# Investigating RSA-1-dependent PP2A functions in *C. elegans* mitotic spindle assembly

by

Karen Irene Lange

A thesis submitted in partial fulfillment of the requirements for the degree of

Doctor of Philosophy

in

Molecular Biology and Genetics

Department of Biological Sciences
University of Alberta

# Abstract

Spindle assembly pathways are conserved in many organisms. Defects in spindle assembly can result in aneuploidy, a common cause of cell death and cancer. A better understanding of spindle assembly pathways is required to fully appreciate how defects in spindle assembly manifest as aneuploidy and cancer. Phosphorylation of spindle assembly proteins is a key mechanism to regulate this process. Phosphatases, such as protein phosphatase 2A (PP2A), dephosphorylate these proteins to precisely regulate their activity. The substrate specificity and subcellular localization of the PP2A complex is regulated by protein interactions with regulatory subunits. In *C. elegans* embryos, a PP2A regulatory subunit, RSA-1, is required for mitotic spindle assembly. *rsa-1(lf)* embryos exhibit a reduction in the number of microtubules at the centrosomes. Loss of *rsa-1* causes a dramatic collapse of the mitotic spindle and, subsequently, a failure in chromosome segregation that results in embryonic lethality. Although it is expected that RSA-1 promotes dephosphorylation of specific proteins important for spindle assembly and/or function, bona fide substrates have not been verified. Potential targets include the microtubule depolymerase, KLP-7, and the microtubule stabilizer, TPXL-1. In *rsa-1(lf)* embryos, centrosomes exhibit increased levels of KLP-7 but decreased levels of TPXL-1, suggesting a potential molecular basis for the *rsa-1* phenotypes. However, it is not clear how RSA-1 regulates KLP-7 and TPXL-1. To investigate the function of the RSA-1/PP2A complex, I performed a genetic screen for suppressors of a temperature-sensitive missense allele, *rsa-1(or598).* This screen recovered interaction suppressor mutations that altered amino acids within either the RSA-1 regulatory subunit itself or the PP2A structural subunit, PAA-1. These mutations highlight key residues that likely play a role

in modulating the regulatory subunit preference of the PP2A holoenzyme. Through my characterization of RSA-1 function in embryos using microscopy-based experiments, I discovered a novel role for RSA-1 in localizing a major mitotic kinase, Aurora A, to microtubules. Furthermore, I propose a model whereby RSA-1 is required for an interaction between Aurora A and TPXL-1, which promotes microtubule localization of the kinase. I also observed that TPXL-1 is located on the chromatin in *C. elegans* embryos in an RSA-1, Aurora A, and RanGTP-dependent manner. I propose that TPXL-1 at the chromatin promotes spindle assembly in a manner similar to nuclear TPX2 in vertebrates.

# Preface

Some of the results presented in Chapter 3 of this thesis have been previously published as K.I. Lange, J. Heinrichs, K. Cheung, & M. Srayko. (2013). Suppressor mutations identify amino acids in PAA-1/PR65 that facilitate regulatory RSA-1/B″ subunit targeting of PP2A to centrosomes in *C. elegans*. *Biology Open, 2*(1), 88-94. These results are presented herein with permission from all co-authors. I was responsible for designing experiments, carrying out experiments, and interpreting the results. Some of the yeast two hybrid constructs were prepared by J. Heinrichs and the anti-PAA-1 antibody was prepared and purified by K. Cheung.

The results presented in Chapter 4 and Appendix B are an original work and have not been previously published. The anti-TPXL-1 antibody was prepared by K. Cheung and purified by J. Tegha-Dunghu. The whole genome sequencing presented in Appendix B was completed by Delta Genomics (Edmonton, Alberta) and Genome Quebec (Montreal, Quebec). Bioinformatics analysis of the sequencing data was performed by Paul Stothard (Department of Agricultural Food and Nutritional Science, University of Alberta).

# Acknowledgements

I would like to thank my husband, Craig, for his love and encouragement over the years I have been working on this thesis. I would also like to thank my family for their unconditional support.

I would like to thank all of my past and present lab mates for discussions, help with techniques, and generally making the lab a fun place to be. I would also like to specifically thank my supervisor, Dr. Martin Srayko, for his guidance and support throughout the course of my graduate work.

# Table of Contents

# List of Tables

# List of Figures

# List of Abbreviations

| | |
|---|---|
| **°C** | Degrees Celsius |
| **abc** | Srayko lab designation for mutant alleles |
| **air** | Aurora/Ipl1-related serine/threonine kinase |
| ***At*** | *Arabidopsis thaliana* |
| **ATP** | Adenosine triphosphate |
| **aui** | Arbitrary units of intensity |
| **B** | Bristol |
| **bli** | Blistered |
| **bmk** | BimC related kinase |
| **bp** | Base pair |
| **bub** | Budding uninhibited by benzimidazole |
| **Ca** | Calcium |
| **cdc** | Cell division cycle |
| **Cdk** | Cyclin-dependent kinase |
| **cDNA** | Complementary DNA |
| ***Ce*** | *Caenorhabditis elegans* |
| **ced** | Cell death abnormality |
| **CPC** | Chromosomal passenger complex |
| **dd** | Dresden, Deutschland, Hyman lab allele designation |
| **dhc** | Dynein heavy chain |
| **DIC** | Differential interference contrast |
| **DNA** | Deoxyribonucleic acid |
| **dpy** | Dumpy |
| **dsRNA** | Double stranded RNA |
| **ebp** | End binding protein |
| **EDTA** | Ethylenediaminetetraacetic acid |
| **EF** | Glutamic acid phenylalanine |
| **EMS** | Ethyl methanesulfonate |

| | |
|---|---|
| **GAP** | GTPase activating protein |
| **gDNA** | Genomic DNA |
| **GEF** | Guanine nucleotide exchange factor |
| **GFP** | Green fluorescent protein |
| **GDP** | Guanine diphosphate |
| **GTP** | Guanine triphosphate |
| **H** | Hawaiian |
| **H2B** | Histone 2B |
| **hcp** | Holocentric chromosome binding protein |
| **HEAT** | Huntingtons, elongation factor 3, PP2A, Tau |
| **Him** | High incidence of males |
| **his** | Histidine |
| ***Hs*** | *Homo sapiens* |
| **InDel** | Insertion/Deletion |
| **IPTG** | Isopropyl β-D-1-thiogalactopyranoside |
| **kbp** | Thousand base pairs |
| **klp** | Kinesin like protein |
| **KMN** | Knl-1/Mis-12/Ndc-80 complex |
| **L1** | Larval stage 1 |
| **L2** | Larval stage 2 |
| **L3** | Larval stage 3 |
| **L4** | Larval stage 4 |
| **LB** | Luria Bertani broth |
| **let** | Lethal |
| **leu** | Leucine |
| **lf** | Loss of function |
| **LG** | Linkage group |
| **lon** | Long |
| **M9** | Minimal *C. elegans* salt buffer |
| **MAP** | Microtubule associated protein |
| **Mbp** | Mega base pairs |

| | |
|---|---|
| **MCAK** | Mitotic centromere associated kinesin |
| **mcrs** | Microtubule-binding microspherule protein |
| **mel** | Maternal effect lethal |
| **mm** | Yeast minimal media |
| **MMDB** | Macromolecular structure database |
| **MT** | Microtubule |
| **MTOC** | Microtubule organizing center |
| **NEBD** | Nuclear envelope breakdown |
| **NGM** | Nematode growth medium |
| **NLS** | Nuclear localizing signal |
| **O/N** | Overnight |
| **or** | Oregon, Bowerman lab allele designation |
| **paa** | Phosphatase 2A regulatory A subunit |
| **pak** | p21-activated kinase |
| **PAGE** | Polyacrylamide gel elctrophoresis |
| **PBS** | Phosphate buffered saline solution |
| **PCR** | Polymerase chain reaction |
| **Plk** | Polo-like kinase |
| **PP1** | Protein phosphatase 1 |
| **PP2A** | Protein phosphatase 2A |
| **PP6** | Protein phosphatase 6 |
| **pph** | Protein phosphatase |
| **pptr** | Protein phosphatase 2A regulatory subunit |
| **ptrn** | Patronin |
| **Rac** | Ras-related C3 botulinum toxin substrate |
| **Ran** | Ras-related nuclear protein |
| **RCC1** | Regulator of chromosome condensation 1 |
| **RFLP** | Restriction fragment length polymorphism |
| **RNA** | Ribonucleic acid |
| **RNAi** | RNA interference |
| **rsa** | Regulator of spindle assembly |

| | |
|---|---|
| **RT** | Room temperature |
| **SAC** | Spindle assembly checkpoint |
| **s.d.** | Standard deviation |
| **SDS** | Sodium dodecyl sulphate |
| **Ska** | Spindle and kinetochore associated |
| **spd** | Spindle defective |
| **sun** | Sad1/UNC- 84 |
| **szy** | Suppressor of *zyg-1* |
| **TBST** | Tris buffered saline solution with Tween-20 |
| **TON2** | Tonneau 2 |
| **TPX2** | Targeting protein for Xenopus klp2 |
| **tpxl** | TPX2 like |
| **trp** | Tryptophan |
| **ts** | Temperature sensitive |
| **ubxn** | UBX-containing protein in nematodes |
| **unc** | Uncoordinated |
| **V** | Volts |
| **Wt** | Wild-type |
| **XMAP** | *Xenopus* microtubule associated protein |
| **YPD** | Yeast extract, peptone, dextrose |
| **zyg** | Zygotic defective |

# 1 Introduction

## 1.1 Mitosis

Mitosis describes the process of a eukaryotic cell dividing into two daughter cells that are genetically identical to the original mother cell. Prior to mitosis, the genome is replicated to generate two copies of all chromosomes that can then be evenly distributed between the daughter cells. There are several characteristic steps involved in mitosis, broadly defined as prophase, metaphase, anaphase, telophase, and cytokinesis. During these phases, the replicated chromosomes condense, align along the metaphase plate, and segregate to the daughter cells. Mitosis is completed when the chromosomes de-condense and the cytoplasm of the daughter cells is separated in cytokinesis. Successful mitosis requires that cells undergo dramatic restructuring and this requires the concerted activities of many proteins, both temporally and spatially.

One challenge faced by all eukaryotic cells is the accurate segregation of the replicated genome to daughter cells during cell division. Defects in chromosome segregation can result in aneuploidy, which can give rise to daughter cells that are either inviable or unresponsive to normal cell division controls, the latter of which is a necessary precedent to cancer. Successful mitosis requires that cells assemble a transient, microtubule based structure that faithfully segregates the sister chromatids. While the exact architecture of this apparatus, termed the mitotic spindle, varies between organisms, there are conserved pathways that are used in the assembly process. Understanding the process of spindle assembly in a genetically tractable model organism such as *Caenorhabditis elegans* will foster a better understanding of spindle assembly and function in general, and provide insight into the molecular basis for human diseases associated with aneuploidy.

In *C. elegans*, a phosphatase regulatory subunit, termed RSA-1, is required for mitotic spindle assembly (Schlaitz et al., 2007). RSA-1 targets a phosphatase to the centrosomes and is presumed to dephosphorylate protein substrates. Depletion of RSA-1 function in *C. elegans* embryos results in a significant decrease in the number of microtubules emanating from the centrosome and a small spindle phenotype. Based on these phenotypes, it is expected that substrates of the RSA phosphatase complex will directly

regulate microtubule dynamics and spindle stability. The primary goal of this thesis was to investigate how the RSA-1-phosphatase complex facilitates spindle assembly in *C. elegans* embryos using genetics and microscopy based techniques.

## 1.2 Mitotic phosphatases and kinases

Cellular events, such as cell division, require that a vast number of proteins are regulated in a coordinated manner. Post-translational modification of proteins is one mechanism used by cells to synchronously regulate the activity of many different proteins. Phosphorylation is a reversible post-translational modification whereby a phosphate group is covalently added to an amino acid of a substrate protein. Phosphorylation can regulate the temporal and spatial behaviour of a protein by altering enzymatic activity, changing binding affinity to other proteins, affecting subcellular localization, or priming the protein for subsequent post-translational modifications. Kinases catalyze the transfer of a terminal phosphate from adenosine tri-phosphate onto a nucleophilic amino acid side chain of a substrate. Phosphatases oppose the action of kinases by removing phosphate groups from substrates.

Proteomics studies in mammalian cells have revealed that fluctuations in phosphorylation levels are especially apparent during mitosis (Olsen et al., 2010). Phosphorylation is critical to regulate spindle assembly and most identified centrosome (Keck et al., 2011) and spindle-associated proteins (Santamaria et al., 2011) have multiple phosphorylation sites. Kinases are well characterized regulators of mitosis (Alexander et al., 2011) and mitotic phosphatases also play many crucial roles in ensuring progression through mitosis (reviewed in Barr, et al., 2011). A balance between the activities of kinases and phosphatases is critical for proper mitosis.

### 1.2.1 Aurora A kinase

The dramatic increase in protein phosphorylation that is observed during mitosis (Olsen et al., 2010) is due to the activity of a variety of kinases including the Aurora kinases, cyclin-dependent kinases (Cdk), and polo-like kinases (Plk). These kinases, and many others, play key roles in ensuring mitosis proceeds correctly (reviewed in Bayliss et al., 2012; Ma and Poon, 2011). This thesis will focus on the mitotic functions of Aurora

A kinase because it has previously been implicated as a major regulator of microtubule dynamics and mitotic spindle assembly.

The kinase activity of Aurora A is required for several key mitotic processes including centrosome maturation (Hannak et al., 2002; Mori et al., 2007), entry into mitosis (Seki et al., 2008), and mitotic spindle assembly (Tsai et al., 2003). Aurora A is found at the centrosomes and along microtubules (Kufer et al., 2002; Ozlü et al., 2005), which facilitates its ability to directly regulate substrates that are required for spindle assembly. Aurora A phosphorylates a consensus motif (R-X-S/T) and several substrates of this kinase have been identified. Many of the verified substrates of Aurora A affect microtubule dynamics and organization. For example, Aurora A phosphorylates one substrate to promote chromatin-mediated microtubule nucleation (Albee et al., 2006; Pinyol et al., 2013; Scrofani et al., 2015) and another substrate that stabilizes kinetochore microtubules by crosslinking (Booth et al., 2011; Wong et al). Aurora A also phosphorylates a microtubule depolymerase, MCAK, to limit its activity and promote microtubule stability (Zhang et al., 2008; Braun et al., 2014). By directly regulating the activity and localization of proteins that affect microtubule dynamics or organization (Sardon et al., 2008; Wong et al., 2008), Aurora A regulates spindle assembly.

Aurora A protein levels are regulated in a cell cycle dependent manner. Aurora A protein levels increase at the start of mitosis (Fumoto et al., 2008) and remain high until Aurora A is targeted for destruction by the anaphase promoting complex in a ubiquitin-dependent manner (Floyd et al., 2008). Degradation of Aurora A by the proteasome is regulated by at least two mechanisms. Phosphorylation can prevent proteasome-dependent degradation of Aurora A in both human cells and *Xenopus* extracts (Horn et al., 2007; Littlepage and Ruderman, 2002). Additionally, binding to TPX2 has been shown to prevent ubiquitin-mediated degradation of Aurora A (Giubettini et al., 2010). This could result in specific pools of Aurora A being protected from degradation, and other pools targeted for destruction.


**Figure 1-1 Regulation of Aurora A catalytic activity**
Aurora A kinase activity can be activated by phosphorylation of the T-loop or binding of activating proteins such as TPX2. This activation can be opposed by phosphatases which dephosphorylate Aurora A.

The catalytic activity of Aurora A is also regulated by several mechanisms (Figure 1-1). The best characterized mechanism of Aurora A activation is phosphorylation on a threonine residue, termed the T-loop, in the kinase domain of Aurora A. The T-loop can be phosphorylated by Aurora A (Bayliss et al., 2003; Eyers et al., 2003) or it can be phosphorylated by other kinases, both at the T-loop as well as additional residues (Zhao et al., 2005). Binding of activating proteins, such as Ajuba, Bora, or TPX2 (Bai et al., 2014; Seki et al., 2008; Zorba et al., 2014), is also able to stimulate Aurora A kinase activity. Aurora A activity has shown to be limited by the activity of phosphatases that dephosphorylate the T-loop phosphorylation of Aurora A (Zeng et al., 2010).

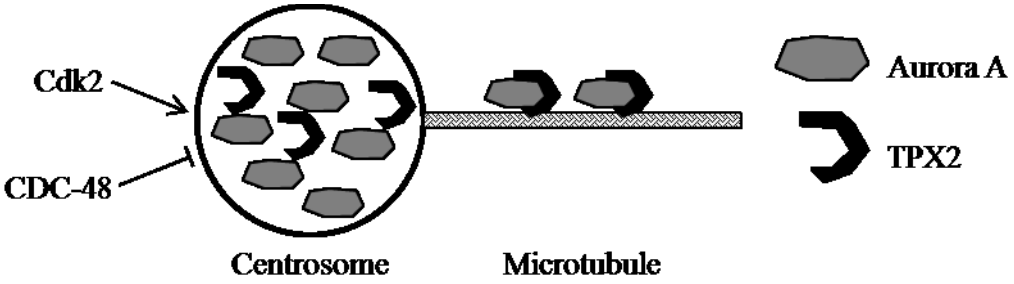


**Figure 1-2. Localization of Aurora A**
Aurora A is located at the centrosomes and on microtubules. Aurora A localization to the centrosome is promoted by Cdk2 and limited by CDC-48. The microtubule localization of Aurora A requires TPX2.

The localization of Aurora A at both the centrosomes and microtubules is tightly regulated and critical for spindle assembly. The targeting of Aurora A to these two locations occurs via distinct mechanisms. Aurora A localization to the centrosomes in mitosis is promoted by the cyclin dependent kinase Cdk2 (Leontovich et al., 2013). In contrast, Aurora A localization to the centrosomes is limited by a AAA ATPase. Depletion of the AAA ATPase CDC-48 leads to early accumulation of Aurora A at the

centrosome and results in premature centrosome maturation and spindle defects (Kress et al., 2014) in both *C. elegans* and human cells. The microtubule localization of Aurora A requires TPX2 (Kufer et al., 2002; Ozlü et al., 2005) and the kinase activity of Aurora A (Sardon et al., 2008). In *C. elegans*, it has been shown that Aurora A is phosphorylated at the T-loop at the centrosome, but that Aurora A on the microtubules is not phosphorylated at this residue (Toya et al., 2011).

In addition to promoting bipolar spindle assembly, Aurora A is a key regulator of mitotic spindle length. This aspect of Aurora A function is dependent on correct localization to the spindle microtubules; conditions that disrupt the recruitment of Aurora A to spindle microtubules result in significantly shorter or collapsed mitotic spindles. For example, small spindles are observed upon depletion of TPX2, which abrogates Aurora A localization to microtubules (Bird and Hyman, 2008; Ozlü et al., 2005). In addition, mutations that disrupt the protein interaction between Aurora A and TPX2 (Ozlü et al., 2005), or depletion of a protein that promotes the association of TPX2 with the microtubules (Chen et al., 2014), also result in collapsed spindles. Despite this correlation between Aurora A's location on the spindle microtubules and spindle stability, the molecular mechanism of how Aurora A regulates spindle length remains elusive.

### 1.2.2 Protein phosphatase 2A (PP2A)

A large phosphatase family called protein phosphatase 2A (PP2A) is required for many cellular processes including mitosis, meiosis, apoptosis, metabolism, various signalling pathways, and DNA replication (reviewed in Lambrecht et al., 2013; Sents et al., 2013). Inhibition or loss of PP2A activity promotes tumour formation (Suganuma et al., 1988) and mutations in PP2A subunits have been identified in many types of cancers including within tissues of the lung (Ruediger et al., 2011), ovary (Rahman et al., 2013), endometrium (Hoang et al., 2014), and liver (Chen et al., 2013).

The PP2A holoenzyme is a heterotrimeric complex composed of a catalytic subunit, a structural subunit, and a regulatory subunit (Figure 1-3). The core of the PP2A enzyme is formed by the catalytic and structural subunit. These two subunits associate with a various regulatory subunit that confers substrate specificity and determines the subcellular localization of the PP2A core enzyme. The many PP2A regulatory subunits are divided into three major families based on sequence similarity and are termed B, B',

or B''. These families of regulatory subunits share no structural similarity with each other. In mammalian cells, many of these genes have multiple splice variants with unique expression patterns and functions. The expression and function of the mammalian PP2A regulatory subunits have previously been published (reviewed in Lambrecht et al., 2013) and some of this information is summarized in Table 1-1.

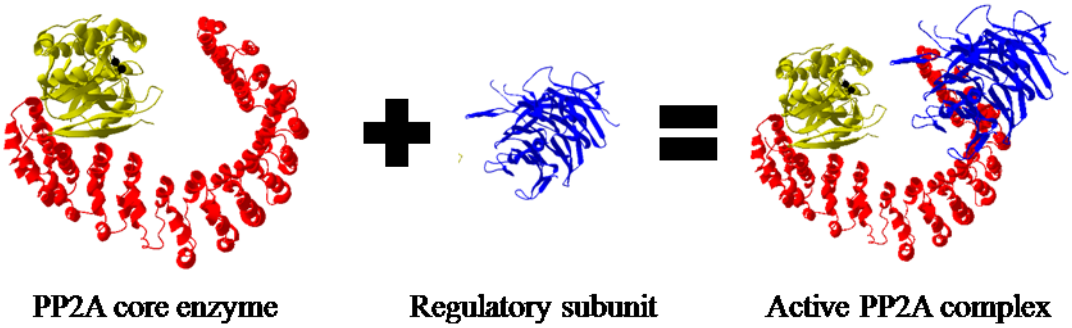


**Figure 1-3. Structure of PP2A holoenzyme**
Crystal structure of the PP2A holoenzyme with a B family regulatory subunit, PR55. MMDB ID: 84473 (Xu et al., 2008). The catalytic subunit is yellow and the structural subunit is red.

| | Gene Name | Protein Names | Tissue expression | Subcellular localization | References |
|---|---|---|---|---|---|
| **B** | PPP2R2A | PR55α, B55α | Ubiquitous | Cytoskeleton, cytoplasm, nucleus, plasma membrane, Golgi, ER | Sontag et al., 1995<br>Strack et al., 1998 |
| | PPP2R2C | PR55γ, B55γ | Brain | Cytoskeleton | Zolnierowicz et al., 1994<br>Strack et al., 1998 |
| **B'** | PPP2R5A | PR61α, B56α | Ubiquitous | Centromere, cytoplasm, mitochondria | McCright et al., 1996<br>Foley et al., 2011 |
| **B''** | PPP2R3A | PR72 | Skeletal muscle, heart | Cytosol, nucleus | Hendrix et al., 1993<br>Zwaenepoel et al., 2008 |
| | PPP2R3C | G5PR | Ubiquitous | Cytosol, nucleus, centrosome | Kono et al., 2002<br>Jakobsen et al., 2011 |

**Table 1-1. Selected mammalian PP2A regulatory subunits from the B, B' and B'' families**
"Ubiquitous" tissue expression means it has been observed in all tissues investigated to date. This is not a comprehensive list of PP2A regulatory subunits and functions. A more detailed survey of mammalian PP2A regulatory subunits has previously been reviewed in Lambrecht et al., 2013.

Several PP2A regulatory subunits have characterized roles in mitosis in human cells. For example, B-subunit B55α/PPP2R2A was identified in an RNAi based screen for factors required for mitotic exit (Schmitz et al., 2010) and B'-subunit B56α/PPP2R5A is

required to promote the interaction between kinetochores and microtubules (Foley et al., 2011; Kruse et al, 2013). Copy number variants of B55α/PPP2R2A have been identified as a susceptibility gene in prostate cancer (Cheng et al., 2014) so it is likely that this gene contributes to the tumour suppressor activity of PP2A. Since many PP2A regulatory subunits have known functions in mitosis, it is difficult to determine which ones are responsible for the tumour suppressor function of PP2A. One or several of the PP2A regulatory subunits may confer the tumour suppressor ability of PP2A and this could vary in different tissues. Other regulatory subunits with mitotic roles or even regulatory subunits with currently uncharacterized mitotic functions could also contribute to PP2A tumour suppressor activity.

### 1.3 **The importance of spindle assembly**

In all eukaryotes, the mitotic spindle is critical to ensure that each daughter cell will receive precisely one complement of the genome. While chromosome gain has been shown to promote large-scale phenotypic changes that drive evolution (reviewed in Chen et al., 2012), aneuploidy is more often deleterious for an organism (reviewed in Ricke and van Deursen, 2013). Many levels of regulation exist to promote the efficiency and fidelity of spindle assembly to limit the occurrence of aneuploidy.

Aneuploidy is associated with, and can cause, many types of cancers (reviewed in Gordon et al., 2012; Holland and Cleveleand, 2012; Ricke and van Deursen, 2013). Mouse models that have a high incidence of aneuploidy were shown to be predisposed to cancer. There are many molecular mechanisms that can give rise to aneuploidy such as the disruption of spindle assembly (Aguirre-Potolés et al., 2012), inappropriate kinetochore-microtubule attachments (Diaz-Rodríguez et al., 2008), deregulation of the spindle assembly checkpoint (Schliekelman et al., 2009), or lack of correction of kinetochore-microtubule attachment errors (Ricke et al., 2011). In addition to its link to cancer, chromosomal instability in mice has also been shown to cause premature aging (Baker et al., 2004; Baker et al., 2006). Aneuploidy in human cells results in similar defects as those observed in mice. A rare autosomal recessive genetic disorder, termed mosaic variegated aneuploidy syndrome (MVA), is characterized by severe chromosome segregation errors due to a mutation in a key spindle assembly checkpoint protein, BubR1

(Wijshake et al., 2012). This mutation causes premature sister chromatid separation and results in aneuploidy in approximately one quarter of somatic cells (Schmid et al., 2014). While this syndrome has a high incidence of spontaneous abortion, individuals born with MVA are predisposed to early onset cancer and display premature aging phenotypes, growth retardation, and have a reduced life span (Pinson et al., 2014). Proper spindle assembly and function is essential for the posterity of all eukaryotic cells. A better understanding of the regulation of microtubules and mitotic spindle assembly will help to explain how these components impact cellular health and disease.

Tumors with specific gene expression or protein activity patterns have been shown to respond differentially to various cancer treatments. It is a challenge to find biomarkers that can be used to predict if a patient will respond to a specific treatment. For example, Aurora A kinase is hyperactive in many cancer cell lines and tumors (Nikonova et al., 2013) and overexpression of Aurora A in cancer cell lines has been shown to confer resistance to a chemotherapeutic agent that targets microtubules, Taxol (Anand et al., 2003; Li et al., 2011). As such, Taxol is not an effective anti-cancer treatment for tumours that have increased Aurora A activity. The challenge is to determine whether Aurora A is active in a tumour or not. Aurora A activity is commonly measured by phosphorylation of a threonine residue in the catalytic T-loop domain (Littlepage et al., 2002). However, binding of TPX2 to Aurora A is able to activate the kinase activity independently of T-loop phosphorylation (Dodson et al., 2012; Zorba et al., 2014). Therefore, T-loop phosphorylation is not necessarily indicative of Aurora A activity in cells. A more thorough understanding of Aurora A activation *in vivo* is critical for predicting tumor response to Taxol treatment (Shagisultanova et al., 2015) and selecting chemotherapeutic agents that will most effectively treat patients. Additionally, small molecule inhibitors of Aurora A have shown promising anti-tumor properties in clinical trials (Malumbres and Pérez de Castro, 2014) and could potentially attenuate the Aurora A mediated Taxol resistance (Scharer et al., 2008). A better understanding of how Aurora A is regulated in healthy cells will allow for better predictive methods to determine Aurora A activity in tumours.

## 1.4 **Structure of the mitotic spindle**

The mitotic spindle is a bipolar microtubule-based structure that facilitates the proper segregation of replicated chromosomes into the future daughter cells during cell division. Microtubules are the major structural component of the mitotic spindle, however, many other proteins associate with the mitotic spindle (Sauer et al., 2005) and proteomic analysis has identified more than 1100 proteins on mammalian metaphase spindles (Bonner et al., 2011). Several non-protein components of the spindle have also been implicated in contributing to its structure and organization. These include macro-molecules such as RNA (Blower et al., 2005), poly-ADP-ribose (Chang et al., 2004), and glycogen (Groen et al., 2011), however the roles of non-protein components of the spindle will not be explored in this thesis.

### 1.4.1 Microtubules

Microtubules are polymers of α/β-tubulin heterodimers that interact in a "head to tail" fashion to form protofilaments and the protofilaments interact laterally to form a hollow polymer approximately 25 nm in diameter (Figure 1-4A). The organization the α/β-tubulin dimers in the protofilaments generates an intrinsic polarity in the microtubule lattice. At one end, termed the minus-end, the α-tubulin is exposed while at the plus-end the β-tubulin is exposed (Mitchison, 1993). The kinetic properties of the microtubule ends vary with the plus-end being more dynamic than the minus-end. Microtubules have an intrinsic property termed dynamic instability whereby they undergo phases of polymerization and depolymerization and can stochastically switch between growth and shrinking (Mitchison and Kirschner, 1984; Figure 1-4B). The transition from growing to shrinking is called catastrophe and the transition from shrinking to growing is called a rescue.

While individual microtubules are dynamic, they are able to form higher order structures that are stable. For example, the steady-state metaphase mitotic spindle is overall a stable structure, even though it is composed of individual microtubules that are dynamic throughout mitosis (Wadsworth and Salmon, 1986).

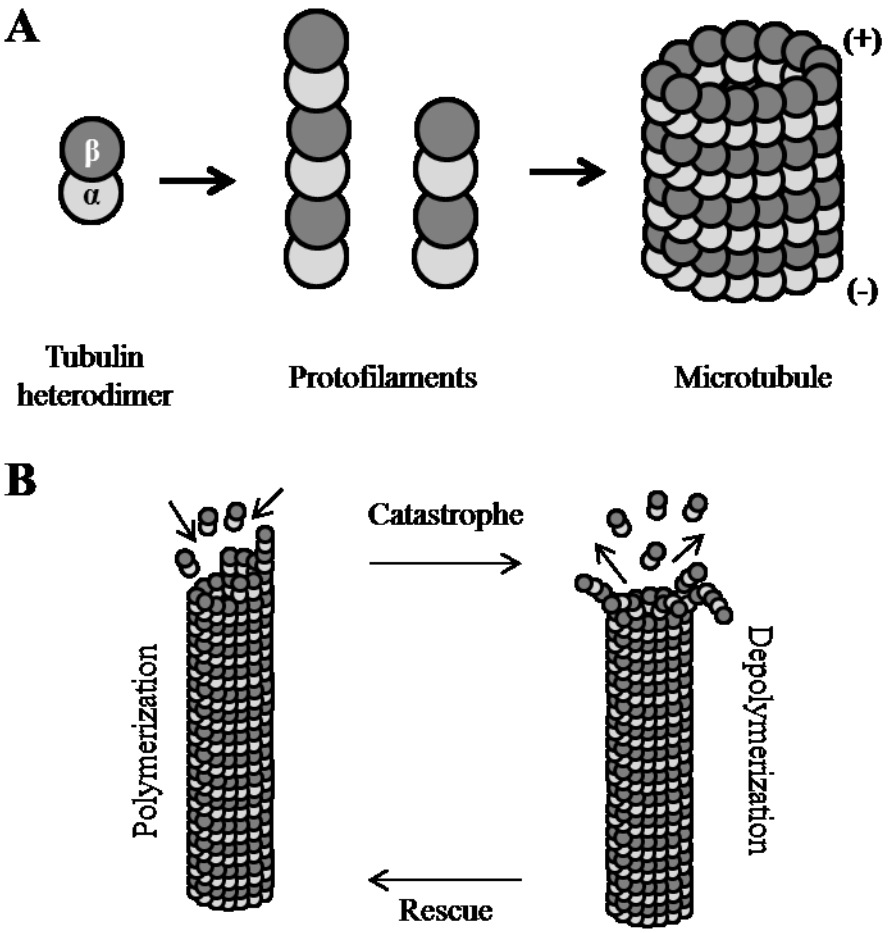


**Figure 1-4. Microtubule structure and dynamic instability**
A) The structure of an α/β-tubulin heterodimer, protofilaments, and microtubule. B) Schematic of microtubule dynamics.

#### *1.4.1.1 Microtubule populations in the spindle*

The microtubules in the mitotic spindle can be divided into three classes: kinetochore microtubules, inter-polar microtubules, and astral microtubules (Figure 1-5). Kinetochore microtubules are anchored at the spindle pole or centrosome and are directly attached to a kinetochore at the chromatin. There are proteins on the spindle that specifically interact with kinetochore microtubules (Goodwin and Vale, 2010; Meunier and Vernos, 2011), making these microtubules molecularly distinct from others within the spindle. Kinetochores microtubules are the most stable microtubules in the mitotic spindle and are resistant to conditions that generally depolymerize microtubules, such as cold treatment (reviewed in Inoué and Salmon, 1995). Kinetochores remain connected to microtubules

that are growing or shrinking (reviewed in Guo et al., 2013) and thus accommodate changes in pole-to-pole or pole-to-chromatin distance.


**Figure 1-5. Microtubule populations in the spindle**
Schematic of the different types of microtubules that make up the mitotic spindle at metaphase. The populations are kinetochore microtubules (red), spindle or inter-polar microtubules (yellow), and astral microtubules (green).

Inter-polar microtubules typically account for the bulk of the spindle mass (Nazarova et al., 2013). They provide structural support and rigidity to the spindle and may or may not extend to the spindle poles. These microtubules can overlap at the spindle equator, which generates anti-parallel microtubules that can interact via microtubule-associated proteins. This class of microtubules can also interact with the proteins on the chromatin to help position the chromosomes during spindle assembly.

Astral microtubules originate from the centrosome or spindle pole and radiate out without interacting with the chromatin. This population of microtubules can interact with the cell cortex and are important to position the spindle in the cell (Noatynska et al., 2012). The astral microtubules increase in length and density during anaphase (Wühr et al., 2010) and this population of microtubules can interact with motor proteins at the cortex to provide the force for pole separation during anaphase (Grill et al., 2001; Grill et al., 2003).

Organisms from different phylogenetic backgrounds have dramatic differences in the number of the microtubules in each of these populations. The kinetochore microtubules can either be a single microtubule that attaches to a single kinetochore, like in the budding yeast *S. cerevisiae* or a bundle of microtubules like in higher eukaryotes (Joglekar et al., 2008). The number of astral microtubules also varies dramatically between organisms. For example, *S. cerevisiae* has approximately 20 astral microtubules

(Dammermann et al., 2012) while *C. elegans* has over 2000 microtubules emanating from each centrosome (O'Toole et al., 2012).

#### *1.4.1.2 Regulation of microtubule dynamics in the spindle*

Experiments with tubulin solutions *in vitro* have shown that temperature, microtubule-binding drugs, and tubulin concentration can change the dynamic properties of microtubules (Inoué & Salmon, 1995). In living cells and cell extracts, microtubule dynamics are primarily regulated by microtubule associated proteins. These proteins can promote microtubule nucleation, polymerization, depolymerization, or stabilization. The activities of these proteins are controlled spatially and temporally to allow the microtubule cytoskeleton to form higher order structures and perform various functions in the cells.

Microtubule nucleation refers to the formation of a new microtubule polymer. The best characterized protein that promotes microtubule nucleation in cells is gamma-tubulin. Gamma-tubulin forms a complex that acts as a template for a microtubule to nucleate on (Guillet et al., 2011; Kollman et al., 2010). While gamma-tubulin can promote microtubule nucleation, it is not absolutely required for microtubule formation *in vivo. C. elegans* embryos depleted of gamma-tubulin microtubules can still nucleate around centrosomes, but the microtubule arrays are disorganized (O'Toole et al., 2012). Gamma tubulin can also promote microtubule nucleation at sites other than the centrosomes such as along an existing microtubule (Bucciarelli et al., 2009; Goshima et al., 2008).

Microtubule polymerization occurs when tubulin subunits are added on to the end of a microtubule. Typically this occurs at the plus-end of the microtubule. A microtubule polymerase, XMAP215, tracks with the plus-end of a growing microtubule and facilitates the addition of tubulin dimers to the polymer (Brouhard et al., 2008; Kerssemakers et al., 2006). This activity promotes the growth of long microtubules and contributes to larger mitotic spindle size (Srayko et al., 2003; Barr and Gergely, 2008).

There are several mechanisms that can promote the catastrophe of a microtubule and result in depolymerization. Lowering the effective concentration of free tubulin will promote microtubule de-polymerization. Proteins such as stathmin bind and sequester tubulin to locally lower the tubulin concentration and promote microtubule disassembly

(Curmi et al., 1997). During mitosis, stathmin is inactivated by phosphorylation to promote microtubule stability and spindle assembly (Gadea and Ruderman, 2006). Another mechanism to promote microtubule catastrophes is by the catalytic activity of microtubule depolymerases. One of the best studied microtubule depolymerases is MCAK. MCAK is a kinesin-13 family member that uses the energy from ATP hydrolysis to promote microtubule disassembly (Ohi et al., 2004). MCAK associates with the plus-end of microtubules and stimulates a conformational change or curve in the protofilaments and results in microtubule depolymerization (Burns et al., 2014). Loss of this microtubule depolymerization via *klp-7(RNAi)* in *C. elegans* embryos results in a significant increase in microtubule number during mitosis (Srayko et al., 2005) and meiosis (Han, 2014). Microtubule length and formation can also be influenced by microtubule severing enzymes such as katanin (Srayko et al., 2006; Zhang et al., 2011) or figetin (Mukherjee et al., 2012).

Cells use several mechanisms to stabilize microtubules. Some proteins such as HURP interact directly with the microtubule lattice to stabilize the interaction between the protofilaments of the microtubule to prevent disassembly (Yang and Fan, 2008). However, the regulation of MT polymer assembly and disassembly can involve a complex hierarchy of regulatory enzymes. One such mechanism involves preventing depolymerization by antagonizing the activity of microtubule destabilizing proteins. For example, patronin and MCRS1 compete with MCAK to bind the minus-end of microtubules (Goodwin and Vale, 2010; Meunier and Vernos, 2011). By antagonizing the interaction of MCAK with microtubules these proteins result in an overall decrease of microtubule catastrophes.

It is often challenging to distinguish between factors that promote microtubule nucleation and factors that stabilize existing microtubules. Because both of these biochemically different mechanisms increase microtubule number, the consequences of removing either activity could manifest as superficially similar phenotypes. For example, TPX2 is known to bind microtubules and can promote microtubule formation from tubulin *in vitro* (Schatz et al., 2003; Brunet et al., 2004; Wittmann et al., 2000). However, it remains unclear how TPX2 performs this function *in vivo*. Since TPX2 binds the polymer, it could directly stabilize microtubules or it could interact with other proteins. It

has been shown that TPX2 promotes branched microtubule nucleation through an interaction with augmin and gamma tubulin (Petry et al., 2013). Additionally, TPX2 is also known to bind to other factors that promote microtubule formation such as Aurora A (Bayliss et al., 2003). Since factors like TPX2 can have multiple roles in regulating microtubule dynamics it is difficult to determine which phenotypes are associated with which activities.

### 1.4.2 Centrosomes

Centrosomes are the dominant site of microtubule nucleation and organization in most animal cells. During mitosis, the centrosomes are located at the spindle poles and play a key role in organizing the mitotic spindle (reviewed in Chavali et al., 2015). Each centrosome is composed of a pair of centrioles that can recruit peri-centriolar material that creates a matrix that nucleates and organizes microtubules. The microtubules emanate from centrosomes with their minus-ends embedded in the centrosome matrix and the plus-end of the microtubule growing outwards. During mitosis the centrosomes undergo a maturation process whereby they increase in size and capacity for microtubule nucleation (Hannak et al., 2002). During centrosome maturation, many proteins are recruited to the centrosome but the exact number of centrosomal proteins varies between organisms. *Drosophila* centrosomes are composed of more than 250 proteins (Müller et al., 2010), while *S. cerevisiae* centrosomes comprise 18 proteins (Keck et al., 2011). Many of the proteins at the centrosome have coiled-coil domains that allow them to act as scaffolds for other proteins (Kuhn et al., 2014).

In addition to their role as a microtubule organizing center, centrosomes also act as signalling centers during mitosis (reviewed in Arquint et al., 2014). For example, centrosomes promote nuclear envelope breakdown independently of their ability to nucleate microtubules (Portier et al., 2007). When centrosomes are manipulated to be a further distance from pro-nuclei, there is a significant delay in nuclear envelope breakdown (Hachet et al., 2007; Portier et al., 2007). Many regulators of mitosis are located at the centrosome to coordinate various mitotic processes. For example, the centrosomal localization of Aurora A is regulated to coordinate centrosome maturation with cell cycle progression (Kress et al., 2014).

### 1.4.3 Chromatin and kinetochores

Microtubules form a connection with the chromatin at the centromere through a large multi-subunit complex called the kinetochore. The human kinetochore is a large structure and contains at least 196 proteins (Tipton et al., 2012). The kinetochore can be divided into two main structures termed the inner and outer kinetochore. The inner kinetochore is composed of proteins that interact with centromeric DNA. During mitosis the centromeric chromatin is specified by a specialized histone in the nucleosome. This centromeric H3 is required to recruit all other kinetochore proteins to the centromere (Oegema et al., 2001). The outer kinetochore proteins interact with microtubules. In *S. cerevisiae* a single microtubule interacts with a single kinetochore, while in human cells upwards of 35 microtubules interact with the kinetochore (McEwen et al., 1997). The KMN (KNL-1/MIS-12/NDC-80) network is the main structure at the kinetochore that makes end-on attachments to microtubules (reviewed in Varma and Salmon, 2012). The RZZ (ROD-1/ZWILCH/ZW10) complex recruits dynein to the kinetochore to allow for the kinetochore to interact laterally with microtubules and promotes efficient spindle assembly.

Microtubules that are attached to kinetochores are more stable than other microtubules populations in the spindle, but they are still dynamic. Specific protein complexes are required to facilitate the interaction of the kinetochore with depolymerizing microtubules. The interaction between the kinetochore and dynamic microtubules is formed by the Dam1 complex in yeast (Joglekar et al., 2006) or the SKA complex (Schmidt et al., 2012) in mammals and *C. elegans*. Once correctly formed, this connection is very stable and kinetochores can remain attached to microtubules even when they are growing or shrinking (reviewed in Guo et al., 2013).

The interaction of the kinetochore with microtubules is monitored by the spindle assembly checkpoint in order to delay anaphase until the chromosomes are correctly bi-oriented in the spindle (reviewed in Sacristan and Kops, 2014). Unattached kinetochores recruit checkpoint proteins, such as Mad2, to the kinetochore and this will cause a delay in anaphase onset until the checkpoint is satisfied.

## 1.5 **Assembly of the mitotic spindle**

After nuclear envelope breakdown, a bipolar spindle assembles around the chromatin. This requires the nucleation and precise organization of the microtubule cytoskeleton to form the transient and essential structure of the mitotic spindle. Several distinct molecular pathways contribute to mitotic spindle assembly and these processes contribute to the robustness of spindle assembly. The contribution of various molecular mechanisms that contribute to spindle assembly in different cell types varies dramatically. For example, the dominant spindle assembly pathway in *C. elegans* requires centrosomes and centrosomal microtubules while other organisms, such as *Xenopus,* utilize chromatin-mediated microtubule nucleation for spindle assembly.

### 1.5.1 "Search and capture"

The term "search and capture" has been used to describe the mechanism of spindle assembly whereby centrosomes nucleate intrinsically dynamic microtubules that probe the cytoplasm in search of the chromosomes (Mitchison and Kirschner, 1984). When a microtubule encounters a kinetochore it can then attach and this eventually forms the bipolar spindle (Mitchison and Kirshener, 1985; Holy and Leibler, 1994). In some organisms, such as *C. elegans,* centrosomes play a dominant role in microtubule nucleation and organization and are absolutely required for spindle assembly.

Mathematical simulations indicate that the "search and capture" model of spindle assembly does not account for how quickly chromosomes can align in human cells (Wollman et al., 2005). Experimentally, human cells can assembly a spindle in 20-30 minutes, whereas the mathematical models indicate "search and capture" alone would require more than 120 minutes to assemble the human mitotic spindle (Wollman et al., 2005).These results suggest that additional mechanisms of spindle assembly exist in human cells to increase the efficiency of the process. This hypothesis was further supported by experiments in *Drosophila* (Basto et al., 2006) and mammalian cells (Khodjakov et al., 2000) that indicated centrosomes were not essential for mitotic spindle assembly.

### 1.5.2 RanGTP-mediated spindle assembly

In *Xenopus* extracts, bipolar spindles can assemble around chromatin in the absence of both centrosomes and kinetochores (Heald et al., 1996). This observation indicates that chromatin is sufficient to promote the nucleation of microtubules that can then be organized into a bipolar spindle structure. The chromatin produces a signal that promotes the nucleation and organization of microtubules. The small Ras-related nuclear GTPase, Ran, is required for chromatin-mediated spindle assembly. Ran can exist in either a GTP or GDP bound state. A guanine nucleotide exchange factor called RCC1 promotes the exchange of GDP to the RanGTP bound state. RCC1 is found on the chromatin and in *Xenopus* extracts RCC1 coated beads are sufficient to assemble bipolar spindle structures (Halpin et al., 2011). RCC1 activity on the chromatin generates a gradient of RanGTP (Kalab et al., 2002). The activity of RCC1 is opposed by RanGAP, which activates the GTPase activity of Ran. In most animals, RanGAP is found in the cytoplasm and is important to limit the RanGTP gradient to the area near the chromatin.

RanGTP contributes to spindle assembly through various mechanisms. RanGTP alters microtubule dynamics by increasing the rescue frequency (Wilde et al., 2001; Yokoyama et al., 2013), which leads to an increase in microtubule stability and therefore microtubule number around the chromatin. Microtubule nucleation in the proximity of the chromatin is not sufficient to form a spindle; microtubules need to be organized in order to form a bipolar spindle. RanGTP also directs an increase in the amount of a microtubule motor, Eg5, on the microtubules (Wilde et al., 2001), which is essential for organizing the microtubules into a bipolar structure (Kollu et al., 2009).

The exact molecular mechanism for how RanGTP promotes the nucleation of microtubules around the chromatin remains to be determined. It is known that TPX2 is required for RanGTP-mediated spindle assembly; *Xenopus* extracts depleted of TPX2 are unable to nucleate microtubules around the chromatin (Gruss et al., 2001). TPX2 activity is inhibited by binding to importin and RanGTP promotes the dissociation of TPX2 from this inhibitory association (Gruss et al., 2001). TPX2 mutants that are unable to bind importin are constitutively active and are sufficient to promote microtubule formation (Schatz et al., 2003). While TPX2 is known to be a key player in Ran-mediated nucleation of microtubules around the chromatin, how TPX2 promotes microtubule

formation during spindle assembly is unknown. TPX2 could nucleate microtubules directly, it could promote the stability of microtubules that are already nucleated, or it could promote the activity of other spindle assembly factors. These possibilities are not mutually exclusive and TPX2 could contribute to multiple spindle assembly pathways. A further complication is that TPX2 is also a major activator of Aurora A. Aurora A has a prominent role in centrosome maturation, leading to the production of microtubules, but it has also been implicated in nuclear processes in human cells (Katayama et al., 2008). Indeed, Aurora A has been observed to be transiently associated with the chromatin in *C. elegans* (Toya et al., 2011), suggesting that it could regulate spindle assembly via centrosome- and chromatin-dependent pathways.

### 1.5.3 The chromosomal passenger complex

The chromosomal passenger complex (CPC) is required for chromatin-mediated spindle assembly (Sampath et al., 2004) independently from RanGTP (Maresca et al., 2009).The CPC is composed of four conserved subunits: Aurora B kinase, a kinase activator INCENP, and two scaffold proteins Borealin and Survivin (Gassmann et al., 2004). The CPC has several functions that lead to the stability of microtubules near the chromatin which can then be organized to produce the mitotic spindle. CPC-dependent microtubule formation occurs via at least two distinct mechanisms. Phosphorylation of the tubulin sequestering protein, stathmin, by Aurora B locally inhibits its activity near the chromatin (Gadea and Ruderman, 2006) which promotes microtubule stability. Additionally, Aurora B phosphorylation of the microtubule depolymerase, MCAK, can inhibit its activity near the chromatin (Zhang et al., 2007; Ems-McClung et al., 2013) which also promotes microtubules stability near the chromatin.

In addition to promoting microtubule stability near the chromatin, the CPC contributes to spindle assembly in other ways. Another critical role for the chromosome passenger complex during spindle assembly is the correction of errors in microtubule-kinetochore attachment. Aurora B is active at improperly attached kinetochores and promotes the release of the microtubules to correct the error (Sarangapani et al., 2013). The CPC is also important after sister chromatid segregation to regulate spindle midzone assembly and cytokinesis (Speliotes et al., 2000).

## 1.6 **Regulation of spindle length**

One important aspect of spindle assembly is the regulation of mitotic spindle length. While spindle size can vary dramatically between organisms and different cell types, in any given cell type the spindle length is very consistent (reviewed in Goshima and Scholey, 2010). It has been shown that cell volume or size correlates directly with spindle length in many cell types (Decker et al., 2011; Good et al., 2013; Hara and Kimura, 2009), however, cell size is not the only factor that contributes to the regulation of spindle length. This is apparent in very large cells where an upper limit to spindle size is observed (Wühr et al., 2008). Spindle-associated proteins and other molecules have intrinsic properties that regulate the size of the spindle. This was clearly shown in experiments with cell extracts from two *Xenopus* species. *X. laevis* has larger eggs than *X. tropicalis* and, as a result, embryonic *X. laevis* cells have larger spindles. In cell free extracts from these species, the spindles recapitulate the *in vivo* size (Brown et al., 2007). When these extracts are combined the spindles that form are an intermediate length between the *in vivo X. laevis* and *X. tropicalis* spindle sizes (Brown et al., 2007). This indicates that diffusible factors within the respective cytoplasm contribute to spindle length in these systems.

Factors that are known to affect spindle length can be classed into three general categories: those that form gradients on the spindle, those that affect microtubule dynamics, and motor proteins. The balance between these various factors contributes to the steady-state spindle length that is observed in cells.

### 1.6.1 Centrosome size and gradients affect spindle length

Gradients are known to affect many aspects of spindle assembly (reviewed in Weaver and Walczak, 2015). In *C. elegans,* there is a strong correlation between the centrosomal levels of the TPX2-like protein, TPXL-1, and spindle size (Greenan et al., 2010). This correlation has also been observed in human cells (Bird and Hyman, 2008). Higher levels of centrosomal TPXL-1 correlate with a broader gradient of TPXL-1 on the microtubules and a longer spindle (Greenan et al., 2010). While this observation has been well documented, it is unknown how a gradient of TPXL-1 on the microtubules affects spindle length.

TPXL-1 is known to recruit Aurora A to the microtubules (Ozlü et al., 2005) and conditions that prevent Aurora A from localizing to the microtubules result in a shorter spindle (Ozlü et al., 2005). These observations suggest that TPXL-1 and Aurora A may work in the same pathway to promote spindle length. The molecular mechanism for how they regulate spindle length is unknown. They may alter downstream effectors that regulate microtubule dynamics or motor proteins that can directly affect spindle length.

### 1.6.2 Microtubule dynamics affect spindle size

Microtubule dynamics can directly affect spindle length. For example, conditions that result in an increase in microtubule catastrophes, such as cold treatment or microtubule binding drugs can result in significantly shorter spindles (Inoué & Salmon, 1995). Mathematical modelling experiments have also shown that several aspects of microtubule dynamics affect spindle length. Both the lifetime of an individual microtubule as well as the stability of the microtubules in the spindle affect spindle length (Burbank et al., 2007; Loughlin et al., 2010). Generally, any condition that results in increased microtubule depolymerization results in shorter spindles.

Many proteins in cells affect microtubule dynamics and therefore these factors also contribute to spindle length. For example, loss of a microtubule stabilizing protein, HURP, results in shorter spindles in both *Drosophila* (Yang and Fan, 2008) and *Xenopus* (Koffa et al., 2006). In human cells, loss of proteins that protect microtubule minus-ends from depolymerases, such as patronin (Goodwin and Vale, 2010) or MCRS1 (Meunier and Vernos, 2011), also result in shorter spindles. Overexpression of the microtubule depolymerase, MCAK, increases levels of microtubule depolymerization and results in shorter spindles (Domnitz et al., 2012) and depletion of MCAK can result in increased spindle length (Mitchison et al., 2005).

### 1.6.3 Microtubule motor proteins and spindle size

Many microtubule motor proteins are known to affect spindle length. The best characterized microtubule motor that affects spindle length is Eg5/BimC/BMK-1. Eg5 is a plus-end directed motor that binds to microtubules and can crosslink adjacent microtubules (Cole et al., 1994). On antiparallel microtubules, this crosslinking and plus-end movement results in the microtubule minus-ends being separated (Figure 1-6). In the

**Figure 1-6. Plus-end directed microtubule motors promote spindle elongation**
Plus-end motors, such as Eg5, can crosslink microtubules and provides the force to push minus ends of microtubules apart. Microtubule minus-ends are enriched at the spindle poles and the action of Eg5 leads to spindle elongation in organisms.

mitotic spindle, microtubule minus-ends are aligned at the spindle pole so this action results in spindle elongation. When Eg5 is chemically inhibited with monastrol, the spindle collapses (Kapoor et al., 2000).

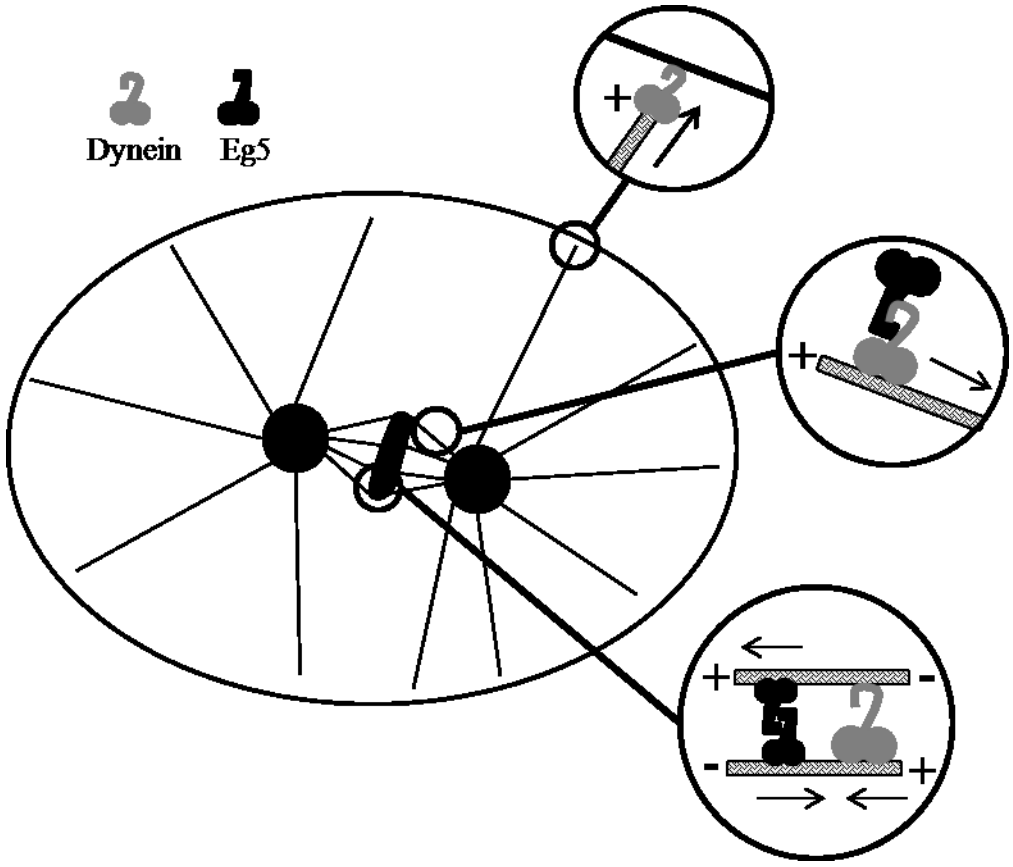


**Figure 1-7. Dynein affects spindle length**
Dynein is a minus-end directed motor that affects spindle length through a variety of mechanisms. When anchored at the cortex, dynein provides an outward force on the spindles. Dynein also functions to localize Eg5 at the minus-end of microtubules at spindle poles. Dynein can also oppose the activity of plus-end directed motors.

Conceptually, minus-end directed motors could directly antagonize plus-end directed motors to maintain spindle length. If the function of a minus-end directed motor was to simply antagonize the plus-end directed motors, then depletion of the minus-end directed motor should result in spindle elongation. Contrary to this hypothesis, when the function of the minus-end motor, dynein, is disrupted it results in a small spindle phenotype in *C. elegans* and budding yeast (Hamill et al., 2002; Hepperla et al., 2014). Dynein, a minus-end directed motor, has several functions in the mitotic spindle that could affect spindle length (Figure 1-7). In addition to antagonizing Eg5 activity by sliding antiparallel microtubules (Ferenz et al., 2009), dynein is also anchored to the cortex and provides an outward force on the spindle poles through interactions with the astral microtubules (Couwenbergs et al., 2007; Nguyen-Ngoc et al., 2007) and dynein also transports Eg5 to the spindle poles (Gable et al., 2012; Uteng et al., 2008).

## 1.7 *C. elegans* as a model for microtubule dynamics and spindle assembly

*C. elegans* is a small round worm that was established as a model organism in the 1960s (Brenner, 1974). Since then it has proven to be a useful research tool for many areas of biology and *C. elegans* are suited for use in genetics, cell biology, and high throughput analyses (Labbé and Roy, 2006). Many tools are available for forward or reverse genetics in *C. elegans* and the large single-celled embryo of *C. elegans* is especially useful for microscopy-based cell biology experiments.

The *C. elegans* genome was the first fully sequenced genome of a multicellular organism (The *C. elegans* Sequencing Consortium, 1998). Approximately 21,000 protein coding genes have been identified in the *C. elegans* genome and over 7,500 of these genes have clear human orthologs (Shaye and Greenwald, 2011). The conservation of protein coding genes between humans and *C. elegans* allows conserved pathways to be investigated in worms. The results from experiments performed in *C. elegans* can often lead to a better understanding of human health and disease states.

### 1.7.1 Stereotypical cell divisions in the *C. elegans* embryo

After meiosis is completed, the first mitotic cell division in *C. elegans* takes approximately fifteen minutes. The events of the first mitosis in *C. elegans* are highly reproducible both temporally and spatially, so perturbations such as mutations or RNAi

treatments that have even minor deviations from wild-type can be studied. Spindle assembly in *C. elegans* is dominated by centrosomal microtubule nucleation and provides an excellent system to understand how the centrosomes contribute to spindle assembly.

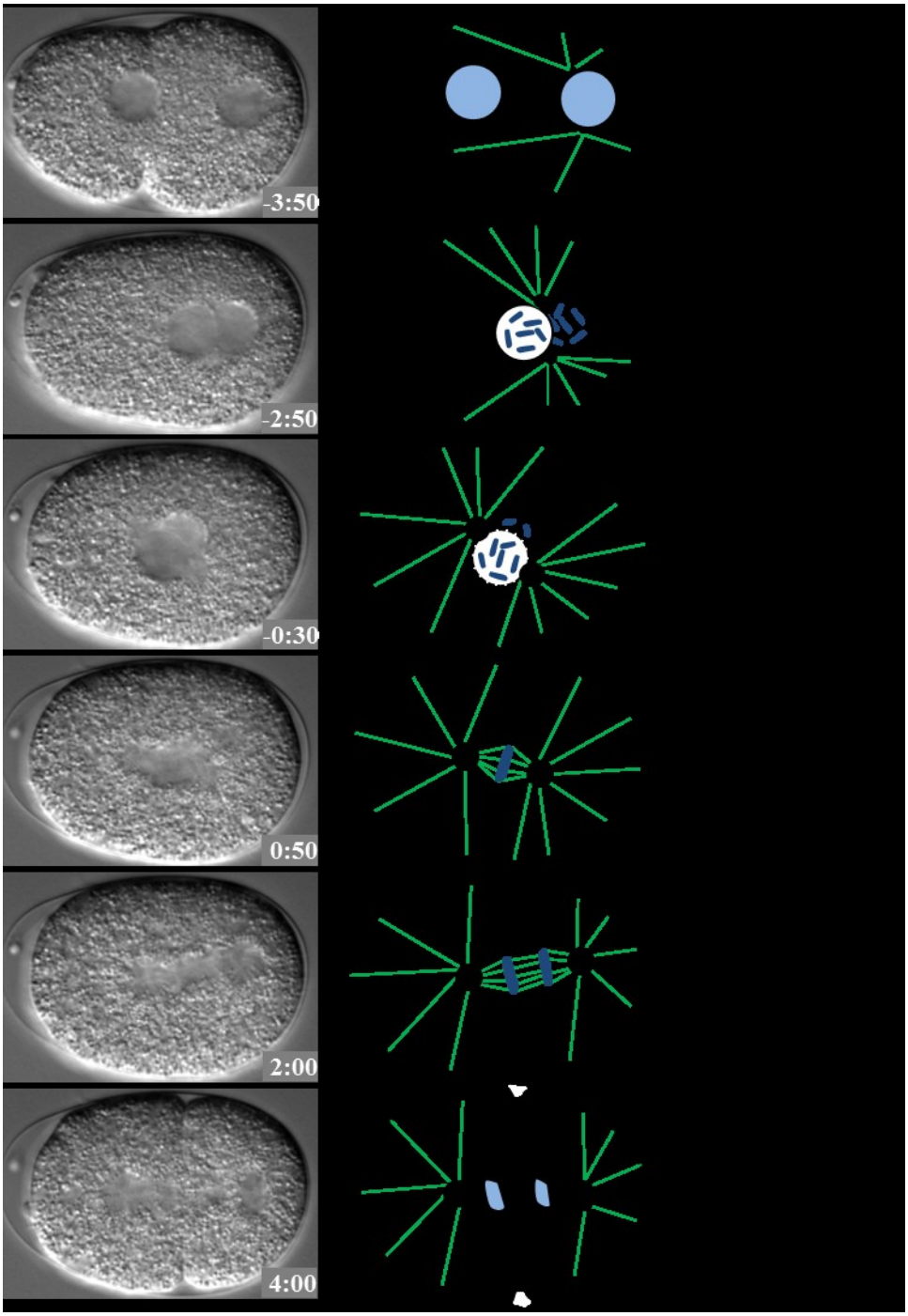


**Figure 1-8. The first mitosis in *C. elegans***
Time 0 is nuclear envelope breakdown (NEBD). Key steps in the first mitotic division of *C. elegans* are shown with DIC images and schematics.

The first mitotic division in *C. elegans* has been very well characterized (Figure 1-8; reviewed in Müller-Reichert et al., 2010). Briefly, after a fertilized oocyte completes meiosis the nuclear envelopes form and the maternal pronucleus migrates towards the paternal pronucleus at the posterior of the embryo. Centrioles are brought into the cytoplasm during fertilization and they begin to recruit maternal peri-centriolar material to form the centrosomes. Prophase begins when the chromosomes condense, which happens shortly before the pronuclei meet. After the pronuclei meet, they center and rotate to align the centrosomes along the long axis of the embryo. The nuclear envelope then breaks down and cytoplasmic proteins can penetrate the permeable nuclear envelope (Hayashi et al., 2012). After nuclear envelope breakdown, microtubules interact with the chromatin and the chromosomes congress between the centrosomes. The *C. elegans* chromosomes are holocentric (reviewed in Maddox et al., 2004), which means that kinetochores form along the entire length of the chromosomes. Once the chromosomes are aligned, the embryo proceeds into anaphase where the chromosomes are segregated by a mechanism involving force generators that pull on the astral microtubules to separate the centrosomes and chromosomes. Once the chromosomes are segregated, they begin to de-condense, the nuclear envelope reforms and the cytokinetic furrow ingresses. The first division in *C. elegans* is asymmetric with the anterior daughter cell being slightly larger than the posterior daughter (Rabilotta et al., 2012).

Many of the well characterized spindle assembly factors are present in *C. elegans* and have conserved roles in spindle assembly. For example, *C. elegans* embryos require Aurora A for centrosome maturation and spindle assembly (Ozlü et al., 2005; Schumacher et al., 1998) and RanGTP is required to bias microtubule growth towards the chromatin (Srayko et al., 2005). There are some key differences in *C. elegans* spindle assembly. Notably, the spindle assembly checkpoint functions differently in *C. elegans* embryos compared to most other eukaryotic systems used to study spindle assembly. In many animal cells, the spindle assembly checkpoint will cause an arrest in mitosis until the checkpoint is satisfied. However, *C. elegans* embryos will pause if chromosomes are not properly aligned, however this delay will only last a few minutes (Encalada et al., 2004). The cell will then enter anaphase and attempt to complete cytokinesis despite defects in spindle assembly or chromosome alignment. This can be an advantage to

working with *C. elegans* because if a protein is required early in mitosis for spindle assembly and also later in mitosis, then the later phenotypes can still be observed and characterized. Mitotic arrest in this example would preclude an analysis of anaphase and telophase.

While many factors are highly conserved between humans and *C. elegans*, some proteins are not. For example, the TPX2-like protein in *C. elegans* is missing the protein domain that is known to interact with RanGTP (Figure 1-9) so it has been proposed that the *C. elegans* TPXL-1 protein may only perform a subset of spindle assembly functions that TPX2 performs (Karsenti, 1995).

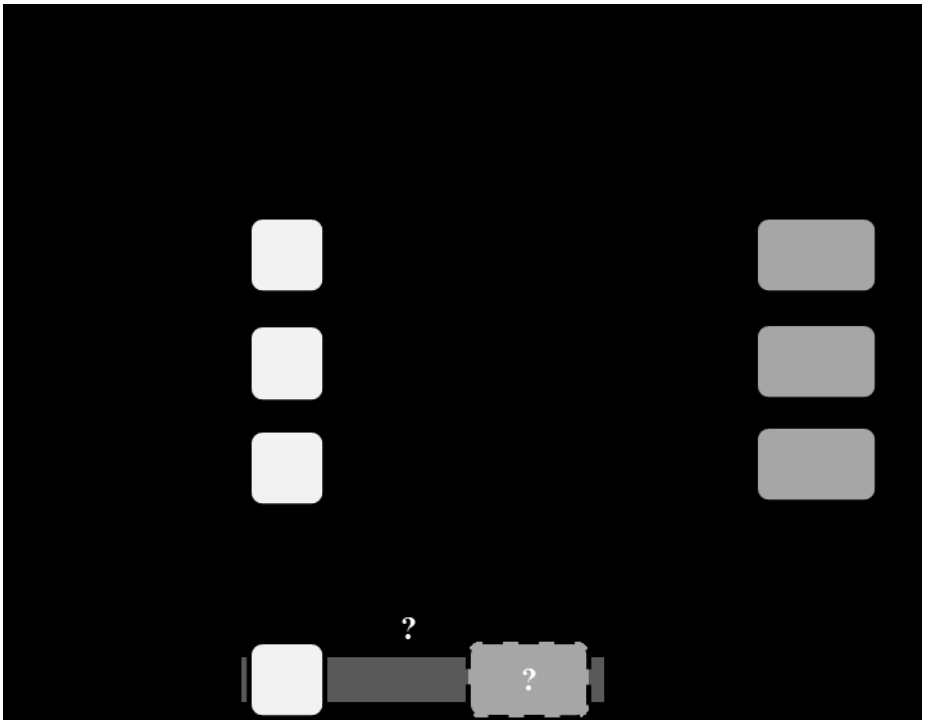


**Figure 1-9. TPX2-like proteins in various eukaryotes**
While TPX2-like proteins have roles in spindle assembly in many eukaryotes, the protein is not highly conserved. For example, the TPX2 protein is highly conserved in vertebrates and *A. thalania*, but the *C. elegans* and *D. melanogaster* protein share no sequence identity. Questions marks on the *C. elegans* protein indicate domains that have been proposed but have not been verified experimentally. This figure is a summary of information that was presented in the following publications: Brunet et al., 2004; Eckerdt et al., 2008; Goshima, 2011; Ozlü et al., 2005; and Vos et al., 2008.

### 1.7.2 Microtubules in post-embryonic tissues

Microtubules and the proper regulation of microtubule dynamics are critical during the development of eukaryotic organisms. This is especially apparent in multicellular organisms where different cell and tissue types modify the microtubule cytoskeleton for

specialized functions. *C. elegans* is also an excellent model to investigate post-embryonic roles of microtubules and microtubule dynamics.

The dynamic properties of microtubules in a specific cell type are variable at different times in development. For example, during development of the *C. elegans* egg laying apparatus the precursor cells have shorter microtubules with a slower growth rate and higher frequency of catastrophe than the differentiated cells (Lacroix et al., 2014). The difference in microtubule dynamics in these cells is due to activities of different microtubule-associated proteins. In precursor cells, depletion of the microtubule depolymerizing protein KLP-7 with RNAi did not affect microtubule dynamics, while in differentiated cells, *klp-7(RNAi)* decreased the levels of catastrophes (Lacroix et al., 2014). This suggests that the KLP-7 protein regulates microtubules in these differentiated cells but not in their precursor cells and therefore KLP-7 activity is regulated differently in different cells. Other proteins that affect microtubule dynamics could also play important roles during post-embryonic development.

### 1.8 *rsa-1* is a regulator of *C. elegans* spindle assembly

The *rsa-1* gene was initially identified in a large scale RNAi-based DIC microscopy screen that investigated 98% of the predicted genes in *C. elegans* for embryogenesis defects (Sonnichsen et al., 2005). In the early embryo, *rsa-1(RNAi)* was observed to have spindle elongation defects. *rsa-1(RNAi)* was embryonic lethal with a few escapers that either arrested in L1 or became sterile adults (Sonnichsen et al., 2005).

The role of *rsa-1* in the first mitotic division was further characterized by a systematic analysis of 40 genes that were proposed to affect microtubule dependent processes (Srayko et al., 2005). An analysis of microtubule dynamics in *rsa-1(RNAi)* embryos found that the microtubule growth rate was similar to wild-type but the number of microtubules observed growing from the centrosomes was approximately one quarter the level in wild-type embryos (Srayko et al., 2005). This result suggested that the spindle elongation defects observed by Sonnichsen et al. may be a consequence of the decrease in microtubule numbers in *rsa-1(RNAi)* embryos.

Further investigation revealed that the RSA-1 protein shares sequence similarity with the B'' family of PP2A regulatory subunits (Schlaitz et al., 2007). A B'' regulatory

subunit in the small flowering plant *Arabidopsis thalinana*, TONNEAU2/TON2, is required to organize acentrosomal microtubule arrays (Camilleri et al., 2002; Azimzadeh et al., 2008; Kirik et al., 2012) suggesting a potential conserved role for this protein family in regulating the microtubule cytoskeleton. It remains unknown if a human B'' regulatory subunit has a role in regulating microtubule dynamics or organization. In human cells, the PP2A core enzyme has been observed at the centrosome using immunofluorescence (Sontag et al., 1995) and the most similar human B'' regulatory subunit to RSA-1, G5PR, has been identified as a centrosomal protein in a proteomics assay (Jakobsen et al., 2011). Therefore it is plausible that G5PR could function to regulate the microtubule cytoskeleton in human cells, but currently there is no direct evidence to support this hypothesis.

RSA-1 was found to co-precipitate with the structural (PAA-1) and catalytic (LET-92) subunits of the *C. elegans* PP2A complex (Schlaitz et al., 2007) indicating that RSA-1 likely is a bona fide PP2A regulatory subunit. It was found that RSA-1 localizes to the centrosomes and is required for the PP2A catalytic subunit, LET-92, to be recruited to the centrosome (Schlaitz et al., 2007). To date, no substrates of the RSA-1/PP2A complex have been verified. Many proteins that affect microtubule dynamics and spindle assembly are found at the centrosomes during at least part of the cell cycle (Boxem et al., 2008; Kuhn et al., 2014) and could potentially be substrates of the RSA-1/PP2A complex.

Live imaging of *rsa-1(RNAi)* embryos with fluorescent markers indicated that there are two primary mitotic phenotypes in the first mitotic division: 1) a significant decrease in the levels of microtubules observed from the centrosomes 2) a collapse of the mitotic spindle (Schlaitz et al., 2007). In order to determine if the spindle collapse was the result of the decrease in microtubule number, the authors co-depleted the MCAK-like microtubule depolymerase, KLP-7. *klp-7(RNAi)* embryos display a significant increase in the levels of microtubules growing from the centrosome (Srayko et al., 2005). *rsa-1(RNAi);klp-7(RNAi)* embryos exhibited near wild-type levels of microtubules but the spindle collapse was still observed (Schlaitz et al., 2007). This suggests that the spindle collapse observed in *rsa-1(RNAi)* is not a consequence of a decrease in microtubule number.

A decrease in the overall number of centrosomal microtubules could be caused by several different mechanisms. For example, there could be a decrease in the level of microtubule nucleation, microtubules that nucleate could be unstable, or a combination of these mechanisms. Since the *rsa-1(RNAi);klp-7(RNAi)* co-depletion had a wild-type level of microtubule nucleation this suggests that the centrosomes are capable of nucleating microtubules and it is more likely that RSA-1 is required to promote microtubule stability. In *rsa-1(RNAi)* there was a significant increase in the levels of KLP-7 at the centrosome (Schlaitz et al., 2007). While an increase in KLP-7 microtubule depolymerase at the centrosome could explain why there are fewer microtubules in *rsa-1(lf)* embryos, it remains unknown how RSA-1 controls the recruitment of KLP-7 to the centrosome.

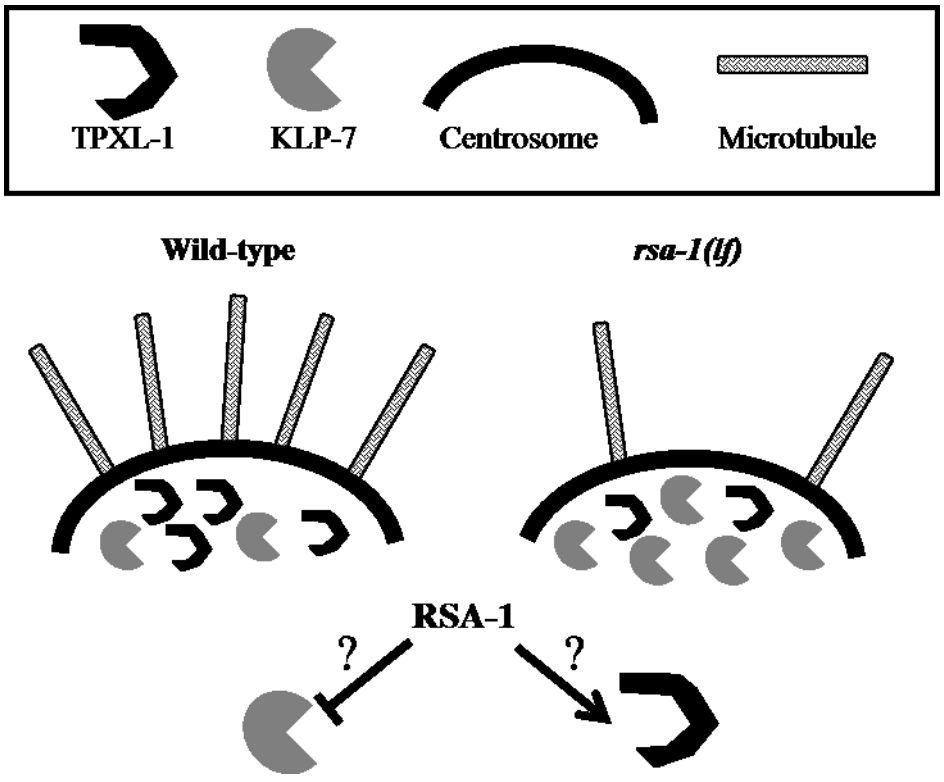


**Figure 1-10. Schematic of RSA-1 function at the centrosome**
At the centrosome, RSA-1 is known to promote levels of TPXL-1 while limiting levels of KLP-7. It is unknown how RSA-1 regulates the localization of these proteins to the centrosome and it may be direct or indirect.

Like in other organisms, the *C. elegans* TPX2-like protein, TPXL-1, is critical for maintaining spindle length. *tpxl-1(RNAi)* embryos exhibit a spindle collapse (Ozlü et al., 2005) similar to that observed in *rsa-1(RNAi)*. In *rsa-1(RNAi)* embryos there is a

significant decrease in the levels of TPXL-1::GFP at the centrosome (Schlaitz et al., 2007), and it has been proposed that this is the direct cause of the spindle collapse phenotype in *rsa-1(lf)* embryos. However, the mechanism of how RSA-1 affects centrosomal levels of TPXL-1 or why the decrease in centrosomal TPXL-1 causes a spindle collapse is unknown.

Taken together, the simultaneous increase in levels of KLP-7 and decrease in levels of TPXL-1 at the centrosome could explain the phenotypes observed in *rsa-1(RNAi)* early embryos. However, the mechanism that RSA-1 uses to limit KLP-7 and promote TPXL-1 centrosomal recruitment is not known. RSA-1/PP2A could dephosphorylate these proteins directly to affect their subcellular localization, or one or more intermediate effectors may be present in the pathway.

### 1.9 **The goals of this thesis**

The primary goal of this thesis was to elucidate the mechanism by which RSA-1 regulates spindle length and microtubule nucleation in *C. elegans* embryos. The observation that *rsa-1(lf)* embryos have decreased levels of TPXL-1 and increased levels of KLP-7 at the centrosome suggests that RSA-1 may directly regulate these proteins. I sought to determine if these proteins were direct substrates of the RSA-1/PP2A complex.

### 1.10 **Summary of this thesis**

Herein, I investigate how a decrease in the function of RSA-1 causes defects in *C. elegans* spindle assembly. The results in this thesis have been divided into two chapters, the first of which contains a detailed characterization of a specific missense allele of *rsa-1*. I determined that this amino acid substitution causes a decrease in RSA-1 function because the protein is unable to recruit the structural subunit of the PP2A holoenzyme to the centrosomes. In a genetic screen for suppressors of this mutation I was able to identify an interaction interface between the RSA-1 and PAA-1 proteins and I recovered extragenic suppressors that could reveal new components of the RSA-1 pathway. The second chapter of results presents experiments where I directly tested various hypotheses for why loss of *rsa-1* function results in the spindle-collapse phenotype in *C. elegans* embryos. Through this work, I uncovered a novel role for RSA-1 in regulating the subcellular location of Aurora A kinase. I also determined that the *C. elegans* TPX2-like

protein locates to the chromatin in an RSA-1, Aurora A, and RanGTP-dependent manner, which suggests that the *C. elegans* TPXL-1 protein may have a similar role in chromatin-mediated spindle assembly as the vertebrate TPX2 protein.

# 2 Materials and Methods

## 2.1 *Caenorhabditis elegans* nomenclature

When the *C. elegans* genome was cloned and sequenced every predicted gene was given a systematic name. For example, C25A1.9 is the ninth gene on the C25A1 cosmid. Characterized genes in *C. elegans* are given an italicized three or four letter name followed by a hyphen and a number. For example, *rsa-1* was named *regulator of spindle assembly-1* because it was the first gene identified with a role in this specific process. Proteins are written as the gene but in all capital letters and not italicized. For example, RSA-1 is the protein produced by the *rsa-1* gene.

Alleles of a gene are italicised and parenthesised after the gene name. They are given a unique identifier that designates the laboratory where the allele originated. For example, *or598* refers to the five-hundred ninety-eighth allele identified in Dr. Bruce Bowerman's lab in Eugene, Oregon. A plus sign is the designation for wild-type alleles. When dsRNA has been used to reduce the function of a gene, the term *RNAi* is used similarly to an allele designation. Italicized roman numerals indicate the chromosome a gene is located on. Autosomes are designated by the roman numbers I-V and X for the sex chromosome. Genotypes are written in numerical order (I-V, with X last) and mutations are described left to right as designated by the *C. elegans* genetic map. Semi-colons are used to separate chromosomes. Heterozygous genotypes are written with a slash separating the homologous chromosomes.

Transgenes are named with the laboratory allele designation, followed by *Ex* if it is extra-chromosomal or *Is* if it is integrated, and followed by a number. The genotype of the transgene is written in square brackets.

*C. elegans* strains are named by two or three capitalized letters followed by a number. The strain name indicates its origin, for example, MAS1 is the first worm strain that originated from Dr. Martin Srayko's laboratory.

## 2.2 *C. elegans* strains and maintenance

Unless otherwise indicated, all strains were maintained at 20 °C on nematode growth medium (NGM) seeded with an auxotrophic strain of *Escherichia coli,* OP50, as

previously described (Brenner, 1974). For all experiments, temperature-sensitive strains were shifted to the restrictive temperatures as L4 larvae unless otherwise indicated. Worm strains were generated in the Srayko lab or obtained from the *Caenorhabditis* Genetics Center, Bruce Bowerman, Tony Hyman, or Dave Pilgrim.

| Strain | Genotype |
|---|---|
| **CB4856** | Hawaiian genetic background |
| **EU1395** | *rsa-1(or598) I; ruIs32[unc-119(+), pie-1p::GFP::his-11] III; ddIs6[unc-119(+), pie-1p::GFP::tbg-1]* MEL, TS |
| **MAS7** | *klp-7(tm2143) III* MEL, TS |
| **MAS23** | *dpy-5(e61), rsa-1(or598) I* MEL, TS |
| **MAS24** | *rsa-1(or598) I; unc-5(e53) IV; dpy-11(e249) V; lon-2(e670) X* MEL, TS |
| **MAS37** | *unc-119(ed3) III; abcIs3[unc-119(+), pie-1p::ebp-2::GFP]* |
| **MAS39** | *rsa-1(or598) I,* MEL, TS |
| **MAS40** | *rsa-1(or598) I; bli-2(e768) II; unc-32(e189) III* MEL, TS |
| **MAS53** | *rsa-1(or598) I; paa-1(abc3) III* |
| **MAS59** | *rsa-1(or598, abc6) I* |
| **MAS61** | *rsa-1(or598) I; paa-1(abc8) III* |
| **MAS65** | *rsa-1(or598) I; paa-1(abc12) III* |
| **MAS67** | *rsa-1(or598) I; paa-1(abc14) III* |
| **MAS75** | *rsa-1(or598, abc20) I* |
| **MAS76** | *rsa-1(or598, abc21) I* |
| **MAS78** | *rsa-1(or598) I; paa-1(abc23) III* |
| **MAS91** | *itIs37[unc-119(+), pie-1p::mCherry::his-58] IV; ruIs57[unc-119(+), pie-1p::GFP::tbb-2]* |
| **MAS97** | *rsa-1(or598) I* in Hawaiian genetic background MEL, TS |
| **MAS99** | *rsa-1(or598) I; dpy-1(e1) paa-1(abc2) unc-32(e189) III* |
| **MAS101** | *dpy-1(e1) paa-1(abc2) unc-32(e189) III* |
| **MAS104** | *paa-1(abc13) III* |
| **MAS105** | *paa-1(abc5) III* |
| **MAS113** | *rsa-1(or598)I; abcIs3[unc-119(+), pie-1p::ebp-2::GFP]* MEL, TS |
| **MAS118** | *paa-1(abc14) III* |
| **MAS136** | *rsa-1(or598)I; itIs37[unc-119(+), pie-1p::mCherry::his-58]IV; ruIs57[unc-119(+), pie-1p::GFP::tubulin]* MEL, TS |
| **MAS139** | *paa-1(abc8) III* |
| **MAS140** | *rsa-1(or598, abc27) I* |
| **MAS146** | *rsa-1(or598, abc24) I* |
| **MAS153** | *rsa-1(or598) I; paa-1(abc11) III* |
| **MAS154** | *rsa-1(or598) I; paa-1(abc26) III* |
| **MAS158** | *rsa-1(or598) I; paa-1(abc5) III* |

**Table 2-1. *C. elegans* strains and genotypes.**
Worm strains used in this thesis. If a strain was outcrossed, only the final strain is listed here. Strains that are maternal effect lethal (MEL) or temperature sensitive (TS) are indicated.

| Strain | Genotype |
|---|---|
| **MAS159** | *rsa-1(or598, abc29) I* |
| **MAS163** | *rsa-1(or598) I; paa-1(abc13) III* |
| **MAS164** | *rsa-1(or598) I; paa-1(abc9) III* |
| **MAS165** | *rsa-1(or598) I; paa-1(abc15) III* |
| **MAS171** | *rsa-1(or598) I; paa-1(abc2) III* |
| **MAS172** | *rsa-1(or598) I; paa-1(abc7) III* |
| **MAS173** | *rsa-1(or598) I; paa-1(abc28) III* |
| **MAS175** | *rsa-1(or598) I; paa-1(abc10) III* |
| **MAS176** | *paa-1(abc2) III* |
| **MAS228** | *rsa-1(or598) I; klp-7(tm2143) III* MEL, TS |
| **MAS229** | *rsa-1(or598) I;ddIs12[unc-119(+), pie-1p::tpxl-1::GFP]* MEL, TS |
| **MAS230** | *rsa-1(or598)I;ddIs206[unc-119(+), pie-1p::tpxl-1(RNAi resistant,F15D,F18D)::GFP]* |
| **MAS231** | *rsa-1(or598), abc17* |
| **MAS234** | *rsa-1(or598) I; abc19* |
| **MAS235** | *rsa-1(or598) I; abc25* |
| **MAS241** | *ddIs12[unc-119(+), pie-1p::tpxl-1::GFP]; itIs37[unc-119(+), pie-1p::mCherry::his-58] IV* |
| **MAS242** | *rsa-1(or598)I; ddIs12[unc-119(+), pie-1p::tpxl-1::GFP];itIs37[unc-119(+), pie-1p::mCherry::his-58] IV* MEL, TS |
| **MAS244** | *bsIs20[mCherry::tbb-2]; ddIs12[unc-119(+), pie-1p::tpxl-1::GFP]* |
| **MT464** | *unc-5(e53) IV; dpy-11(e224) V; lon-2(e678) X.* |
| **MT465** | *dpy-5(e61) I; bli-2(e768) II; unc-32(e189) III.* |
| **N2** | Wild-type. |
| **OD142** | *unc-119(ed3) III; ltIs78 [(pKO5) pie-1::GFP::TEV::Stag::air-1 spliced coding + unc-119(+)]* |
| **TH32** | *ruIs32[unc-119(+), pie-1p::GFP::his-11] III; ddIs6[unc-119(+), pie-1p::GFP::tbg-1]* |
| **TH53** | *unc-119(ed3) III; ddIs12[unc-119(+), pie-1p::tpxl-1::GFP]* |
| **TH92** | *ddIs[unc-119(+), pie-1p::tpxl-1(RNAi resistant)::GFP] I; unc-119(ed3) III* |
| **TH125** | *unc-13(e1091) rsa-1(dd13)/hT2g I* MEL |
| **TH311** | *unc-119(ed3) III; ddIs206[unc-119(+), pie-1p::tpxl-1(RNAi resistant,F15D,F18D)::GFP]* |

**Table 2.1 continued.**
Worm strains used in this thesis. If a strain was outcrossed, only the final strain is listed here. Strains that are maternal effect lethal (MEL) or temperature sensitive (TS) are indicated.

### 2.3 **Genomic DNA extraction for PCR**

1 - 20 gravid hermaphrodites were picked into 5 – 30 µL worm lysis buffer (50 mM KCl, 10 mM Tris-HCl pH 8.3, 2.5 mM $MgCl_2$, 0.45% NP-40/Igepal-CA-630, 0.45% Tween-20, 0.01% gelatin) with approximately 600 µg/mL of Proteinase K in a PCR tube (200 µL). The worms were lysed in a thermocycler running the following program: 65 °C

for 1 hour, 95 °C for 15 minutes. 5 µL of this gDNA was then used as the template for PCR or frozen at -20 °C. Frozen gDNA samples were thawed on ice immediately before use.

### 2.4 **Polymerase chain reactions**

All PCR reactions were performed with NEB Taq Polymerase and NEB Taq Pol buffer supplied with $MgCl_2$ from the manufacturer. Oligonucleotides were ordered from Integrated DNA Technologies and 100 mM stocks were made in TE pH 7.5 (10 mM Tris, 1 mM EDTA). For working stocks, primers were diluted to 10 mM with $ddH_2O$. Specific details about the primer sequences and PCR conditions are outlined in Appendix A.

### 2.5 **Sanger sequencing of DNA**

All sequencing primers used are listed in Appendix A. Sequencing reactions were performed according to the standard operating procedure of the University of Alberta Molecular Biology Services Unit. Reactions were set up as follows: 2 µL BigDye Terminator v3.1 premix, 6 µL 2.5x buffer (5 mM $MgCl_2$, 200 mM Tris pH 9.0), 1 µL 10 mM primer, 50-200 ng of PCR template or 100-400 ng of plasmid template, and brought up to volume with $ddH_2O$. The reaction was placed in a thermocycler for 25 cycles of 96 °C for 30 seconds, 50 °C for 15 seconds, and 60 °C for 2 minutes. Ethanol precipitation in a 1.5 mL Eppendorf tube was used to clean up the sequencing samples. The sample was added to 2 µL of NaOAc/EDTA (1.5 M sodium acetate, 250 mM EDTA) and 80 µL of cold 95% ethanol was then added. The sample was left for 15 minutes at 4 °C. The sample was centrifuged at 4 °C for 15 minutes and the supernatant was removed. 500 µL of cold 70% ethanol was added and the sample was centrifuged at 4 °C for 5 minutes. The supernatant was removed and the sample was air dried. The pellet was then delivered to MBSU for electrophoresis and sequence analysis on the 3730 Genetic Analyzer (Applied Biosystems) by the MBSU staff. Sequencing results were provided as electropherograms and text files. Electropherograms were examined using the Sequencing Scanner 2.0 (Applied Biosystems) and text files were analyzed using A Plasmid Editor 2.0 (Wayne Davis, University of Utah). Multiple sequences were aligned using ClustalW 2.0 (EMBL-EBI).

## 2.6 **Genetic screen for suppressors of *rsa-1(or598)***

### 2.6.1 Chemical mutagenesis

Three independent rounds of chemical mutagenesis were performed as follows. L4 hermaphrodites homozygous for *rsa-1(or598)* were washed with M9 (42 mM $Na_2HPO_4$, 22 mM $KH_2PO_4$, 86 mM NaCl, 1 mM $MgSO_4$) into a 15 mL falcon tube. The volume was brought to 4 mL and 20 µL of EMS was added following appropriate safety precautions. The worms were incubated with gentle agitation for 4 hours at room temperature. The worms were then rinsed five times with 10 mL of M9. Mutagenized hermaphrodites were placed onto 10 cm NGM plates (~25 worms per plate) and incubated at 20 °C.

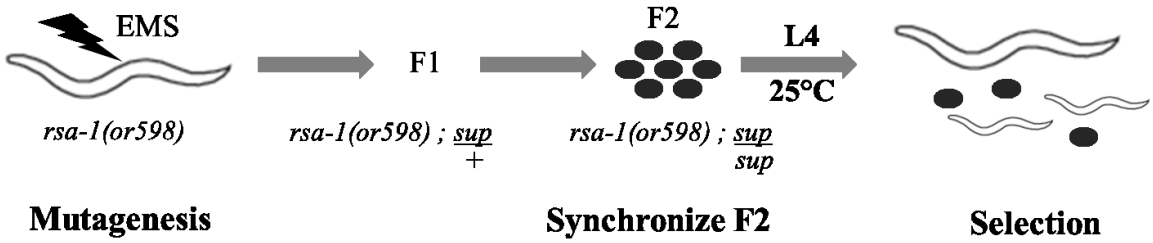


**Figure 2-1. Genetic screen for suppressors of *rsa-1(or598)***
Homozygous *rsa-1(or598)* worms were mutagenized with EMS. Gravid F1 hermaphrodites were treated with alkaline hypochlorite to isolate the F2 embryos. These worms were synchronized and when they were L4 they were shifted to the semi-restrictive temperature of 25 °C to select for suppressors of *rsa-1(or598)*.

### 2.6.2 Isolation of suppressors of *rsa-1(or598)*

To determine the number of haploid genomes screened, the number of F1 hermaphrodites was estimated. When the F1 generation was gravid, the hermaphrodites were split into pools and each was treated with alkaline hypochlorite solution to isolate the F2 embryos. These embryos were incubated in M9 solution with gentle agitation overnight to synchronize the population as L1 larvae and were then plated onto NGM plates at 20 °C. When the synchronized F2 generation was L4, the plates were shifted to the restrictive temperature of 25 °C. At this temperature the *rsa-1(or598)* mutant has a hatching rate of 3.1% (± 2.0%). Any plate where the F3 were observed to have a higher hatching rate potentially contains a suppressor mutation. A single hermaphrodite from any pool with a hatching rate that was higher than 5% was isolated and was maintained at 25 °C. Strains were deemed a true suppressor if they were able to be propagated at 25 °C

and each was then given an allele designation. An overview on how suppressors were isolated is depicted in Figure 2-1.

### 2.6.3 Characterization of *ras-1(or598)* suppressors

The hatching rate of each suppressor allele was quantified at 26 °C. Seven L4 larval hermaphrodites were grown individually on NGM plates at 26 °C. After 24 hours the hermaphrodites were moved to a new plate and after an additional 24 hours the hermaphrodites were removed from the second plate. The hatching rate was determined by the number of larvae that hatched, divided by the total number of eggs laid.

To determine the genetic behaviour of each suppressor, hermaphrodites were mated back to the un-mutagenized *rsa-1(or598)* strain. The F1 from this cross were shifted to 26 °C as L4 and the hatching rates were determined. These hermaphrodites were homozygous for *rsa-1(or598)* but heterozygous for the suppressor allele. A suppressor is dominant if it can suppress the *rsa-1(or598)* mutation as a heterozygote and recessive if it cannot. Suppressors were not organized into complementation groups because almost all suppressors were determined to be dominant.

To reduce the number of background mutations from the suppressor strains, they were backcrossed to the *rsa-1(or598)* strain and homozygotes from the F2 were isolated. Several suppressors had very high hatching rates (>90%) and were not outcrossed because any background mutations presumably did not affect the viability of the strain.

### 2.6.4 Genetic mapping of suppressors

Linkage analysis was performed with six phenotypic markers (Figure 2-2). Each mapping strain was mated with *rsa-1(or598)* males to generate males that are homozygous for *rsa-1(or598)* but heterozygous for the visible markers. These males were then mated to a non-outcrossed suppressor strain. Alternatively, males homozygous for the suppressor were mated directly with the mapping strains. Hermaphrodites from the F1 generation were singled onto a new plate to prevent mating with male siblings. Worms from the F2 that were homozygous for the visible markers were shifted to 26 °C as L4 larvae. As a control, phenotypically wild-type hermaphrodites were also shifted to verify the genetic behavior of the suppressor. After 48 hours these plates were screened for the presence/absence of viable progeny. Plates that did not have hatched eggs were scored as

not having the suppressor allele. This approach determined if the suppressor allele segregated independently from the visible marker. A $\chi^2$ test was used to determine the likelihood that deviations in the expected genetic segregation frequencies were due to chance alone. Decisions were made at 95% confidence, whereby $\chi^2$ value greater than 3.84 indicated that the suppressor did not segregate independently from the visible marker and was likely on the same chromosome.

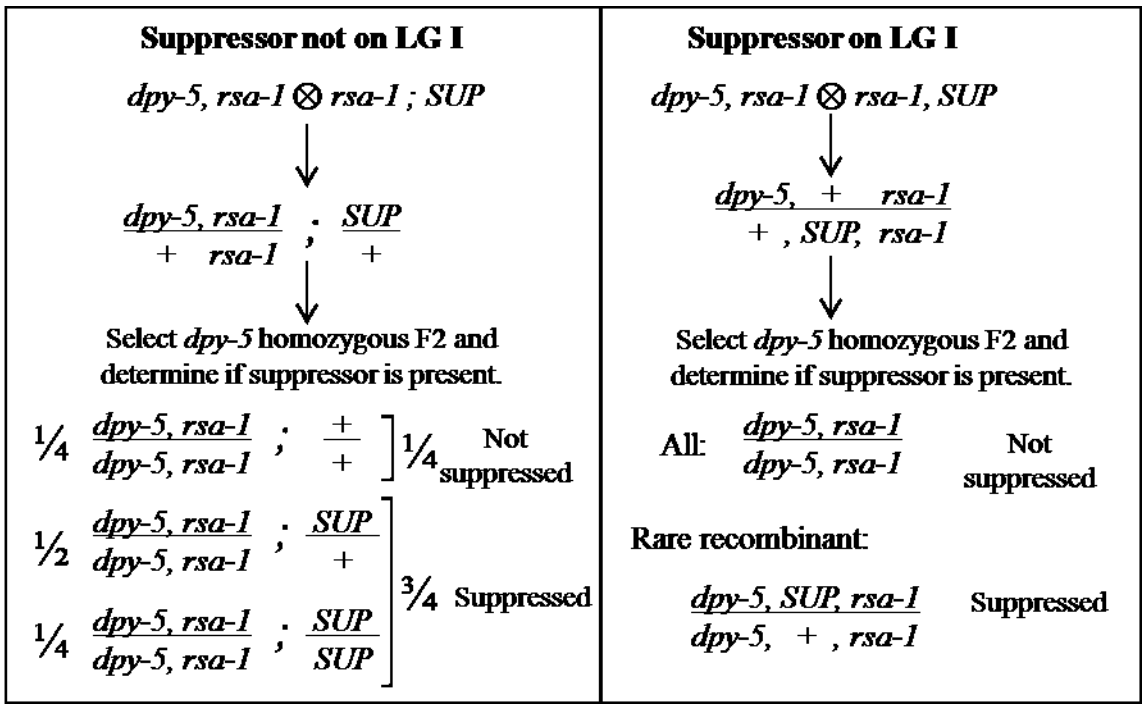


**Figure 2-2. Genetic mapping of a dominant suppressor with LG1.**
A strain containing the suppressor is mated with a hermaphrodite homozygous for both *rsa-1(or598)* and a recessive morphological marker *dpy-5(e61).* The F1 generation is allowed to self-fertilize and Dpy F2 progeny are screened to determine if the suppressor allele is present. If the suppressor is unlinked to the marker then it will show classical Mendelian inheritance of a dominant gene. If the suppressor is linked to the marker then most Dpy progeny will not be suppressed but rare recombinants may be recovered that are suppressed.

### 2.6.5 Snip-SNP mapping of LGIII

A wild isolate of *C. elegans* from Hawaii (H) was found to contain a high density of single nucleotide polymorphisms (SNPS) (Wicks, et al., 2001). Similar to mutations that cause visible morphological phenotypes, these SNPs can be used in mapping experiments. Genetic variations between the Hawaiian and Bristol strain that affect restriction enzyme cut sites were accessed from www.wormbase.org. Fourteen SNPs were chosen that spanned chromosome III and are summarized in Table 2-2.

The *rsa-1(or598)* allele was introduced into the Hawaiian genetic background by back-crossing it with CB4856 six times. This strain was named MAS97 and was confirmed to be homozygous for all Hawaiian snip-SNPs used for the analysis. The original strain used for the genetic screen, MAS39, was homozygous for the Bristol snip-SNPs.

| SNP Name | Genetic Position | Genomic Position |
|---|---|---|
| **pkP3055** | III: -14.86 | III:2216771 |
| **pkP3094** | III: -8.89 | III:2892594 |
| **dbP8** | III: -7.35 | III:3202340 |
| **pkP3046** | III: -5.33 | III:3591549 |
| **pkP3096** | III: -4.12 | III:3923462 |
| **snp_B0284[1]** | III: -3.18 | III:4388630 |
| **pkP3047** | III: -1.71 | III:5431295 |
| **pkP3099** | III: -1.47 | III:5625493 |
| **snp_C05D11[1]** | III: -1.29 | III:6404569 |
| **pkP3101** | III: -0.91 | III:6872547 |
| **pkP3102** | III: -0.85 | III:6980484 |
| **pkP3071** | III: 4.81 | III:10714089 |
| **pkP3074** | III: 11.75 | III:11678556 |
| **pkP3075** | III: 16.32 | III:12302078 |

**Table 2-2. Genetic location of SNPs for Snip-SNP mapping of LG3**

#### *2.6.5.1 Generation of recombinants for SNP mapping*

For SNP mapping, recombination events between the suppressor and visible markers were detected. Briefly, the suppressor was linked to *unc-32* and/or *dpy-1.* These strains were then mated to a Hawaiian strain. Wild-type F2 were screen for suppression of *rsa-1(or598)*. Wild-type non-suppressed hermaphrodites were analyzed to determine if they had a recombinant or parental genotype. Recombinants would give rise to Unc or Dpy progeny. Recombinants #1-8 were Unc-non-suppressed and #9-24 were Dpy-non-suppressed. Genomic DNA from a population of each recombinant was then isolated and analyzed by PCR and restriction digest.

#### *2.6.5.2 Determination of SNP identity from recombinants*

All snip-SNPs were determined by PCR and restriction enzyme digests. SNP PCR reactions were 15 µL dd$H_20$, 2.5 µL 10x Taq buffer, 1.25 µL of each 10 mM primer, 1 µL of 10 mM dNTPs, 1µL Taq, and 3 µL of gDNA as template. All snip-SNPs used the same PCR program as follows: 95 °C for 2 minutes and 30 cycles of 95 °C for 30 seconds, 57 °C for 30 seconds, and 72 °C for 1 minute. Restriction enzymes were used

according to manufacturer's instructions. Agarose gel electrophoresis with ethidium bromide was used to visualize the RFLPs. A sample SNP mapping gel is shown in Figure 2-3.

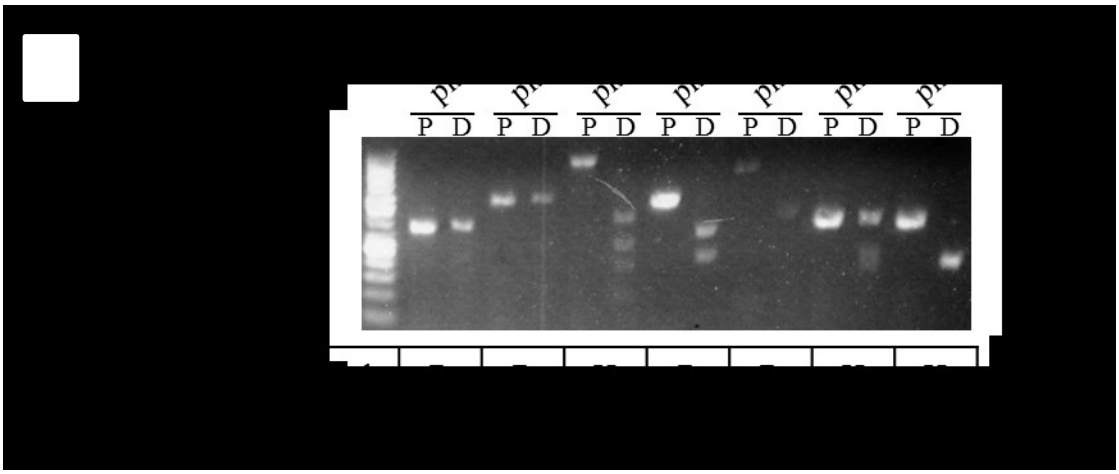


**Figure 2-3. Snip-SNP analysis of five unc-non suppressed recombinants**
A) A representative agarose gel from Snip-SNP mapping is shown. gDNA from an Unc, Non-suppressed recombinant was analyzed using PCR (P) and restriction enzyme digestion (D). The asterisk indicates an inconclusive result on this gel.

## 2.7 **Yeast two hybrid analysis**

Physical interactions between two proteins of interest can be detected by fusing one protein to a DNA binding domain and the other to a transcription activator domain. If the proteins of interest interact it will result in the transcription of a downstream reporter gene.

### 2.7.1 *Saccharomyces cerevisiae*

The yeast strain used was L40 (MATa trp1 leu2 his3 LYS2::lexA-HIS3 URA3::lexA-LacZ). Yeast were maintained on YPD (0.5% yeast extract, 1% peptone, 1% dextrose, 2% agar). For analysis, yeast were grown on synthetic minimal medium that was prepared as follows for a total volume of 250 mL: 5 g agar (omitted for liquid cultures), 1.68 g yeast nutrient base (Bio101 Systems, 4027-012), 1.25 g ammonium sulphate, $H_2O$ was added up to 200 mL and the pH was brought to 5.8 with sodium hydroxide. This was autoclaved and then 12.5 mL of 40% dextrose, 25 mL of essential amino acid mix (300 mg/L L-isoleusine, 1.5 g/L L-alanine, 200 mg/L L-arginine, 300 mg/L L-lysine, 200 mg/L L-methionine, 500 mg/L L-phenylalanine, 2 g/L L-threonine, 300 mg/L L-tyrosine), and 6.25 mL 800 mg/L adenine, 6.25 mL 800 mg/L uracil. Depending on the

drop-out media being made, the following were also added: 6.25 mL 800 mg/L L-tryptophan, 6.25 mL 4 g/L L-leucine, and/or 6.25 mL 800 mg/L L-histidine. Agar plates were stored at 4 °C and liquid media was stored at room temperature. Drop-out media is abbreviated to communicate which amino acids are lacking in the media. For example, "-trp-leu" is yeast minimal media lacking tryptophan and leucine.

### 2.7.2 Construction of yeast two hybrid vectors

The cDNA for *paa-1*, *let-92*, and *rsa-1* were obtained from Open BioSystems and sequenced to verify they were wild-type. The cDNA were first TA cloned using the pGemT system (as per manufacturer's instructions) using primers listed in Appendix A. All cloning primers were designed such that the gene would be in frame with the N-terminal fusions of the yeast expression vectors. Traditional cloning was used to sub-clone the cDNA from pGemT into the yeast vectors. *paa-1* was sub-cloned in the pAct2.2 vector (Addgene), *let-92* was sub-cloned in the pLexA vector (Addgene), and *rsa-1* was sub-cloned into both pLexA and pAct2.2. The pLexA::RSA-1, pLexA::LET-92, and pLexA::PAA-1 constructs were cloned by J. Heinrichs.

### 2.7.3 PCR based mutagenesis

PCR based mutagenesis was used to create cDNA that contained the same lesions as the mutants identified in the *rsa-1(or598)* suppressor screen. PCR based mutagenesis was performed on the cDNA prior to being sub-cloned into the yeast expression vectors to minimize the chance of other errors being introduced into the yeast plasmid backbone. This approach was used to generate the *rsa-1(or598)* D319G amino acid substitution, the *rsa-1(abc6)* G319S intragenic suppressor lesion, and the *paa-1(abc8)* V106I amino acid substitution.

PCR-based mutagenesis uses overlapping forward and reverse primers that contain the desired nucleotide substitution. The primers are 42 nucleotides long to allow them to anneal to the template even with the mismatch from the mutation. Pfu was used as the DNA polymerase for this application because it has proof-reading ability. The extension step of the PCR reaction is 10 minutes long to allow the entire plasmid to be synthesized in the reaction. The primers were phosphorylated so that the PCR product would be able to be circularized by Taq ligase. In this reaction, the newly synthesized DNA is not

methylated. DpnI was added to specifically degrade the methylated template so that only the plasmid synthesized by the PCR reaction was transformed into *E. coli*.

The protocol is as follows: The reaction was hot-started with 17 µL PT1.1x Master Mix (500 mM KCl, 15 mM $MgCl_2$, 100 mM Tris-HCl pH8, 0.1% BSA), 1 µL 10 mM NAD, 0.5 µL each phosphorylated primer (See Appendix A for complete list of primers), 0.5 µL DMSO, 0.3 µL Taq ligase, 10 ng of template. Then 1 µL of Pfu was added and the PCR conditions were as follows: 95 °C x 2 min, (95 °C x 1 min, 55 °C x 1 min, 65 °C x 10 min) x30 cycles, and 65 °C x 7 min. 1 µL of DpnI was added and incubated for 5 hours at 37 °C prior to transformation into DH5α. The cDNA was fully sequenced to verify that no other mutations were introduced and then the constructs were sub-cloned into the yeast expression vectors using the same approach described in section 2.7.2.

### 2.7.4 Yeast transformation

Plasmid DNA for yeast transformations was isolated from *E. coli* (DH5α) with a CTAB precipitation. Briefly, a 125 mL culture of DH5α with the appropriate plasmid was grown overnight. The bacteria were spun down in a 50 mL falcon tube and the supernatant was discarded. The pellet was resuspended in 1.25 mL of GTE (50 mM glucose, 25 mM Tris pH 8, 10 mM EDTA) and 2 mL of 0.2 M NaOH/1% SDS was added and mixed gently and left at room temperature for 5 minutes. 1.85 mL of KAc (3 M potassium acetate, 2 M acetic acid) was added and mixed gently. The tube was chilled in an ice water bath for 5 minutes and then centrifuged at 4 °C for 10 minutes. The supernatant was transferred to a new tube, 500 µL of 5% CTAB was added, and the tube was centrifuged for 10 minutes at 4 °C. The supernatant was discarded and 4 mL of $NH_4Ac$/EDTA (1 M ammonium acetate, 10 mM EDTA) added to the pellet. Then 10 mL of cold 95% ethanol was added and centrifuged at 4 °C for 10 minutes. The pellet was then washed with 5 mL of 70% ethanol and the pellet allowed to air dry at room temperature. The pellet was suspended in 500 µL of TE pH 7.5 and the DNA concentration was determined using a spectrophotometer (NanoVue).

Yeast were grown in liquid YPD for 48 hours in a shaking incubator at 30 °C. 1 mL of the culture was removed, centrifuged, and most of the supernatant was removed. 100 µg of carrier DNA (salmon sperm DNA, Sigma) and 5 µg of each plasmid was added. The sample was vortexed until no yeast pellet remained. 500 µL of PEG/LiAc/TE (40%

polyethylene glycol, 100 mM lithium acetate pH 7-7.4, 10 mM Tris pH 7.5, 10 mM EDTA) was added and the tube was gently mixed and left at room temperature overnight. The sample was spun down, the supernatant removed, and the yeast were plated on the appropriate drop-out media to select for transformants. Plates were incubated for at least 48 hours at 30 °C and then stored at 4 °C. A negative control with no plasmid DNA added was performed in parallel to all transformations to ensure yeast were unable to grow on drop-out media without plasmid DNA.

#### 2.7.5 Detecting protein interactions

The reporter gene for this analysis was HIS3, which allows for growth of an otherwise auxotrophic strain on media lacking histidine when the LexA DNA binding domain and the Act2.2 activation domain are in close proximity to each other. Yeast were transformed with both pLexA and pAct2.2 fusion constructs and TRP1 and LEU2 were used as positive selection markers. To ensure that the yeast retained the plasmids, they were maintained under selection on SD-trp-leu media. The positive control for this assay was pLexA::RAS and pAct2.2::RAF (Addgene) which have previously been shown to have a strong protein interaction. Liquid cultures of yeast were incubated in a shaking incubator at 30 °C in SD-trp-leu media for 48-60 hours. Serial dilutions (1, 0.1, 0.01, and 0.001) of the yeast were plated on SD-trp-leu and SD-trp-leu-his agar plates and incubated at 20 °C, 25 °C, and 30 °C. After two to four days of growth a photo was taken.

### 2.8 **RNA interference by feeding**

The *E. coli* strain HT115(DE3) and L4440 vector (Addgene) were used for all RNAi feeding experiments. HT115 contains and IPTG-inducible T7 polymerase and the L4440 vector has T7 promoters flanking the multiple cloning site. This *E. coli* is capable of synthesizing dsRNA from any DNA that is inserted at this site. When *C. elegans* eat *E. coli* that contain dsRNA, it invokes the *C. elegans* RNAi machinery and provides an efficient and specific knockdown of any complementary transcripts in the worm. RNAi bacterial clones with the appropriate insert in L4440 were obtained from an RNAi library (Kamath et al., 2003) or cloned into L4440 if they were absent from the library. See Appendix A for details on all cloning primers. The L4440 vector without an insert in the multiple cloning site was used at the negative control for all RNAi experiments.

HT115(DE3) *E. coli* with the appropriate RNAi vector was used to inoculate 5 mL of LB (1 mg/mL granulated tryptone, 0.5 mg/mL yeast extract, 0.5 mg/mL NaCl) with 50 mg/mL of ampicillin. RNAi plates (NGM, 1 mM IPTG, and 25 mg/mL carbenicillin) were seeded with overnight cultures and left at room temperature overnight to express double-stranded RNA. RNAi plates were used immediately or stored at 4 °C for up to one week. To reduce the risk of contaminating the RNAi plate with OP50 bacteria, L4 hermaphrodites were placed on an unseeded RNAi plate for 30 minutes to 1 hour prior to being put on the seeded RNAi plate. Hermaphrodites were incubated on the RNAi plates for 10 - 28 hours.

Effective RNAi knockdown was confirmed using one or more of the following methods: 1) embryonic lethality 2) microscopy to verify the appropriate loss of function phenotype, 3) a western blot to verify that the protein levels decreased with the RNAi treatment, or 4) loss of fluorescence of a GFP-tagged version of the protein after RNAi treatment.

### 2.9 **Determining antibody specificity**

The rabbit-α-PAA-1 (C-terminus, amino acids 288–590) and rabbit-α-TPXL-1 (full length) antibodies were generated by K. Cheung with the University of Alberta animal facility. The PAA-1 antibody was purified by K. Cheung and the TPXL-1 antibody was purified by T. Denghu. To verify these antibodies were specific to their intended targets, immunostaining and western blot analysis was performed on embryos that were treated with RNAi against the target (Figure 2-4). In western blots, the antibodies recognized a single band of the appropriate size that was depleted after RNAi treatment. The staining patterns specific to each antibody were decreased after RNAi treatment. The antibodies were determined to be specific to their intended targets and were used in further analysis.

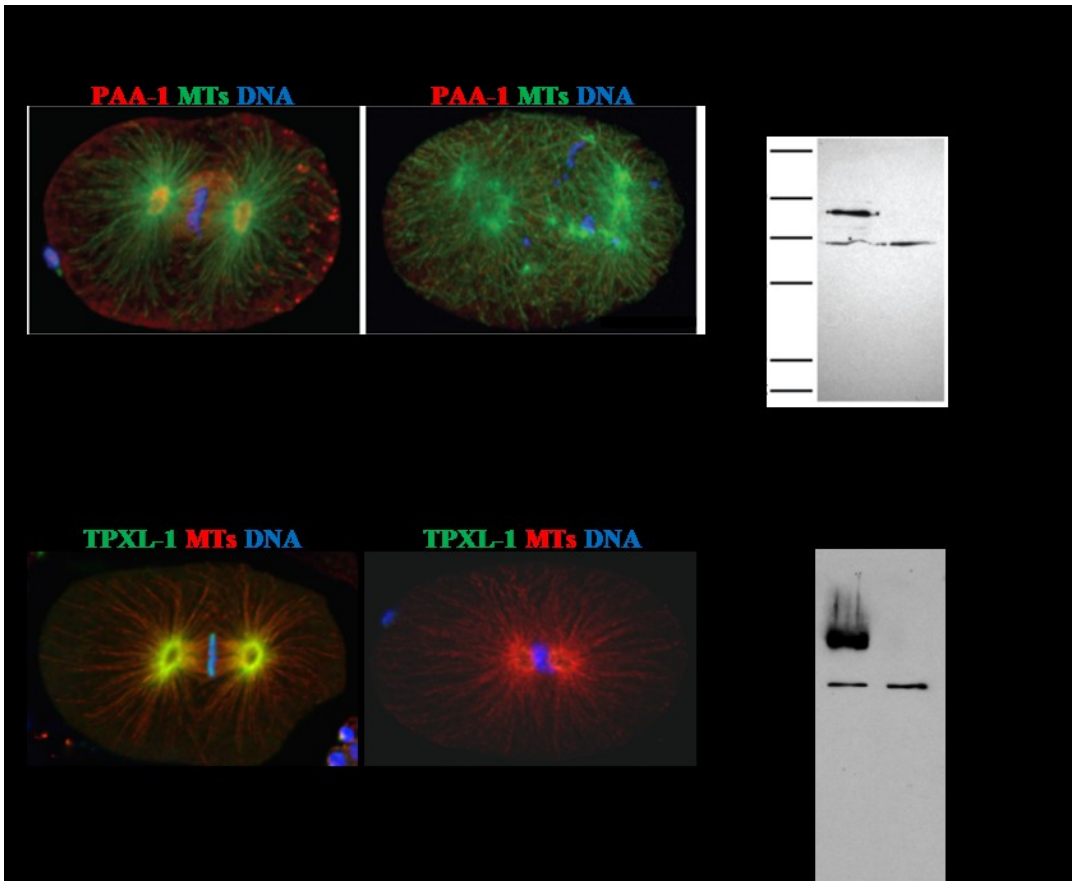


**Figure 2-4. Verifying specificity of α-PAA-1 and α-TPXL-1 antibodies.**
A) Immunostaining with α-PAA-1 in control and *paa-1(RNAi)* treated embryos. B) Western blot with α-PAA-1 in control and *paa-1(RNAi)* treated embryos. C) Immunostaining with α-TPXL-1 in control and *tpxl-1(RNAi)* treated embryos. D) Western blot with α-TPXL-1 in control and *tpxl-1(RNAi)* treated embryos.

### 2.10 Immunofluorescence staining of *C. elegans* embryos

25-35 young adult hermaphrodites were picked into 5 µL of dd$H_2O$ on a poly-lysine-coated slide (Sigma-Aldrich, P0425). An 18 $mm^2$ coverslip was placed on the worms. Gentle pressure was applied to the cover slip so that the embryos were expelled from the gonad and the slides were immediately frozen in liquid nitrogen. The cover slip was removed using a razor blade and the slides were fixed in -20 °C methanol (100%) for 15 minutes. Slides were washed in PBS for 5 min at room temperature or overnight at 4 °C. All incubations occurred in a humid chamber to prevent the slide from drying out. Slides were blocked with 100 µL 25% goat serum diluted in PBS for 30 min – 1 hour. 75 µL of primary antibody solution was used per slide (5% goat serum, 0.01% triton-X, mouse and/or rabbit primary antibody as per Table 2-3, and brought to volume with PBS). Slides

were washed twice for 10 minutes in PBS. 75 µL of secondary antibody solution was used per slide (5% goat serum, 0.01% triton-X, 0.5 µg of each appropriate secondary antibody (goat-anti-rabbit IgG or goat anti-mouse IgG conjugated to Alexa488, Alexa546, or Alexa647), and brought to volume with PBS). For experiments that used both rabbit anti-RSA-1 and rabbit anti-PAA-1 antibodies, fixed embryos were first treated with rabbit anti-PAA-1 which was converted to goat using 30 µl of 5 µg/mL of DyLight488 conjugated goat anti-rabbit FAB fragments (Jackson Laboratories). DAPI (5 µg/mL) was used to stain chromatin for 5 minutes. Slides were washed twice for 5 minutes in PBS. 4 µL of mounting media (90% glycerol, 0.5% p-phenylenediamine, 20 mM Tris-HCl pH 8.8) was added to the slide and mixed well. A 22 x 22 mm coverslip was placed on the slide and the edges sealed with nail polish. The slides were stored at -20 °C.

| Target | Source | Conc. (mg/mL) | IF[1] Dilution | WB[2] Dilution | Details |
|---|---|---|---|---|---|
| **α-Tubulin** | Mouse | 1 | 1/100 | 1/1000 | Sigma (DM1A) |
| **PAA-1** | Rabbit | 1.41 | 1/50 | 1/1000 | Lange *et al.*, 2013 |
| **RSA-1** | Rabbit | 2.42 | 1/100 | 1/1000-2000 | Schlaitz *et al.*, 2007 |
| **TPXL-1** | Rabbit | 3 | 1/100 | 1/1000 | Made by K. Cheung |
| **ZYG-9** | Rabbit | 0.97 | 1/100 | N/A | Srayko *et al.*, 2003 |
| **AIR-1** | Rabbit | 5 | 1/200 | N/A | Han, 2014 |
| **TBG-1** | Rabbit | 3.89 | 1/200 | N/A | O'Toole *et al.*, 2012 |

**Table 2-3 Primary antibodies used in this thesis**
[1] Immunofluorescence [2] Western blot

### 2.11 **Microtubule regrowth assay**

L4 hermaphrodites of the appropriate genotype were put at 26 °C overnight. The next day, 30 animals, now young adults, were dissected in 5 µL of $ddH_2O$ on a poly-lysine-coated glass microscope slide (Sigma-Aldrich, P0425). An 18 x 18 mm coverslip was placed on the worms and gentle pressure was applied so that the embryos were expelled from the gonad. The slide was incubated for 8 minutes on an aluminum block in an ice bath to depolymerize the microtubules. The slide was put at 26 °C in a humid chamber for 0, 15, 30, or 90 seconds to allow the microtubules to regrow. The slide was then frozen in liquid nitrogen and the standard immunostaining protocol (Section 2.10) was followed.

## 2.12 **Protein sample preparations**

### 2.12.1 Whole worm protein sample

Twenty to fifty gravid hermaphrodites were picked into 5 µL water. An equal volume of 2x Laemmli loading buffer (Sigma-Aldrich, S3401) was added and the sample was incubated at 95 °C for five minutes. The sample was either loaded onto an SDS-PAGE gel immediately or frozen at -20 °C. Frozen samples were incubated at 95 °C for five minutes just prior to loading into an acrylamide gel.

### 2.12.2 Embryo preparation

Thirty to two-hundred gravid hermaphrodites were picked into 1 mL of M9. Worms were spun at 1000g for 1 minute and the M9 was removed without disrupting the pelleted worms and 1 mL of M9 was added. This wash was repeated twice and the worms were left in 50 µL of M9. 50 µL of freshly prepared alkaline hypochlorite (1 M NaOH, 35% sodium hypochlorite (Sigma-Aldrich, 425044)) was added to the pellet and the sample was vortexed for three minutes. 400 µL of embryo wash buffer (100 mM Tris pH 7.5, 100 mM NaCl, 0.1% Tween-20) was added and it was spun at 1000g for 1 minute. The supernatant was removed and the pellet washed with embryo wash buffer three times. The pellet was left in 10 µL of buffer and an equal volume of 2x Laemmli loading buffer was added. The sample was frozen at -20 °C or used immediately. Prior to loading onto the gel the sample was sonicated at room temperature in a sonicating water bath for 10 minutes and then incubated at 95 °C for 5 minutes.

### 2.12.3 Quantitative embryo preparation

Gravid hermaphrodites were washed off of five to ten 100 mm NGM plates with M9 into a 50 mL Falcon tube. The worms were left at room temperature for 10 minutes for gravity to pellet the worms. The supernatant was removed the pellet was washed twice with M9. The supernatant was removed to 1 mL and the worms were transferred to a 1.5 mL Eppendorf tube. The supernatant was again removed and the worms were resuspended in 100 µL of M9. An equal volume of freshly prepared alkaline hypochlorite solution (1 M NaOH, 35% sodium hypochlorite) was added and the sample was vortexed for 3 minutes. The sample was then passed through a 25 gauge needle three times and 400 µL of embryo wash buffer (100 mM Tris pH 7.5, 100 mM NaCl, 0.1% Tween-20)

added and the sample was spun at 1000g for 1 minute. The supernatant was removed and the pellet washed with embryo wash buffer three times. The pellet was left in 100 µL of the buffer and an equal volume of the appropriate lysis buffer was added, H100 + 10% glycerol (50 mM HEPES pH 7.4, 1 mM EGTA, 1 mM $MgCl_2$, 100 mM KCl, 10% glycerol, 0.05% NP-40, protease inhibitor (Roche, 11-836-170-001), and phosphatase inhibitors (Sigma, P0044 and P5726)). The sample was frozen in liquid nitrogen and then sonicated on ice for 5 minutes (15 seconds with a 45 second break). The sample was spun at 13000 rpm in a 4 °C centrifuge for 20 minutes and the supernatant retrieved. A colorimetric assay (BioRad Protein Assay, 500-0006) was used to determine the protein concentration and aliquots were frozen at -80 °C or used immediately.

### 2.13 **Lambda protein phosphatase treatment**

100 µg of protein in lysis buffer without phosphatase inhibitors was incubated at 30 °C for 30 minutes with 5 µL lambda protein phosphatase (New England Biolabs, P0753) in 1x NEBuffer PMP supplemented with 1 mM $MnCl_2$. The reaction volume was brought to 50 µL with HPLC grade $H_2O$ (Sigma-Aldrich, 270733). Negative controls did not contain the lambda phosphatase.

### 2.14 **SDS-PAGE and Western blot**

Proteins were separated via SDS-PAGE using a stacking gel (3.7% Acrylamide/Bis, 130 mM Tris pH 6.8, 1% SDS, 1% ammonium persulfate, and 0.1% TEMED) and a 10% acrylamide resolving gel containing (10% Acrylamide/Bis, 390mM Tris pH 8.8, 1% SDS, 1.5% ammonium persulfate, and 0.04% TEMED). A pre-stained protein ladder (7-175 kDa, New England Biolabs or PageRuler Plus, Thermo Scientific) was used to estimate the relative mass of the proteins. Gels were run at room temperature with running buffer (25 mM Tris, 192 mM glycine, 0.1% SDS, pH 8.3). Appropriate running conditions were determined empirically for each protein being resolved. Proteins were transferred from the acrylamide gel to a nitrocellulose membrane at 90V for 1 hour in cold transfer buffer (20% methanol, 25 mM Tris, 192 mM glycine). Proteins were detecting after SDS-PAGE using various methods as described in section 2.16.

### 2.15 **Phos-tag SDS-PAGE**

Proteins were loaded into a 3.7% stacking gel (3.7% Acrylamide/Bis, 130 mM Tris pH 6.8, 1% SDS, 1% ammonium persulfate, and 0.1% TEMED) with an 8% acrylamide resolving gel (8% Acrylamide/Bis, 390 mM Tris pH 8.8, 1% SDS, 1.5% ammonium persulfate, and 0.04% TEMED) with an appropriate concentration of Phos-Tag (Wako Pure Chemical Industries) and $MnCl_2$ added as per the manufacturer's instructions. Running conditions were determined emperically. Prior to blotting, the membrane was incubated on a rotating platform at room temperature in transfer buffer with 1mM EDTA for 20 minutes, replacing the solution once. The membrane was washed for 10 minutes in regular transfer buffer. The proteins were transferred onto a nitrocellulose membrane by electro-blotting for 2 hours at 100V. Proteins were detected after western blotting using various methods as described in section 2.16.

### 2.16 **Visualizing proteins after SDS-PAGE or Western blot**

#### 2.16.1 Coomassie staining

The polyacrylamide gel was immersed in five volumes of coomassie staining solution (0.25% coomassie brilliant blue R-250 (BioRad, 101-0400), 45% methanol, 10% acetic acid) on a rotating platform at room temperature for 1 hour. The gel was rinsed with methanol:acetic acid solution (45% methanol, 10% acetic acid) three times and then incubated overnight in methanol:acetic acid solution with a knotted Kim-wipe in the container. The gel was put in water and a photo was taken of it.

#### 2.16.2 Ponceau staining

A nitrocellulose membrane was stained for 5 minutes in Ponceau solution (0.1% Ponceau S (Sigma, P3504), 5% acetic acid) and rinsed in $H_20$. A photo was taken of the membrane. The membrane was immersed in 0.1 M NaOH for 30 seconds and rinsed in running distilled water for 3 minutes. The membrane was subsequently used for immune-detection of proteins.

#### 2.16.3 Antibody detection of proteins

8% skim milk powder in TBST (50 mM Tris, 150 mM NaCl, 0.05% Tween 20, pH 7.6) was used to block the nitrocellulose membrane for one hour at room temperature

with gentle agitation or overnight at 4 °C. The membrane was incubated in primary antibody in 4% skim milk powder in TBST for one hour at room temperature or overnight at 4 °C. Amounts of primary antibodies used are listed in Table 2-3. The membrane was washed three times in TBST for 10 minutes. The primary antibodies were detected with species-specific HRP-conjugated secondary antibodies (1:5000; Bio-Rad Laboratories) in 4% skim milk powder in TBST that were incubated for one hour at room temperature or overnight at 4 °C. The membrane was washed three times in TBST for 10 minutes. ECL detection buffer (Thermo Scientific) was put on the membrane for 5 minutes and the blot was wrapped in saran wrap and exposed to film.

## 2.17 **Microscopy**

Confocal microscopy was performed with an Olympus IX81 inverted microscope with a Yokogawa CSU-10 spinning disc. All images were collected with a 60X oil objective (NA 1.42) and captured with a Hamamatsu Orca R2 camera using MetaMorph software. When require, a temperature control device was used to maintain a constant temperature while imaging embryos on the confocal microscope (Tegha-Dunghu et al., 2014).

Widefield microscopy was performed with an Olympus IX81 inverted microscope with a dry 10X (NA 0.3), dry 20X (NA 0.7), or oil 60X (NA 1.42) objective. Images were captured with a Hamamatsu Orca R2 camera using MetaMorph software.

### 2.17.1 Imaging of fixed embryos

Z-stacks over 12.2 µm were captured on the confocal microscope with planes 0.2 µm apart. Acquisition settings were optimized to ensure that no channel was saturated. Images were de-convolved using Huygens essential. Out of focus planes were removed from the stack and maximum projections were generated for creating figures. Quantitative analysis was performed on raw images that were obtained with the same acquisition settings for all of the embryos.

### 2.17.2 Time lapse microscopy of *C. elegans* embryos

1-5 young adult worms were dissected in 5 µL of egg buffer (118 mM NaCl, 48 mM KCl, 2 mM $CaCl_2$, 2 mM $MgCl_2$, 25 mM HEPES pH 7.3) on a 22 $mm^2$ cover slip. The coverslip was then placed on a 2% agarose pad (2% agarose in egg buffer). Images were

captured starting prior to nuclear envelope breakdown and were taken at regular intervals, usually every ten seconds, until at least telophase.

#### 2.17.3 DIC microscopy of whole worms

Ten worms were anaesthetized in sodium azide (100 μM sodium azide in M9) on 20 mm x 50 mm coverslip and mounted on agarose pads. When the worms were immobilized, they were imaged on the widefield microscope using the 10x and 20x objectives. For adult worms that could not be captured in the full frame of the camera, multiple overlapping images were acquired and composites assembled with Adobe Photoshop.

#### 2.17.4 GFP stream acquisitions of EBP-2::GFP

MAS37 or MAS113 were incubated at 26 °C and single celled embryos from young adult worms were imaged. GFP streams with 300 ms exposure and 2x2 binning were captured 45 seconds after nuclear envelope breakdown. A temperature control was used to maintain the embryo at 25.7±0.5 °C.

### 2.18 **Spindle length and chromatin separation measurements**

Time-lapse live imaging of TH32 and EU1395, which express γ-tubulin::GFP, was used to calculate spindle length. Spindle length was determined by measuring the length of a line drawn between the centers of each of the γ-tubulin foci. To compare the rate of centrosome separation during anaphase, the distance between the centrosomes over time was calculated.

Chromatin separation was calculated using mCherry::histone. Measurements began at the first frame after anaphase onset where chromatin separation was observed. A perpendicular line was drawn between each chromatin mas and this distance was averaged over several embryos.

### 2.19 **Quantification of PAA-1 levels at the centrosome**

All embryos in this analysis were in the first mitosis. Only embryos after nuclear envelope breakdown to anaphase were analyzed. Every embryo that was imaged was included in the analysis unless the image quality was too poor to be included; for example, if the embryo was below a worm carcass. Only the planes of the Z-stack that

contained the centrosomes were used in the analysis and the anterior and posterior centrosomes were analyzed separately. The pixel intensity was summed for the planes that contained the centrosome. As outlined in Figure 2-5, circles with a fixed diameter were placed on the images and the integrated pixel intensity inside the circle was calculated. The circle in the cytoplasm was used to subtract background staining from the analysis. The ratio of the intensity of PAA-1 to RSA-1 was determined and the average was calculated.

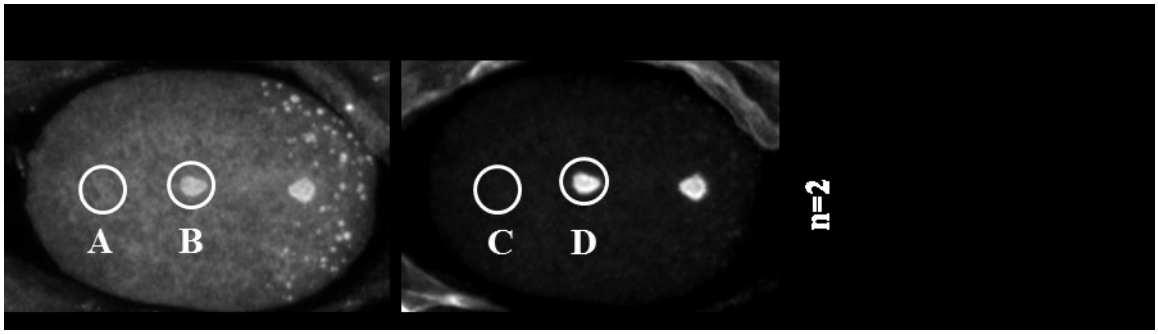


**Figure 2-5. Quantification of PAA-1 levels at the centrosome.**
The integrated pixel intensity of a circle on the centrosome and in the cytoplasm on PAA-1 and RSA-1 images was determined. These values were then entered into the formula shown where n is the number of centrosomes included in the analysis.

### 2.20 **Linescans of TPXL-1**

Metamorph software was used to create 24 bit TPXL-1::GFP and mCherry::Tubulin RGB composite images. Representative embryos were chosen that best represented all embryos in the set and a line scan perpendicular to the spindle was calculated and graphed. Maximum pixel intensity was 256 bits units per channel and images are shown with arbitrary units of intensity.

### 2.21 **Quantification of GFP from live embryos**

To quantify levels of GFP in living embryos, time lapse acquisitions were started at 1 minute and 30 seconds after nuclear envelope breakdown and images were acquired every 10 seconds for two minutes. Microscope settings were constant for all embryos analyzed. Only centrosomes that were in focus were included in the analysis and the first frame of the acquisition was used to minimize the effects of photo-bleaching. For tubulin::GFP, integrated signal intensity at the centrosome was calculated. For TPXL-1::GFP, average pixel intensity at the centrosome, chromatin, or in a representative location in the cytoplasm was calculated.

# *3* Results: Characterizing *rsa-1(or598)*

## 3.1 Genetic Characterization of *rsa-1(or598)*

The *rsa-1(or598)* allele was identified in a genetic screen for temperature-sensitive embryonic lethal mutations in *C. elegans* (O'Rourke et al., 2011). Consistent with the previously published characterization of this allele, I found that it had decreasing embryonic viability as temperature increased (Figure 3-1). At 20 °C *rsa-1(or598)* homozygotes have an embryonic viability of 82.7 % (s.d. 12.4%, n=2119). The *rsa-1(or598)* homozygotes have 100% embryonic lethality at 26 °C and no hatching was ever observed at this temperature (n=1887).

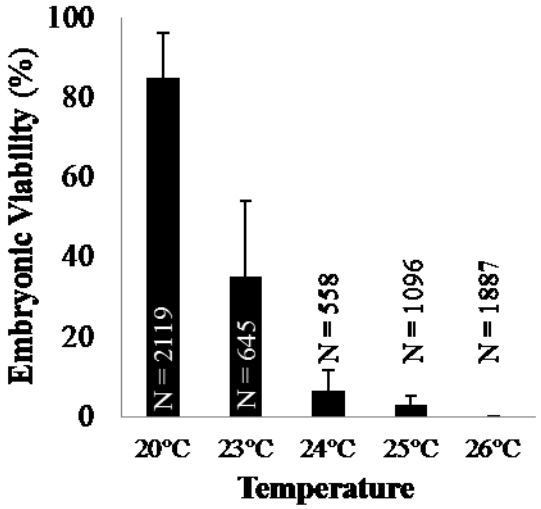


**Figure 3-1. *rsa-1(or598)* was a temperature sensitive allele**
Hatching rates of *rsa-1(or598)* homozygous hermaphrodites at permissive and restrictive temperatures. N is the number of embryos included in the analysis.

### 3.1.1 Temperature sensitivity of *rsa-1(or598)*

*rsa-1(or598)* was previously reported to be a fast acting temperature-sensitive allele (O'Rourke et al., 2011); embryos produced at 15 °C were shifted to 24 °C for approximately one minute and a phenotype was observed in the *rsa-1(or598)* embryos. Since this is a fast acting allele, this could limit how *rsa-1(or598)* strains are manipulated in the laboratory. For example, if shifting hermaphrodites from 26 °C to the permissive temperature for one minute affects the embryonic viability of the strain, then accurate analysis of the embryonic viability would need to be carried out and analyzed entirely at the restrictive temperature.

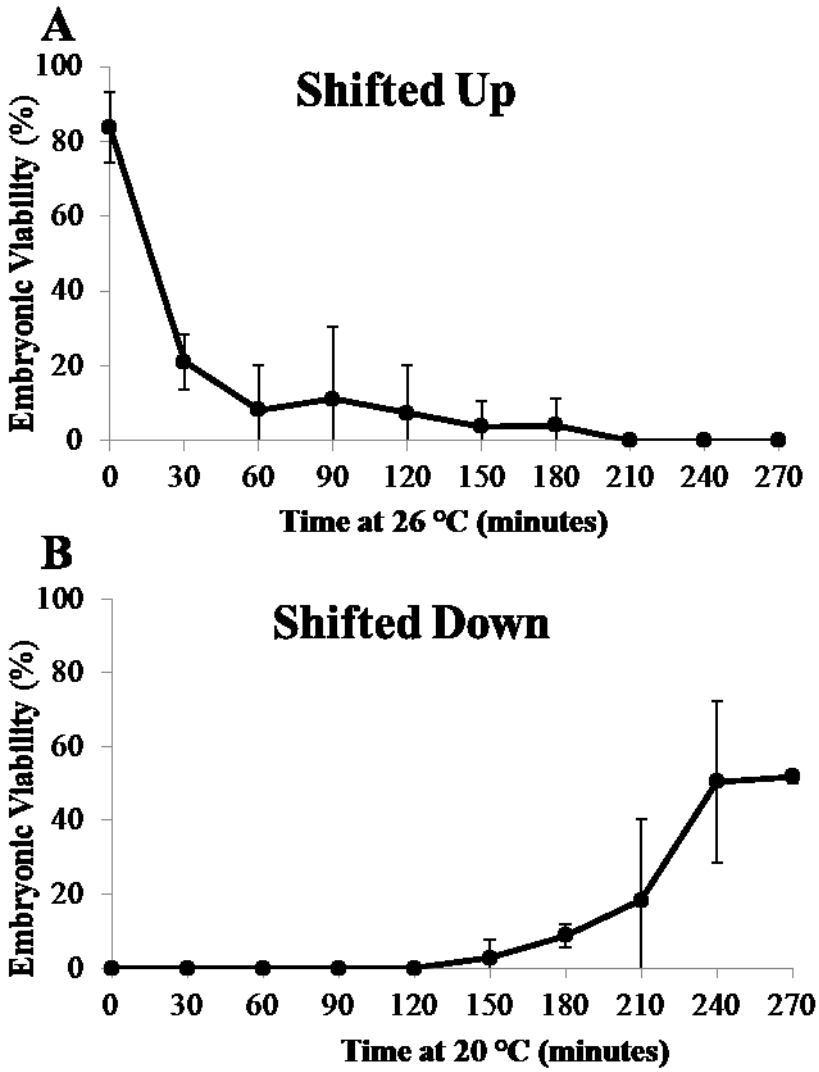


**Figure 3-2. *rsa-1(or598)* was not fast acting on embryonic viability**
A) Hatching rate of embryos produced by hermaphrodites that were put at 20ºC as L4 and the next day shifted to 26ºC as young adults at time 0. Hermaphrodites were moved to new plates every 30 minutes and the embryonic viability at each time point was determined. B) Hatching rate of embryos produced by hermaphrodites that were put at 26ºC as L4 and the next day shifted down to 20ºC as young adults at time 0. Error bars are the standard deviations.

In order to determine the effect of temperature on the hatching rates of worms, I performed two temperature shift experiments. First, L4 hermaphrodites were incubated at 20 °C overnight and then shifted up to 26 °C as young adults. After 3 hours and 30 minutes the hatching rate was 0% (Figure 3-2A). This indicated that accurate embryonic viabilities could not be obtained by shifting gravid adults to the restrictive temperature. For subsequent experiments, hermaphrodites were placed at the restrictive temperature as L4 to accurately determine the embryonic viability of the progeny. Next, I investigated

how quickly embryonic viability is restored to embryos laid by hermaphrodites shifted from a restrictive to permissive temperature. L4 hermaphrodites were incubated at 26 °C overnight and then shifted down to 20 °C as young adults. These hermaphrodites produced only dead embryos until 2 hours and 30 minutes at the permissive temperature of 20 °C (Figure 3-2B). For subsequent experiments, worms were never left at room temperature for more than 30 minutes to ensure that the calculated embryonic viabilities at the restrictive temperature were accurate.

### 3.1.2 Genetic behaviour of *rsa-1(or598)*

To determine if the *rsa-1(or598)* allele was recessive or dominant, I mated homozygous hermaphrodites with wild-type males. The F1 progeny from this cross are heterozygous for *rsa-1(or598).* The embryonic viability of embryos produced by the heterozygous F1 hermaphrodites was determined and compared to wild-type and *rsa-1(or598)* homozygous hermaphrodites at the same temperature (Figure 3-3).

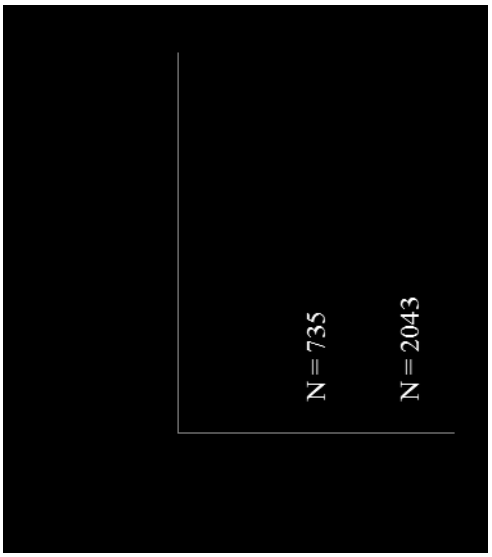


**Figure 3-3. *rsa-1(or598)* was recessive**
Hatching rates of embryos produced by *rsa-1(or598)* homozygous, *rsa-1(or598)* heterozygous, and wild-type hermaphrodites at 25ºC. ** indicates a p-value of <0.0001.

At 25 °C the embryonic viability of wild-type hermaphrodites was 99.8% (s.d. 1.9%, n=2043) and the embryonic viability of *rsa-1(or598)* homozygous hermaphrodites was 3.1% (s.d. 2.1%, n=1096). The *rsa-1(or598)* heterozygote exhibited an embryonic viability of 98.2% (s.d. 4.6, n=735) which was significantly different from homozygotes.

Since the mutant phenotype was not observed in heterozygotes, I concluded that the *rsa-1(or598)* allele was recessive.

### 3.1.3 *rsa-1(or598ts)* embryos are partially rescued by wild-type sperm

Embryonic lethality can be caused by a deficiency in either maternal or zygotic contributions or both. Maternal-effect lethality refers to essential genes where the maternal genotype determines the phenotype of the embryo. The embryo requires maternal contributions of mRNA and protein in the cytoplasm and if a mutation prevents the contribution of an essential component embryonic lethality results. Even if the zygote is heterozygous for a recessive maternal-effect lethal allele, the presence of a wild-type copy in the zygote genome would be unable to rescue the phenotype because transcription is repressed in the single celled *C. elegans* embryo (Guven-Ozkan et al., 2008).

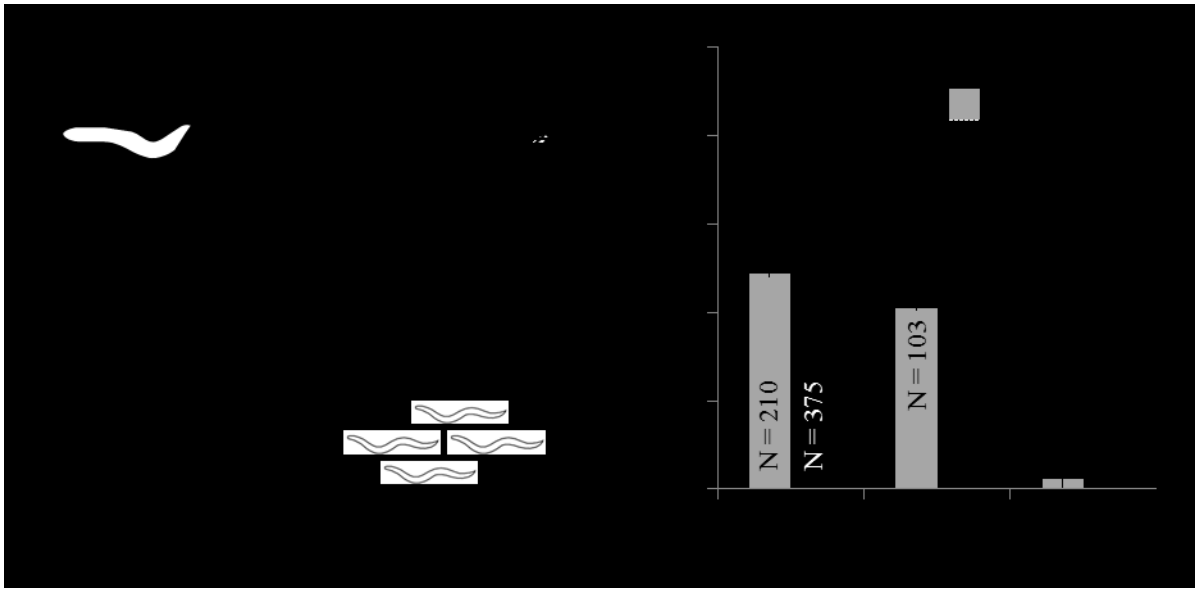


**Figure 3-4. *rsa-1(or598)* causes zygotic and maternal effect lethality**
A) Dumpy *rsa-1(or598)* homozygous hermaphrodites were mated with wild-type or *rsa-1(or598)* (not shown) males. The embryonic viability of the mated hermaphrodite was calculated. B) Hatching rates of *rsa-1(or598)* homozygous hermaphrodites mated with either wild-type or *rsa-1(or598)* homozygous males to generate F1 embryos with the genotype indicated. Error bars are the standard deviation and N is the number of embryos included in the analysis.

To test if *rsa-1(or598)* is maternal-effect lethal, I mated *dpy-5(e61) rsa-1(or598)* hermaphrodites to either wild-type (Figure 3-4A) or *rsa-1(or598)* males. In these crosses the maternal genotype was homozygous for *rsa-1(or598)* but the F1 embryos were either heterozygous or homozygous for *rsa-1(or598)*.The recessive *dpy-5* allele was included to

verify that mating crosses were successful. At all temperatures tested, the F1 embryos that were heterozygous for the *rsa-1(or598)* allele had a higher embryonic viability than homozygous embryos (Figure 3-4B).

These results indicated that a wild-type *rsa*-1 allele introduced by the male was able to partially rescue the embryonic lethality associated with *rsa-1(or598)*. This was particularly evident at 26 °C where *rsa-1(or598)* homozygote embryos were completely inviable, while the heterozygous outcross F1 showed 2.4 % embryonic viability (s.d 4.6%, n=126). This indicates that the maternal genotype resulted in approximately 97% of the embryonic lethality but 3% of the embryonic viability is due to zygotic expression of *rsa-1* at 26 °C. In other words, my results indicate that the *rsa-1(or598)* allele causes both maternal and zygotic-effect lethality. I propose that a maternal contribution of *rsa-1* is required for early development and that *rsa-1* is also required later during embryogenesis when the zygotic genome is transcribed.

### 3.1.4 Complementation test with two *rsa-1* alleles, *or598* and *dd13*

I performed a complementation test with *rsa-1(or598)* and a previously characterized allele, *rsa-1(dd13).* The *rsa-1(dd13)* disrupts a splice site near the C-terminus of the protein and was predicted to be a null allele because the protein was not detected in Western blots (Schlaitz et al., 2007). However, the antibody used in this analysis is for a C-terminal peptide that would not be included in a truncated RSA-1(dd13) protein. The *rsa-1(dd13)* allele was recessive and has 0% embryonic viability at all temperatures so it was maintained in a heterozygous state (Schlaitz et al., 2007). The lethal *rsa-1(dd13)* allele was balanced with hT2g, a balancer that expresses a pharyngeal GFP marker. As outlined in Figure 3-5A, I mated the balanced *rsa-1(dd13)* strain with *rsa-1(or598)* males and selected F1 progeny without a GFP positive pharynx. The F1 were allowed to self-fertilize and the embryonic viability was determined (Figure 3-5B). Surprisingly, *rsa-1(dd13)* and *rsa-1(or598)* complemented each other. The *rsa-1(dd13)/rsa-1(or598)* genotype exhibited a significantly higher embryonic viability than either allele alone at every temperature tested.

This was a surprising result because usually complementation indicates that the alleles are in different genes. Since both of these mutants have the same phenotype and the

mutagenic lesions were already identified in the *rsa-1* gene, it was difficult to interpret the complementation results. One possibility is that the two *rsa-1* alleles cause the same phenotype via a different molecular mechanism. If each mutant gene creates a protein that is missing one key function, then when both alleles are present the two mutations can functionally compensate for each other.

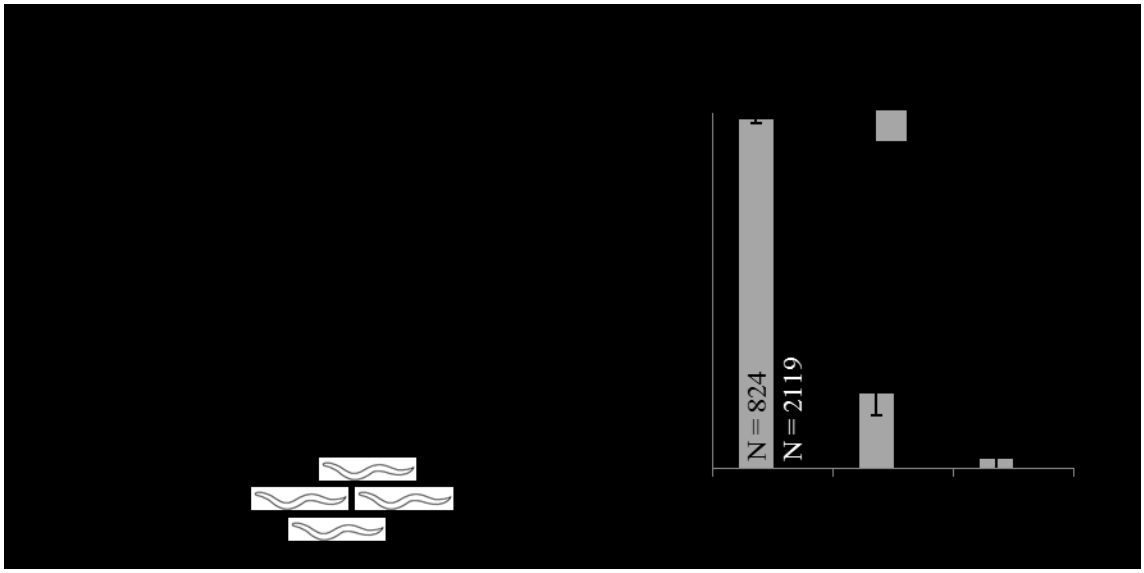


**Figure 3-5. *rsa-1(or598)* complements *rsa-1(dd13)***
A) EU1374 was mated with TH125. Viability of non-GFP F1 progeny was calculated. B) Hatching rates of embryos produced by *rsa-1(or598)/rsa-1(dd13)* hermaphrodites at permissive and restrictive temperatures. *dd13* homozygous hatching rates are not included in the graph because it exhibits 0% embryonic viability at all temperatures. * indicates a p-value of <0.05 and ** indicates a p-value of <0.0001. Error bars are the standard deviation and N is the number of embryos included in the analysis.

## 3.2 *rsa-1(or598)* phenotypes in the early embryo

Previously, loss of *rsa-1* function has been shown to cause multiple phenotypes in the early embryo (O'Rourke et al., 2011; Schlaitz et al., 2007). To determine if *rsa-1(or598)* embryos exhibit these phenotypes, I investigated a set of stereotypical behaviours that occur shortly following fertilization in the *C. elegans* single-celled embryo (as described in section 1.5.1, Figure 1-8).

### 3.2.1 Nuclear envelope breakdown and spindle positioning

In wild-type *C. elegans* embryos, the female pronucleus migrates from the anterior of the embryo to the posterior where it joins the male pronucleus. The two pronuclei then move to the center of the embryo and rotate to correctly position the centrosomes for cell division (Figure 3-4A). The nuclear envelopes break down within 16 seconds (s.d. 11.4

seconds, n=5) seconds of each other. At 26°C *rsa-1(or598)* embryos exhibited asynchronous nuclear envelope breakdown (Figure 3-6B) and spindle assembly in the posterior of the embryo (Figure 3-6A). Consistently, male pronuclear envelope break down occurred 80 seconds (s.d. 25.8 seconds, n=5) before the female pronucleus. In *rsa-1(or598)* embryos the female pronucleus did not finish migrating to meet the male pronuclei at the initiation of nuclear envelope breakdown. In *rsa-1(or598)* embryos the centrosomes and pronuclei did not properly center and rotate so the mitotic spindle was mis-positioned to the posterior side of the cell. This posterior positioning of the mitotic spindle led to an exaggerated asymmetric division in *rsa-1(or598)* embryos at 26 °C with *rsa-1(or598)* embryos having a smaller posterior cell than the wild-type counterparts (Figure 3-6B).

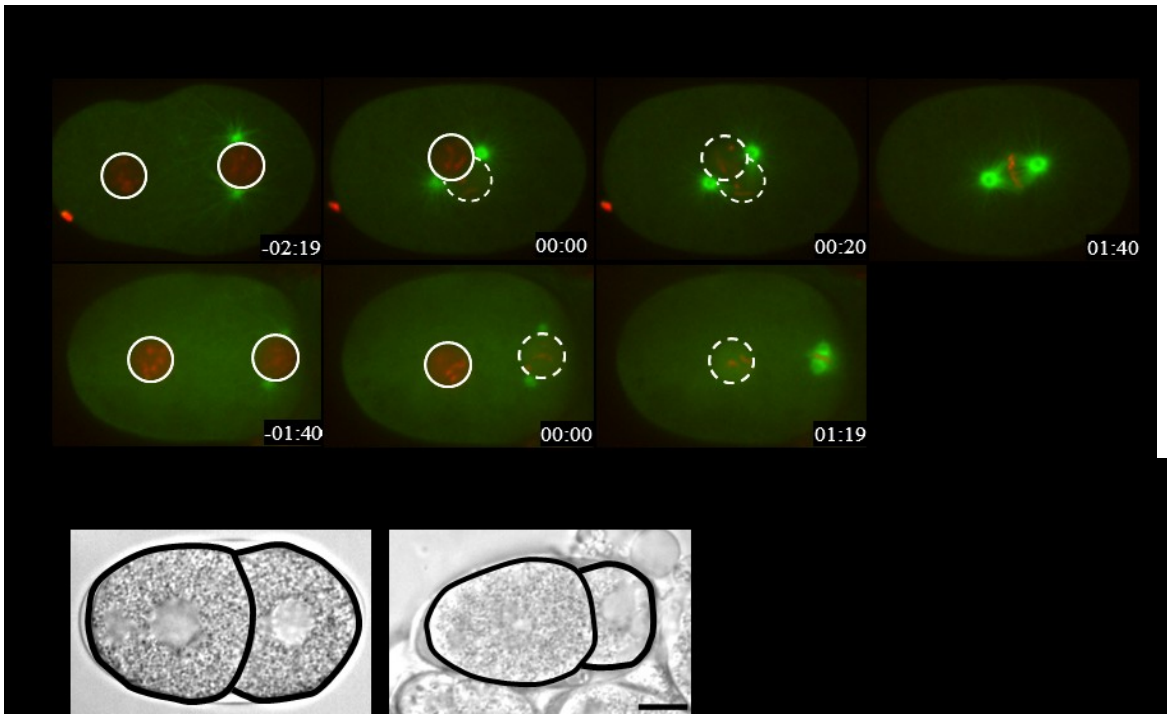


**Figure 3-6. NEBD and spindle position in *rsa-1(or598)***
A) Tubulin::GFP and mCherry::Histone in wild-type and *rsa-1(or598)*. Solid lines indicate nuclear envelopes and dashed lines indicates nuclear envelope breakdown. Time 0 is male nuclear envelope breakdown. Female nuclear envelope breakdown and metaphase occur in the same frame in the *rsa-1(or598)* embryo. B) DIC of wild-type and *rsa-1(or598)* after cytokinesis. The scale bar is 10 µm.

### 3.2.2 Spindle collapse

Spindle assembly occurs after nuclear envelope breakdown. As the spindle assembles the centrosomes move further apart. At nuclear envelope breakdown (Figure 3-7B, time 0), the wild-type centrosomes were 11.0 µm (s.d. 1.0 µm, n=2) apart and by metaphase

the distance between the centrosomes increased to 14.87 µm (s.d. 0.74 µm, n=5). In *rsa-1(or598)* embryos that were incubated at 26 °C and imaged at 20 °C, the centrosomes always moved closer together by an average of 1.8 µm (s.d. 1.2 µm, n=6) after nuclear envelope breakdown. This phenotype, where the distance between the centrosomes decreases during spindle assembly, is called a spindle collapse (Figure 3-7A).

The spindle collapse phenotype in *rsa-1(or598)* embryos was more severe when embryos were kept at 26 °C while imaging (Figure 3-6A). For subsequent microscopy experiments, a temperature control device was used on the microscope to maintain the embryos at a restrictive temperature for imaging (Tegha-Dunghu et al., 2014).

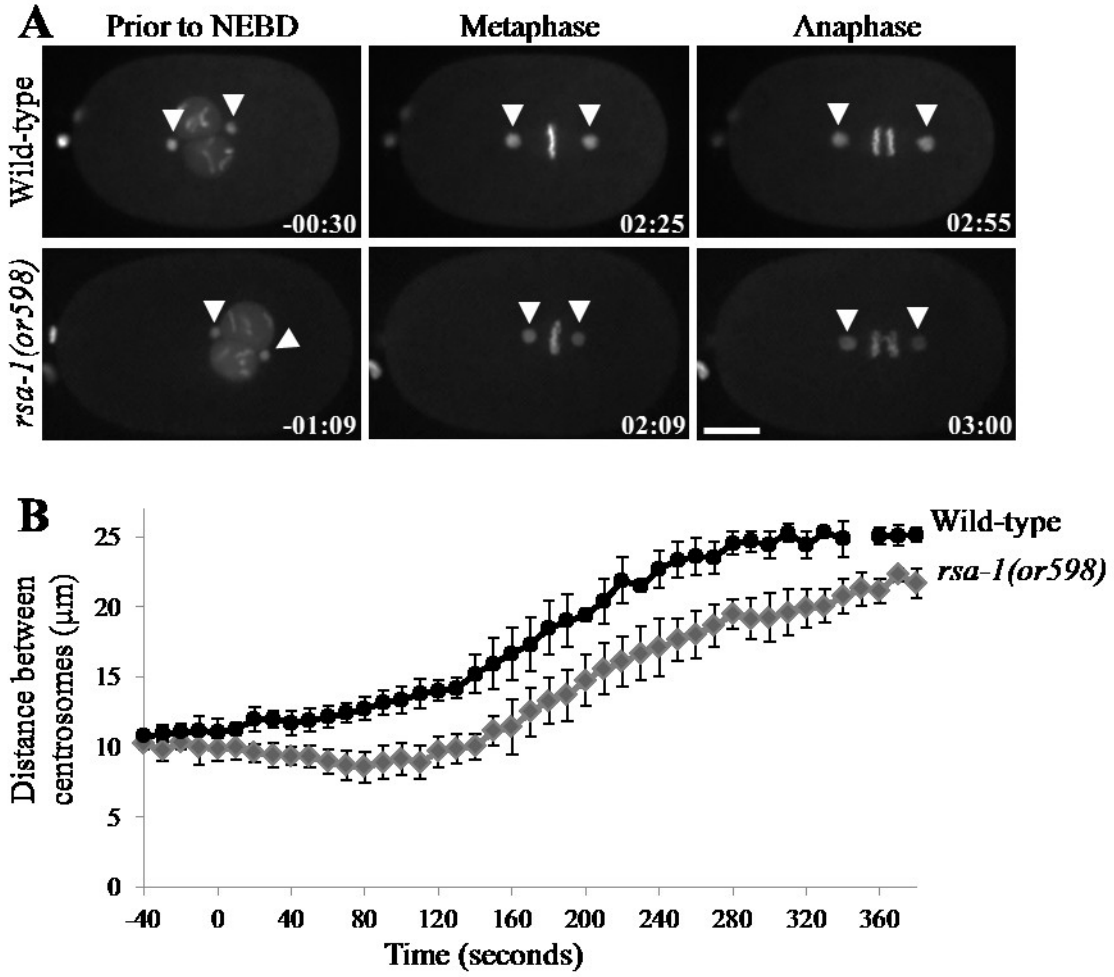


**Figure 3-7. Spindle collapse in *rsa-1(or598)* embryos.**
A) Time lapse microscopy of wild-type and *rsa-1(or598)* embryos that express gamma-tubulin::GFP and histone::GFP. Hermaphrodites were incubated at 26 °C overnight and then imaged at room temperature. The scale bar is 10 µm. Arrow heads indicate the centrosomes. B) The distance in micrometers between the center of the centrosomes from pronuclear migration to telophase is plotted. Time 0 is nuclear envelope breakdown.

### 3.2.3 Chromosome segregation errors

Spindle assembly defects observed in *rsa-1(or598)* embryos resulted in chromosome segregation errors and aneuploidy of the daughter cells. It is likely that this aneuploidy is the cause of the lethality in the embryos. There were two distinct causes observed for the

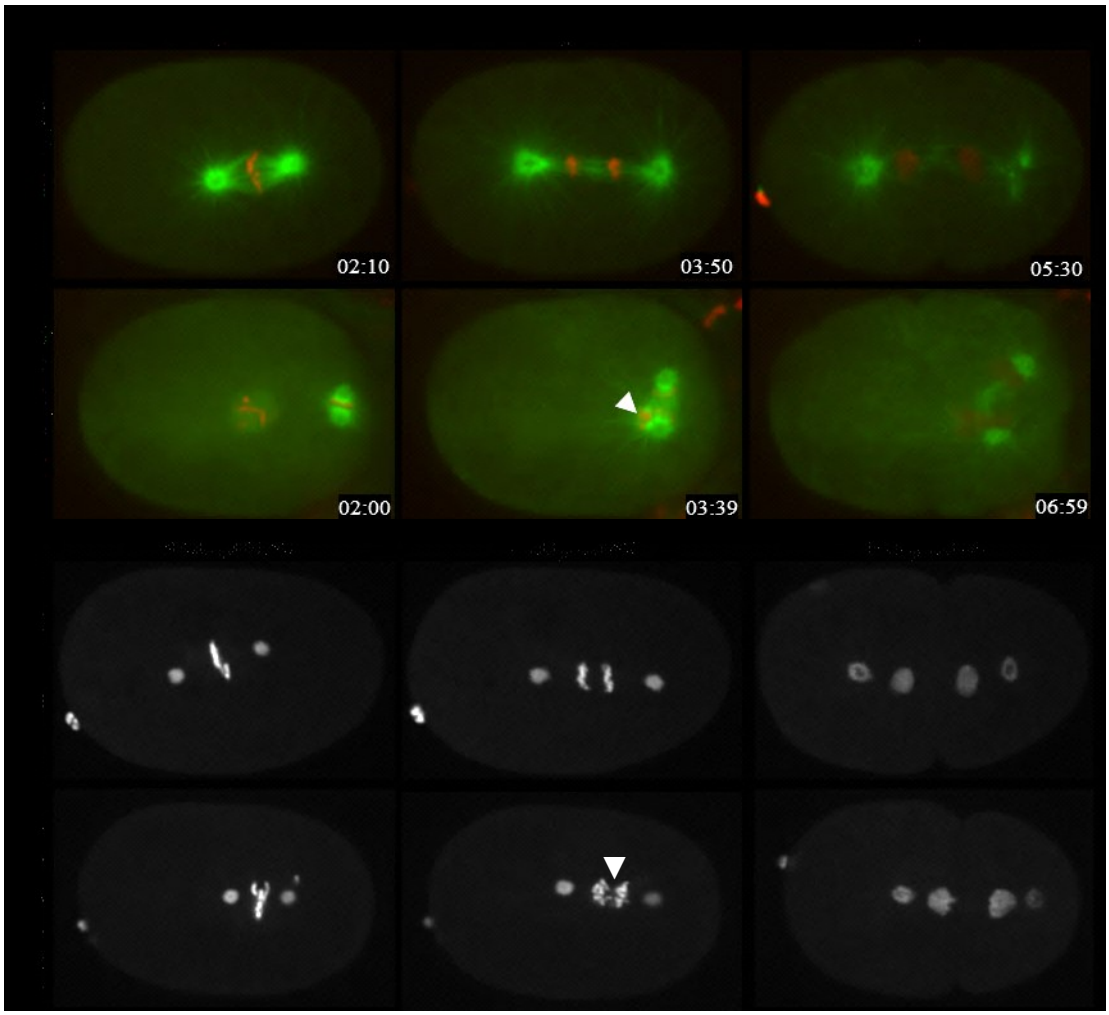


**Figure 3-8. Chromosome segregation errors in *rsa-1(or598)* embryos**
A) The arrow head indicates the *rsa-1(or598)* maternal chromosomes that were incorporated into the spindle after spindle assembly. Time 0 is nuclear envelope breakdown. B) Chromosome segregation errors in *rsa-1(or598)* embryos that incorporated all chromosomes in the spindle. The arrowhead indicates lagging chromosomes.

chromosome segregation errors in *rsa-1(or598)*. Firstly, as described in Section 3.2.1, pronuclear migration was disrupted in *rsa-1(or598)* early embryos. This resulted in assembly of the spindle without the maternal complement of chromosomes. The chromosomes excluded from the spindle either remained in the anterior of the embryo or migrated towards the spindle later in mitosis, such as at the onset of anaphase (Figure

3-8A). Even when these chromosomes joined the spindle, they were not correctly incorporated in the spindle proper, often resulting in only one daughter cell receiving all of the maternal chromosomes. *rsa-1(or598)* embryos also exhibited chromosome bridges and lagging chromosomes during anaphase. Often the chromosomes that appeared to be bi-oriented during metaphase exhibited a lag during anaphase, resulting in chromosomes situated in the spindle mid-zone during anaphase (Figure 3-8B).

### 3.2.4 Level of microtubules emanating from the centrosomes

*rsa-1(RNAi)* has been reported to cause a significant decrease in the number of microtubules that grow from the centrosomes (Srayko et al., 2005). To determine if the *rsa-1(or598)* allele also displays this phenotype the levels of centrosomal microtubules during metaphase were measured (Figure 3-9A).

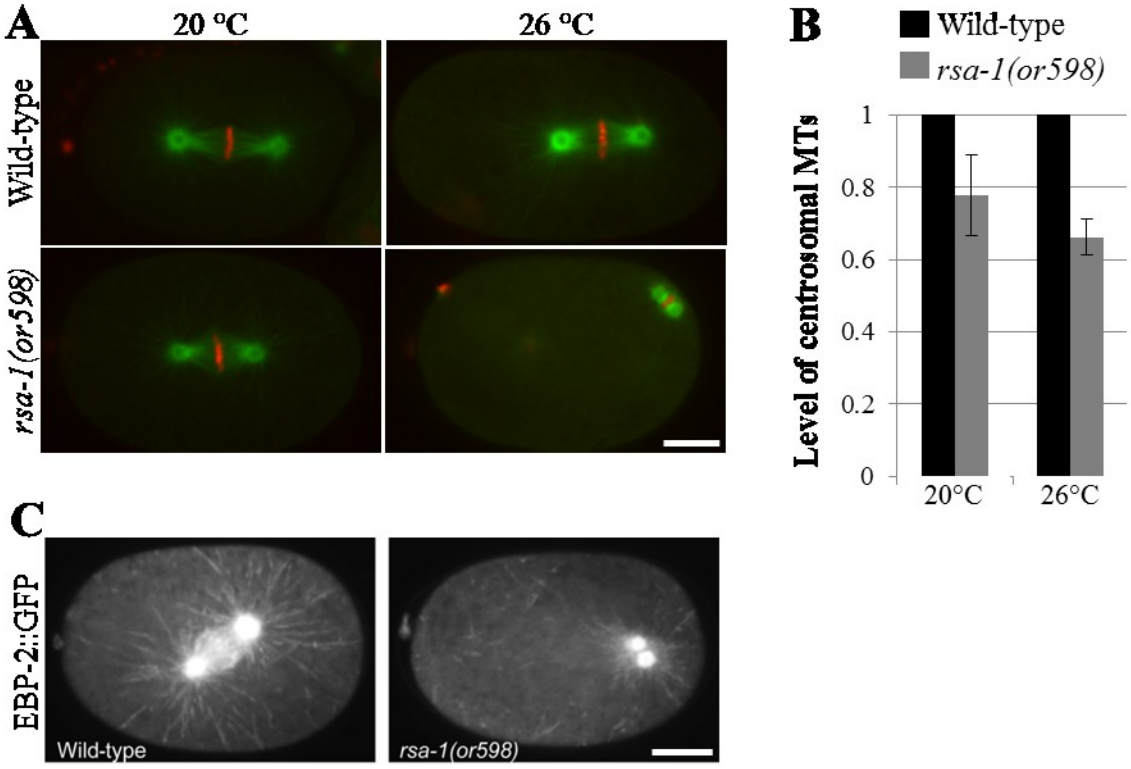


**Figure 3-9. *rsa-1(or598)* results in fewer centrosomal microtubules**
A) Time-lapse microscopy of MAS96 and MAS136, which express tubulin::GFP and mCherry::Histone, at 20°C and 26°C. The frame shown is 10-20 seconds before the onset of anaphase. B) Integrated signal intensity of the centrosome during metaphase in *rsa-1(or598)* embryos relative to wild-type. n=5 embryos for each temperature. C) A 20 second projection of a streamed movie of the microtubule plus end tracking protein EBP-2::GFP is shown for wild-type and *rsa-1(or598).* The scale bars are 10 µm.

At 20 °C and 26 °C, *rsa-1(or598)* have fewer microtubules than wild-type (Figure 3-9B) although the microtubule deficiency was more severe at the restrictive temperature of 26 °C. EBP-2 decorates the polymerizing microtubules. Twenty-second projections of the microtubule plus end tracking protein, EBP-2::GFP, show how much an individual microtubule grew in 20 seconds (Figure 3-9C). In *rsa-1(or598)* embryos, there was a decrease in both the number of growing microtubules and the distance each microtubule polymerized during that time. These results are consistent with previous reports that *rsa-1* is required to promote microtubule growth or stability in embryos.

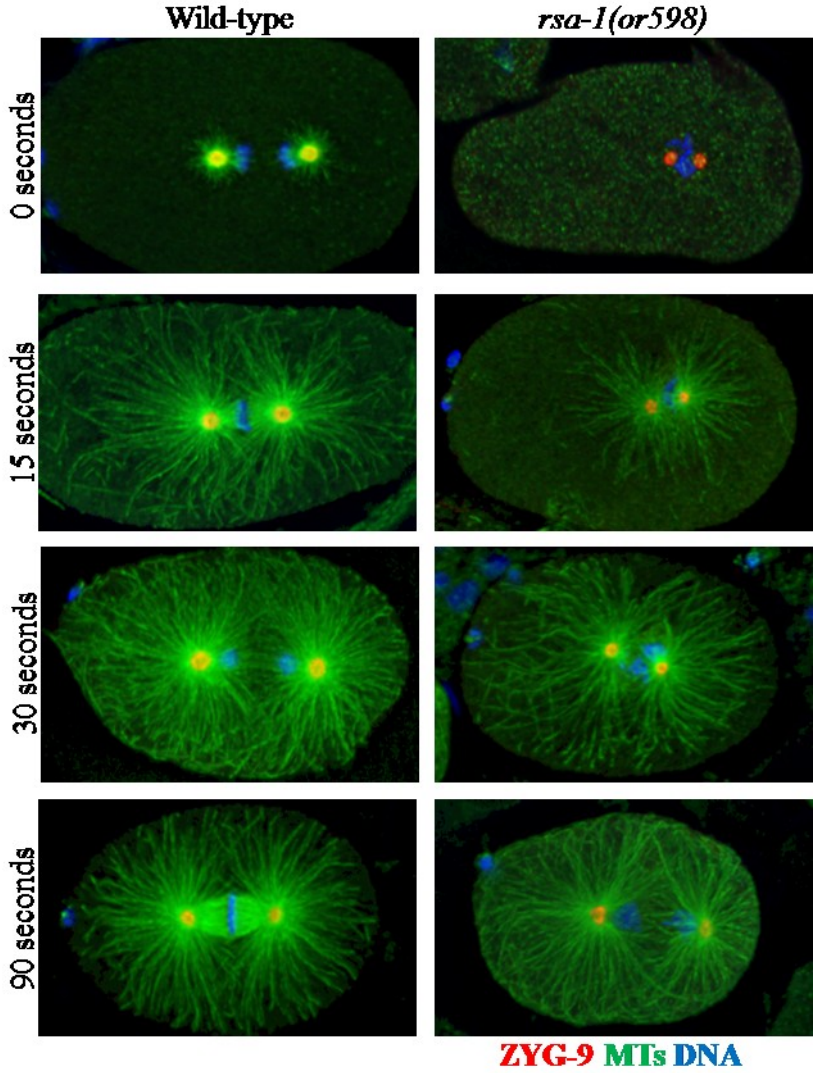


**Figure 3-10. Microtubules polymerize slower in *rsa-1(or598)* embryos**
Prior to fixation and immunostaining, microtubules were depolymerized with cold treatment and then allowed to regrow at 26 ºC for the amount of time indicated. ZYG-9 (red) is a centrosomal marker, microtubules are green, and DAPI stains the DNA.

To assess the ability of centrosomes to nucleate microtubules, the microtubules were depolymerized by cold treatment and allowed to re-grow at 26 °C (Figure 3-10). After 15 seconds of re-polymerization both wild-type and *rsa-1(or598)* embryos had microtubules emanating from the centrosomes, however wild-type embryos had longer microtubules that spanned the cytoplasm to reach the cortex while *rsa-1(or598)* had shorter microtubules. After 30 seconds at 26 °C wild-type and *rsa-1(or598)* embryos had long microtubules, although wild-type embryos had a greater density of microtubules. These results indicated that microtubule growth was not as robust in *rsa-1(or598)* embryos as it is in wild-type.

#### 3.2.5 Conclusion of *rsa-1(or598)* phenotypes

It was previously shown that depletion of *rsa-1* function in embryos results in a decrease in microtubule number from the centrosome and a spindle collapse (Schlaitz et al., 2007). Further investigation of *rsa-1(or598)* embryos has revealed that there are also spindle positioning defects, asynchronous nuclear envelope breakdown, and chromosome segregation errors when *rsa-1* function is compromised by the missense mutation in this allele.

### 3.3 **Immunofluorescence imaging RSA-1(or598)**

During the first mitotic division RSA-1 was located to the centrosomes (Schlaitz et al., 2007). To determine if the *rsa-1(or598)* point mutation affects the ability of RSA-1 to locate to the centrosomes in the cell, I performed immunofluorescence with C-terminal α-RSA-1 peptide antibody (Figure 3-11). At 26 °C the RSA-1(or598) protein was observed at the centrosomes which indicated that the mutation did not disrupt the location of RSA-1 during the first mitosis. Since RSA-1(or598) is still located at the centrosome, this suggests that the mutation disrupts the activity or function of RSA-1.

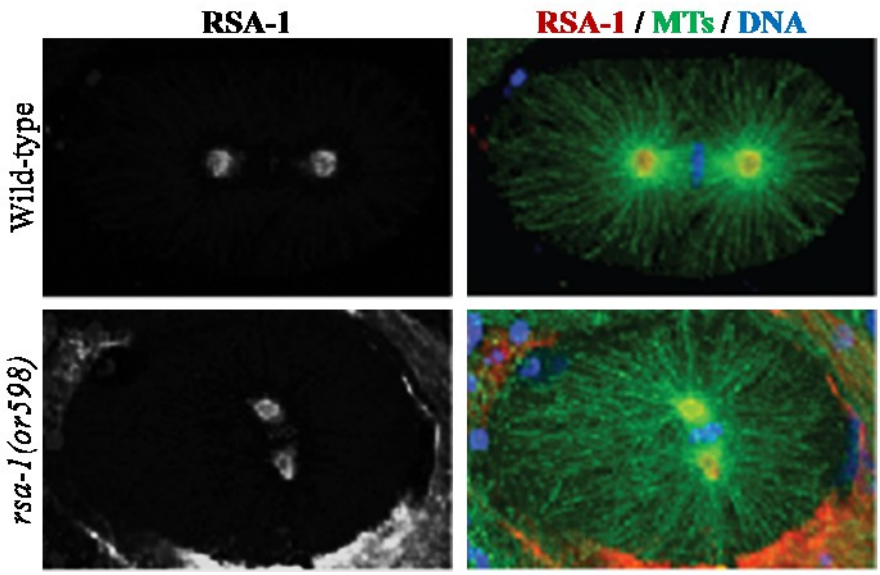


**Figure 3-11. RSA-1 localizes to centrosomes in *rsa-1(or598)* embryos**
Immunostaining of RSA-1 in metaphase embryos at 26 °C. RSA-1 is observed at the centrosome in wild-type and *rsa-1(or598)* embryos.

### 3.4 *rsa-1(or598)* phenotypes during late embryogenesis

At 25 °C, *rsa-1(or598)* exhibited an embryonic viability of 3.1% (s.d. 2.1%, n=1096) (Figure 3-1). However, 100% of the embryos that hatched at this temperature arrested during L1 and did not have a healthy appearance. This suggested that the *rsa-1(or598)* allele was not able to support development later during embryogenesis. When a homozygous *rsa-1(or598)* hermaphrodite was mated with a wild-type male, the F1 embryos were heterozygous for *rsa-1(or598)* and had an embryonic viability of 40.8% (s.d. 38.5%, n=103) at 25 °C (Figure 3-4B). The viable F1 progeny did not arrest as L1 larvae. In this experiment, all maternal contributions of the RSA-1 protein were from the *or598* allele. The wild-type *rsa-1* allele was contributed paternally and presumably was only expressed in the zygote after the two cell stage (Guven-Ozkan et al., 2008). These data suggest that the *rsa-1* gene was also expressed later during embryogenesis and was necessary for proper embryonic development. The cause of the L1 larval arrest was not investigated in this thesis.

## 3.5 **Post embryonic *rsa-1(or598)* phenotypes**

### 3.5.1 Sterility

It was previously observed that shifting L1 *rsa-1(or598)* hermaphrodites to 26 °C leads to sterile adults (O'Rourke et al., 2011), but the basis for this sterility was not reported. Sterility can be caused by several defects including germ-line proliferation, somatic gonad development, oogenesis, spermatogenesis, or fertilization. In order to identify the cause of the sterility, L1 hermaphrodites were incubated at 26 °C and observed at regular intervals using DIC microscopy (Figure 3-12A). Worm length and gonad development are reliable features that can be used to determine the age of *C. elegans* larvae. However, *rsa-1(or598)* larvae exhibited mutant phenotypes that affected both worm size and gonad development so it was not possible to accurately determine the developmental age of each worm analyzed using these methods. I used the time of incubation at 26 °C to compare larvae between genotypes. Time points were chosen based on the development of wild-type worms whereby all worms are L1 at 0 hours, L2 at 20 hours, L3 at 28 hours, L4 at 44 hours, and gravid adults at 60 hours.

At L1, L3, L4 and adult time points the *rsa-1(or598)* hermaphrodites were significantly larger than wild-type worms (Figure 3-12B). At each time point the variation in the length of worms observed in *rsa-1(or598)* was greater than in wild-type.

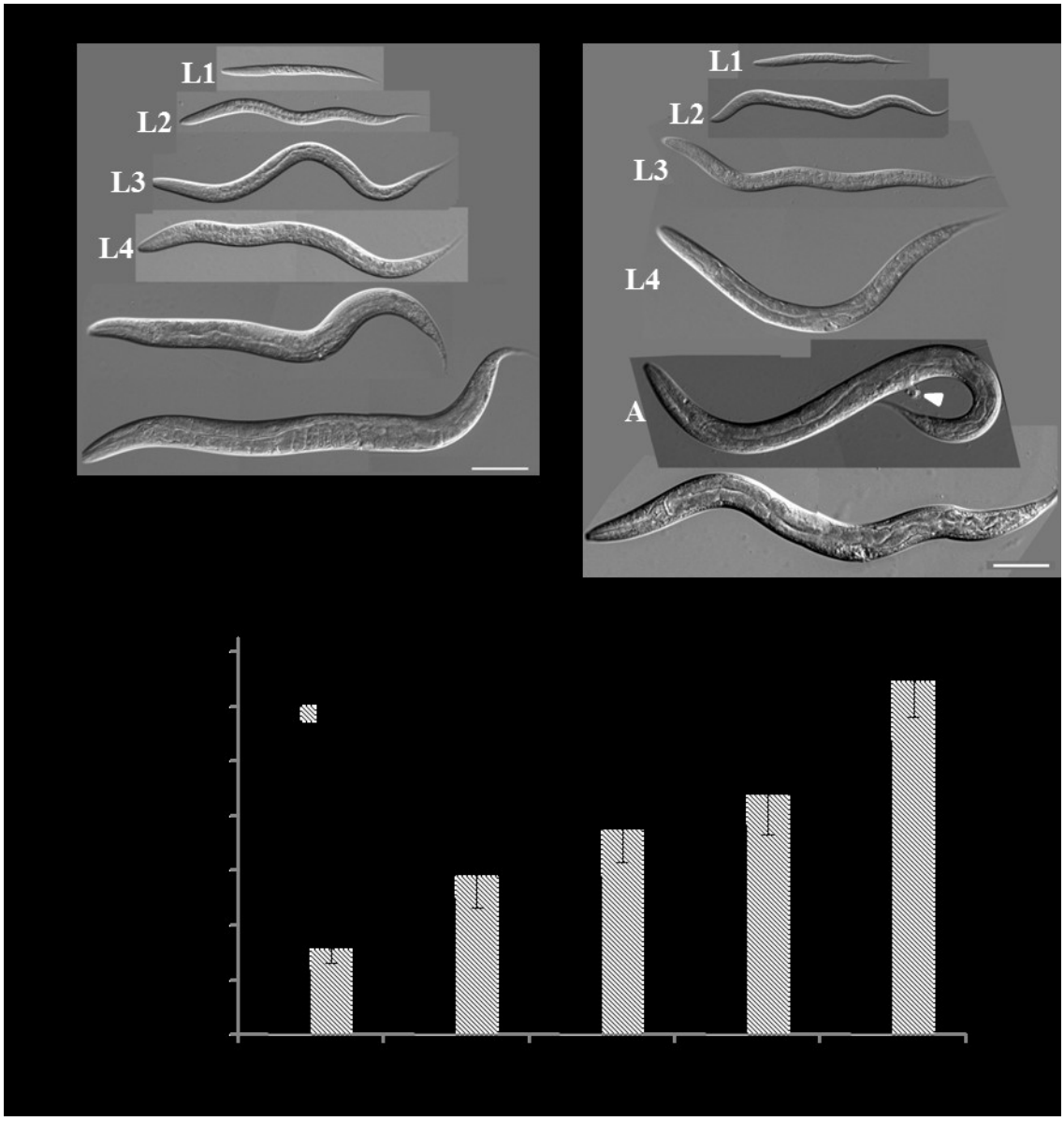


**Figure 3-12. Length of wild-type and *rsa-1(or598)* worms**
A) Representative wild-type and *rsa-1(or598)* hermaphrodites that were incubated at 26°C beginning as L1 larvae. The arrowhead indicates a protruding vulva. The scale bar is 100 µm. B) Length was determined from measuring each worm from the tip of its nose to the end of its tail. Worms were put at 26 °C as L1 larvae and incubated for the length of time indicated. Error bars are standard deviation. * indicates a p-value of <0.05 and ** indicates a p-value of <0.0001.

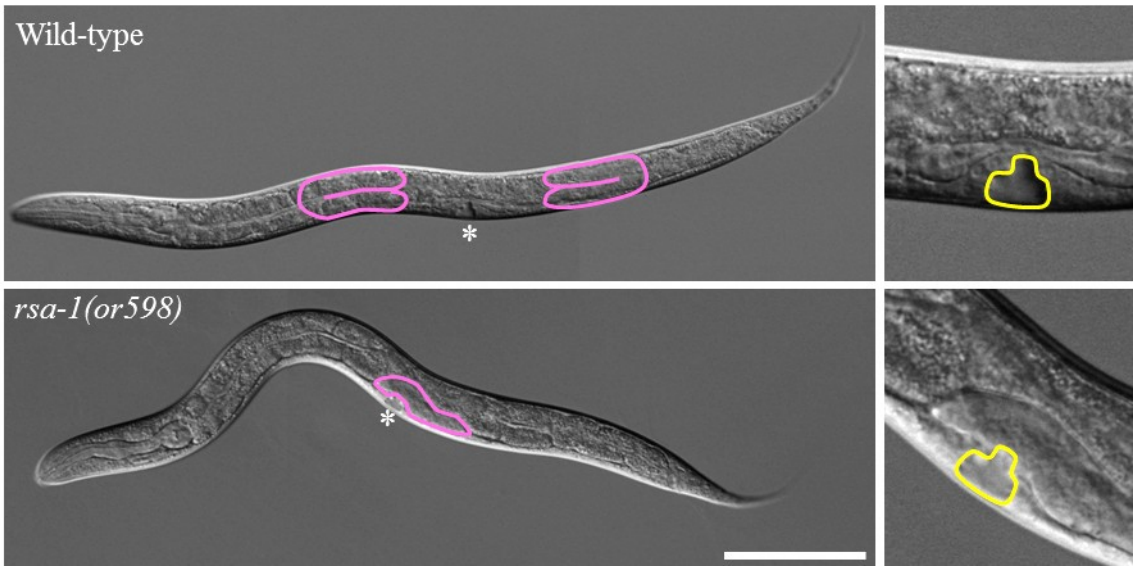


**Figure 3-13. L4 developing vulva and gonad in wild-type and *rsa-1(or598)* hermaphrodites**
The pink regions contain all germ-line nuclei that were observed. A close up of the developing vulva is shown on the right with the yellow region highlighting the developing vulva. Asterisk indicates the location of the vulva. The scale bar is 100 µm.

During the L4 larval stage in wild-type hermaphrodites the developing gonad had two lobes that extended out from the vulva and loop back, the germ-line nuclei are at the distal ends of the gonad arms, and the developing vulva has a characteristic "podium" shape (Figure 3-13). At the time point when wild-type worms were L4, *rsa-1(or598)* hermaphrodites exhibited the characteristic "podium" shaped vulva. However, in L4 *rsa-1(or598)* hermaphrodites, migration of the gonad was rarely observed and the germ-line nuclei were proximal to the vulva (Figure 3-13).

All of the *rsa-1(or598)* worms that were shifted to 26 °C as L1 developed into sterile hermaphrodites, with no eggs laid. After 52-60 hours at 26 °C all wild-type worms were healthy gravid adults (n=22) while *rsa-1(or598)* hermaphrodites did not have oocytes visible in the gonad arms (n=31). Specific germ-line and gonad defects in individual *rsa-1(or598)* hermaphrodites varied, but many had a protruding vulva (42%), and/or defects in migration or looping of the gonad (52%). These results suggest that *rsa-1* may play a role in migration of the distal tip cell during gonad arm extension. Future experiments involving long time-lapse imaging of developing worm gonads and closer inspection of the distal tip cell could be used to address this possibility.

### 3.5.2 *rsa-1(or598)* causes a high incidence of males

At 20 °C, the *rsa-1(or598)* allele causes a high incidence of males or Him phenotype. 7.4% ± 4.7% of live progeny from a self-fertilized *rsa-1(or598)* hermaphrodite are male (n=1023) while self-fertilized wild-type hermaphrodites have male progeny less than 0.05% of the time (n=1947). The cause of the high incidence of males in *rsa-1(or598)* progeny is unknown but is usually caused by chromosome non-disjunction during meiosis. Consistent with a role for RSA-1 in spindle function, a Him phenotype could be caused by defects during gametogenesis that lead to mistakes in chromosome pairing or increased levels of chromosome non-disjunction during the meiotic divisions. Live-cell imaging could be performed on adult worm gonads to help distinguish between these possibilities.

## 3.6 Genetic screen for suppressors of *rsa-1(or598)*

A genetic screen for suppressors of *rsa-1(or598)* was performed to identify other genes in the *rsa-1* pathway. Since the RSA-1 protein did not have any identified protein domains, intragenic suppressors could highlight regions of the protein that are important for its function. Extragenic suppressors could highlight substrates of the RSA-1/PP2A complex or indicate pathways that interact with *rsa-1*.

A suppressor of *rsa-1(or598)* was defined as any second site mutation that exhibited embryonic viability at 26 °C and could be maintained at 25 °C. Chemical mutagenesis with EMS was used to generate random mutations in an outcrossed strain carrying the *rsa-1(or598)* allele. The F2 progeny of the mutagenized worms were then incubated at 25 °C to select for suppressor mutations.

| Round of mutagenesis | Haploid genomes | Number of suppressors | Suppressor alleles |
|---|---|---|---|
| **1** | 17,000 | 1 | *abc2* |
| **2** | 51,000 | 4 | *abc3, abc27-29* |
| **3** | 160,000 | 20 | *abc5-15, abc17-21,abc23-26* |

**Table 3-1. Details of *rsa-1(or598)* EMS suppressor screen**

Three independent rounds of mutagenesis were performed resulting in a total of approximately 200,000 haploid genomes screened (Table 3-1). Twenty-five independent suppressors were isolated. Several suppressors were out-crossed one to four times to

remove background mutations from the stains (Figure 3-14). In many cases the viability of the strains increased, likely due to the removal of unlinked deleterious mutations.

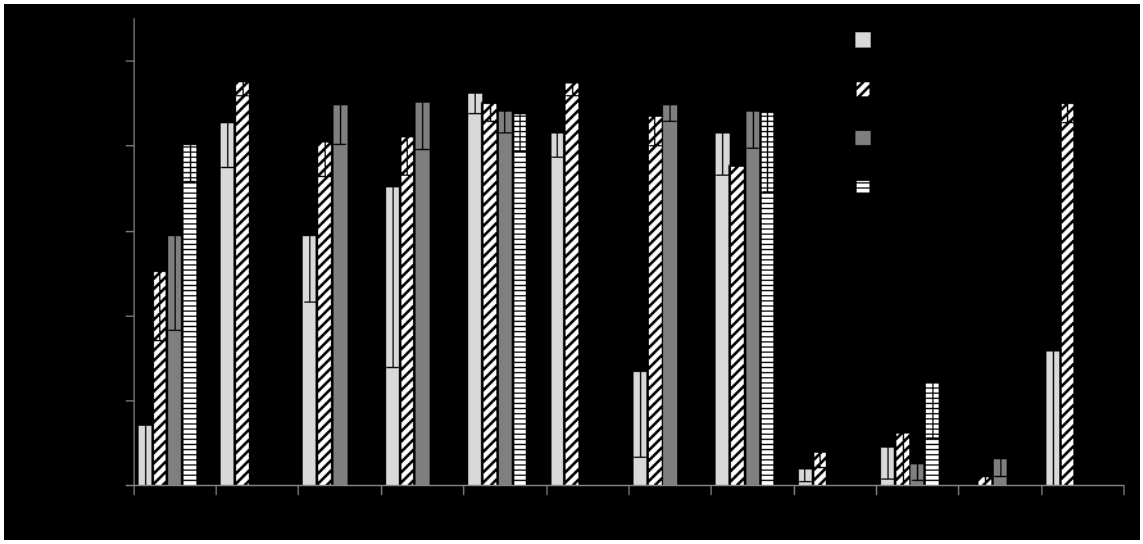

**Figure 3-14. Outcrossing of the *rsa-1(or598)* suppressors**
Hatching rates for *rsa-1(or598)* suppressor strains that were out-crossed one to four times. Error bars are the standard deviation.

Strong suppressors exhibited embryonic viabilities approaching 100%, however several weak suppressors were also isolated. Notably, the *abc17, abc18, abc19,* and *abc25* alleles had embryonic viabilities less than 20% at 26 °C. All of the suppressor strains had a healthy wild-type appearance at permissive temperatures except the originally isolated *abc25* suppressor containing strain, which was dumpy.

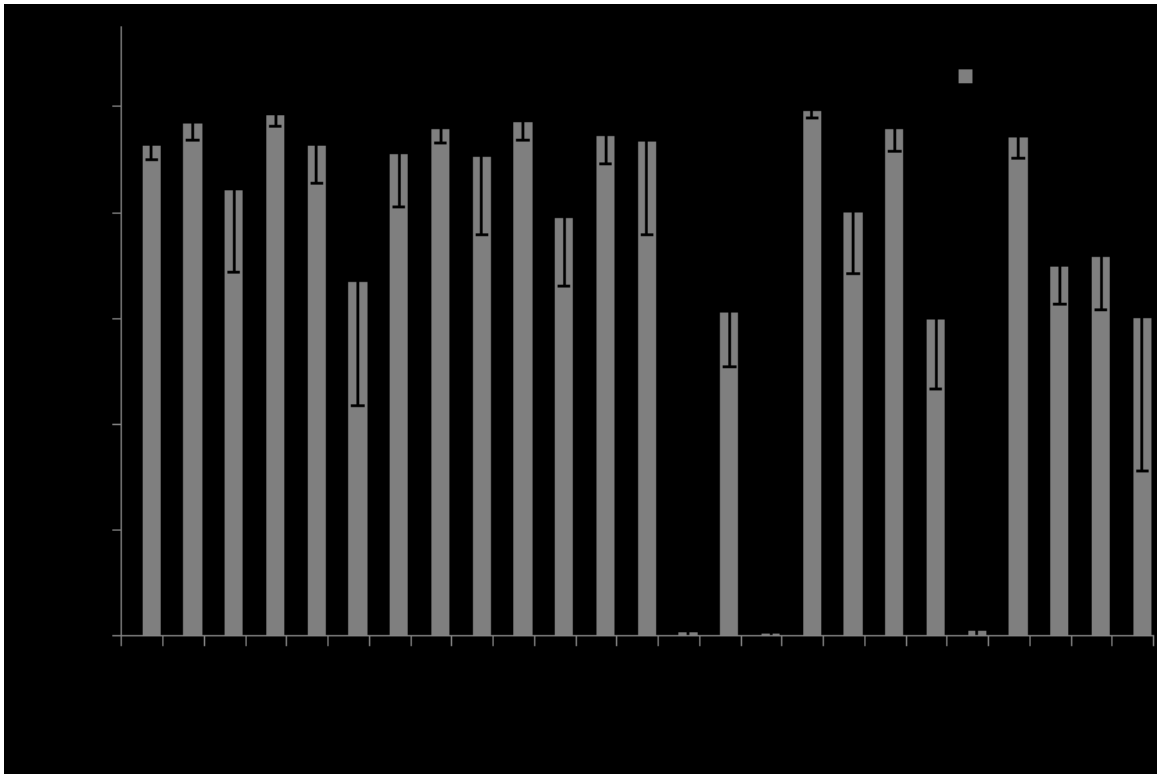

**Figure 3-15. Embryonic viabilities of *rsa-1(or598)* suppressors at 26 °C**
Homozygous and heterozygous hatching rates for embryos produced by the *rsa-1(or598)* suppressors. All strains have the *rsa-1(or598)* mutation which has 0% embryonic viability at 26 °C on its own. Error bars are the standard deviation.

To determine if the suppressors were recessive or dominant they were mated with the original *rsa-1(or598)* strain to generate F1 progeny that were homozygous for *rsa-1(or598)* and heterozygous for the suppressor allele. Recessive suppressors would be unable to suppress the *rsa-1(or598)* phenotype at 26 °C and produce embryos with an embryonic viability of 0% at this temperature. All of the suppressors were dominant because their embryonic viabilities were greater than 0% at 26 °C (Figure 3-15, Table 3-2). As heterozygotes, most of the suppressors conferred embryonic viabilities that were similar to their homozygous hatching rates. However, *abc17*, *abc19*, abc24, *abc25,* and *abc27* had hatching rates that were significantly lower as heterozygotes. *abc2, abc18*, *abc20, and abc23* had embryonic viabilities that were significantly higher as heterozygotes. This observation could be caused by the nature of the suppressor allele or by unrelated mutations that were not removed by out-crossing.

| | | Embryonic Viability | | | | | |
|---|---|---|---|---|---|---|---|
| | Out- | Homozygous | | | Heterozygous | | |
| Allele | crossed | Avg | s.d. | n | Avg | s.d. | n |
| *abc2* | 3x | 80.8 | 9.2 | 506 | 92.5 | 2.6 | 1227 |
| *abc3* | | 97.6 | 1.7 | 584 | 96.7 | 3.0 | 758 |
| *abc5* | 1x | 95.5 | 3.6 | 292 | 84.1 | 15.4 | 832 |
| *abc6* | | 96.7 | 2.6 | 633 | 98.5 | 2.1 | 465 |
| *abc7* | 2x | 89.8 | 9.2 | 576 | 92.7 | 7.1 | 685 |
| *abc8* | | 76.1 | 20.2 | 385 | 66.9 | 23.4 | 813 |
| *abc9* | 2x | 90.4 | 11.1 | 449 | 91.1 | 10.1 | 582 |
| *abc10* | 4x | 94.4 | 3.1 | 791 | 95.8 | 2.7 | 1002 |
| *abc11* | 1x | 95.1 | 3.1 | 758 | 90.5 | 14.8 | 590 |
| *abc12* | | 87.8 | 10.8 | 393 | 97.0 | 3.2 | 403 |
| *abc13* | 2x | 89.8 | 3.9 | 707 | 78.9 | 12.9 | 866 |
| *abc14* | | 85.3 | 12.4 | 224 | 94.4 | 5.2 | 467 |
| *abc15* | 3x | 88.4 | 19.2 | 455 | 93.5 | 17.6 | 723 |
| *abc17* | 1x | 8.3 | 4.1 | 973 | 0.8 | 1.3 | 630 |
| *abc18* | | 2.2 | 4.5 | 313 | 61.0 | 10.0 | 346 |
| *abc19* | 4x | 18.3 | 10.5 | 769 | 0.6 | 0.9 | 623 |
| *abc20* | | 83.0 | 11.9 | 188 | 99.1 | 1.2 | 451 |
| *abc21* | | 69.0 | 14.6 | 210 | 79.9 | 11.5 | 134 |
| *abc23* | | 80.3 | 7.3 | 623 | 95.8 | 4.2 | 476 |
| *abc24* | | 98.7 | 1.7 | 396 | 59.7 | 13.1 | 529 |
| *abc25* | 2x | 6.6 | 4.5 | 1019 | 1.1 | 1.2 | 548 |
| *abc26* | 2x | 90.4 | 4.9 | 794 | 94.3 | 4.0 | 848 |
| *abc27* | | 96.7 | 2.2 | 573 | 69.7 | 7.0 | 422 |
| *abc28* | | 70.8 | 28.4 | 449 | 71.6 | 9.9 | 962 |
| *abc29* | | 82.6 | 7.8 | 511 | 60.2 | 29.0 | 334 |

**Table 3-2. Embryonic viability of *rsa-1(or598)* suppressors at 26 °C**
s.d. is the standard deviation and n is the number of embryos tallied.

### 3.7 **Mapping *rsa-1(or598)* suppressors**

To determine which chromosome the suppressor mutations were located on, linkage analysis with visible markers was performed. All suppressors except *abc18, abc27, abc28,* and *abc29* were mapped.

Linkage analysis of the suppressors was performed with the following phenotypic markers located at the center of their respective linkage groups: *dpy-5(e61) I, bli-2(2768) II, unc-32(e189) III, unc-5(e53) IV, dpy-11(e249) V,* and *lon-2(e670) X*. Since all of the suppressors are dominant, the expectation was that 75% would be suppressed and 25% would not be suppressed. A $\chi^2$ test was used to decide if the suppressor segregated independently from the marker or not. A $\chi^2$ value of less than 3.84 was used to determine that the suppressor segregated independently from the marker.

| Allele | LG I | | | LG II | | | LG III | | | LG IV | | | LG V | | | LG X | | |
|---|---|---|---|---|---|---|---|---|---|---|---|---|---|---|---|---|---|---|
| | Sup. | Not | $\chi^2$ | Sup. | Not | $\chi^2$ | Sup. | Not | $\chi^2$ | Sup. | Not | $\chi^2$ | Sup. | Not | $\chi^2$ | Sup. | Not | $\chi^2$ |
| ***abc2*** | 26 | 31 | **26.3** | 7 | 10 | **10.4** | 1 | 53 | **154.1** | 7 | 8 | **6.4** | 20 | 24 | **20.5** | 16 | 11 | **3.6** |
| ***abc3*** | 40 | 7 | **2.6** | 37 | 6 | **2.8** | 10 | 42 | **86.3** | 18 | 6 | **0.0** | 18 | 6 | **0.0** | 22 | 2 | **3.6** |
| ***abc5*** | 9 | 6 | **1.8** | 16 | 3 | **0.9** | 0 | 9 | **27.0** | 10 | 6 | **1.3** | 18 | 7 | **0.1** | 18 | 5 | **0.1** |
| ***abc6*** | 0 | 22 | **66.0** | 18 | 4 | **0.5** | 22 | 10 | **0.7** | 18 | 6 | **0.0** | 28 | 15 | **2.2** | 26 | 10 | **0.1** |
| ***abc7*** | | | **N/A** | 16 | 1 | **3.3** | 0 | 24 | **72.0** | 10 | 6 | **1.3** | 17 | 7 | **0.2** | 17 | 2 | **2.1** |
| ***abc8*** | 11 | 8 | **3.0** | 20 | 9 | **0.6** | 0 | 41 | **123.0** | 10 | 24 | **37.7** | 25 | 16 | **4.3** | 34 | 10 | **0.1** |
| ***abc9*** | 13 | 7 | **1.1** | 20 | 5 | **0.3** | 1 | 16 | **43.3** | 17 | 5 | **0.1** | 12 | 7 | **1.4** | 19 | 3 | **1.5** |
| ***abc10*** | 22 | 1 | **5.2** | 17 | 2 | **2.1** | 1 | 22 | **61.2** | 3 | 4 | **3.9** | 14 | 14 | **9.3** | 15 | 11 | **4.2** |
| ***abc11*** | 17 | 4 | **0.4** | 18 | 3 | **1.3** | 2 | 18 | **45.1** | 12 | 6 | **0.7** | 14 | 7 | **0.8** | 16 | 5 | **0.0** |
| ***abc12*** | 18 | 6 | **0.0** | 23 | 7 | **0.0** | 1 | 19 | **52.3** | 13 | 7 | **1.1** | 10 | 13 | **12.2** | 21 | 9 | **0.4** |
| ***abc13*** | 11 | 7 | **1.9** | 15 | 7 | **0.5** | 0 | 14 | **42.0** | 6 | 7 | **5.8** | 8 | 7 | **3.8** | 12 | 7 | **1.4** |
| ***abc14*** | 11 | 5 | **0.3** | 24 | 4 | **1.7** | 0 | 9 | **27.0** | 13 | 4 | **0.0** | 16 | 6 | **0.1** | 14 | 6 | **0.3** |
| ***abc15*** | 14 | 7 | **0.8** | 14 | 0 | **4.7** | 8 | 11 | **11.0** | 16 | 2 | **1.9** | 13 | 4 | **0.0** | 12 | 6 | **0.7** |
| ***abc17*** | 0 | 22 | **66.0** | 14 | 7 | **0.8** | 6 | 14 | **21.6** | 1 | 20 | **55.3** | 2 | 22 | **56.9** | 8 | 12 | **13.1** |
| ***abc19*** | 18 | 6 | **0.0** | 14 | 8 | **1.5** | 12 | 5 | **0.2** | 24 | 21 | **11.3** | 17 | 31 | **40.1** | 39 | 8 | **1.6** |
| ***abc20*** | 1 | 21 | **58.2** | 18 | 6 | **0.0** | 18 | 7 | **0.1** | 9 | 4 | **0.2** | 14 | 7 | **0.8** | 12 | 5 | **0.2** |
| ***abc21*** | 3 | 12 | **24.2** | 16 | 5 | **0.0** | 6 | 6 | **4.0** | 12 | 5 | **0.2** | 12 | 4 | **0.0** | 17 | 5 | **0.1** |
| ***abc23*** | 19 | 4 | **0.7** | 22 | 3 | **2.3** | 1 | 41 | **118.1** | 14 | 2 | **1.3** | 16 | 4 | **0.3** | 17 | 4 | **0.4** |
| ***abc24*** | 0 | 19 | **57.0** | | | **N/A** | | | **N/A** | 11 | 4 | **0.0** | 15 | 7 | **0.5** | 16 | 7 | **0.4** |
| ***abc25*** | 11 | 7 | **1.9** | 11 | 14 | **12.8** | 15 | 6 | **0.1** | 11 | 8 | **3.0** | 14 | 10 | **3.6** | 11 | 12 | **9.1** |
| ***abc26*** | 3 | 17 | **38.4** | 11 | 5 | **0.3** | 0 | 20 | **60.0** | 5 | 11 | **16.3** | 7 | 10 | **10.4** | 2 | 12 | **27.5** |

**Table 3-3 Genetic mapping to assign suppressors to a linkage group**
$\chi^2$ value of > 3.84 are gray. "Sup" refers to the number of suppressed hermaphrodites scored.

The mapping was performed with the original non-outcrossed suppressor strains. Many weak suppressor strains exhibited very poor embryonic viability, in which case the $\chi^2$ test was not able to provide an unambiguous genetic map position. Weak suppressors could be scored as "not suppressed" even when a copy of the suppressor allele was present and this skewed the mapping data to suggest that alleles did not segregate independently from multiple markers. Several suppressors mapped to multiple chromosomes (Table 3-3). For example, *abc2* had $\chi^2$ values of greater than 3.84 for all chromosomes except the X. However, the $\chi^2$ value for linkage group III was much greater than 3.84 so the suppressor allele was probably located on chromosome III.

### 3.8 **Identification of intragenic suppressors**

Eight suppressors did not segregate independently from the *dpy-5* marker on linkage group I (Table 3-3) so I concluded that these suppressors were likely located on this chromosome. Since the *rsa-1* gene was located on chromosome I, it was sequenced in the linked and unmapped suppressors. Second-site mutations in *rsa-1* were identified in six of these strains (Table 3-4).

| Genotype | Base pair sub. | Amino acid sub. |
|---|---|---|
| *rsa-1(or598)* | A956G | D319G |
| *rsa-1(or598, abc6)* | G955A | G319S |
| *rsa-1(or598, abc20)*<br>*rsa-1(or598, abc21)* | C1004T | S335L |
| *rsa-1(or598, abc24)*<br>*rsa-1(or598, abc27)* | G967A | D323N |
| *rsa-1(or598, abc29)* | C1099A | L367M |

**Table 3-4. Mutations in intragenic suppressors**
Nucleotide positions are in the spliced transcript C25A1.9a.

All of the intragenic suppressors were missense mutations that were predicted to cause amino acid substitutions in the RSA-1 protein (Figure 3-16). For comparison, a previously characterized allele, *rsa-1(dd13)*, which causes a splice site mutation that results in a truncated protein, is included in the figure.

The intragenic mutations were clustered near the original *or598* lesion and the 6 mutations affected four residues in total. One suppressor, *abc6*, mutated the same residue as the *or598* allele. In the wild-type RSA-1 protein, amino acid 319 is an aspartic acid residue while in the *or598* mutant it is a glycine. The *abc6* mutation does not revert this

amino acid to wild-type, instead the suppressor mutant had a serine at this position. The transitions G967A and C1004T both independently arose twice in the suppressor screen. *abc29* is the mutation that is farthest away from the original *or598* lesion and is 49 amino acids downstream. Since these mutations are contained in a domain they could provide information about this region. Without additional experiments and information, these alleles are not informative.

The original *or598* mutation and two suppressors affect amino acids in a region of RSA-1 that has similarity to a characterized calcium binding domain in human PP2A B'' regulatory subunit called PR72. PR72 has been shown to bind two calcium ions with two EF hand domains (Janssens et al., 2003) termed EF1 and EF2. The possibility that RSA-1 could bind calcium ions is explored in section 5.2.3 of this thesis.

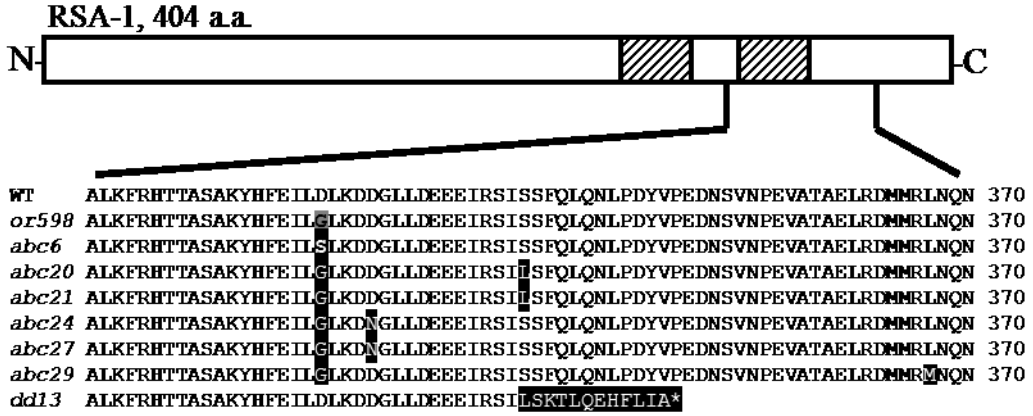


**Figure 3-16. Intragenic suppressors of *rsa-1(or598)***
Partial amino acid sequence of RSA-1 in Wild-type, *rsa-1(or598)*, intragenic suppressors, and the predicted protein caused by the *rsa-1(dd13)* splice site mutation. The striped boxes indicate the region of RSA-1 that has similarity to the $Ca^{2+}$ binding EF hands of human PP2A B'' regulatory subunit PR72.

### 3.9 SNP-mapping to refine *abc2* map position

Sixteen suppressors were linked to *unc-32* on chromosome III (Table 3-3). Since the suppressors were dominant, complementation testing could not be used to ensure they belonged to the same complementation group. Nevertheless, *abc2* was chosen as a representative suppressor to further refine the map position on the chromosome. The *abc2* mapping data had one recombination event between *abc2* and *unc-32* in the 53 progeny that were analyzed. This suggested that *abc2* was approximately 2 cM away from *unc-32* on the chromosome. Since this type of analysis was unable to determine if the suppressor

was to the left or right of the marker, I concluded that *abc2* was between -2 and +2 cM on LG III.

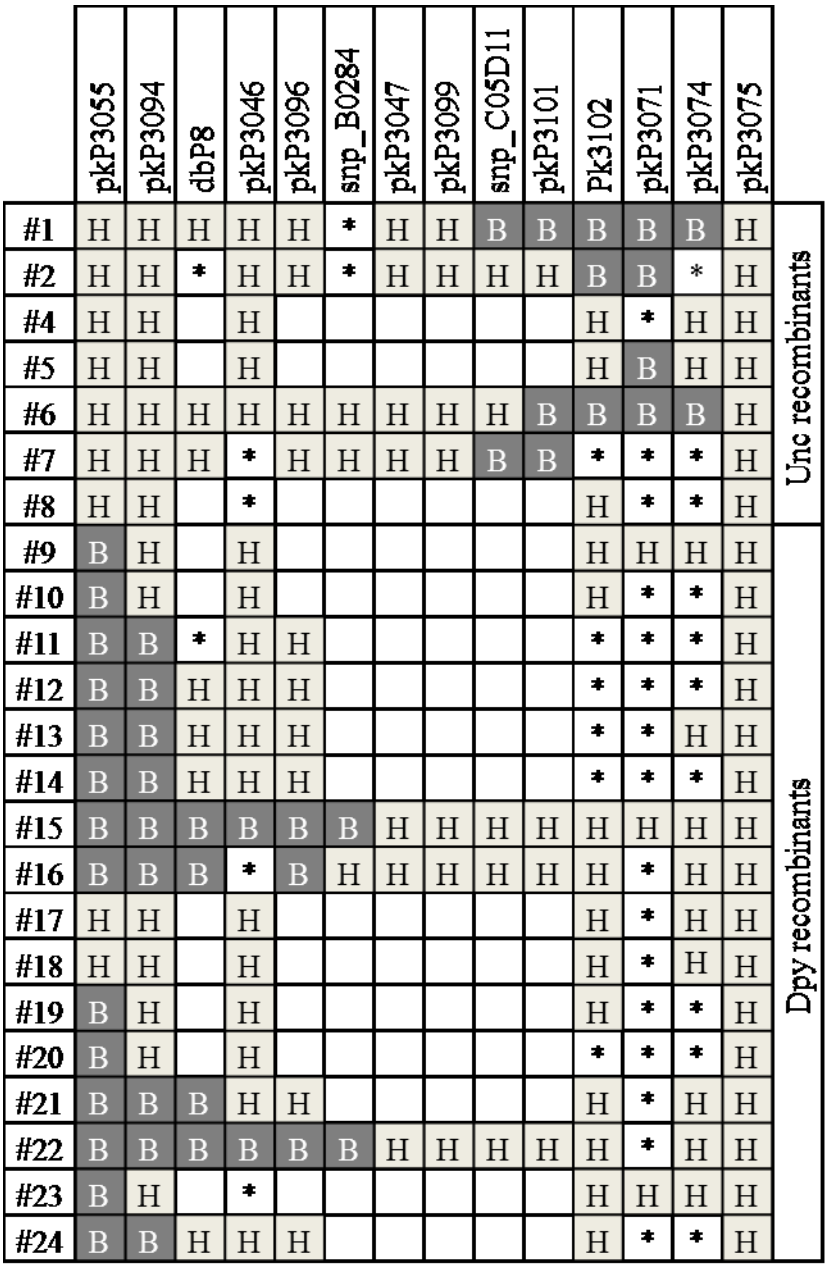

| | pkP3055 | pkP3094 | dbP8 | pkP3046 | pkP3096 | snp_B0284 | pkP3047 | pkP3099 | snp_C05D11 | pkP3101 | Pk3102 | pkP3071 | pkP3074 | pkP3075 | |
|---|---|---|---|---|---|---|---|---|---|---|---|---|---|---|---|
| #1 | H | H | H | H | H | * | H | H | B | B | B | B | B | H | Unc recombinants |
| #2 | H | H | * | H | H | * | H | H | H | H | B | B | * | H | |
| #4 | H | H | | H | | | | | | | H | * | H | H | |
| #5 | H | H | | H | | | | | | | H | B | H | H | |
| #6 | H | H | H | H | H | H | H | H | H | B | B | B | B | H | |
| #7 | H | H | H | * | H | H | H | H | B | B | * | * | * | H | |
| #8 | H | H | | * | | | | | | | H | * | * | H | |
| #9 | B | H | | H | | | | | | | H | H | H | H | Dpy recombinants |
| #10 | B | H | | H | | | | | | | H | * | * | H | |
| #11 | B | B | * | H | H | | | | | | * | * | * | H | |
| #12 | B | B | H | H | H | | | | | | * | * | * | H | |
| #13 | B | B | H | H | H | | | | | | * | * | H | H | |
| #14 | B | B | H | H | H | | | | | | * | * | * | H | |
| #15 | B | B | B | B | B | B | H | H | H | H | H | H | H | H | |
| #16 | B | B | B | * | B | H | H | H | H | H | H | * | H | H | |
| #17 | H | H | | H | | | | | | | H | * | H | H | |
| #18 | H | H | | H | | | | | | | H | * | H | H | |
| #19 | B | H | | H | | | | | | | H | * | * | H | |
| #20 | B | H | | H | | | | | | | * | * | * | H | |
| #21 | B | B | B | H | H | | | | | | H | * | H | H | |
| #22 | B | B | B | B | B | B | H | H | H | H | H | * | H | H | |
| #23 | B | H | | * | | | | | | | H | H | H | H | |
| #24 | B | B | H | H | H | | | | | | H | * | * | H | |

**Figure 3-17 Summary of all Snip-SNP mapping results**
Bristol (B) or Hawaiian (H) genotypes were determined for a variety of RFLPs on chromosome III (shown along the top). Asterisks indicate results were inconclusive and blank squares were not tested. Recombinants #1-8 are Unc-Non-suppressed and #9-24 are Dpy-Non-suppressed.

The snip-SNP mapping of twenty three recombinants refined the position of *abc2* between -3.18 and -1.29 cM on chromosome III (Figure 3-17 and Figure 3-18). Recombinants #1, 7, 15 and 22 were the most informative recombinants and additional

polymorphisms could have been used to further refine the map position. This region on chromosome III represented over 2 Mbp and more than 600 predicted genes. *paa-1,* the gene that encodes the structural subunit of the PP2A complex, is in this region. Genomic DNA from an *abc2* strain was isolated and the *paa-1* gene was sequenced. A single base pair substitution that results in a missense mutation was identified in *paa-1*.

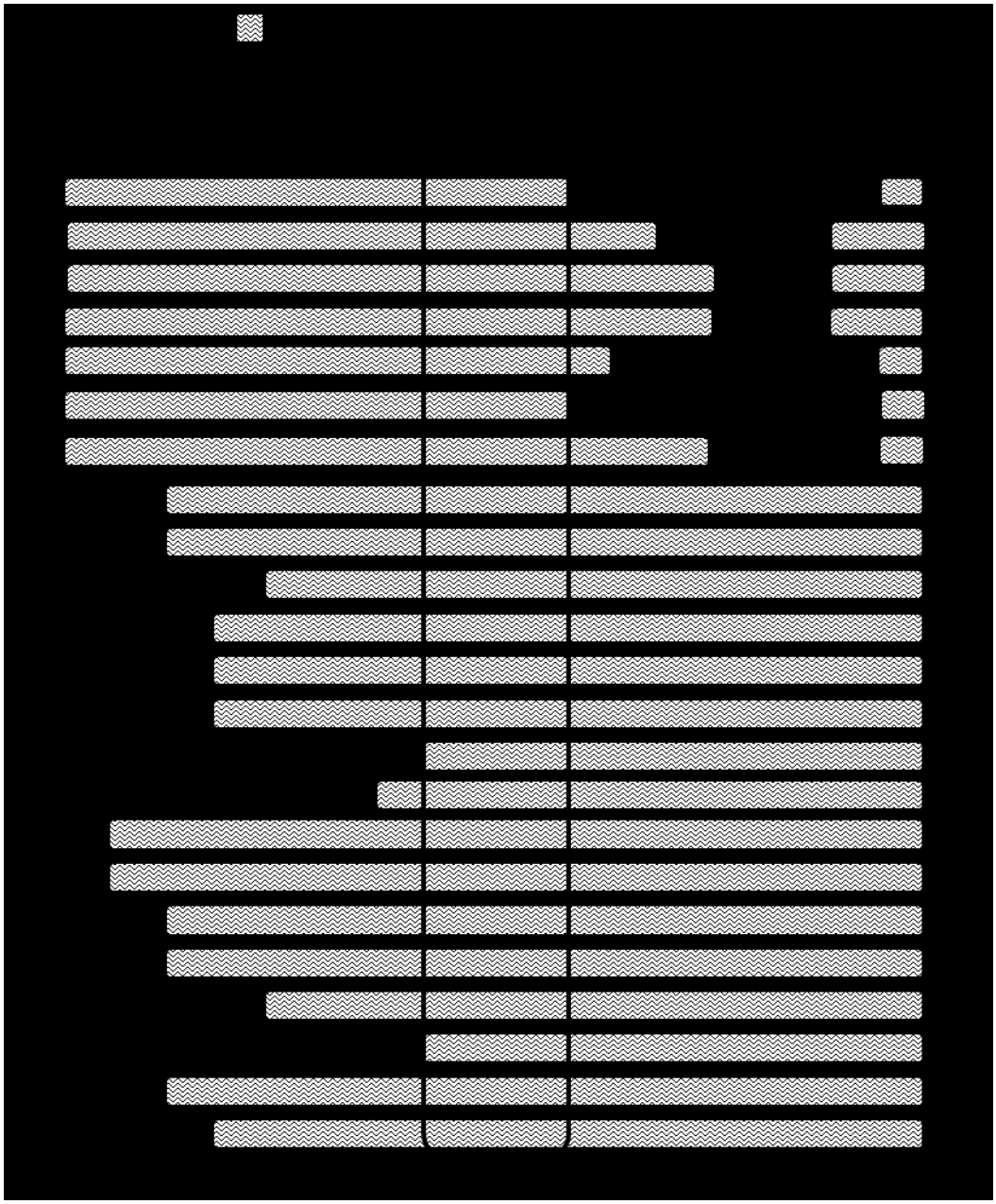

**Figure 3-18. Schematic of recombinant chromosomes**
Summary of all Snip-SNP mapping data as a schematic of the inferred chromosomes generated from the recombination events. *abc2* was mapped between -3.18 and -1.29 cM on LG III.

### 3.10 **Identification of suppressor mutations in *paa-1***

The observation that *abc2* had a mutation in the *paa-1* gene prompted me to sequence *paa-1* in the remaining suppressors that were linked to LG III as well as the unmapped suppressors. Mutations in *paa-1* were identified in sixteen of the suppressors and were divided into five groups based on the affected residue in *paa-1* (Table 3-5). Independently isolated mutations that affected the same residue were identified in four of the five groups of suppressors in *paa-1*. The C67T transition arose nine times. Two lesions were observed in the *paa-1* coding region in the *abc13* suppressor strain.

The *paa-1* gene is highly conserved between *C. elegans* and humans; the PAA-1 protein shares 62.9% identity and 76.6% similarity with the human PP2A structural subunit PPP2R1A/PR65α. The amino acids mutated by the *paa-1* suppressors all affected conserved residues between humans and *C. elegans* (Figure 3-19), which suggested that these suppressor mutations could provide information about the human protein.

| Suppressors | Base pair sub. | Amino acid sub. |
|---|---|---|
| *paa-1(abc2)*<br>*paa-1(abc23)* | G451A | G151R |
| *paa-1(abc3)*<br>*paa-1(abc5)*<br>*paa-1(abc7)*<br>*paa-1(abc9)*<br>*paa-1(abc10)*<br>*paa-1(abc11)*<br>*paa-1(abc12)*<br>*paa-1(abc15)*<br>*paa-1(abc18)* | C67T | R23C |
| *paa-1(abc8)*<br>*paa-1(abc28)* | G316A | V106I |
| *paa-1(abc13)* | G316A, C461G | V106I, S154C |
| *paa-1(abc14)*<br>*paa-1(abc26)* | G68A | R23H |

**Table 3-5. Mutations and amino acid substitutions in *paa-1* that suppress *rsa-1(or598)***
Nucleotide positions are in the spliced transcript F48E8.5.1.

The crystal structure for the human PP2A structural subunit,PR65α, has been solved several times (Cho and Xu, 2006; Groves et al., 1999; Strack et al., 2002; Xu et al., 2006; Xu et al., 2008). The protein consists of 15 tandem HEAT repeats that are joined with a short linker, forming a horseshoe shape. Each HEAT repeat is composed of two helices

with one facing the outside and the other facing the inside of the semi-circle shape. Since the PP2A structural subunit is so highly conserved, the *C. elegans* PAA-1 protein likely has a very similar structure. The amino acids affected by the suppressor mutations are all located on the ridge between helices and in the inner helix of HEAT repeats 1 to 4. This suggested that this region of the protein could be involved in an RSA-1 related function.

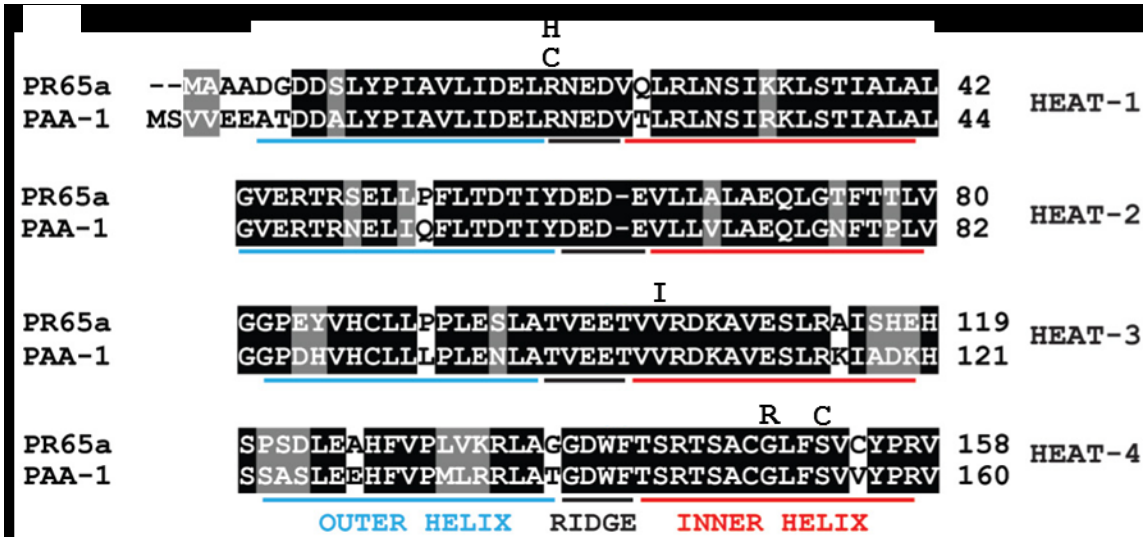


**Figure 3-19. *rsa-1(or598)* suppressors cause missense mutations in *paa-1***
Protein alignment of PAA-1 with the human PP2A structural subunit, PR65α. Amino acid substitutions in suppressors are indicated with above the sequence.

### 3.11 *paa-1(abc2)* is an allele-specific suppressor

To determine if suppression by *paa-1(abc2)* was specific to the *rsa-1(or598)* mutation, I tested if *paa-1(abc2)* could suppress the embryonic lethality caused by the *rsa-1(dd13)* allele. This allele affects splicing of the *rsa-1* gene and was previously predicted to be a null allele (Schlaitz et al., 2007). The *rsa-1(dd13); paa-1(abc2)* double mutant had 0% embryonic viability (n=85) while *rsa-1(or598); paa-1(abc2)* had an embryonic viability of 80.8% (s.d. 9.2%, n=506). Therefore, I concluded that *paa-1(abc2)* was an allele specific suppressor because it was unable to suppress the *rsa-1(dd13)* allele.

### 3.12 *rsa-1(or598)* disrupts the protein interaction with PAA-1

RSA-1 is required to recruit the core PP2A complex, PAA-1 and LET-92, to the centrosomes (Schlaitz et al., 2007). Since suppressor mutations were identified in RSA-1 and PAA-1, it was possible that these were interaction suppressors. Interaction suppressors are allele-specific and the *paa-1(abc2)* suppressor was unable to suppress

*rsa-1(dd13)* which provided support for this hypothesis. To investigate the possibility that the intragenic and *paa-1* suppressors might be interaction suppressors, immunostaining with a α-PAA-1 and α-RSA-1 antibodies was performed (Figure 3-20).

In wild-type and *rsa-1(or598)* embryos, the RSA-1 protein was observed at the centrosomes. The RSA-1 protein was not detected in *rsa-1(dd13)* and *rsa-1(RNAi)* embryos, which was consistent with previous results (Schlaitz et al., 2007). In wild-type embryos, specific staining for PAA-1 was observed in the cytoplasm, nuclear envelope, on the centrosomes, on the spindle, and at P-granules. In *rsa-1(or598)* embryos, the subcellular localization of PAA-1 to the centrosomes was specifically disrupted. In *rsa-1(RNAi)* embryos, PAA-1 was not observed at the centrosomes, which was consistent with previous results indicating that RSA-1 targets PP2A to the centrosomes (Schlaitz et al., 2007). Unexpectedly, PAA-1 was observed at the centrosomes in *rsa-1(dd13)* embryos. This allele is predicted to disrupt a splice site in the transcript that introduces a premature stop codon. Since the RSA-1 protein was not detected in *rsa-1(dd13)* embryos, it was hypothesized that *dd13* could be a null allele (Schlaitz et al., 2007). However, these results show that PAA-1 was recruited to the centrosome in *rsa-1(dd13),* suggesting that a truncated, but partially functional RSA-1(dd13) protein is sufficient for the centrosomal localization of PAA-1.

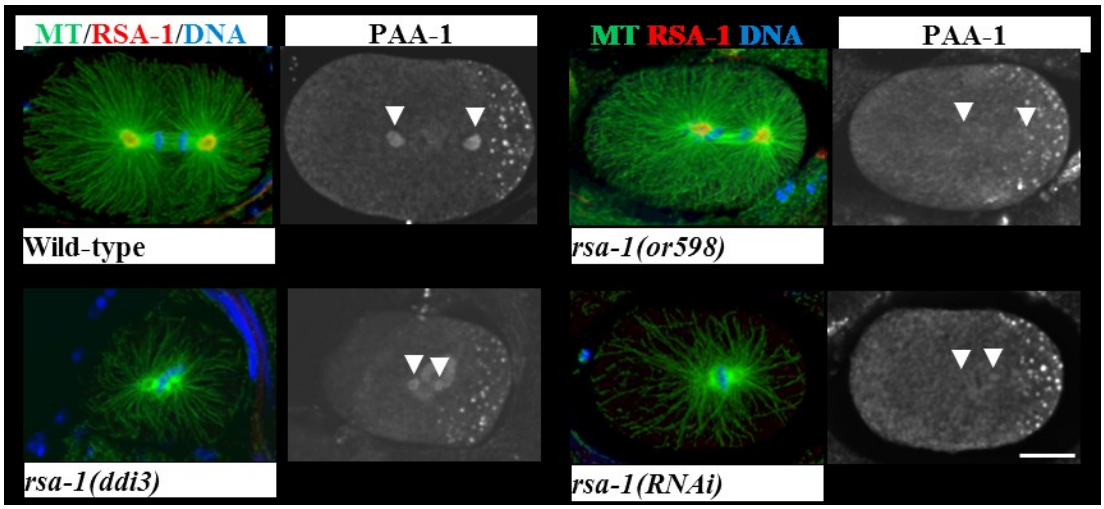


**Figure 3-20. Centrosomal localization of PAA-1 is sensitive to *rsa-1* function**
Immunostaining of PAA-1 and RSA-1 in wild-type, *rsa-1(or598*), *rsa-1(dd13),* and *rsa-1(RNAi)* at 26°C. Arrowheads indicate the centrosomes and the scale bar is 10 µm. PAA-1 is not recruited to the centrosomes in *rsa-1(RNAi)* or *rsa-1(or598)* embryos.

The immunostaining results showed that RSA-1(or598) cannot efficiently recruit PAA-1 to the centrosome, but this could be due to an indirect interaction with an intermediate protein. To test whether or not the *or598* mutation disrupted a physical interaction between the PAA-1 and RSA-1 proteins, a yeast two hybrid assay was performed (Figure 3-21). Growth of yeast on the selective media (SC-trp-leu-his) indicated that the two proteins, one fused to the activation domain (AD) and one to the DNA-binding domain (BD), are capable of a protein interaction.

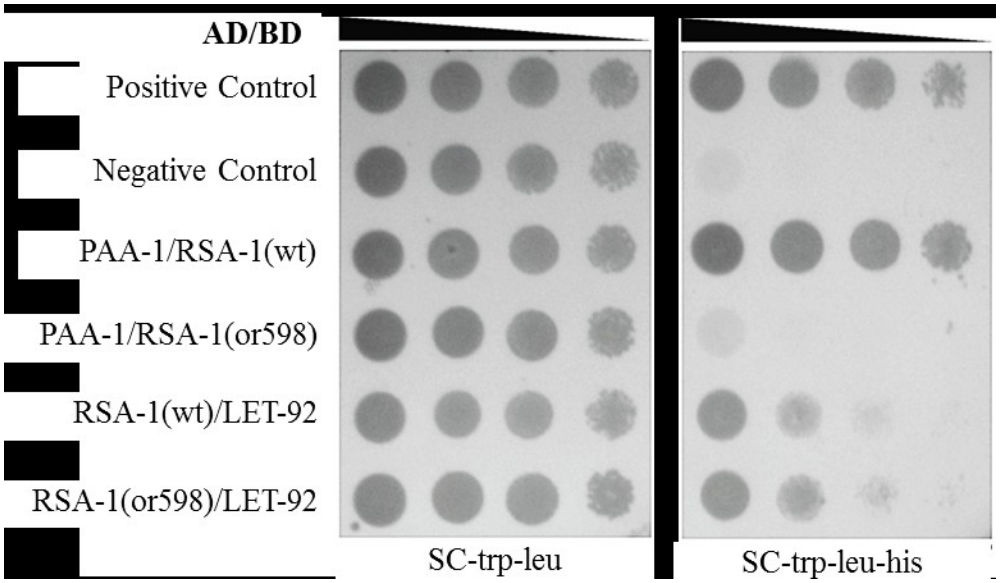


**Figure 3-21. Yeast two hybrid assay with RSA-1 and PP2A core subunits**
Yeast transformed with two plasmids and dilutions plated on control (SC-trp-leu) and selective (SC-trp-leu-his) media. Each construct was a fusion protein with either a transcription activating domain (AD) or a DNA binding domain (BD). PAA-1 is the structural PP2A subunit and LET-92 is the catalytic subunit. The *rsa-1(or598)* missense mutation disrupts the protein interaction with PAA-1 but not LET-92.

Growth on the selective media was observed with the RSA-1/PAA-1 constructs and the RSA-1/LET-92 constructs. These results suggested that wild-type RSA-1 was able to interact with the structural and catalytic subunits of the PP2A complex. RSA-1(or598) did not grow on the selective media when PAA-1 was present but did grow with LET-92, suggesting the *rsa-1(or598)* missense mutation specifically disrupted the protein interaction between RSA-1 and PAA-1.

### 3.13 **Suppressors in PP2A restore RSA-1/PAA-1 interaction**

Since the *rsa-1(or598)* mutation specifically disrupted the protein interaction between RSA-1 and PAA-1, I hypothesized that the intragenic and *paa-1* suppressors should

restore this protein interaction. One representative allele from each class of the four intragenic suppressor and five *paa-1* suppressors were used for this analysis. Each of these strains were immunostained to determine if PAA-1 was observed at the centrosomes in these embryos (Figure 3-22). Both RSA-1 and PAA-1 localized to the centrosomes in all of the representative intragenic and *paa-1* suppressors strains.

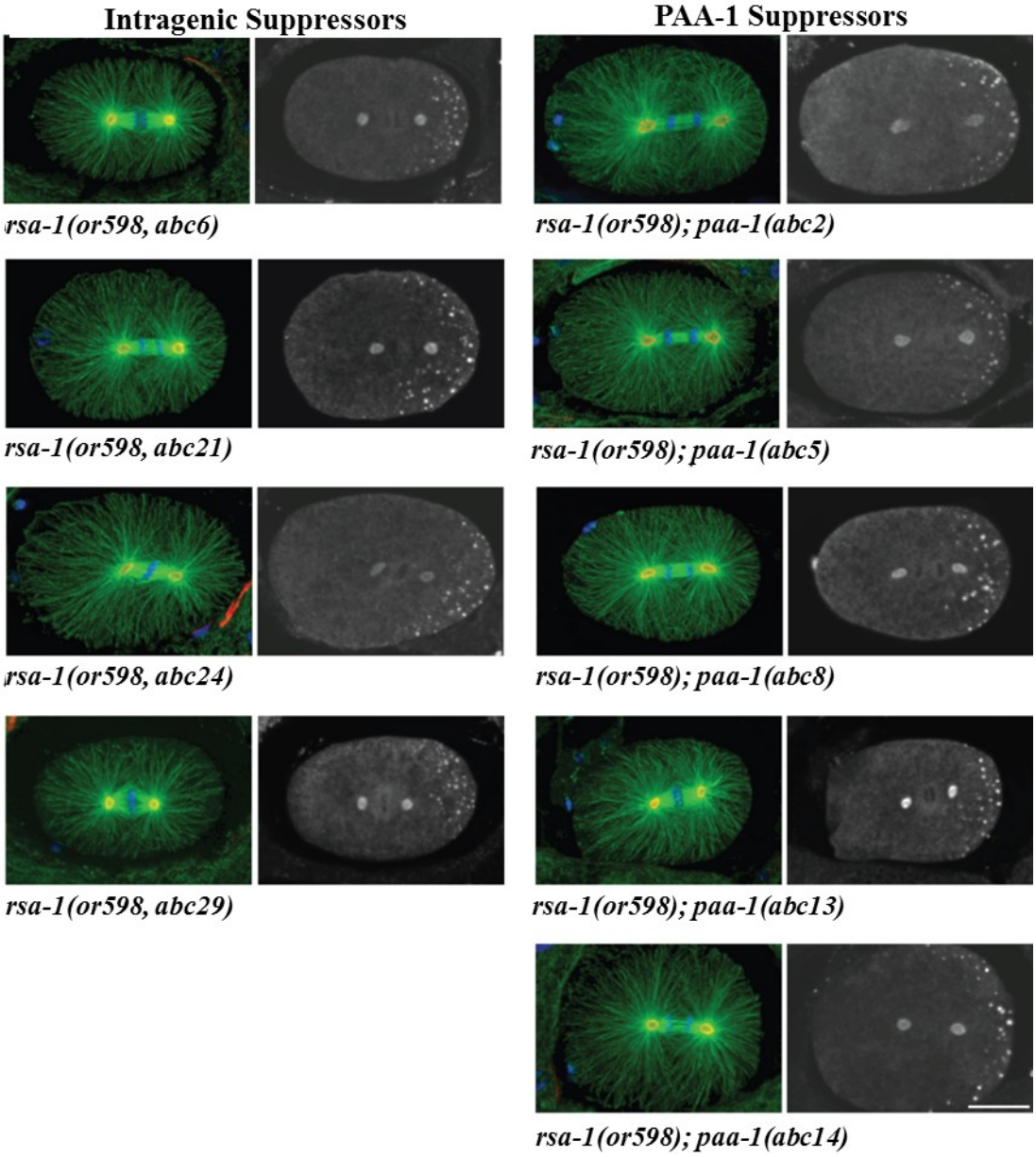


**Figure 3-22. Localization of PAA-1 in PP2A subunit suppressors**
Immunostaining of PAA-1 and RSA-1 in suppressors at 26°C. The scale bar is 10 µm. All intragenic and *paa-1* suppressors restore PAA-1 recruitment to the centrosome.

To determine if the suppressors restored the PAA-1 to wild-type levels, the ratio of the fluorescence intensity of PAA-1 to RSA-1 was calculated. Embryos from wild-type, *rsa-1(or598)*, one representative intragenic suppressor, and one representative *paa-1* suppressor strain were analyzed (Figure 3-23). The data showed that levels of the PAA-1 protein were significantly reduced in *rsa-1(or598)* embryos and that the suppressor mutations restored wild-type levels of centrosomal PAA-1.

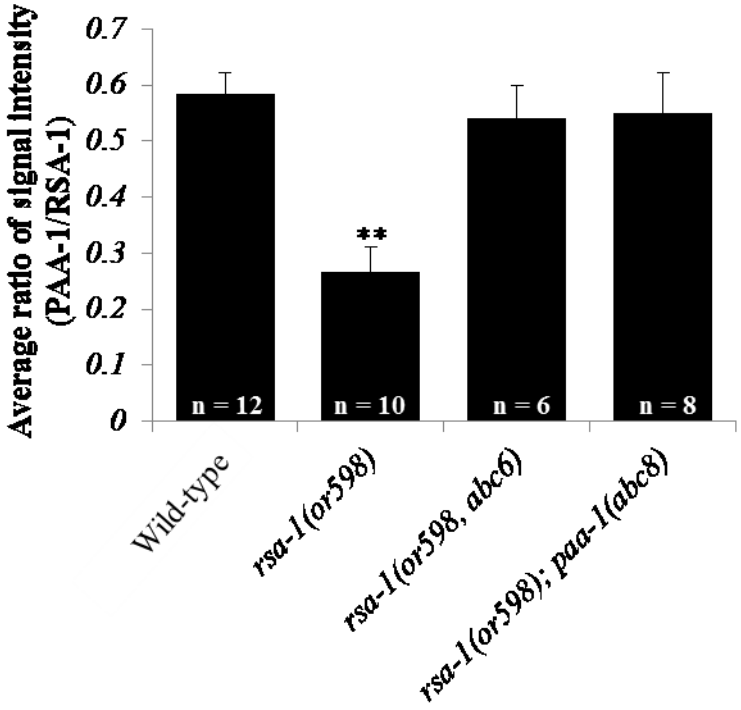


**Figure 3-23. Quantification of PAA-1 levels at the centrosome**
The average integrated signal intensity of PAA-1 at the centrosome relative to RSA-1. n is the number of centrosomes in the analysis. ** indicates a p-value of less than 0.0001. Suppressors restore PAA-1 levels at the centrosome to wild-type levels.

To confirm that the centrosomal location of PAA-1 in the suppressor strains was due to a restored protein interaction between RSA-1 and PAA-1, a yeast two hybrid assay was performed (Figure 3-24). RSA-1(abc6) contains the D319S alteration and this mutant protein was found to interact with the wild-type PAA-1 protein as determined by growth on selective media. I also found that the single amino acid substitution in PAA-1(abc8), V106I, restored the protein interaction with the mutant RSA-1(or598) protein.

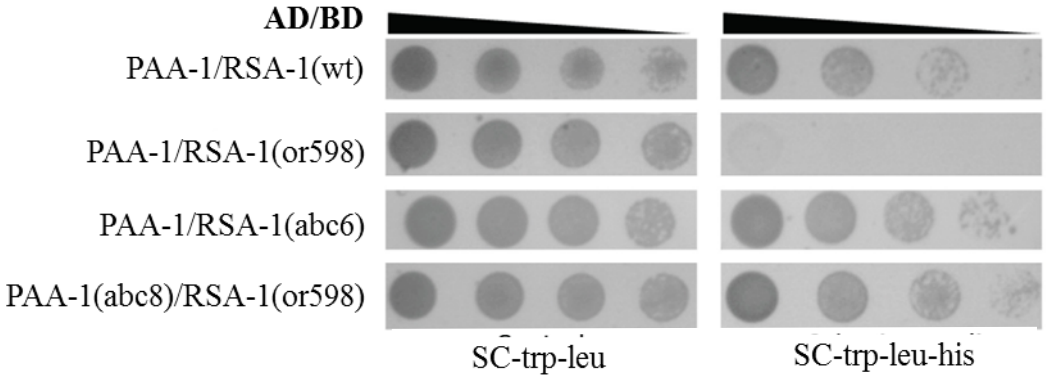


**Figure 3-24. Yeast two hybrid assay with interaction suppressors.**
Yeast transformed with two plasmids and plated on control (SC-trp-leu) and selective (SC-trp-leu-his) media. Each construct was a fusion protein with either a transcription activating domain (AD) or a DNA binding domain (BD. Representative intragenic and *paa-1* mutation restore protein interaction between RSA-1 and PAA-1.

### 3.14 PAA-1 mutations have no obvious deleterious phenotypes

To determine if the *paa-1* suppressors cause embryonic lethality in an *rsa-1(+)* background, strains were generated with the representative *paa-1* suppressors in an otherwise wild-type genetic background. Sequencing of the *rsa-1* and *paa-1* genes was used to confirm the genotypes of the strains. At 26 °C the only strain that caused embryonic lethality was *paa-1(abc2)* (Table 3-6). However, the embryonic viability of the strain that contained *paa-1(abc2)* was highly variable ranging from 21.7% to 100% suggesting that an unrelated mutation could be responsible for the decreased viability.

| Genotype | Avg | s.d | n |
|---|---|---|---|
| *paa-1(abc2)* III | 77.8 | 25.1 | 481 |
| *paa-1(abc5)* III | 99.4 | 1.4 | 480 |
| *paa-1(abc8)* III | 96.9 | 2.8 | 327 |
| *paa-1(abc13)* III | 97.4 | 2.0 | 348 |
| *paa-1(abc14)* III | 97.8 | 4.1 | 322 |

**Table 3-6. *paa-1* mutations in an otherwise wild-type background**
Embryonic viability (%) at 26˚C. s.d. is the standard deviation and n is the total number of embryos.

*paa-1(RNAi)* resulted in 100% embryonic lethality (n=986). Since the mutations in *paa-1* recovered as suppressors of *rsa-1(or598)* did not cause embryonic lethality, then the mutant PAA-1 proteins must be able to fulfill their wild-type functions. These data were consistent with the α-PAA-1 immunostaining results because the localization of PAA-1 was not obviously disrupted (Figure 3-22). In the strains that contained *paa-1*

suppressor mutations, PAA-1 localization to P-granules, the nuclear envelope, and the spindle was not obviously disrupted.

### 3.15 **Further characterization of the non-interaction suppressors: *abc17, abc19,* and *abc25***

The identity of three suppressor mutations remains unconfirmed. These suppressors all exhibited embryonic viabilities less than 20%, and the linkage analysis was not conclusive. While the identity of these suppressors is required to fully elucidate the basis for suppression of *rsa-1(or598)*, an initial characterization was nonetheless performed to provide clues on how the mutations might restore embryonic viabilities to *rsa-1(or598)* embryos.

Preliminary results pertaining to these suppressor alleles are also presented in Appendix B of this thesis. These results have been omitted from this chapter because they are preliminary and have not been repeated. The appendix includes whole genome sequencing data and RNAi experiments to test whether candidate genes confer suppression of *rsa-1(or598)*.

#### 3.15.1 Dpy phenotype in *abc25* suppressor

When *abc25* was isolated in the suppressor screen, the worms had an obvious Dpy phenotype. It was possible that the Dpy phenotype was caused by a mutation unrelated to the suppressor or that the suppressor mutation caused the Dpy phenotype. To distinguish these possibilities the Dpy *abc25* strain was mated with *rsa-1(or598)* males. The wild-type F1 from this cross were then self-fertilized to determine if the Dpy phenotype was linked to the suppressor phenotype (Figure 3-25A). In this cross, 69% of the Dpy F2 progeny were not suppressed (Figure 3-25B). This indicated that the suppressor and Dpy mutation segregated independently and were not caused by the same mutation. Three wild-type suppressed F2 were generated in this cross and were used to isolate an *abc25* homozygous strain that did not segregate Dpy progeny.

| | Not Sup | Sup | $\chi^2$ |
|---|---|---|---|
| Dpy | 11 (69%) | 5 (31%) | 2.0 |
| WT | 10 (77%) | 3 (23%) | --- |

**Figure 3-25. Determining if *abc25* confers a Dpy phenotype**
A) Scheme to determine if the Dpy phenotype is linked to *abc25*. B) Summary of the F2 progeny from crossing MAS80 hermaphrodite to MAS39 males. A $\chi^2$ value $> 3.84$ indicates that the suppressor and Dpy phenotypes are linked.

### 3.15.2 DIC microscopy of abc17, abc19, and abc25

Since *abc17, abc19,* and *abc25* exhibited embryonic viabilities of under 20% (Table 3-2) it suggested that they may only weakly suppress the *rsa-1(or598)* phenotype or that they cause lethality. DIC microscopy of the first mitotic division was performed to determine which mitotic phenotypes were present in these suppressors (Figure 3-26). For this analysis the hermaphrodites were cultured at 26 °C and imaged at room temperature.

Using DIC microscopy, many key features of the first mitosis can be observed in wild-type embryos (Figure 3-26). The female pronucleus migrates to the posterior of the embryo where it meets the male pronucleus and then they center and rotate in the embryo. This rotation places the centrosomes and spindle parallel to the length of the embryo. After nuclear envelope breakdown the centrosomes and the spindle can be observed in most embryos. During anaphase the spindle rocks and elongates as the DNA is segregated. A cytokinetic furrow ingresses and divides the two daughter cells apart. In

*C. elegans* the first division is asymmetric with a larger anterior and smaller posterior cell.

In *rsa-1(or598)* embryos, the pronuclei met in the posterior of the cell (5/5) but usually failed to properly center and rotate (1/5). In addition, pole-to-pole distances, discernable using DIC optics, indicated that the metaphase spindle was always smaller than wild-type. In some embryos cytokinesis failed (1/5) and in the remainder of embryos that successfully completed cytokinesis the posterior cell was smaller than the posterior cells observed in wild-type embryos.

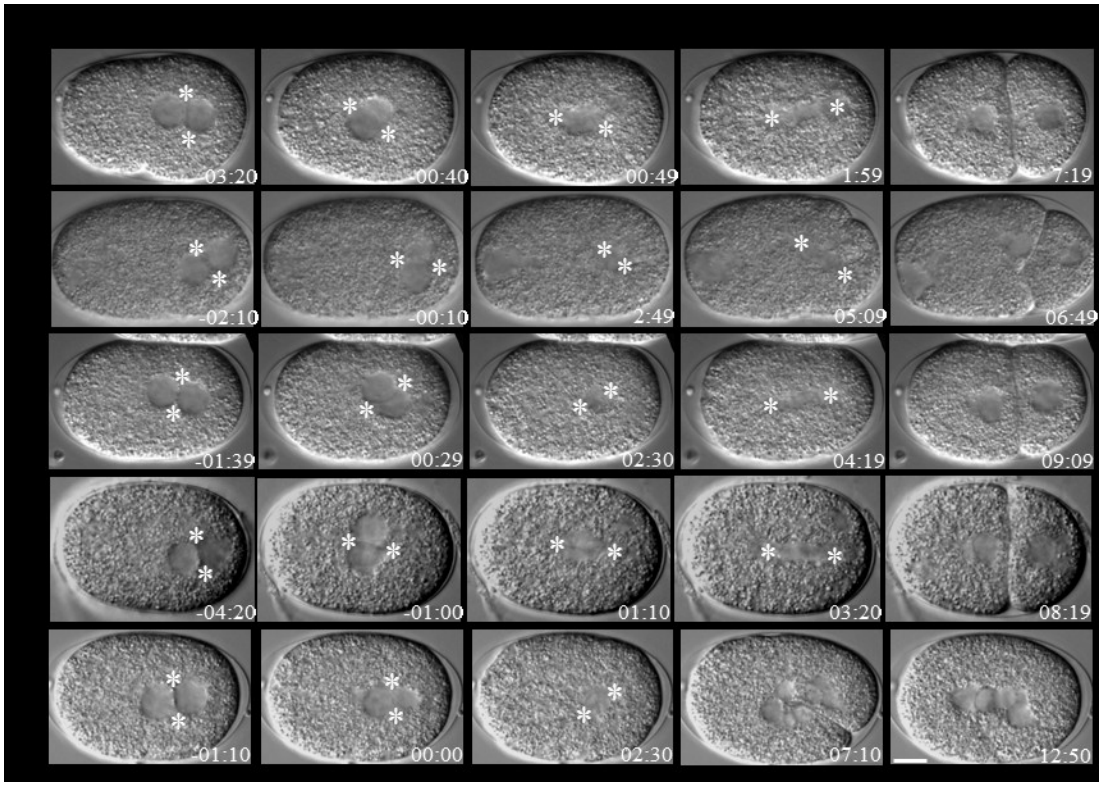


**Figure 3-26. The first mitosis in *abc17, abc19,* and *abc25*suppressor containing strains**
DIC images of the first mitotic division in *C. elegans* embryos. Asterisks indicate the location of the centrosomes. Time 0 is nuclear envelope breakdown and the scale bar is 10 μm. All suppressor alleles are in the *rsa-1(or598)* background.

In *rsa-1(or598), abc17* embryos the pronuclei usually met in the posterior of the embryo but often failed to center (3/7) and/or rotate (4/7). The spindles that were observed in these embryos were similar in size to *rsa-1(or598)* embryos and all of the embryos were able to complete cytokinesis.

Several of the *rsa-1* phenotypes were suppressed in *rsa-1(or598); abc19* embryos. The pronuclei always met, centered, and rotated like wild-type embryos. During metaphase

most of the spindles still appeared smaller in size however some mitotic spindles appeared to be a wild-type length (1/4). All of the *rsa-1(or598); abc19* embryos were able to successfully complete cytokinesis.

In six *rsa-1(or598); abc25* embryos the pronuclei never centered and in only one embryo did the pronuclei rotate correctly. After nuclear envelope breakdown, it was difficult to detect the centrosomes or mitotic spindle in the DIC images in the *rsa-1(or598); abc25* embryos. Most embryos were able to successfully complete cytokinesis (4/6) but some embryos failed and resulted in a multinucleated cell.

### 3.15.3 Suppression of L1 arrest at 25 °C

At 25 °C, *rsa-1(or598)* exhibits embryonic viability of 3.1% and all of the embryos that hatch at this temperature arrest in L1. Since the genetic screen for suppressors selected for suppression at 25 °C, viable suppressors would be required to rescue the embryonic lethality and L1 arrest at this temperature. In *rsa-1(or598)* 100% of the progeny arrest in L1, while in *abc17, abc19,* or *abc25* only 6-14% of the progeny arrest in L1 (Figure 3-27). Since the L1 arrest phenotype is likely the result of a defect in *rsa-1* function later in embryogenesis, it suggests that these suppressors also function at this time.

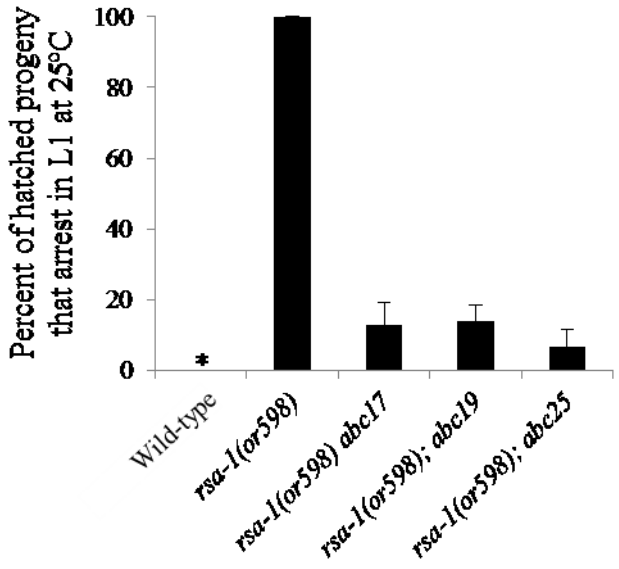


**Figure 3-27. Suppression of L1 arrest phenotype**
The percent of viable progeny at 25ºC that arrested in L1. Asterisk indicates that no progeny arrested at L1 in wild-type.

### 3.15.4 Suppression of Him phenotype

At 20 °C *rsa-1(or598)* self-fertilized hermaphrodites were observed to have 7.4% male progeny whereas self-fertilized wild-type hermaphrodites very rarely had male progeny. The suppressor strains with *abc17, abc19,* and *abc25* were able to partially suppress the Him phenotype. In these strains, self-fertilized hermaphrodites had approximately 1% male progeny (Table 3-7). This suggests that these suppressor alleles also function to suppress the chromosome non-disjunction that results in the Him phenotype.

| Genotype | % male progeny | s.d. | n |
|---|---|---|---|
| Wild-type | 0 | 0 | 1947 |
| *rsa-1(or598)* | 7.4 | 4.7 | 1023 |
| *rsa-1(or598), abc17* | 0.9 | 0.4 | 1389 |
| *rsa-1(or598); abc19* | 0.9 | 1.1 | 939 |
| *rsa-1(or598); abc25* | 1.3 | 1.1 | 1258 |

**Table 3-7. Suppression of Him phenotype at 20ºC**
The percent of progeny that are male at 20ºC is shown. s.d. is the standard deviation and n is the total number of viable progeny tallied.

### 3.15.5 PAA-1 localization in *abc17, abc19,* and *abc25*

Immunostaining was used to determine if *abc17, abc19,* and *abc25* were able to suppress the *rsa-1(or598)* phenotype of not recruiting PAA-1 to the centrosomes (Figure 3-28A). Since the embryonic viabilities of these strains was very low, it was likely that the embryos observed will not successfully complete embryogenesis. For example, *abc17* has an embryonic viability of 8.3% (s.d. 4.1, n=973). It was possible that the PAA-1 was recruited to the centrosome in these 8.3% of embryos and not in the other 91.7%. If this was true, then only one out of twelve embryos would show PAA-1 at the centrosomes and a sample size of six would not be likely to detect this small subset of suppressed embryos. Alternatively, the suppressors could recruit PAA-1 to the centrosomes in all embryos but the PAA-1 protein could still be less efficient at interacting with RSA-1(or598) and only in 8.3% of the embryos was the complex PAA-1 able to fulfill its function in the embryo. The observation of PAA-1 at the centrosome would likely indicate the mechanism of suppression, but not observing PAA-1 at the centrosome is less meaningful because it could simply indicate that not enough embryos were analyzed.

Immunostaining results indicated that PAA-1 was recruited to the centrosomes in *abc19* and *abc25* suppressors but not in *abc17* (Figure 3-28A). These results were

quantified (Figure 3-28B) and *abc19* and *abc25* both restored the level of PAA-1 at the centrosome to wild-type levels. *abc17* had significantly less PAA-1 at the centrosome compared to wild-type embryos and was similar to the levels of centrosomal PAA-1 in *rsa-1(or598)* embryos.

Unexpectedly PAA-1 recruitment to the P-granules was disrupted in the *rsa-1(or598);abc19* embryos (3/9). The P-granules were only visible in one third of the embryos, and the P-granules that were visible in these embryos exhibited a weak fluorescence signal. This suggests that *abc19* somehow affects recruitment of PAA-1 to the P-granules. It is possible that when less PAA-1 is sequestered in the P-granules, a greater pool of PAA-1 is available to interact with RSA-1 and be recruited to the centrosome. This could, in theory, overcome an inefficient protein interaction between PAA-1 and RSA-1(or598).

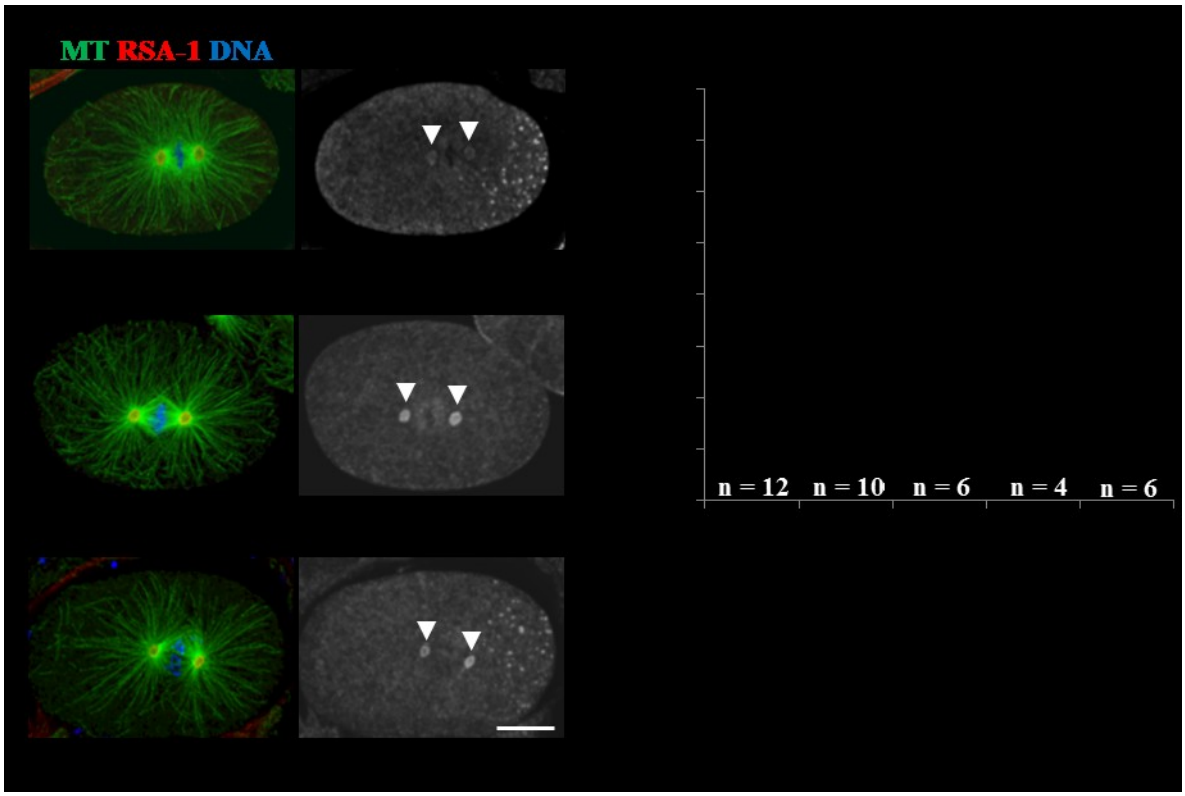


**Figure 3-28. Localization of PAA-1 in *abc17, abc19,* and *abc25***
A) Immunostaining of PAA-1 and RSA-1 in the currently unidentified suppressors homozygous and heterozygous at 26°C. The scale bar is 10 µm. B) The average integrated signal intensity of PAA-1 at the centrosome relative to RSA-1. ** indicates a p-value of <0.0001. n is the number of centrosomes included in the analysis and arrowheads indicate centrosomes.

### 3.15.6 Suppression of *rsa-1(RNAi)*

To determine if the unidentified suppressors require the presence of RSA-1(or598) to confer suppression, embryonic viabilities were determine for each suppressor after *rsa-1(RNAi)* treatment. *rsa-1(RNAi)* in wild-type worms have 6% embryonic viability. However, in the suppressor strains no embryonic viability was observed in *rsa-1(RNAi)* embryos. This suggests that these suppressors require the RSA-1(or598) protein to confer suppression. It is also possible that since these are weak suppressors a larger sample size is required to detect suppression of *rsa-1(RNAi).*

| | Control | | | *rsa-1(RNAi)* | | |
|---|---|---|---|---|---|---|
| **Genotype** | **Avg** | **s.d.** | **n** | **Avg** | **s.d.** | **n** |
| Wild-type | 99.0 | 1.1 | 703 | 6.0 | 6.1 | 217 |
| *rsa-1(or598)* | 0.0 | 0.0 | 159 | 0.0 | 0.0 | 287 |
| *rsa-1(or598), abc17* | 1.2 | 1.3 | 343 | 0.0 | 0.0 | 207 |
| *rsa-1(or598); abc19* | 0.005 | 0.004 | 207 | 0.0 | 0.0 | 206 |
| *rsa-1(or598); abc25* | .06 | .08 | 179 | 0.0 | 0.0 | 336 |

**Table 3-8. Suppression of *rsa-1(RNAi)***
Embryonic viabilities at 26 °C on RNAi control and *rsa-1(RNAi)* feeding plates. Only embryos laid between 24-48 hours on the feeding plates were included in this analysis. This experiment was performed with the original, non-out-crossed suppressor strains.

## 3.16 **Sanger sequencing of potential suppressors**

To identify the mutations in *abc17, abc19,* and *abc25,* several candidate suppressors were selected and sequenced (Table 3-9). Since many suppressor mutations were previously identified in *rsa-1* and *paa*-1, these two genes were sequenced in *abc17, abc19,* and *abc25* but no suppressor mutations were identified. Genes that were previously known to affect microtubule dynamics, spindle assembly, or mitotic progression were chosen as candidate suppressors. No mutations were identified in any of these genes. Whole genome sequencing was performed to identify mutations in these strains and is described in Appendix B.

| Allele | No mutations found in: |
|---|---|
| *abc17* | *rsa-1, paa-1, tpxl-1, cdc-25.1, sur-6* |
| *abc19* | *rsa-1, paa-1, klp-7, air-1* |
| *abc25* | *rsa-1, paa-1, klp-7* |

**Table 3-9. Sanger sequencing of candidate suppressors**
The introns for these genes were sequenced in the suppressors to determine if any mutations were present. In the case of *rsa-1*, I was looking for mutations in addition to the original *or598* lesion.

# 4 Results: Investigating RSA-1 function

## 4.1 Investigating the cause of the *rsa-1(or598)* spindle collapse

*rsa-1(or598)* and *rsa-1(RNAi)* embryos exhibited a spindle collapse phenotype whereby the centrosomes moved towards the chromatin mass. In the early *C. elegans* embryo, the mitotic spindle is under tension (Labbé et al., 2004). Forces originating from the cell cortex act on the centrosomes through contacts with astral microtubules (Nguyen-Ngoc et al., 2007). Similarly, kinetochore microtubules and motor proteins in the spindle oppose this force. For the centrosomes to move towards the chromatin in *rsa-1(lf)* embryos there has to be force generated within the spindle to move the centrosomes. The origin of the force that causes the spindle collapse is not known, but could be caused by several mechanisms. For example, microtubules that are anchored to the centrosome and attached to a kinetochore could cause the spindle to shorten because of the activity of microtubule depolymerization, overactive microtubule motor proteins, or both.

To elucidate the cause of the spindle collapse phenotype, I used RNAi to test various components of the mitotic spindle for their role in this process. In fission yeast, loss of antagonistic motor proteins can rescue spindle length defects (Syrovatkina et al., 2013), so I used similar logic to design the experiments with *rsa-1*. If a protein is required for the spindle collapse in *rsa-1(or598)* then reduction of these components with RNAi should suppress the spindle collapse phenotype in *rsa-1(or598)* embryos.

### 4.1.1 Kinetochores are required for the *rsa-1(or598)* spindle collapse

It was previously reported that the spindle collapse in *tpxl-1(RNAi)* embryos can be prevented by interfering with kinetochore function by *hcp-3(RNAi)* (Ozlü et al., 2005). Since the *rsa-1* spindle collapse is thought to be the same as that observed in *tpxl-1* depleted embryos, then I hypothesized that the *rsa-1* spindle collapse would also require functional kinetochores. However, a test for whether kinetochores are also required for the spindle collapse in *rsa-1* compromised embryos has not been reported so I performed these experiments.

CENP-A is a specialized centromeric H3 that specifies where kinetochores will form along the chromosome. In *C. elegans* the centromeric H3 is encoded by the *hcp-3* gene and is required to recruit all other components of the kinetochore (Oegema et al., 2001;

Kitagawa, 2009). *hcp-3(RNAi)* resulted in normal pronuclear migration and nuclear envelope breakdown but the chromosomes did not congress and align correctly. Premature centrosome separation was also observed (Figure 4-1A). When *rsa-1(or598)* embryos were treated with *hcp-3(RNAi)* a spindle collapse was never observed (n=6). These results indicated that kinetochores were required for the spindle collapse observed in *rsa-1(or598)* embryos (Figure 4-1A). These results were quantified and the spindles in *rsa-1(or598);hcp-3(RNAi)* embryos were significantly longer than in *rsa-1(or598)* embryos (Figure 4-1B).

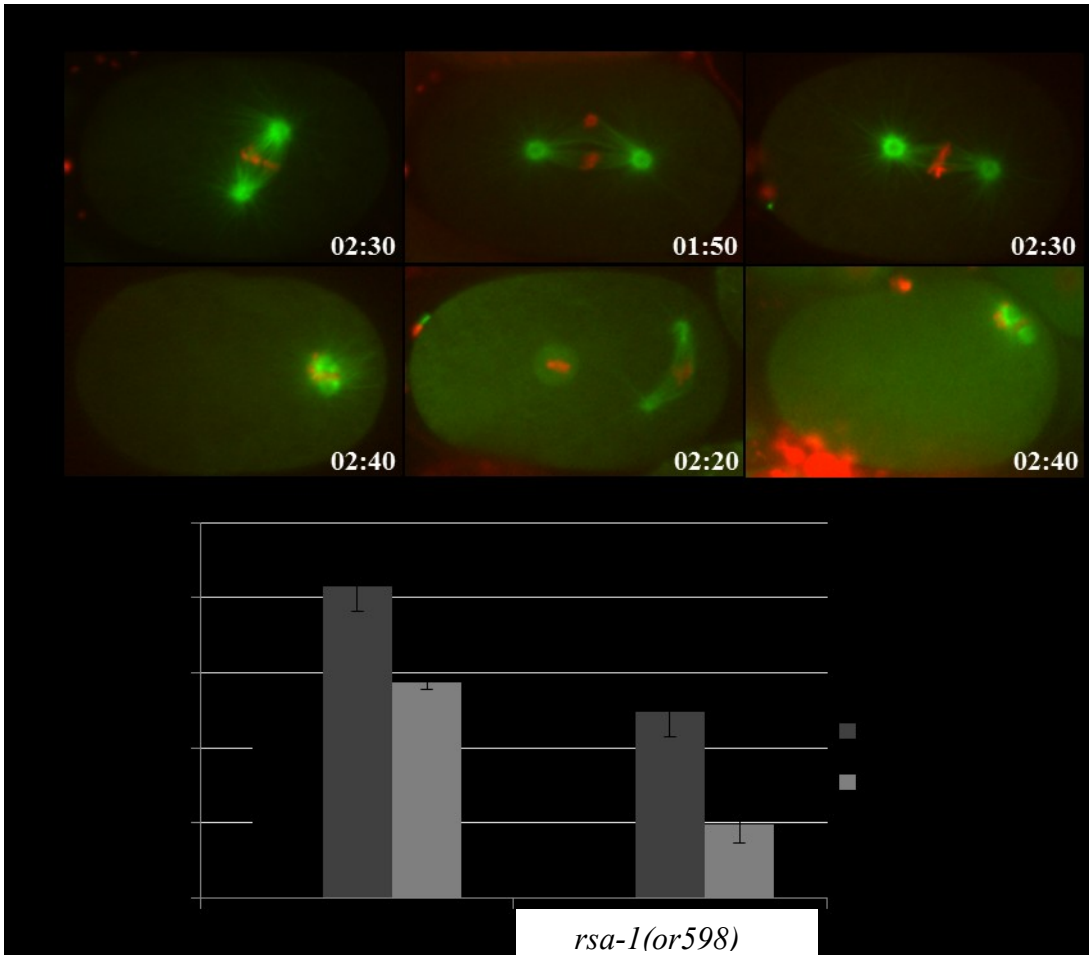


**Figure 4-1. Spindle collapse requires kinetochores but not spindle assembly checkpoint**
A) GFP::tubulin and mCherry::Histone images from time-lapse captures. Time 0 was nuclear envelope breakdown. B) Average distance between the centrosomes at 150-170 seconds after nuclear envelope breakdown. Error bars are the standard deviations.

Another kinetochore component, BUB-1, is required for the spindle assembly checkpoint but not for kinetochore formation. BUB-1 is a kinase that signals when a kinetochore is not correctly bi-oriented in the spindle and prevents the onset of anaphase

until the spindle is properly assembled. In early *C. elegans* embryos the spindle assembly checkpoint will delay, but not arrest, mitosis. As such, BUB-1 is not essential for mitosis or mitotic spindle assembly in early embryos. However, *bub-1(RNAi)* results in embryonic lethality due to defects late in embryogenesis (Sonnichsen et al., 2005).

To determine if the spindle assembly checkpoint was required for the spindle collapse observed in *rsa-1(or598)* embryos, RNAi was used to deplete BUB-1 in the embryos. *bub-1(RNAi)* was determined to be effective because there was 0% embryonic viability (n=148) after 24 hours of RNAi feeding. While the distance between the centrosomes was slightly increased in *bub-1(RNAi)* embryos, *rsa-1(or598); bub-1(RNAi)* embryos still exhibited a spindle collapse phenotype (Figure 4-1A,B). These data suggested that kinetochores, but not the spindle assembly checkpoint, were required for the spindle collapse phenotype observed in *rsa-1(or598)* embryos. As the kinetochore is a large protein complex, many other components of the kinetochore could be tested to determine if they are required for the spindle collapse or not.

### 4.1.2 Microtubule motor proteins are not required fro the *rsa-1(or598)* spindle collapse

Mitotic spindle assembly in vertebrate cells requires several key microtubule motor proteins, with Eg5 and Kif15 having key roles (van Heesbeen et al., 2014). Eg5 is also known as BimC or kinesin-5. Eg5 is required in human cells to crosslink anti-parallel microtubules and provide an outward force on the spindle that can separate the centrosomes (Kapitein et al., 2005). Another vertebrate kinesin that plays an important role in spindle assembly is Kif15 (also referred to kinesin-12 or Klp2). Like Eg5, Kif15 also promotes spindle elongation during spindle assembly (Tanenbaum et al., 2009), however on kinetochore microtubules Kif15 opposes centrosome separation (Sturgill and Ohi, 2013). Recently, it was shown that overexpression of Kif15 in human cells decreased the mitotic spindle length (Sturgill et al., 2014). Since these motors have key roles in spindle assembly in vertebrates, I sought to determine if they have a role in the *rsa-1(lf)* spindle collapse.

In *C. elegans,* the Eg5 homolog, BMK-1, is not essential for mitotic spindle assembly. BMK-1 is phosphorylated by Aurora B and found on the meiotic and mitotic spindle (Bishop et al., 2005). The only mitotic phenotype observed in *bmk-1(RNAi)* embryos is

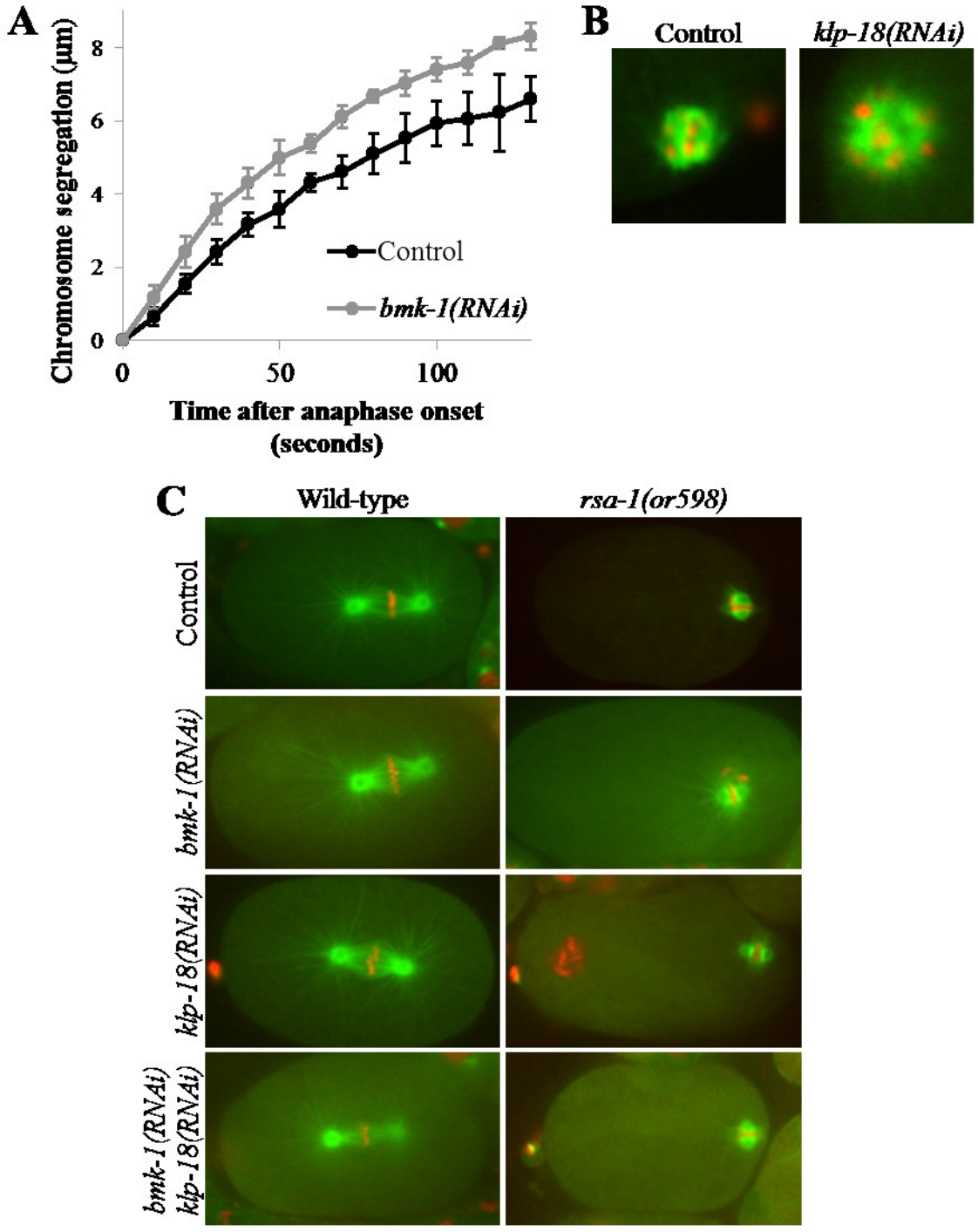


**Figure 4-2. Depletion of BMK-1 or KLP-18 does not suppress *rsa-1(or598)* spindle collapse**
A) Distance between the chromosomes during anaphase in control and *bmk-1(RNAi)* embryos. Error bars are the standard deviation. B) Close-up of the second meiotic spindle in *rsa-1(or598)* and *rsa-1(or598); klp-18(RNAi)* embryos that express GFP::tubulin and mCherry::histone. C) Metaphase wild-type and *rsa-1(or598)* embryos with control, *bmk-1(RNAi), klp-18(RNAi)*, or double RNAi treatment.

an increased rate of centrosome separation during anaphase suggesting that BMK-1 opposes centrosome separation during anaphase (Saunders et al., 2007). To verify that the *bmk-1(RNAi)* treatment was effective, the segregation rate of the chromosomes during anaphase was measured. *bmk-1(RNAi)* was considered effective because the chromosome segregation rate during anaphase was increased in *bmk-1(RNAi)* embryos (Figure 4-2A). Since *rsa-1(lf)* embryos exhibit a collapsed spindle phenotype, it is possible that RSA-1 is normally required to limit the activity of BMK-1 during spindle assembly. This hypothesis predicts that loss of *rsa-1* would lead to excessive BMK-1 activity and cause the spindle collapse. However, in *rsa-1(or589); bmk-1(RNAi)* embryos, a spindle collapse phenotype was observed (Figure 4-2C, n=6). These results indicated that aberrant BMK-1 activity is not what generates the force for the spindle collapse in *rsa-1(or598)* embryos.

In *C. elegans,* the Kif15 homolog, KLP-18 is required for meiotic spindle assembly (Segbert et al., 2003). During mitosis, KLP-18 is found at the spindle poles and spindle midzone but loss of KLP-18 does not result in obvious mitotic phenotypes except for abnormal pronuclei number which is a consequence of the meiotic phenotypes (Segbert et al., 2003). In human cells excessive Kif15 activity leads to a spindle collapse (Sturgill et al., 2014). If RSA-1 was required to limit the activity of KLP-18 then loss of *rsa-1* would lead to hyperactive KLP-18 and that could be the driving force for the spindle collapse in *rsa-1(lf)* embryos. Embryos were imaged starting from meiosis to verify that the *klp-18(RNAi)* treatment was effective due to the presence of unorganized meiotic spindles (Figure 4-2B). The *rsa-1(or598); klp-18(RNAi)* embryos exhibited a spindle collapse (Figure 4-2C, n=5), which indicated that excessive KLP-18 activity is not responsible for the force implicated in the spindle collapse.

While a double mutant for both *bmk-1* and *klp-18* does not result in any observed mitotic phenotypes (Connolly et al., 2014), it is possible that their mitotic roles may only be observed when the protein is overactive. If BMK-1 and KLP-18 performed a redundant function during mitosis, then loss of one of these kinesin proteins might not suppress the spindle collapse phenotype associated with loss of *rsa-1*. To test this hypothesis I performed a double RNAi treatment. *rsa-1(or598); bmk-1(RNAi); klp-18(RNAi)* embryos exhibited a spindle collapse phenotype (Figure 4-2C, n=2). These

results indicated that these kinesin proteins are not the driving force for the spindle collapse in *rsa-1(lf)* embryos.

### 4.2 **Removal of *klp-7* function in *rsa-1(or598)***

KLP-7 is the *C. elegans* homolog to the vertebrate microtubule depolymerase, MACK. Depletion of KLP-7 causes an increase in centrosomal microtubule nucleation in *C. elegans* embryos (Srayko et al., 2005). It was previously reported that *rsa-1(RNAi); klp-7(RNAi)* embryos exhibited a spindle collapse phenotype and they also exhibited almost wild-type microtubule levels (Schlaitz et al., 2007). The result suggested that RSA-1 could be a negative regulator of KLP-7 and that the reduction of microtubules in *rsa-1(RNAi)* embryos results from overactive KLP-7. This hypothesis was further supported when increased levels of the KLP-7 protein were observed at the centrosomes in *rsa-1(RNAi)* embryos (Schlaitz at al., 2007). Because RNAi was used to deplete both genes, and the effectiveness of RNAi is variable and gene-dependent, a strong conclusion based on genetic epistasis is not possible. Therefore, I tested this hypothesis by constructing a double mutant: r*sa-1(or598) I; klp-7(tm2143) III*. The *klp-7(tm2143)* allele is an 875bp deletion that removes all of exon 3 and most of exon 4 from K11D9.1a (Han, 2014). The KLP-7 protein is not detected by western blot in this mutant (Han, 2014). At 26 °C, *klp-7(tm2143)* resulted in variable embryonic viability that ranged from 0 to 32.4%. However, in the double mutant the embryonic viability was 0% (Table 4-1).

| Genotype | Embryonic viability (%) | s.d. | N |
|---|---|---|---|
| *rsa-1(or598) I* | 0.0 | --- | 1887 |
| *klp-7(tm2143) III* | 12.4 | 12.3 | 162 |
| *rsa-1(or598) I; klp-7(tm2143) III* | 0.0 | --- | 119 |

**Table 4-1. Embryonic viability at 26 °C of *rsa-1(or598); klp-7(tm2143)* double mutant**
s.d. is standard deviation and n is the number of embryos tallied.

Immunostaining of the *rsa-1(or598) I; klp-7(tm2143) III* double mutant was consistent with the results observed by Schlaitz et al.; the spindle collapse was observed but there was a visible increase in the number of microtubules emanating from the centrosomes (Figure 4-3). This confirmed that the decrease in microtubule number and spindle collapse are independent phenotypes, and that increased KLP-7 activity is likely

responsible for the reduction in microtubule outgrowth at the centrosomes in *rsa-1(or598ts)* embryos.

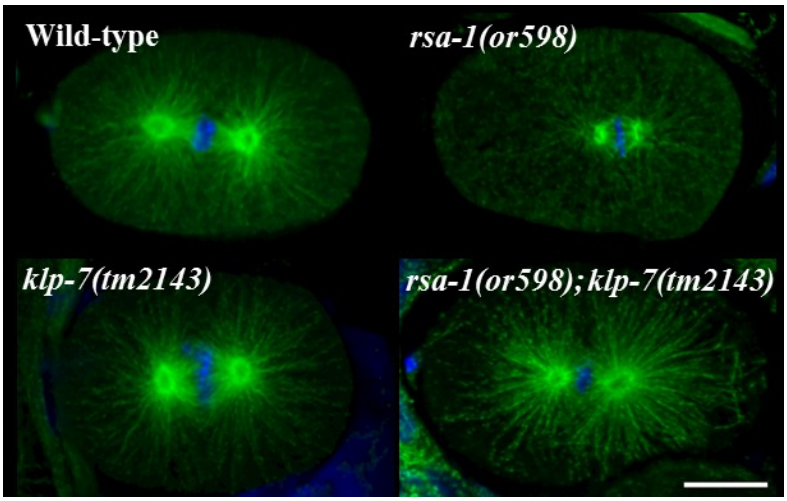


**Figure 4-3. Immunostaining of *rsa-1(or598); klp-7(tm2143)***
Embryos were raised at the restrictive temperature of 26 °C. Microtubules are green and DNA was stained with DAPI (blue). The scale bar is 10 µm. There is an increase in the number of microtubules emanating from the centrosomes in *rsa-1(or598); klp-7(tm2143)* embryos when compared to *rsa-1(or598)* alone.

Time-lapse microscopy of *rsa-1(or598); klp-7(RNAi)* embryos expressing GFP::tubulin and mCherry::histone was performed to determine if any of the *rsa-1(or598)* phenotypes observed in the first mitosis were suppressed by an increase in microtubule levels. Consistent with previous results, *klp-7(RNAi)* embryos exhibited an increase in microtubules that emanated from the centrosome in both the wild-type and *rsa-1(or598)* embryos (Figure 4-4). Additional phenotypes associated with the loss of *rsa*-1 were also diminished in the *rsa-1(or598); klp-7(RNAi)* embryos. In the *rsa-1(or598); klp-7(RNAi)* embryos there was a decreased frequency of asynchronous nuclear envelope breakdown and the spindle was only posteriorly positioned in half of the embryos (Table 4-2). These results indicated that the spindle positioning and nuclear envelope breakdown phenotypes observed in *rsa-1(or598)* embryos are likely due to the reduction of microtubules in *rsa-1(or598)* embryos. These results are not surprising because pronuclear migration and spindle positioning are known to be microtubule dependent processes. The decrease in microtubule number in *rsa-1(lf)* embryos likely makes pronuclear migration and spindle positioning less efficient. An increase in microtubule number can then rescue these phenotypes. Since the spindle still collapses in these embryos, it indicates that this phenotype is independent from microtubule number.

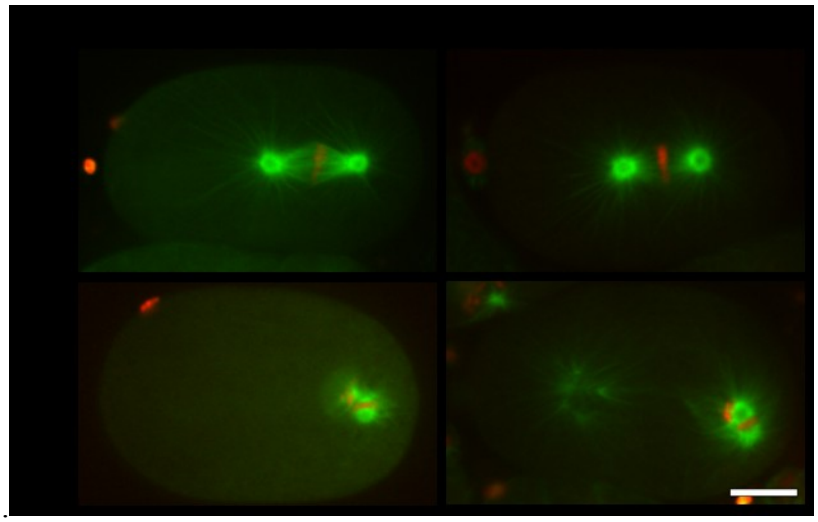

**Figure 4-4. Live imaging of *rsa-1(or598); klp-7(RNAi)* embryos**
Representative metaphase spindles in wild-type and *rsa-1(or598)* after *klp-7(RNAi). E*mbryos expressed mCherry::histone and GFP::tubulin. The scale bar is 10 μm.

Unexpectedly, 25% of the eight *rsa-1(or598); klp-7(RNAi)* embryos imaged in this analysis did not form a bipolar spindle. After nuclear envelope breakdown the chromosomes still collapsed towards the centrosome but a bi-polar structure did not assemble (Figure 4-5A,B). This phenotype was never observed in the *rsa-1(or598)* or *klp-7(RNAi)* control embryos. These results suggest that RSA-1 and KLP-7 may be required in redundant pathways to promote bipolar spindle assembly in *C. elegans*.

| | Control RNAi | | *klp-7(RNAi)* | |
|---|---|---|---|---|
| Phenotype | Wild-type | *rsa-1(or598)* | Wild-type | *rsa-1(or598)*[c] |
| Asynchronous NEBD[a] | 0% (n=0/4) | 100% (n=3/3) | 40% (n=2/5) | 25% (n=1/4) |
| Posterior spindle | 0% (n=0/4) | 100% (n=5/5) | 0% (n=0/5) | 50% (n=3/6) |
| Spindle collapse | 0% (n=0/4) | 100% (n=5/5) | 0% (n=0/5) | 100% (n=6/6) |
| Segregation errors[b] | 0% (n=0/4) | 100% (n=5/5) | 40% (n=2/5) | 100% (n=6/6) |

**Table 4-2. Phenotypes in time-lapse *rsa-1(or598); klp-7(RNAi)* embryos**
[a] Asynchronous nuclear envelope breakdown was defined as a delay between maternal and paternal NEBD of more than 30 seconds. If the time-lapse acquisition began after NEBD the embryos were excluded from this analysis.
[b] Chromosome segregation errors were defined by the appearance of chromosome bridges, lagging chromosomes, or any chromosomes that were not incorporated into the mitotic spindle.
[c] Two *rsa-1(or598); klp-7(RNAi)* embryos did not form a spindle and were excluded from the analysis.

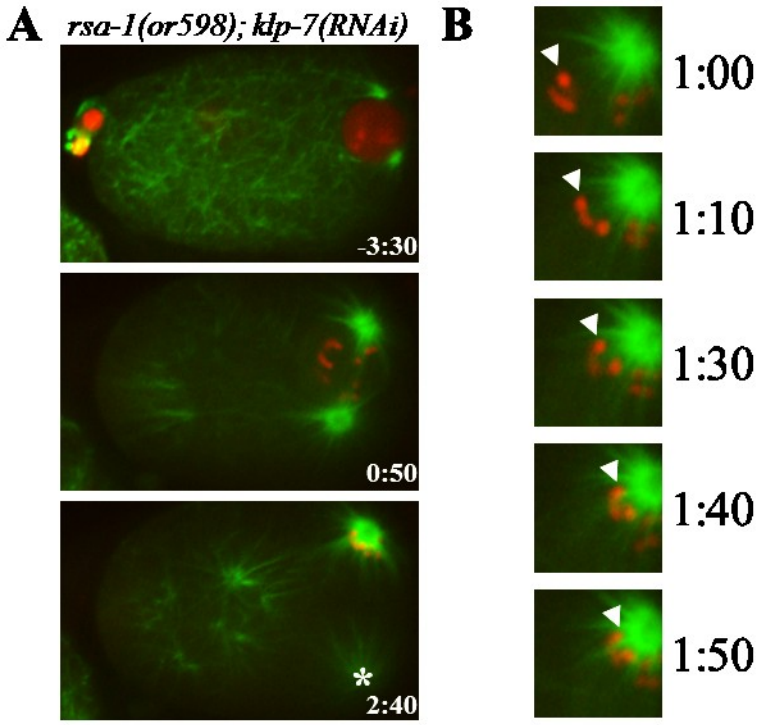


**Figure 4-5. Low-penetrant spindle assembly defect in *rsa-1(or598); klp-7(RNAi)* embryos**
A) Time-lapse microscopy of mCherry::histone and GFP::tubulin in *rsa-1(or598); klp-7(RNAi)*. The asterisk indicates the location of the centrosome that is not in the plane of focus. B) Close up of chromatin moving towards the centrosome. Time 0 is nuclear envelope breakdown.

### 4.3 Mono-polar spindles collapse in *rsa-1(or598)* embryos

The observation of collapsed mono-polar spindles in *rsa-1(or598); klp-7(RNAi)* embryos prompted me to investigate if all mono-polar spindles in *rsa-1(or598)* embryos would exhibit a spindle collapse phenotype.

Centrosomes are attached to the nuclear envelope through the activity of SUN-1, a protein that spans the nuclear envelope, and ZYG-12, a protein that interacts with the centrosome and nuclear envelope (Malone et al., 2003). Depletion of either *sun-1* or *zyg-12* results in centrosomes that can dissociate from the nuclear envelope and migrate away from the male pronucleus. *sun-1(RNAi)* results in transient mono-polar spindles when the centrosomes are too far apart to make bipolar spindles after nuclear envelope breakdown. The mono-polar spindles observed in *rsa-1(or598); sun-1(RNAi)* embryos were smaller than in the *sun-1(RNAi)* embryos (Figure 4-6). These results confirmed that a bipolar spindle is not required for the spindle collapse in *rsa-1(or598)* embryos.

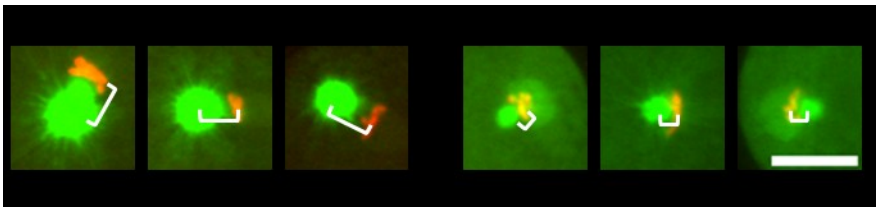

**Figure 4-6. Mono-polar spindles collapse**
Close up view of the chromatin moving towards the centrosome after *sun-1(RNAi)* in *rsa-1(or598)* and wild-type embryos. The brackets highlight the distance from the center of the centrosome (TPXL-1::GFP) to the chromatin mass (mCherry::histone). The scale bar is 10 µm.

## 4.4 Phosphorylation of potential RSA-1/PP2A substrates

One assumption made in this thesis was that the RSA-1/PP2A complex likely dephosphorylates one or more substrates at the centrosome. To date, two candidate substrates have been proposed, KLP-7 and TPXL-1 (Schlaitz et al., 2007). This was based on the observation that *rsa-1(RNAi)* leads to an increase in centrosomal levels of KLP-7 and a decrease of centrosomal TPXL-1 (Schlaitz et al., 2007). However, the mechanism for these changes in protein levels were not explored further and verification of this hypothesis is required. Homologs of KLP-7 and TPXL-1 in vertebrates are known to be regulated by phosphorylation so it is possible that RSA-1 directly regulates these proteins by dephosphorylation. If these are direct substrates of the RSA-1/PP2A complex then removal of RSA-1 activity would cause these proteins to be more phosphorylated in the embryos.

The microtubule depolymerizing kinesin, MCAK, is well characterized and known to be regulated by phosphorylation by Aurora A and Aurora B kinase. KLP-7, the *C. elegans* MCAK homolog, was shown to also be phosphorylated by the Aurora kinases (Han, 2014). However, *rsa-1(RNAi)* did not cause any detectable change in the mobility of KLP-7 on Phos-tag PAGE (Han, 2014). Since RSA-1 was not implicated in affecting phosphorylation of KLP-7 directly, I did not investigate it further as a possible substrate of RSA-1/PP2A.

### 4.4.1 Phosphorylation of TPXL-1

The TPXL-1 protein has previously been shown to be phosphorylated by Aurora A kinase *in vitro* (Ozlü et al., 2005). While it is known that a protein interaction between TPXL-1 and Aurora A is required for TPXl-1 activity in the embryo (Ozlü et al., 2005), it was not verified that TPXL-1 is phosphorylated by Aurora A *in vivo.* Prior to assessing if

RSA-1 and/or PP2A affected the phosphorylation of TPXL-1, I first verified TPXL-1 was phosphorylated in *C. elegans* embryos.

#### *4.4.1.1 TPXL-1 is phosphorylated in embryos*

To determine if TPXL-1 is phosphorylated in *C. elegans* embryos, I isolated protein lysates from embryos and treated them with a commercial phosphatase to remove any phosphate groups from the proteins. The lambda protein phosphatase has a broad specificity and is able to dephosphorylate serines, threonines, and tyrosines. This treatment generates proteins that are non-phosphorylated and can be compared to endogenous, untreated protein lysates. The phosphatase treated protein samples were then separated with PAGE that contained Phos-Tag reagent in the acrylamide. Phos-Tag decreases the mobility of phosphorylated proteins through the acrylamide, resulting in phosphorylated proteins that migrate slower than their non-phosphorylated counterparts (Kinoshita et al., 2006). Depending on the concentration of Phos-tag used in the experiment, it is possible to resolve multiple species that correspond to differential phosphorylation of multiple residues of the protein.

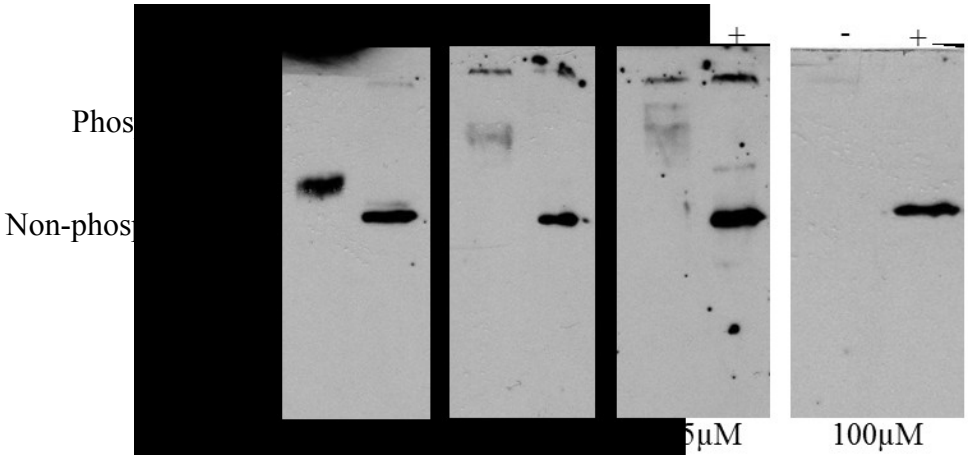


**Figure 4-7. Lambda phosphatase treatment with TPXL-1 western blot**
Each lane contains 100 µg of wild-type embryo protein lysate that was either treated with λ protein phosphatase or not. The samples were run on an 8% acrylamide gel with the indicated concentration of Phos-Tag reagent at 120 V for 2 hrs and transferred for 2 hrs at 90 V. The proteins were then transferred to a nitrocellulose membrane and probed with a TPXL-1 antibody.

With PAGE and western blots, the TPXL-1 protein appeared as a single band of approximately 80 kDa (Figure 2-4D). When wild-type embryo lysates were treated with lambda protein phosphatase the TPXL-1 protein migrated further through the Phos-tag acrylamide gel than the non-treated lysates (Figure 4-7). This increase in mobility after

phosphatase treatment indicates that the endogenous TPXL-1 protein is phosphorylated. The migration of TPXL-1 in the acrylamide gel was more retarded as concentrations of Phos-tag increased. At 100 μM of Phos-tag, the phosphorylated TPXL-1 protein was not detected via western blot presumably because it was unable to enter the poly-acrylamide matrix.

#### *4.4.1.2 Depletion of PAA-1 affects TPXL-1 phosphorylation*

Since TPXL-1 was verified to be a phospho-protein in *C. elegans* embryos, I sought to determine if RSA-1 and/or PP2A are able to affect the phosphorylation state of TPXL-1. If TPXL-1 was a direct substrate of the RSA-1/PP2A phosphatase complex then loss of RSA-1and/or PAA-1 would cause the TPXL-1 protein to be more phosphorylated. Protein preparations from *rsa-1(or598)* hermaphrodites at 26 °C did not exhibit any dramatic change in the phosphorylation state of TPXL-1 (1/6 trials exhibited a mobility shift) (Figure 4-8A). When *rsa-1* function was compromised by treatment with *rsa-1(RNAi)* the TPXL-1 protein also did not appear to be more phosphorylated (0/2 trials) (Figure 4-8B). However, when the structural subunit of the PP2A phosphatase complex was compromised by *paa-1(RNAi)* treatment, the migration of TPXL-1 protein was greatly impeded on Phos-tag gels (5/5 trials) (Figure 4-8B).

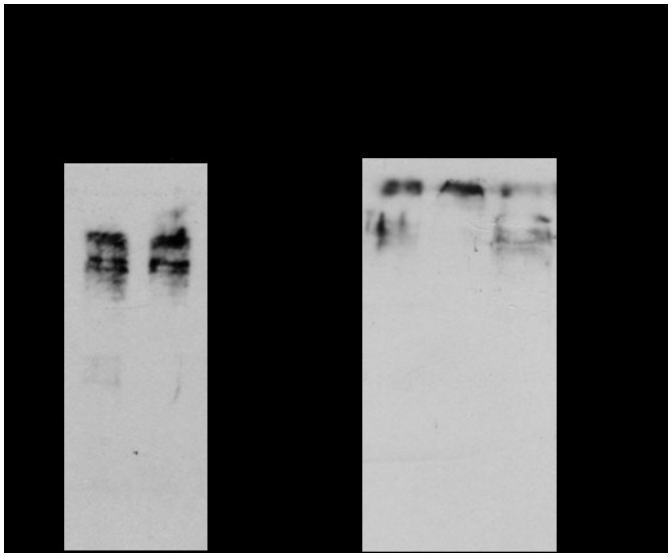

**Figure 4-8. Phos-Tag PAGE with TPXL-1 western blot.**
A) Embryo preparation from 150 hermaphrodites. 50 μM, 8%, 3 hrs 150 V, transfer 2 hrs 100V. B) Embryo preparation from 100 hermaphrodites. 75 μM, 8%, 3 hrs 150 V, transfer 2 hrs 100V. Control embryos were on RNAi plates with L4440 empty vector control. Arrow indicates the most phosphorylated TPXL-1species.

These data suggested that PP2A does affect the phosphorylation state of TPXL-1 *in vivo*. However, RSA-1 is likely not the regulatory subunit that mediates this reaction. It is possible that RSA-1 could affect a small pool of TPXL-1 and that the mobility shift is too subtle to be resolved with Phos-Tag PAGE.

## 4.5 **Location of Aurora A in *rsa-1(or598)* embryos**

Since RSA-1 did not appear to affect the phosphorylation state of either KLP-7 or TPXL-1, I investigated if RSA-1 could affect a regulator of both of these proteins. Aurora A is a major mitotic kinase and known to phosphorylate both TPXL-1 (Ozlü et al., 2005) and KLP-7 (Han, 2014). The *C. elegans* gene for Aurora A is encoded by the *air-1* gene. For simplicity and clarity, I will refer to the AIR-1 protein as Aurora A. If RSA-1 affected the subcellular localization or activity of Aurora A then it could affect pools of both TPXL-1 and KLP-7 in the embryo. An Aurora A antibody was available, so I performed immunostaining of embryos to investigate if *rsa-1(or598)* affected the location of Aurora A in early embryos.

### 4.5.1 Aurora A Immunostaining

In wild-type embryos, Aurora A was observed at the centrosomes and in a graded manner on the microtubules. This halo-like pattern was observed at all stages of mitosis in wild-type embryos (Figure 4-9, Figure 4-10). In *rsa-1(or598)* embryos Aurora A was observed on the centrosomes but not the microtubules during prophase and metaphase (Figure 4-9, n=10/10). This was similar to the phenotype previously observed in *tpxl-1(RNAi)* embryos where TPXL-1 was required to recruit Aurora A to the microtubules (Ozlü et al., 2005; Figure 4-9). Since *rsa-1(or598)* embryos have fewer microtubules than wild-type embryos, it was possible that Aurora A could be present on the microtubules but not visible in these embryos due to the decrease in microtubule number. To address this concern, immunostaining was performed with the *rsa-1(or598) I; klp-7(tm2143) III* double mutant. The *klp-7(tm2143)* allele alone did not affect Aurora A localization, however the *rsa-1(or598) I; klp-7(tm2143) III* double mutant did not have Aurora A on the microtubules during prophase or metaphase (Figure 4-9).

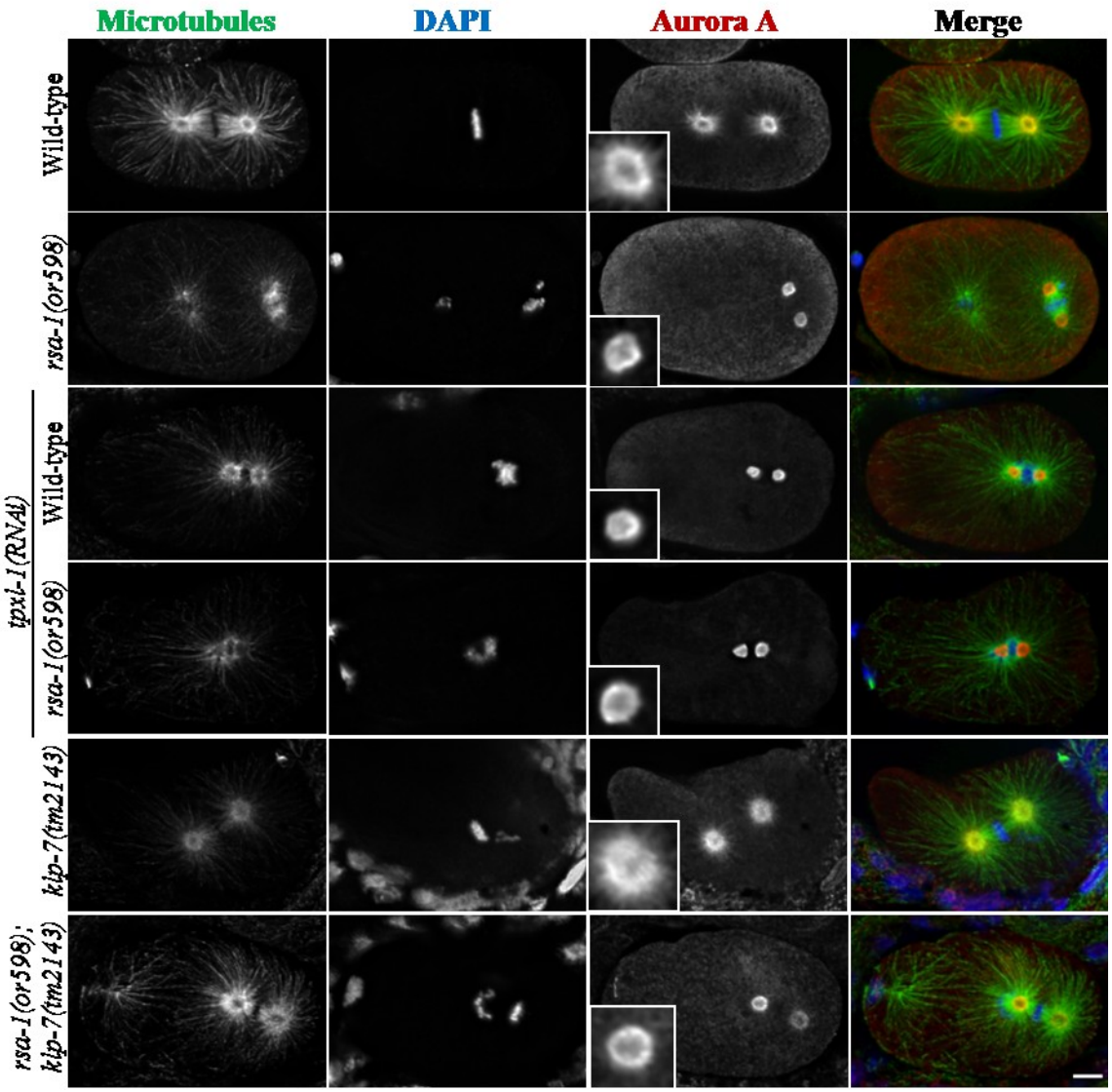


**Figure 4-9. Aurora A localization during spindle assembly**
Immunostaining of Aurora A in metaphase embryos at 26 °C. Microtubules are green, Aurora A is red, and DAPI stains the DNA. Scale bar is 10 µm. Inset is one centrosome. Aurora A staining on the microtubules is lost in *rsa-1(or598)* and *tpxl-1(RNAi)* embryos.

Although both RSA-1 and TPXL-1 seemed to be required for Aurora A location to centrosomal microtubules in spindle assembly, their phenotypes diverged during anaphase and telophase. In *tpxl-1(RNAi)* embryos, Aurora A is contained at the centrosome throughout mitosis. However, during anaphase and telophase in *rsa-1(or598)* embryos, Aurora A was observed on the microtubules (Figure 4-10, n=5/5). In *rsa-1(or598) tpxl-1(RNAi)* embryos, Aurora A was confined to the centrosomes during anaphase (Figure 4-10). These results suggest that RSA-1 affects the localization of Aurora A to the microtubules in a cell cycle dependent manner.

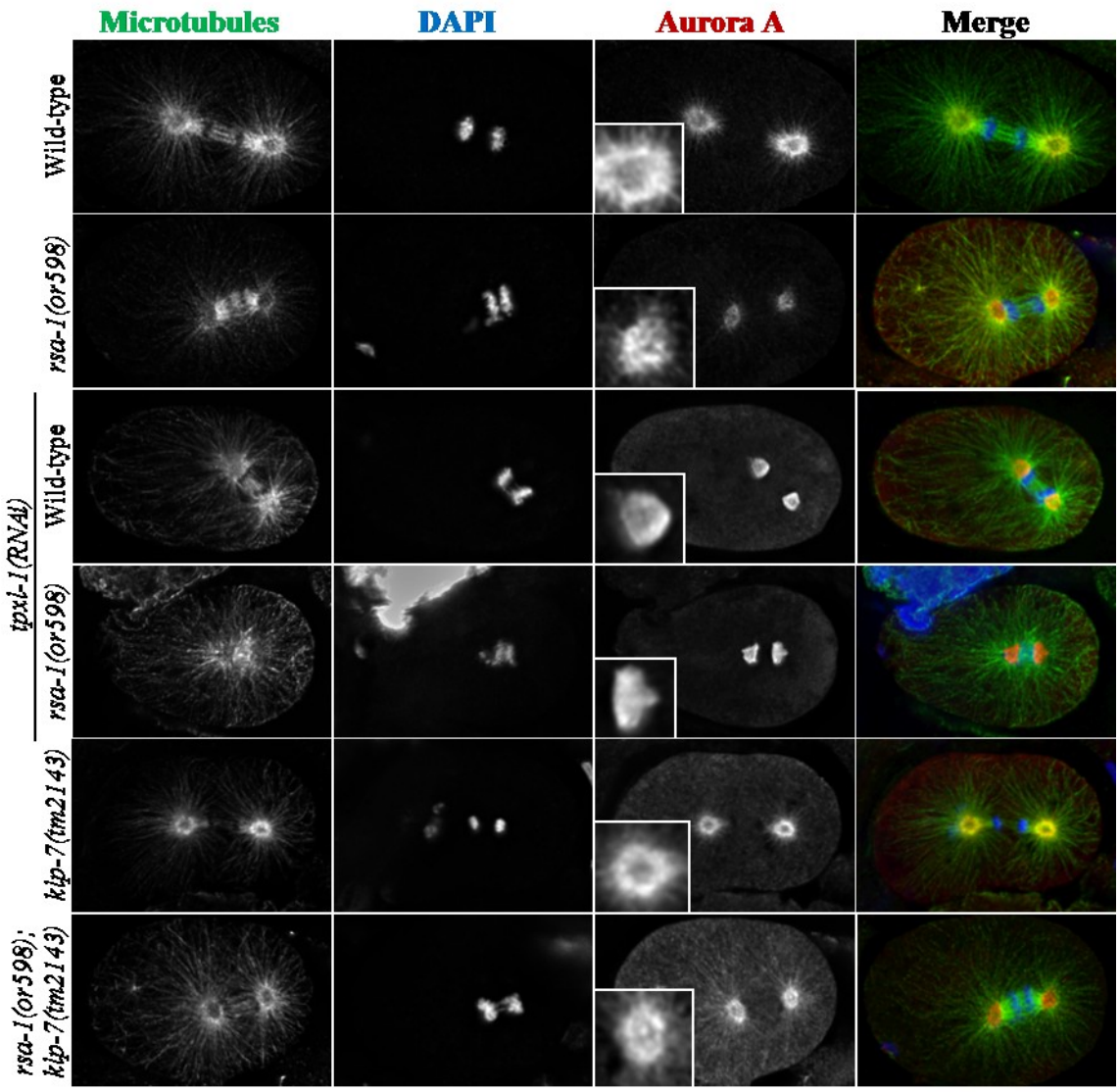


**Figure 4-10. Aurora A localization during anaphase**
Immunostaining of Aurora A in anaphase embryos at 26 °C. Microtubules are green, Aurora A is red, and DAPI stains the DNA. Inset is one centrosome. The scale bar is 10 µm. Aurora A staining on the microtubules is lost in *tpxl-1(RNAi)* embryos but not *rsa-1(or598)* embryos.

Aurora A was previously reported to be transiently associated with the chromatin (Toya et al., 2011). By immunofluorescence, I did not observe Aurora A on the chromatin at any timepoint in mitosis. It was previously reported that cold-treatment of the embryos to depolymerize the microtubules increased the Aurora A staining observed on the chromatin (Toya et al., 2011). Therefore I used this technique to assess Aurora A location on the chromatin. When the microtubules were depolymerized in both wild-type and *rsa-1(or598)* embryos, Aurora A was still not detected on the chromatin (Figure 4-11). These data suggested that Aurora A was either not on the chromatin in these

embryos or was below the level of detection with this antibody. Since Aurora A was not observed on the chromatin, I was unable to assess if *rsa-1(or598)* affects this pool of Aurora A.

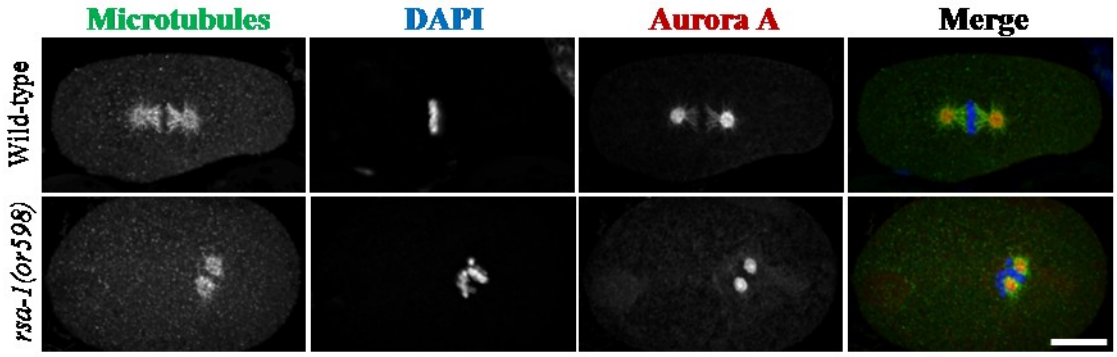


**Figure 4-11. Aurora A after microtubule de-polymerization**
Prior to fixation and immunostaining with an anti-Aurora A antibody, microtubules were depolymerized with cold treatment. Microtubules are green, Aurora A is red, and DAPI stains the DNA. The scale bar is 10 µm.

### 4.5.2 Time-lapse microscopy with Aurora A

The immunostaining results suggested that *rsa-1(or598)* embryos exhibit a dynamic change in the location of Aurora A in mitosis. Live imaging is a better technique to assess how the location of a protein in an embryo can change over time. To verify the immunostaining results and investigate the dynamic localization of Aurora A, a strain expressing AIR-1::GFP (Portier et al., 2007) was acquired from the *Caenorhabditis* Genetics Center (University of Minnesota). The AIR-1::GFP strain was imaged in *rsa-1(RNAi), tpxl-1(RNAi),* and control embryos (Figure 4-12A,B). On the negative controls the Aurora A fluorescence signal was very bright on the centrosomes and microtubules at every stage of mitosis. Notably, AIR-1::GFP signal was brighter in embryos derived from worms cultured at 26 °C (Figure 4-12A) than 20 °C (Figure 4-12B), so it was critical that the control and experimental strains were cultured and imaged at the same temperature. During anaphase in wild-type embryos, a faint AIR-1::GFP signal was observed at the chromatin which was consistent with a previously characterized Aurora A::GFP strain (Toya et al., 2011).

The *rsa-1(RNAi)* embryos exhibited the spindle collapse phenotype which indicated that the RNAi treatment was successful (Figure 4-12A). Prior to nuclear envelope breakdown and during spindle assembly, Aurora A was located at the centrosome. After the onset of anaphase in *rsa-1(RNAi)* embryos, Aurora A was observed at the centrosome

and on the microtubules (Figure 4-12A). Aurora A was not observed on the microtubules of *tpxl-1(RNAi)* embryos at any stage of mitosis (Figure 4-12B). The live imaging confirmed that the localization of Aurora A is dynamic in *rsa-1(RNAi)* embryos. While Aurora A is restricted at the centrosome during spindle assembly, Aurora A can associate with microtubules during anaphase in *rsa-1(RNAi)* embryos.

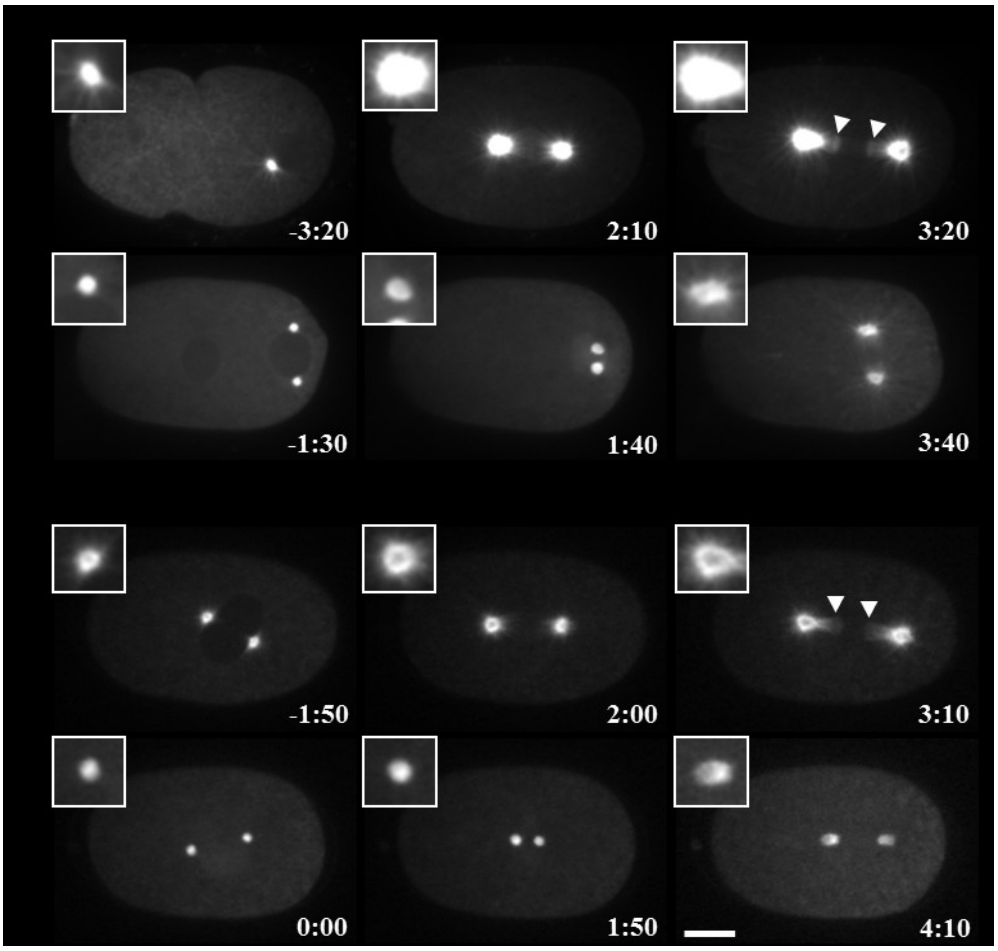


**Figure 4-12. Time lapse microscopy of Aurora A**
A) AIR-1::GFP in control and *rsa-1(RNAi)* embryos imaged at 26 °C B) AIR-1::GFP in control and tpxl-*1(RNAi)* embryos imaged at 20 °C. The scale bar is 10 µm. Arrow heads indicate chromatin localization of Aurora A. Insets are a magnification of one of the centrosomes. Aurora A was observed on the microtubules in *rsa-1(RNAi)* embryos after anaphase. Aurora A was never observed on the microtubules in *tpxl-1(RNAi)* embryos.

### 4.6 **Localization of TPXL-1 in *rsa-1(or598)* embryos**

The TPXL-1 protein has previously been reported to be located at the centrosomes and in a gradient along the microtubules, with highest levels proximal to the centrosomes (Ozlü et al., 2005). *rsa-1(RNAi)* embryos exhibited significantly less TPXL-1 protein at the centrosomes (Schlaitz et al., 2007). To determine if *rsa-1(or598)* embryos showed

any change in TPXL-1 subcellular localization, immunostaining and time lapse microscopy with TPXP-1::GFP were performed.

### 4.6.1 Immunostaining with anti-TPXL-1 antibody

Immunostaining of wild-type embryos with the anti-TPXL-1 polyclonal antibody revealed that the TPXL-1 protein was at the centrosomes, microtubules, and along the chromatin (Figure 4-13). The TPXL-1 immunofluorescence co-localized with the DAPI staining in 18/19 embryos; however, the intensity of the TPXL-1 fluorescence at chromatin varied between embryos and was sensitive to fixation. In *rsa-1(or598)* embryos, TPXL-1 was observed at the centrosomes and on the microtubules, but levels were lower than what was observed in wild-type. In mitotic *rsa-1(or598)* embryos, TPXL-1 was not detected at the chromatin (0/11). Since the TPXL-1 intensity at the chromatin was variable in wild-type embryos, it is possible that in *rsa-1(or598)* embryos TPXL-1 is on the chromatin but the intensity is below the level of detection. Therefore, these results are not conclusive.

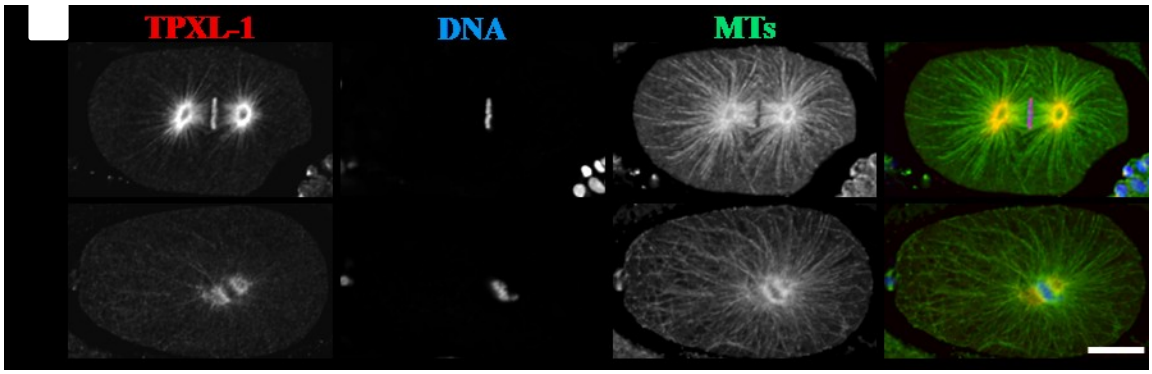


**Figure 4-13. TPXL-1 localization in wild-type and *rsa-1(or598)* embryos**
Localization of TPXL-1 during metaphase in wild-type and *rsa-1(or598)* embryos at 26 °C. The scale bar is 10 µm. In wild-type TPXL-1 is observed on the centrosomes, microtubules, and chromatin. In *rsa-1(or598)* embryos TPXL-1 was not observed on the chromatin.

### 4.6.2 Time lapse microscopy with TPXL-1::GFP

Since the immunostaining results were not conclusive, I confirmed the results with live imaging. In wild-type embryos, TPXL-1::GFP was very bright at the centrosomes and could be observed on the microtubules and chromatin (Figure 4-14A). During anaphase the levels of TPXL-1::GFP increased on the microtubules and chromatin. In *rsa-1(or598)* embryos the TPXL-1::GFP at the centrosomes and on the microtubules was significantly fainter.

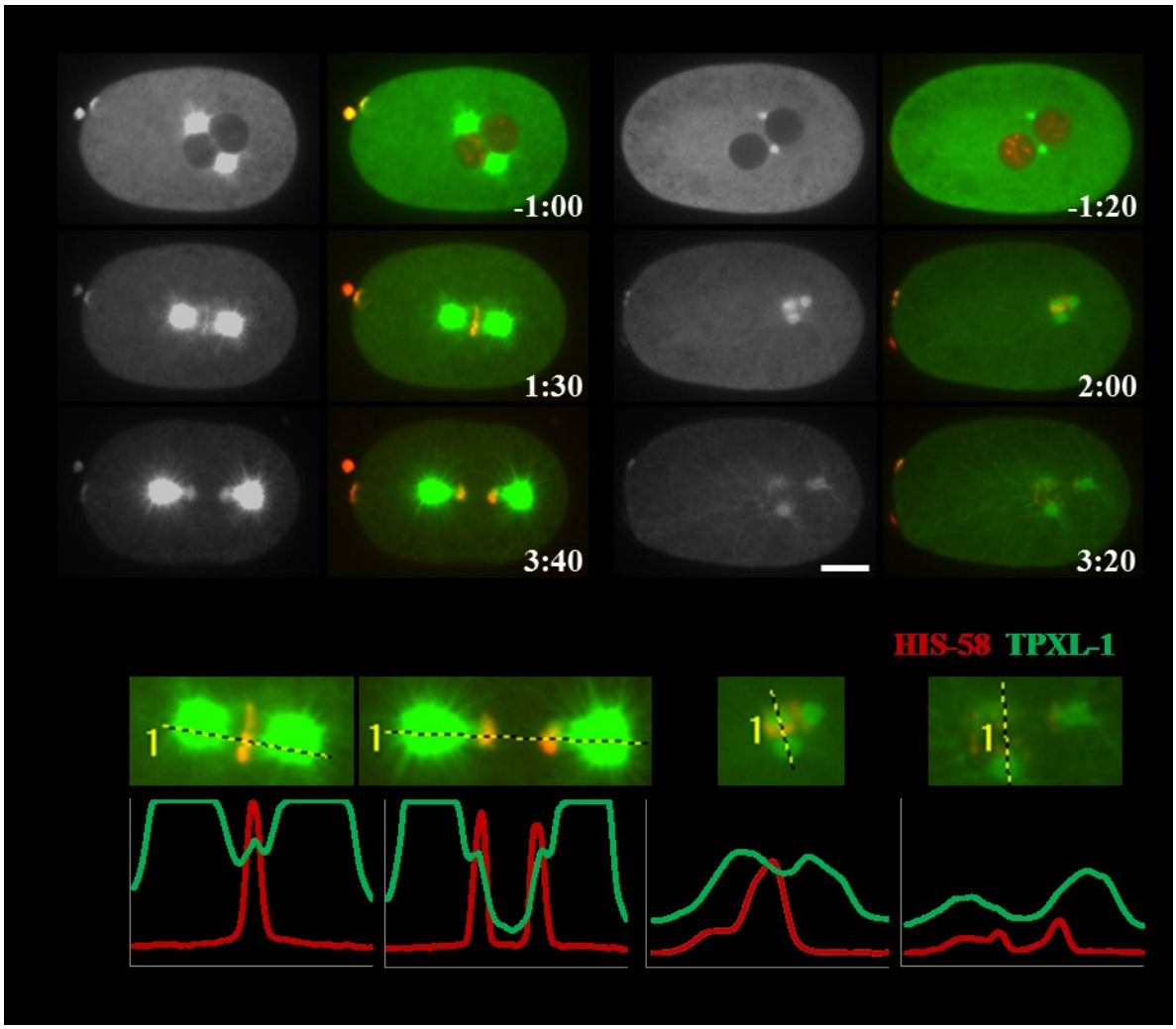


**Figure 4-14. TPXL-1::GFP localization in *rsa-1(or598)* during the first mitosis**
A) TPXL-1::GFP and mCherry::HIS-58 time-lapse microscopy with representative embryos during prophase, metaphase, and anaphase at 26 °C. Scale bar is 10 µm and time 0 is NEBD. B) Line scans of fluorescence intensity during metaphase and anaphase. The black and yellow dashed line was used to make the line scans.

Due to the spindle collapse it was difficult to assess TPXL-1::GFP levels on the chromatin when the centrosomes were saturated (Figure 4-14A). Line scans revealed that, in wild-type embryos, a clear peak of TPXL-1::GFP intensity correlated with the mCherry::chromatin peak (Figure 4-14B). Line scans of *rsa-1(or598)* embryos revealed that there was no peak of TPXL-1::GFP with the chromatin at either metaphase or anaphase. These results are consistent with the immunostaining results so I concluded that RSA-1 is required for TPXL-1 to locate to the chromatin.

### 4.6.3 Quantification of TPXL-1::GFP levels

Levels of TPXL-1::GFP were measured at the centrosome, chromatin, and cytoplasm to quantify how *rsa-1(or598)* affects the localization of TPXL-1. For the cytoplasm measurement, an area with no visible microtubules was selected. While TPXL-1::GFP is also observed on the microtubules, this was not measured in this analysis due to difficulty in measuring protein levels on microtubules. Quantification of TPXL-1::GFP revealed that in *rsa-1(or598)* embryos the levels of TPXL-1 protein was significantly reduced at the centrosomes and at the chromatin (Figure 4-15). There was a slight but significant increase in cytoplasmic levels of TPXL-1::GFP. This increase is likely due to the misplaced TPXL-1::GFP re-locating to the cytoplasm.

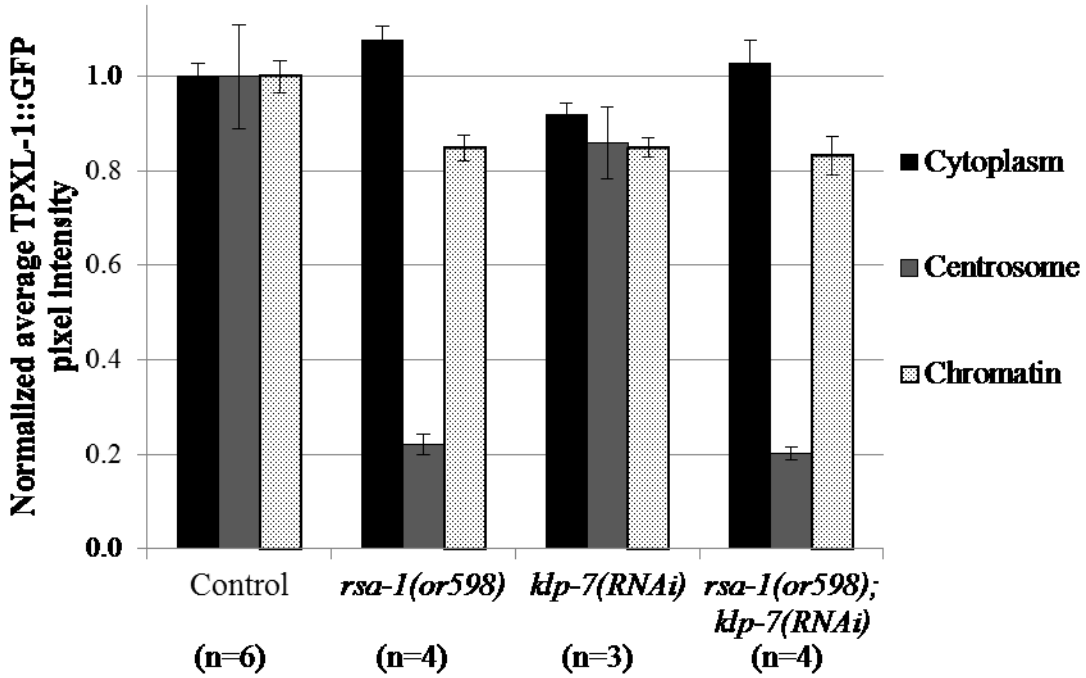


**Figure 4-15. Quantification of TPXL-1::GFP in metaphase embryos**
Imaging was done using standardized conditions that did not saturate the GFP channel. The average pixel intensity for TPXL-1::GFP was calculated at the centrosome, chromatin, and in the cytoplasm in metaphase embryos. The values where then normalized to the RNAi negative control. n is the number of embryos analyzed for each condition.

To determine if the decreased levels of TPXL-1::GFP at the chromatin were because of the decreased levels of microtubules in the *rsa-1(or598)* embryos, I measured TPXL-1::GFP levels in *klp-7(RNAi)* embryos (Figure 4-15). Unexpectedly, *klp-7(RNAi)* embryos showed lower levels of TPXL-1::GFP in the cytoplasm, at the centrosome, and at the chromatin. This is likely a consequence of a limited pool of TPXL-1::GFP in the

embryo. When there are more microtubules for TPXL-1::GFP, this could dilute the TPXL-1::GFP in the embryo. Levels of centrosomal and chromatin TPXL-1::GFP were not significantly different in *rsa-1(or598)* or in the *rsa-1(or598); klp-7(RNAi)* embryos. If levels of TPXL-1::GFP at the centrosome were dependent on microtubule levels then the centrosomal TPXL-1::GFP levels should have increased in the *rsa-1(or598); klp-7(RNAi)* embryos.

## 4.7 **Components required for TPXL-1 at the chromatin**

This thesis has presented evidence that TPXL-1 is located on the chromatin in *C. elegans* embryos. Based on this novel observation, I investigated the molecular mechanism for the location of TPXL-1 to the chromatin. RNAi was used to deplete various components required for spindle assembly in *C. elegans* embryo to determine if they were also required for TPXL-1 to locate to the chromatin. Since RSA-1 was required for TPXL-1 to localize to the chromatin, this approach could illuminate other proteins or pathways that are involved with this function of RSA-1.

### 4.7.1 Aurora A is required for TPXL-1 to localize to the chromatin

Loss of Aurora A in *C. elegans* embryos leads to disorganized, small, bipolar spindles that result in aneuploidy and embryonic lethality (Schumacher et al., 1998). Since Aurora A interacts with TPXL-1 and has been reported to be on mitotic chromosomes in *C. elegans* (Toya et al., 2011), I investigated if Aurora A was required for TPXL-1::GFP to locate to the chromatin.

#### 4.7.1.1 *Reduction of Aurora A with* air-1(RNAi)

*air-1(RNAi)* embryos exhibited small centrosomes, fewer visible microtubules, and small bipolar spindles (Figure 4-16A) which was consistent with the previously described role for Aurora A in centrosome maturation. The small spindles made it difficult to visually assess if TPXL-1 was on the chromatin in *air-1(RNAi)* embryos, however line scans were used to more accurately determine the protein locations (Figure 4-16B). TPXL-1::GFP did not associate with the chromatin in *air-1(RNAi)* embryos. This suggests that Aurora A is required for TPXL-1 to locate to the chromatin, but it is not

clear if the pool of Aurora A at the centrosome, microtubules, or chromatin is responsible.

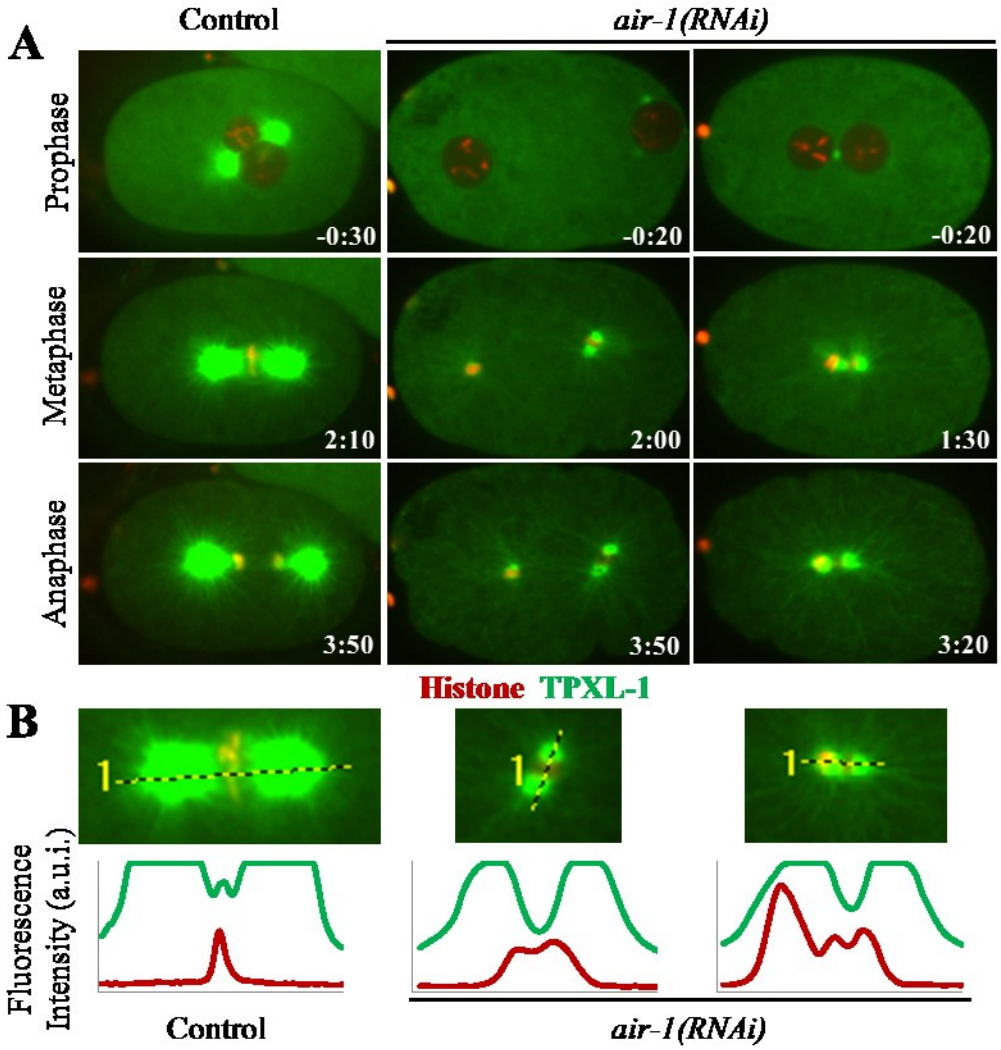


**Figure 4-16. TPXL-1 localization to the chromatin is compromised in when Aurora A is depleted**
A) TPXL-1::GFP and mCherry::Histone time-lapse microscopy with representative embryos during prophase, metaphase, and anaphase at 26 °C. Scale bar is 10 µm and time 0 is NEBD. B) Line scans of fluorescence intensity during metaphase and anaphase. The black and yellow dashed line indicates the region scanned to make the line scans.

#### *4.7.1.2 TPXL-1/Aurora A protein interaction disrupted*

When two conserved phenylalanine residues in the N-terminus of TPXL-1 are mutated, F15D and F18D, the protein interaction between Aurora A and TPXL-1 is no longer detected in co-immunoprecipitations and TPXL-1 is no longer phosphorylated *in vitro* by Aurora A (Ozlü et al., 2005). When these same mutations are introduced into an

RNAi resistant transgene and the endogenous *tpxl-1* is depleted with *tpxl-1(RNAi)*, Aurora A is no longer observed on the microtubules but rather is contained at the centrosome (Ozlü et al., 2005).

Using these same transgenes, I investigated if the protein interaction with Aurora A was required for TPXL-1 to be on the chromatin. For these experiments, *tpxl-1(RNAi)* is used to deplete the endogenous TPXL-1 in the embryos because the transgenes are RNAi resistant. The wild-type RNAi resistant transgene is able to suppress the *tpxl-1(RNAi)* although the spindle is slightly smaller than in control embryos (Figure 4-17). The TPXL-1(WT)::GFP$^{RNAi(R)}$ was observed on the chromatin during metaphase; however, TPXL-1 was not detected on the chromatin during anaphase. When the interaction with Aurora A was disrupted, TPXL-1(F15D,F18D)::GFP$^{RNAi(R)}$ was observed on the chromatin in control embryos, but not on chromatin in *tpxl-1(RNAi)* embryos (Figure 4-17A). Consistent with the previous observation that the protein interaction with Aurora A is essential for TPXL-1 function (Ozlü et al., 2005), the spindle collapsed in these embryos. These results support the hypothesis that Aurora A is required for TPXL-1 to associate with the chromatin.

During the course of this analysis, it appeared that the centrosomal levels of TPXL-1::GFP varied between the wild-type and mutant transgenes. To determine if this was significant, the centrosomal levels of TPXL-1::GFP were quantified (Figure 4-17B). Within the control RNAi embryos, there was no significant differences observed in the centrosomal levels of TPXL-1. When endogenous TPXL-1 was depleted with *tpxl-1(RNAi),* there was approximately 30% less TPXL-1(F15D,F18D) at the centrosome than the wild-type transgene. This decrease was statistically significant, with a p-value of 0.0008. These results indicate that an interaction with Aurora A is also necessary for the efficient centrosomal recruitment of TPXL-1.

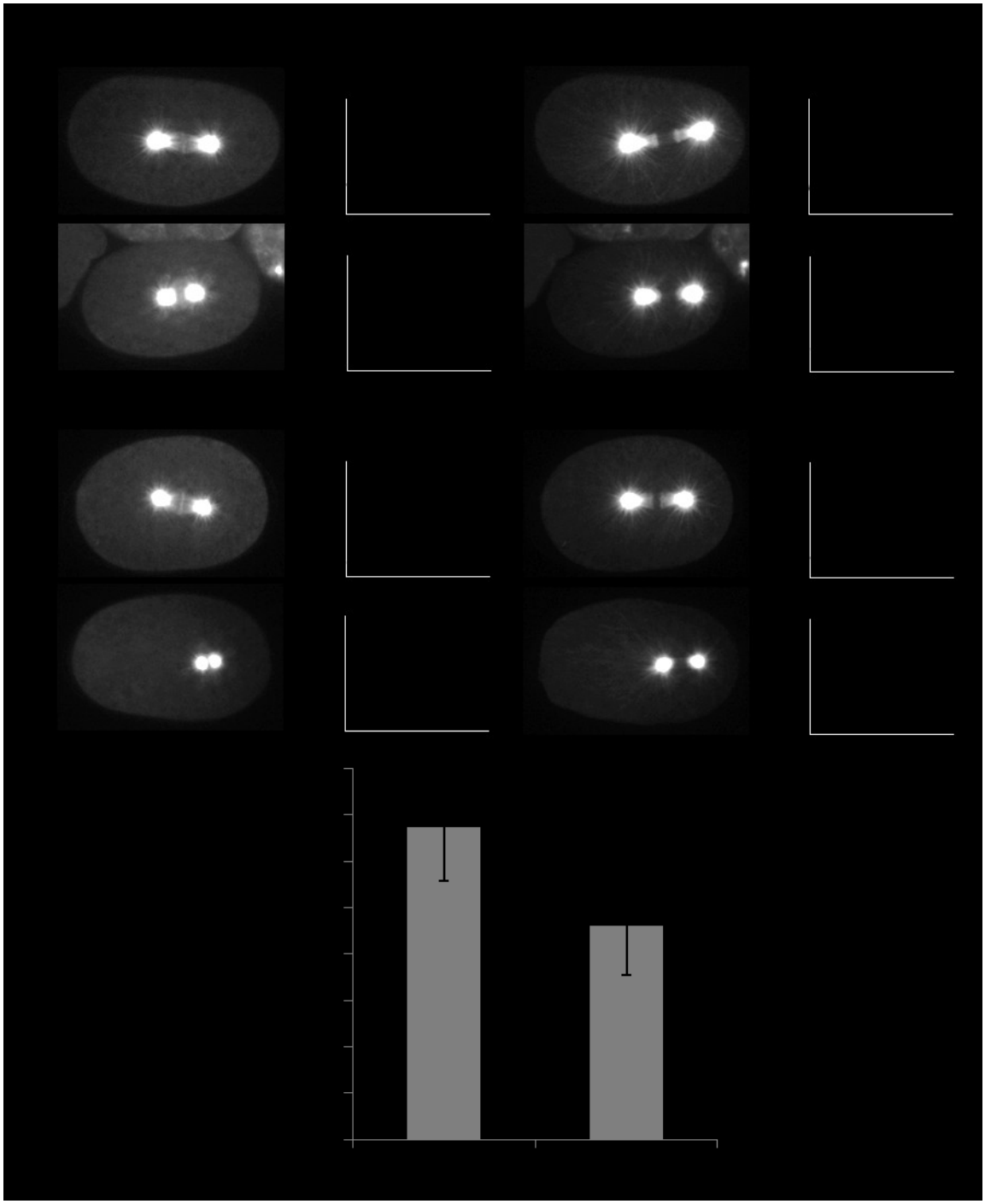

**Figure 4-17. Protein interaction between Aurora A and TPXL-1 is required for TPXL-1 to locate to the chromatin and centrosome**

A) Control embryos have the transgenic *tpxl-1* and the endogenous gene. *tpxl-1(RNAi)* targets the endogenous *tpxl-1* but not the RNAi resistant [RNAi(R)] transgene. Representative line scans across the spindle at metaphase and anaphase are shown. B) Quantification of the integrated signal intensity of TPXL-1(WT)::GFP$^{RNAi(R)}$ or TPXL-1(F15D,F18D)::GFP$^{RNAi(R)}$ at the centrosome relative to background. *tpxl-1(RNAi)* was used to deplete the endogenous TPXL-1. Error bars are the standard deviation.

### 4.7.1 Kinetochores are not required for chromatin localization of TPXL-1

In *C. elegans,* HCP-3 is the centromeric H3 and is required to recruit all other components of the kinetochore (Oegema et al., 2001; Kitagawa, 2009). Depletion of *hcp-3* results in no kinetochores formed on the chromatin and the microtubules are unable to attach to the chromatids. *hcp-3(RNAi)* resulted in normal pronuclear migration and nuclear envelope breakdown but the chromosomes did not align or congress correctly and the centrosomes separated prematurely (Figure 4-18). Line scans across the spindle showed a peak of TPXL-1::GFP that correlated with mCherry::histone in control and *hcp-3(RNAi)* embryos (Figure 4-18). Since TPXL-1 was associated with the chromatin when kinetochores were depleted, TPXL-1 does not require kinetochores to locate to the chromatin.

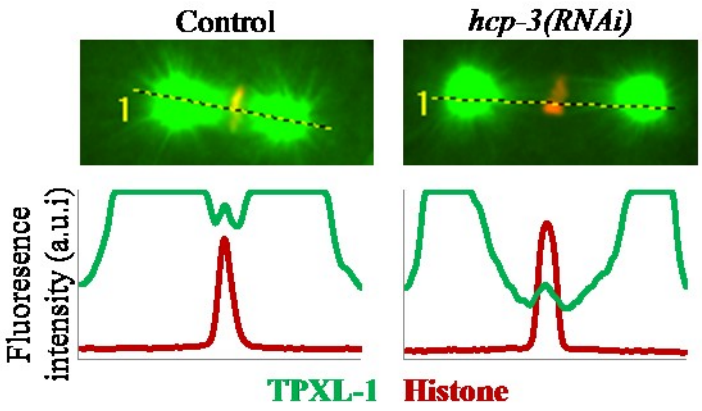


**Figure 4-18. Kinetochores are not required for TPXL-1 to localize to the chromatin**
Line scans of bi-polar spindles in control and *hcp-3(RNAi)* embryos.

### 4.7.2 Chromosomal passenger complex proteins are not required to localize TPXL-1 to chromatin

The chromosomal passenger complex is highly conserved and required for spindle assembly in many organisms (reviewed in van der Horst and Lens, 2014). In human cells, TPX2 has been observed to act as a scaffold that promotes the association of the CPC proteins (Iyer and Tsai, 2012). Since an interaction between TPX2 and the CPC has previously been described, I sought to determine if the TPXL-1 pool at the chromatin requires CPC proteins to locate to the chromatin.

| Human protein | *C. elegans* protein | Function |
|---|---|---|
| Borealin | CSC-1 | Scaffold |
| Survivin | BIR-1 | Scaffold |
| INCENP | ICP-1 | Activator |
| Aurora B | AIR-2 | Kinase |

**Table 4-3. Chromosomal passenger complex in *C. elegans***
A summary of the *C. elegans* orthologs of CPC proteins.

The chromosome passenger complex is composed of four proteins (Table 4-3). In *C. elegans*, the three scaffold proteins CSC-1, BIR-1, and ICP-1 have interdependent localization and all three scaffolds are required for the catalytic subunit of the complex, AIR-2 , to localize (Romano et al., 2003). To determine if the chromosome passenger complex plays a role in targeting TPXL-1 to the chromatin I investigated TPXL-1::GFP in *bir-1(RNAi)* and *air-2(RNAi)* embryos. During mitosis loss of these components of the chromosome passenger complex leads to chromosomes segregation defects and defects in cytokinesis (Speliotes et al., 2000).

During metaphase and anaphase, TPXL-1::GFP co-localized with mCherry::Histone in both *bir-1(RNAi)* and *air-2(RNAi)* (Figure 4-19). This was further assayed with line scans across the spindle in these embryos (Figure 4-20). These data indicated that TPXL-1 did not require the CPC to localize to the chromatin. It is possible that TPXL-1 may interact with the CPC, but that this interaction is not required to recruit TPXL-1 to the chromatin.

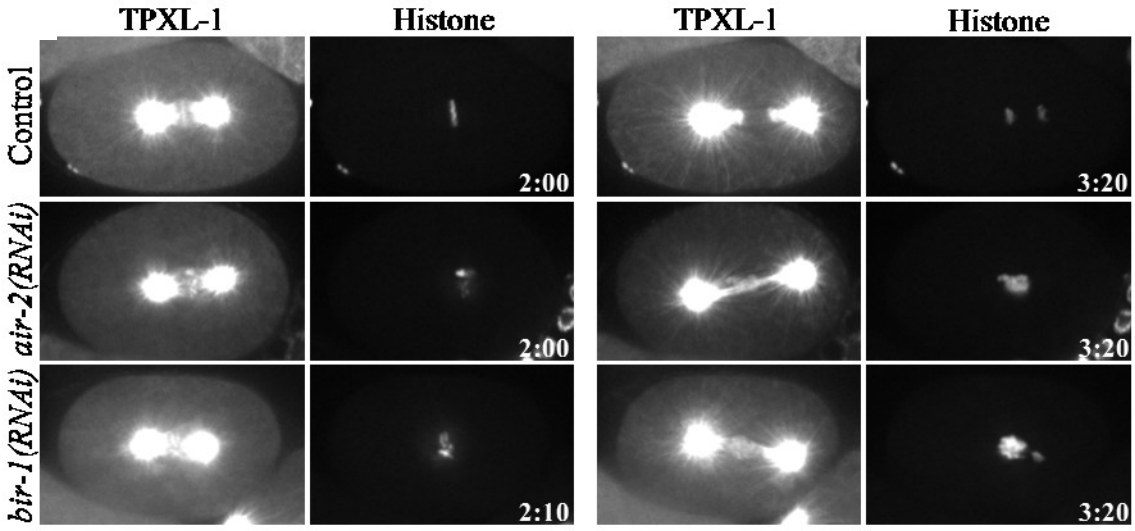


**Figure 4-19. CPC components are not required for TPXL-1 to localize to the chromatin**
Live imaging at 26 °C after 25-27 hours of RNAi feeding with either L4440 empty vector or *air-2(RNAi)* or *bir-1(RNAi)* in a strain expressing TPXL-1::GFP and mCherry histone. Scale bar is 10 µm.

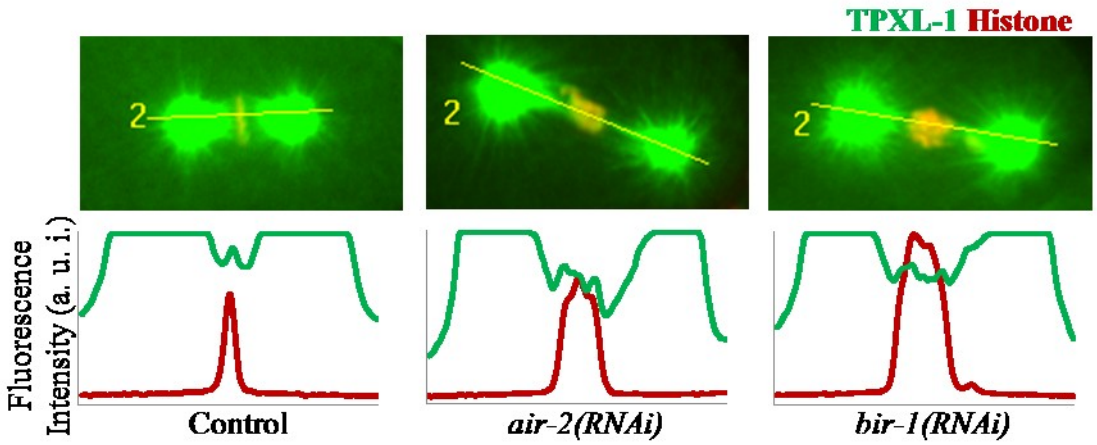


**Figure 4-20. Line scan of TPXl-1 when CPC is compromised**
Line scan perpendicular to the metaphase plate along the spindle at metaphase.

### 4.7.3 RanGTP is required for TPXL-1 to locate to the chromatin

Ran is a small nuclear GTPase that is required in vertebrates for cytoplasm-nuclear transport, spindle assembly, spindle maintenance, and nuclear envelope and nuclear pore assembly at the end of mitosis (Yokoyama and Gruss, 2013). In vertebrates, TPX2 is a well characterized spindle assembly factor that requires Ran to dissociate from importin so it can promote microtubule stability and spindle assembly (Gruss et al., 2001).

The *C. elegans* TPX2-like gene, *tpxl-1*, does not have the C-terminal domain that is predicted to interact with Ran and it is unclear if TPXL-1 has the same roles as TPX2 in promoting Ran-mediated spindle assembly (Karsenti, 2005). Since Ran has well established roles in regulating nuclear levels of TPX2, I investigated if Ran plays a role in the chromatin recruitment of TPXL-1. Specifically, I investigated Ran and related proteins that are characterized to have roles in spindle assembly in *C. elegans* (Table 4-4).

| Human gene | *C. elegans* gene | Description |
|---|---|---|
| Ran | *ran-1* | Small GTPase |
| RanGAP | *ran-2* | Ran GTPase activating protein |
| RCC1 | *ran-3* | Ran guanine exchange factor |
| IMA-2 | *ima-2* | Importin α |
| MEL-28 | *mel-28* | Downstream effector of Ran |

**Table 4-4. Ran associated genes with known roles in early mitotic divisions**
Summary of genes that are involved in the Ran GTPase cycle and show a spindle assembly defect in *C. elegans.* (Adapted from Askjaer et al., 2002).A role for importin β/*imb-1* and RanBP2/*npp-9* have previously been reported but these genes were not analyzed in this thesis.

In *C. elegans* Ran is required for several critical functions including spindle assembly and nuclear envelope assembly, (Askjaer et al., 2002; Bamba et al., 2002). Depletion of Ran in *ran-1(RNAi)* embryos results in several phenotypes including small pronuclei, small embryos, and chromosome segregation errors. In *ran-1(RNAi)* embryos TPXL-1::GFP was not detected at the chromatin (Figure 4-21, Figure 4-22; n=10). These results indicate that Ran, directly or indirectly, is required for chromosomal TPXL-1.

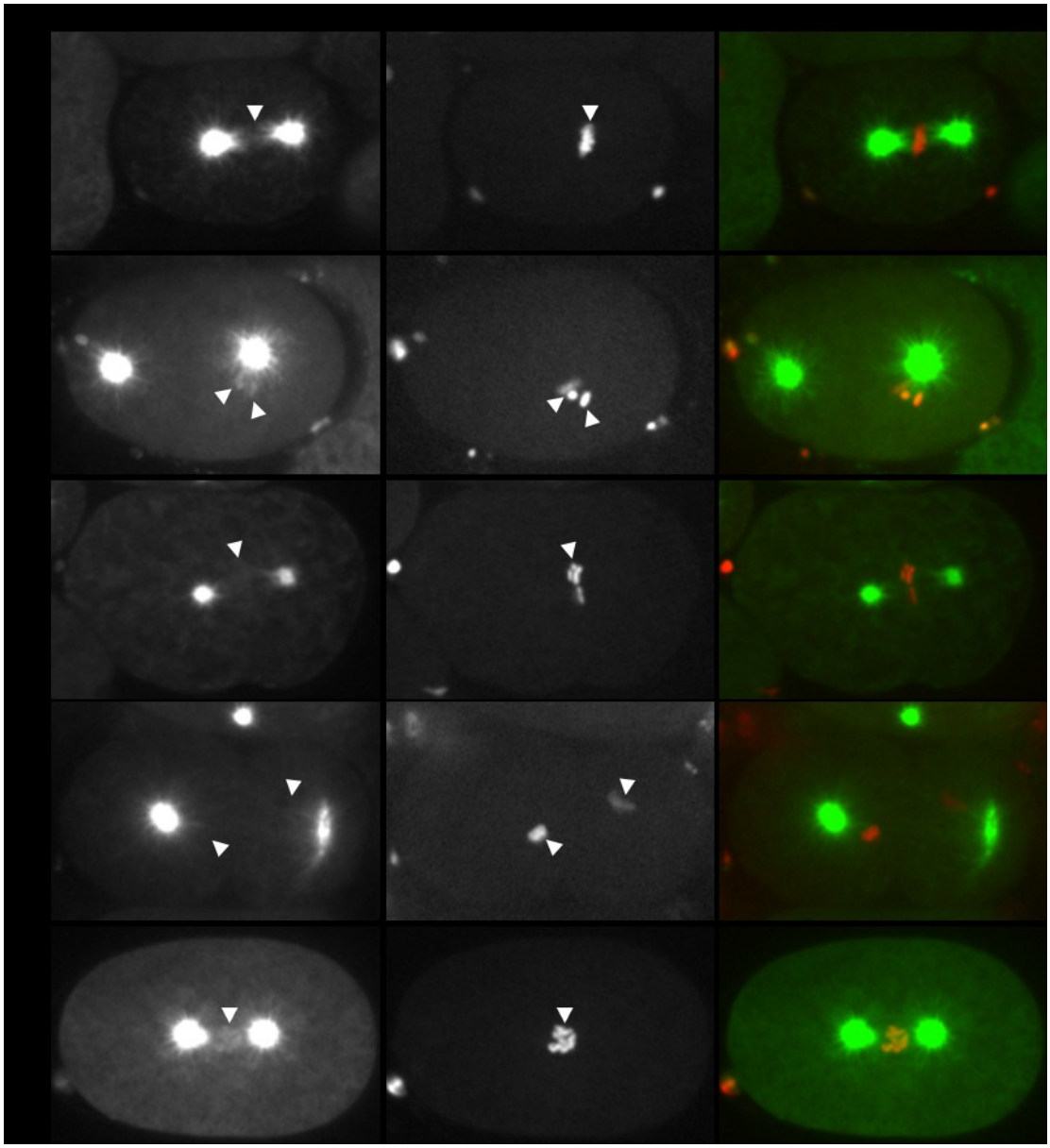

**Figure 4-21. TPXL-1 requires RanGTP to localize to the chromatin**
Live imaging at 26 °C after 24-29 hours of RNAi feeding with either L4440 empty vector or RNAi against a conserved Ran pathway component in a strain expressing TPXL-1::GFP and mCherry histone. Arrow heads indicate the location of the chromatin.

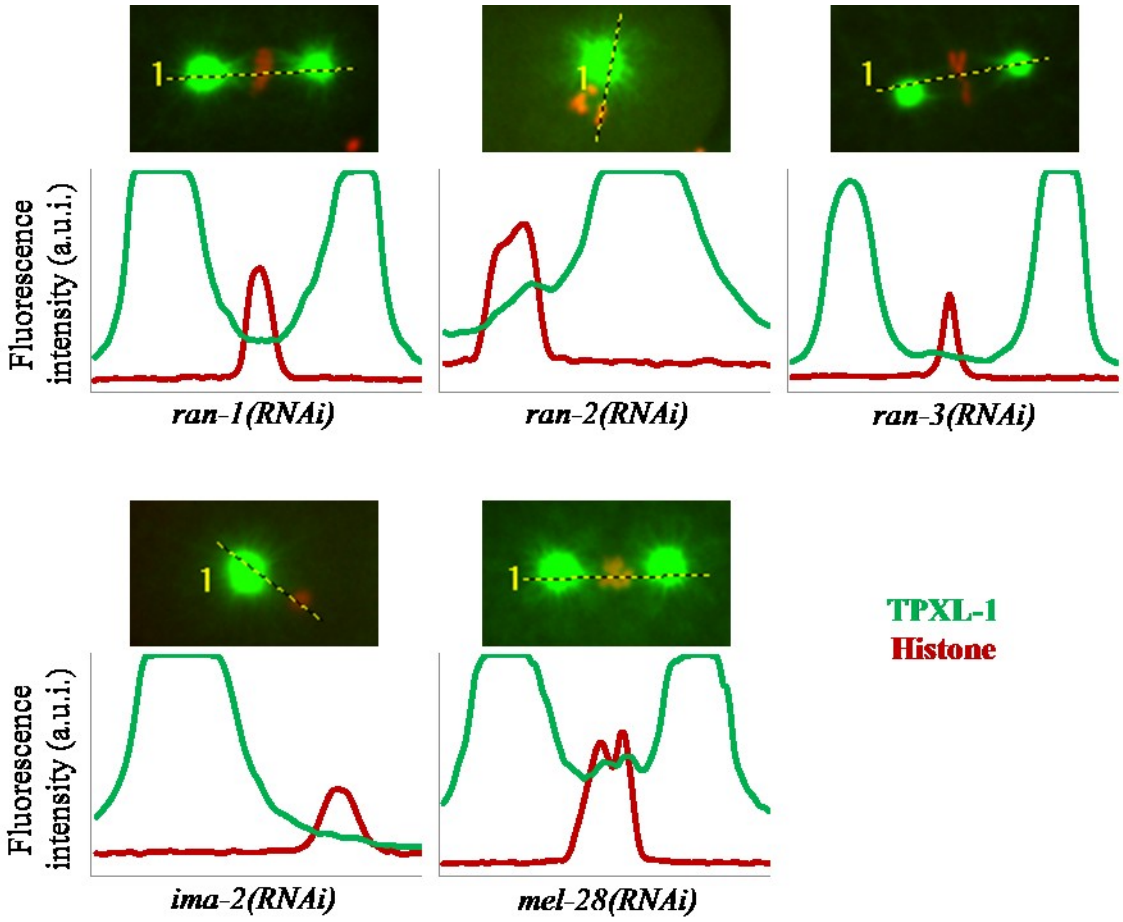


**Figure 4-22. Line-scans TPXL-1 at the chromatin when the Ran pathway is compromised**
Line scan perpendicular to the metaphase plate along the spindle at metaphase or when the chromatin was condensed near a centrosome if no spindle was formed.

In *C. elegans* the RanGAP or GTPase activating protein is encoded by the *ran-2* gene and it is predicted to be a major regulator of the Ran cycle (Askjaer et al., 2002; Bamba et al., 2002). RanGAPs promote the GTPase activity of Ran and stimulate the hydrolysis of GTP to GDP. RanGAPs are usually cytoplasmic or anchored to the cytoplasmic side of the nuclear envelope (Clarke and Zhang, 2008) and play a key role in maintaining the RanGTP gradient around the chromatin. Since Ran has weak GTPase activity without an activator (Clarke and Zhang, 2008), the loss of RanGAP would lead to an excess of RanGTP in the cell. Despite the fact that *ran-2(RNAi)* embryos do not form a bipolar mitotic spindle (Askjaer et al., 2002; Bamba et al., 2002; Figure 4-21), TPXL-1::GFP was still observed at the chromatin in these embryos (Figure 4-21, Figure 4-22; n=8/9 embryos).

RCC1 is the Ran guanine exchange factor or RanGEF and promotes the dissociation of Ran from GDP so it can bind RanGTP. RCC1 is on the chromatin and generates the RanGTP gradient in the nucleus and around the chromatin. The *C. elegans* homolog of RCC1 is RAN-3. Loss of *ran-3* activity causes defects in chromosome condensation, chromosome segregation, and small pronuclei (Askjaer et al., 2002; Bamba et al., 2002). TPXL-1::GFP was not observed on the chromatin in a *ran-3(RNAi)* embryo (Figure 4-21, Figure 4-22; n=1). This is an extremely small sample size because *ran-3(RNAi)* by feeding was only effective in one out of six trials. Injection of dsRNA might be required to achieve efficient knockdown of *ran-3* to increase the sample size for this experiment. Based on these observations, it suggests that it is the GTP bound form of Ran that is required for TPXL-1 to associate with the chromatin.

Importin α/β binds proteins with a nuclear localization signal to import them into the nucleus through the nuclear pore. Once in the nucleus, RanGTP promotes the dissociation of proteins from the importin complex. *C. elegans* have three importin α genes but only one, *ima-2,* plays a role in early mitotic spindle assembly (Askjaer et al., 2002). IMA-2 is associated with mitotic chromosomes but not directly on the spindle (Geles et al., 2002). *ima-2(RNAi)* embryos exhibited a delay in nuclear envelope breakdown and the centrosomes were rocking similar to anaphase embryos when the nuclear envelope broke down (Figure 4-21). TPXL-1::GFP was observed on the mitotic chromatin in less than half of the embryos analyzed (Figure 4-22; n=3/7). This inconsistency may be the result of the fact that some of the embryos may have actually been at a later stage of mitosis. In wild-type embryos, TPXL-1 is excluded from the chromatin during telophase. It is possible that the *ima-2(RNAi)* embryos that did not have TPXL-1 on the chromatin were in telophase and that is why TPXL-1::GFP was not observed on the chromatin.

MEL-28 is a conserved downstream effector of Ran. In *Xenopus* extracts, MEL-28 promotes microtubule nucleation around the chromatin (Yokoyama et al., 2014) and is required for nuclear envelope formation (Gillespie et al., 2007). In *C. elegans*, MEL-28 is required for nuclear envelope assembly but also localizes to the kinetochores and chromatin (Fernandez and Piano, 2006; Galy et al., 2006). To determine if MEL-28 has a role in locating TPXL-1 to the chromatin I imaged TPXL-1::GFP in *mel-28(RNAi)* embryos. TPXL-1::GFP was still associated with the chromatin in *mel-28(RNAi)* embryos

(Figure 4-21, Figure 4-22; n=3). These results indicate that this downstream effect of Ran is not required for TPXL-1 to associate with the chromatin.

### 4.7.4 Loss of PP2A has pleiotropic phenotypes

Since *rsa-1* encodes a regulatory subunit for the PP2A phosphatase, it reasons that the core subunits of PP2A should be required for the same cellular functions as RSA-1. *paa-1(RNAi)* embryos have a pleiotropic phenotype that is more severe than loss of *rsa-1*. In the early *C. elegans* embryo PP2A has roles in nuclear envelope assembly (Asencio et al., 2012), centriole duplication (Kitagawa et al., 2011; Song et al., 2011), spindle assembly (Schlaitz et al., 2007; Lange et al., 2013), and asymmetric partitioning of P-granules (Gallo et al., 2010; Griffin et al., 2011) therefore loss of PP2A has a more severe phenotype than loss of an individual regulatory subunit.

I was not able to accurately determine what mitotic stage the *paa-1(RNAi)* embryos were in because pronuclear migration or other hallmarks of the first mitosis were never observed. In single celled embryos after 25-26 hours of *paa-1(RNAi),* TPXL-1::GFP was only observed in the cytoplasm. However, condensed chromosomes were not observed and as such I was unable to assess if TPXL-1::GFP was on the chromatin in *paa-1(RNAi)* embryos and no conclusions can be drawn from these experiments.

### 4.7.5 Centrosomes are not required for TPXL-1 to locate to the chromatin

Since RSA-1 is located at the centrosomes and affects TPXL-1 at the chromatin, I was interested to see if centrosomes are necessary for TPXL-1 to be observed on the chromatin. I used two RNAi treatments to investigate different aspects of centrosome function. *spd-5(RNAi)* embryos were used to abolish the recruitment of peri-centriolar material to the centrosomes and *tbg-1(RNAi)* was used to generate centrosomes that have a disorganized peri-centriolar matrix.

#### *4.7.5.1 spd-5(RNAi)* does not affect TPXL-1 on the chromatin

SPD-5 is a coiled coil protein that is required to recruit many peri-centriolar proteins to the centrosome including gamma-tubulin and Aurora A kinase (Hamill et al., 2002). Centrosomes do not mature in *spd-5(RNAi)* embryos and microtubules only form around the chromatin after nuclear envelope breakdown (Hamill et al., 2002). Unfortunately,

since TPXL-1::GFP still associated with the microtubules in *spd-5(RNAi)* embryos it was difficult to assess if TPXL-1::GFP was on the chromatin after the microtubules nucleated around the chromatin (Figure 4-23).

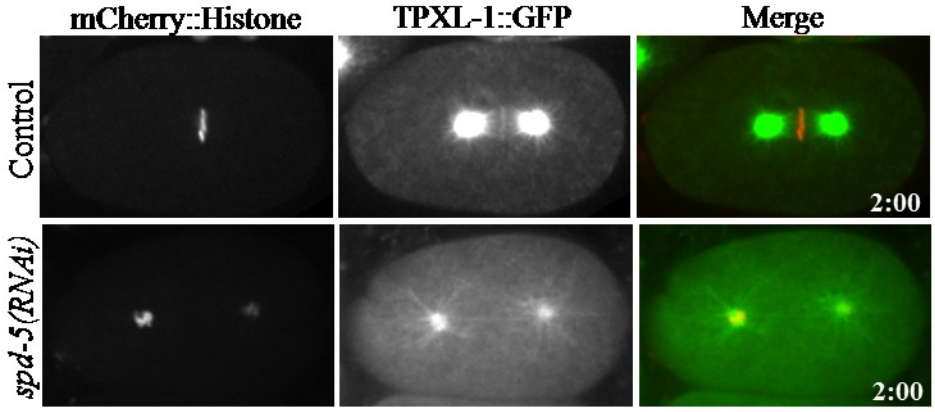


**Figure 4-23. *spd-5(RNAi)* disrupts centrosome formation**
Live imaging at 26 °C after 25-27 hours of RNAi feeding with either L4440 empty vector or *spd-5(RNAi)* in a strain expressing TPXL-1::GFP and mCherry histone. Time 0 is nuclear envelope breakdown.

To distinguish between TPXL-1::GFP on the microtubules and chromatin, I used a strain that expressed mCherry::tubulin (Figure 4-24). For this analysis, the chromatin was defined as regions that were enriched for TPXL-1::GFP but excluded mCherrry::tubulin. In wild-type embryos, the chromosomes were immediately visible following nuclear envelope breakdown and TPXL-1::GFP on the chromatin was visible until telophase. *spd-5(RNAi)* embryos exhibited TPXL-1::GFP on the chromosomes immediately after nuclear envelope breakdown. Once microtubules nucleated around the chromatin it was still difficult to assess if TPXL-1::GFP was on the chromatin. At some time points in mitosis, TPXL-1::GFP could be observed that did not co-localize with the microtubules (Figure 4-24, indicated by asterisks) and is likely associated with the chromatin. Therefore, TPXL-1::GFP does not require centrosomes to be recruited to the chromatin or to be maintained on the chromatin during mitosis.

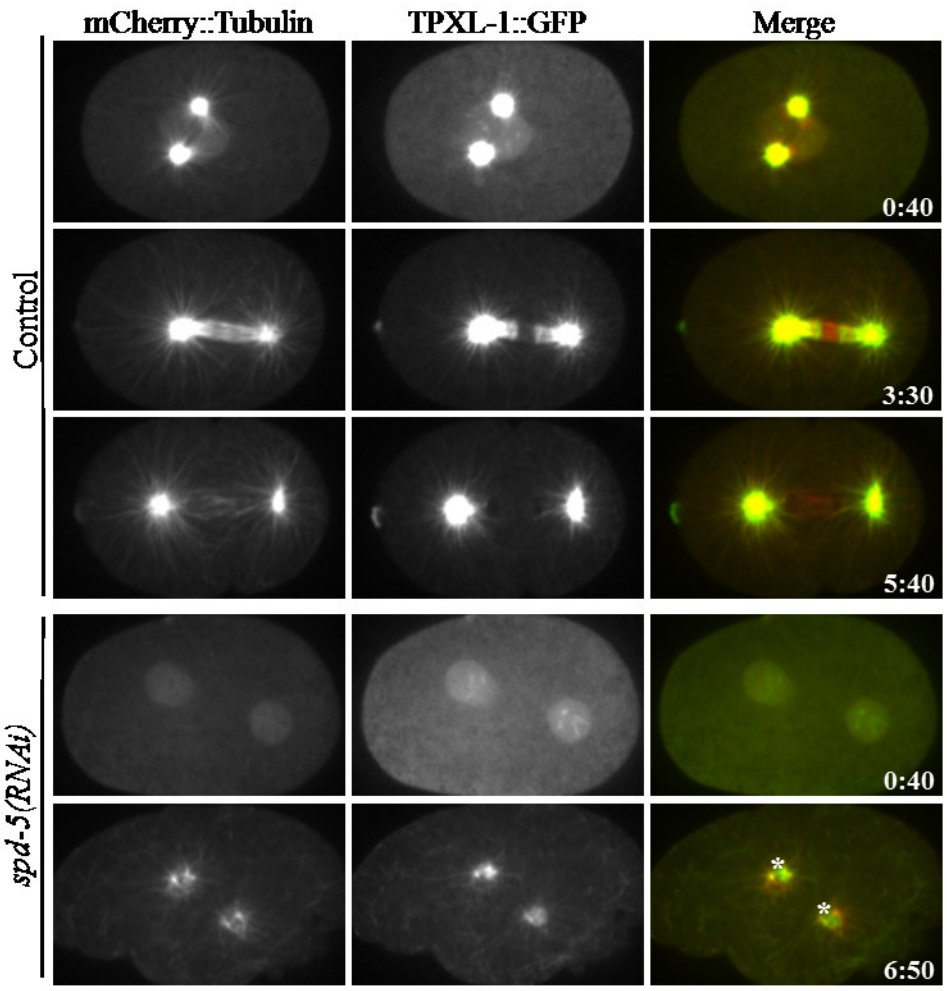


**Figure 4-24. TPXL-1::GFP is on the chromatin in *spd-5(RNAi)***
Live imaging at 26 °C after 26-28 hours of RNAi feeding with either L4440 empty vector or *spd-5(RNAi)* in a strain expressing TPXL-1::GFP and mCherry::tubulin. Time 0 is nuclear envelope breakdown. Asterisks indicate pools of TPXL-1::GFP that do not co-localize with mCherry::tubulin.

#### *4.7.5.2 tbg-1(RNAi)* does not affect TPXL-1 on the chromatin

Experiments done *in vitro* have shown that gamma-tubulin acts as a microtubule nucleator and is thought to promote the nucleation of new microtubules by acting as a template for microtubule growth (Guillet et al., 2011; Kollman et al., 2010). In *C. elegans* embryos, gamma-tubulin/TBG-1 is not required for robust microtubule growth from the centrosomes (Hannak et al., 2002). Instead, TBG-1 plays an important role in organizing the microtubules in the peri-centriolar material to correctly orient the plus end of the microtubule away from the centrosome and into the cytoplasm (O'Toole et al., 2012).

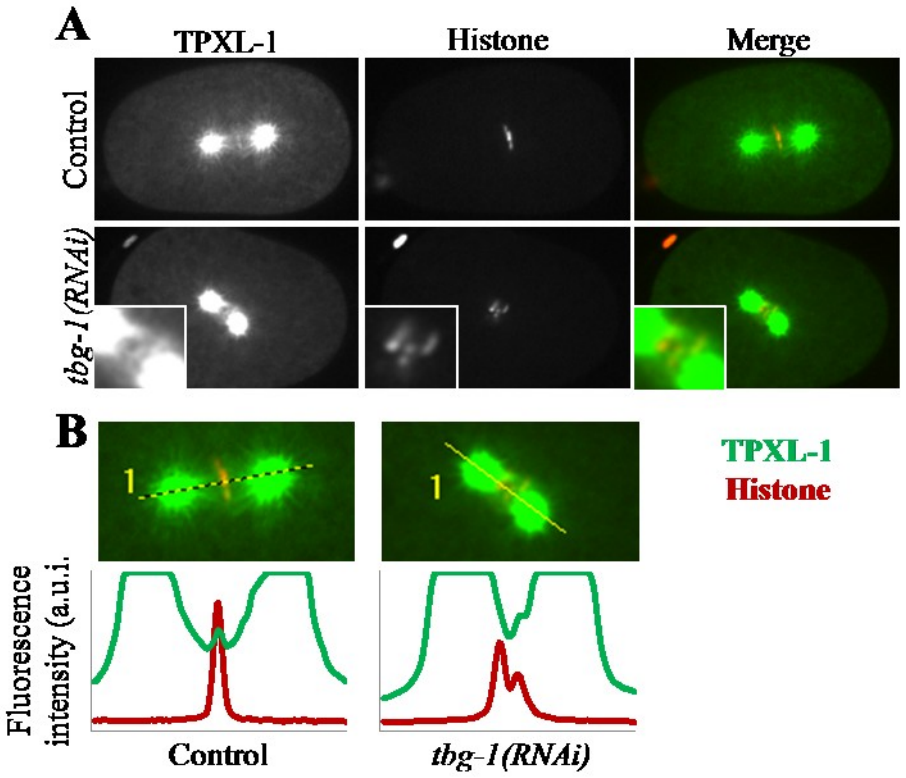


**Figure 4-25. Gamma tubulin does not affect TPXL-1::GFP at the chromatin**
Live imaging at 26 °C after 25-26 hours of RNAi feeding with either L4440 empty vector or *tbg-1(RNAi)* in a strain expressing TPXL-1::GFP and mCherry histone. Insets show a magnification of the chromatin in the *tbg-1(RNAi)* embryo. Line scan perpendicular to the metaphase plate along the spindle at metaphase.

*tbg-1(RNAi)* embryos exhibited spindle assembly defects where the chromosomes were not properly organized between the centrosomes (Figure 4-25). However, TPXL-1::GFP was observed associated with histone in the *tbg-1(RNAi)* embryos. This suggests that gamma tubulin was not required for TPXL-1 to locate to the chromatin.

### 4.7.6 Some MAPs affect TPXL-1 at the chromatin

Since TPXL-1 associates with microtubules, it was possible that other microtubule associated proteins could affect the chromatin localization of TPXL-1.

#### *4.7.6.1 Increased numbers of microtubules does not affect TPXL-1 at the chromatin*

As described in section 4.6.3 of this thesis. Loss of the microtubule depolymerizing kinesin, *klp-7*, resulted in significantly less TPXL-1::GFP at the centrosomes, chromatin, and in the cytoplasm. However, a peak of TPXL-1::GFP intensity is still observed to co-

localize with mCherry::histone (Figure 4-26). These results suggested that increased microtubule numbers does skew the overall distribution of TPXL-1::GFP in the embryo, but that it does not impede TPXL-1::GFP from associating with the chromatin.

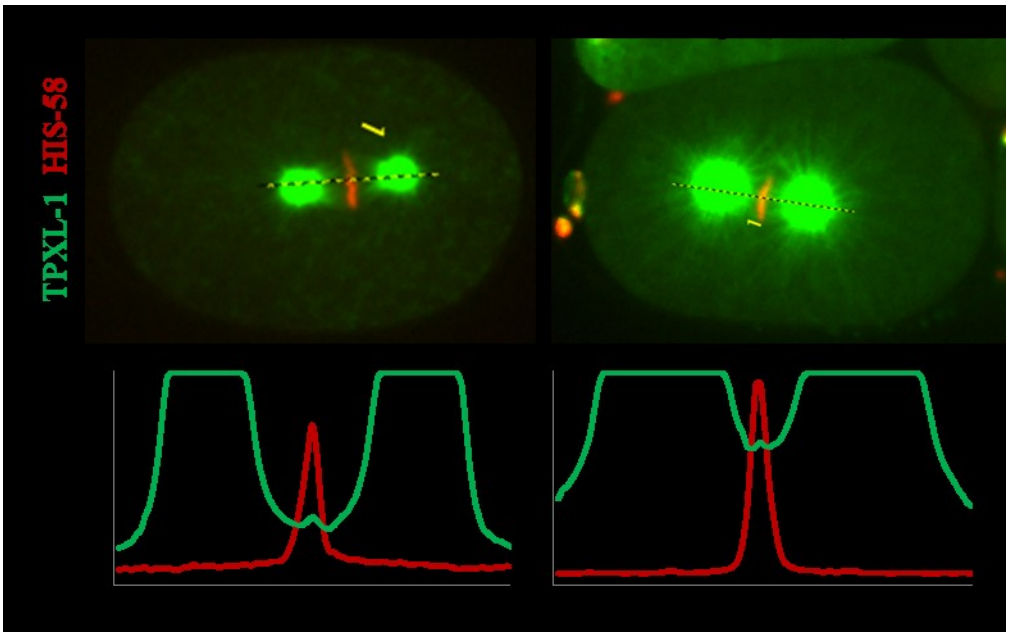


**Figure 4-26. *klp-7(RNAi)* does not affect TPXL-1 at chromatin**
Live imaging at 26 °C after 26-28 hours of RNAi feeding with either L4440 empty vector or *klp-7(RNAi)*. Line scan perpendicular to the metaphase plate along the spindle at metaphase.

#### *4.7.6.2 A microtubule polymerase is required for TPXL-1::GFP to locate to the chromatin*

ZYG-9 is a microtubule polymerase, homologous to XMAP215, that facilitates the addition to tubulin subunits on the plus-end of microtubules. In *C. elegans* ZYG-9 is a centrosomal protein and loss of this function results in a decrease in the number of long microtubules and a short spindle phenotype (Bellanger and Gönczy, 2003; Le Bot, et al., 2003; Matthews et al., 1998; Srayko et al., 2003). Notably, the short spindle phenotype in *zyg-9(RNAi)* embryos is not as severe as the collapsed spindles observed in *rsa-1(RNAi)* or *tpxl-1(RNAi)* embryos.

*zyg-9(RNAi)* embryos exhibited the expected short spindles indicating that the RNAi treatment was successful. Unexpectedly, a peak of TPXL-1::GFP was not observed to co-localize with the mCherry::histone (Figure 4-27).This indicates that ZYG-9 was required for TPXL-1 to associate with the chromatin. The mechanism for how ZYG-9 affects TPXL-1 at the chromatin is unclear, but it may function in the same pathway as RSA-1.

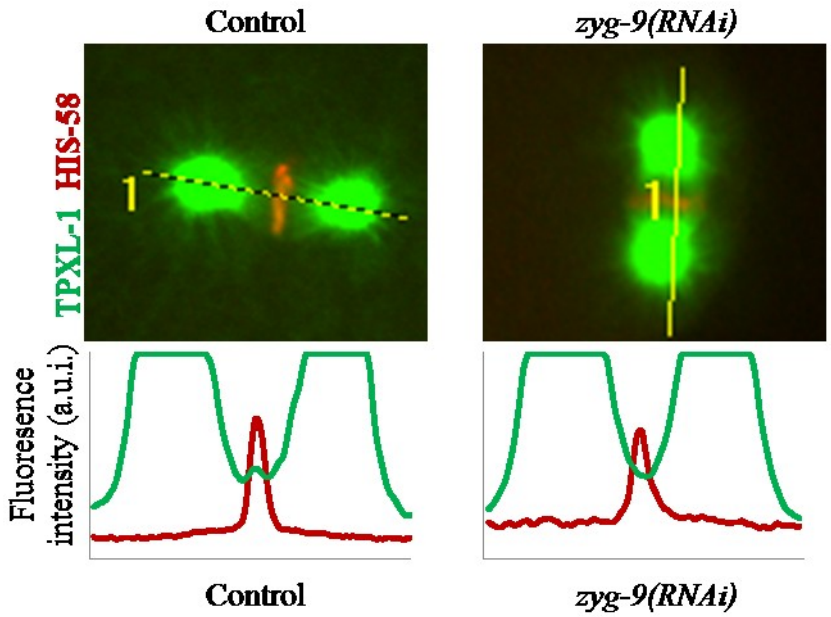


**Figure 4-27. ZYG-9 is required for TPXL-1 to locate to the chromatin**
Live imaging at 26 °C after 27-29 hours of RNAi feeding with either L4440 empty vector or *zyg-9(RNAi)*. Line scan perpendicular to the metaphase plate along the spindle at metaphase.

#### *4.7.6.3 EB proteins do not affect TPXL-1 at the chromatin*

*C. elegans* has three microtubule end binding (EB) protein family members termed *ebp-1, ebp-2*, and *ebp-3*. EB proteins bind the plus ends of actively polymerizing microtubules. The human EB1 protein has many roles in the cell including: regulating microtubule maturation and promoting microtubule dynamics (Maurer et al., 2014), promoting the phosphorylation of kinetochore components (Banerjee et al., 2014), and microtubule stabilization in migrating cells (Morris et al., 2014). However, in *C. elegans,* the function of the EB proteins is unknown. RNAi treatment of any of these genes does not result in any observable phenotypes suggesting that they could be redundant or non-essential. Since EB1 in human cells has been shown to affect both microtubule dynamics and alter kinetochores, I investigated if these proteins played a role in the chromatin localization of TPXL-1. I designed an RNAi construct that was predicted to reduce the function of all three homologs. *ebp-1/2/3(RNAi)* embryos did not exhibit any phenotypes during mitosis or cause embryonic lethality. To verify that this construct was functional, worms expressing EBP-2::GFP were treated with *ebp-1/2/3(RNAi)* and the levels of EBP-2::GFP were visibly reduced (Figure 4-28A) which suggested that the RNAi treatment

was effective but not complete. The *ebp-1/2/3(RNAi)* did not affect the co-localization of TPXL-1 with DAPI (Figure 4-28B). The same results were observed with TPXL-1::GFP co-localizing with mCherry::histone (Figure 4-28C,D). Since this was not a complete knock-down of the EB proteins, it is still possible that they may play a role in the chromatin localization of TPXL-1.

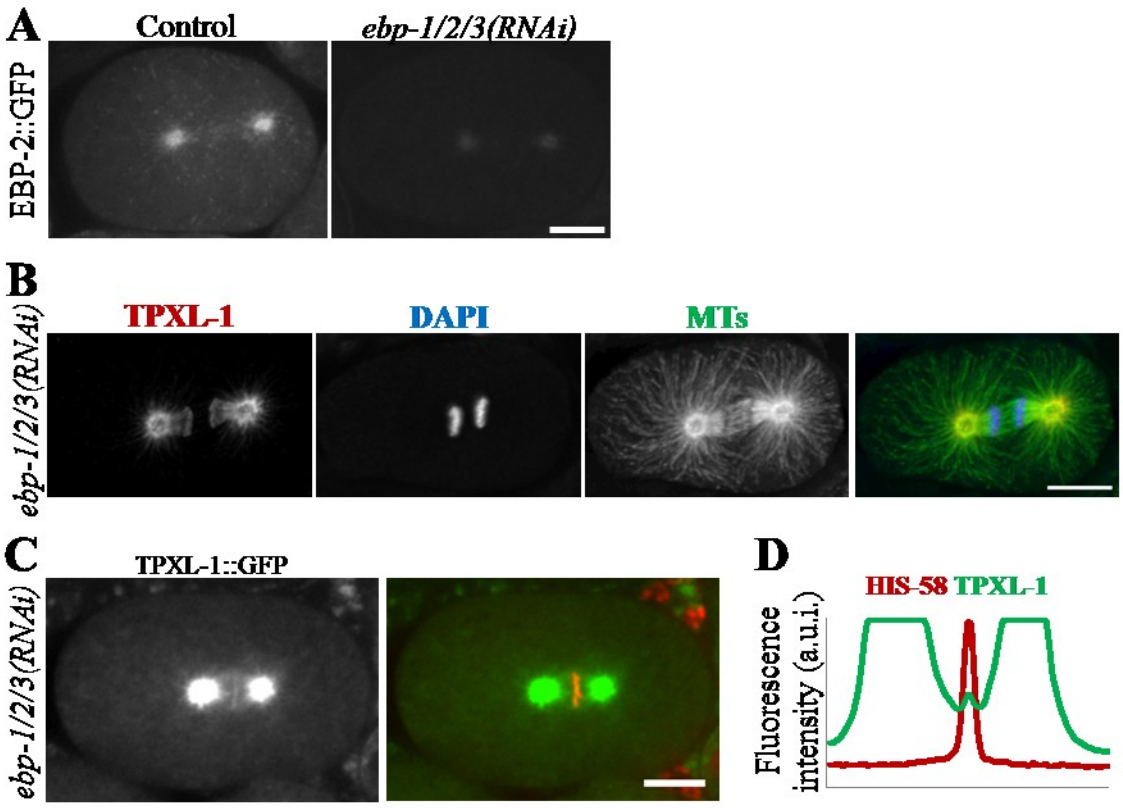


**Figure 4-28. Loss of EBP-1/2/3 does not affect TPXL-1 localization**
A) of EBP-2::GFP fluorescence after *ebp-1/2/3(RNAi)* B) Immunostaining of TPXL-1 in ebp-1/2/3*(RNAi)* embryos at 26 °C.C) Live imaging of TPXL-1::GFP and mCherry::Histone 26 °C after 24 hours of *ebp-1/2/3(RNAi)*. D) Line scan perpendicular to the metaphase plate along the spindle at metaphase. The scale bars are 10 μm.

# 5 Discussion and future directions

The results presented in this thesis were divided into two chapters and an appendix. These results will be discussed together because the findings from both chapters have contributed to a better understanding of RSA-1 function in *C. elegans* embryos.

## 5.1 Summary of *rsa-1(or598)* phenotypes

The *rsa-1(or598)* mutant was discovered in a genetic screen for temperature-sensitive embryonic lethal alleles in *C. elegans* (O'Rourke et al., 2011). This recessive allele has a single point mutation that results in an aspartic acid to glycine mutation at amino acid 319 in the RSA-1 protein (O'Rourke et al., 2011).

I confirmed that *rsa-1(or598)* is a recessive temperature-sensitive allele. I discovered that the embryonic lethality exhibited by *rsa-1(or598)* embryos is the result of a deficiency in a maternal supply of *rsa-1*. However, paternal rescue of some progeny from a homozygous *rsa-1* hermaphrodite indicated that *rsa-1* is also required later in embryogenesis, and that this late embryonic function is likely provided by zygotic transcription. The correct regulation of microtubule dynamics is required for many aspects of development including cell migration and asymmetric divisions. It is possible that *rsa-1* regulates microtubules throughout in development and this is the underlying cause of the L1 arrest phenotype.

DIC microscopy showed that *rsa-1(or598)* embryos exhibited defective pronuclear centration and rotation, small spindles, and defects in chromosome segregation, as previously reported (O'Rourke et al., 2011). Using fluorescence microscopy, I observed that *rsa-1(or598)* embryos exhibited additional phenotypes. I showed that *rsa-1(or598)* had a significant decrease in the levels of centrosomal microtubules, which was consistent with *rsa-1(RNAi)* embryos (Srayko et al., 2005; Schlaitz et al., 2007). Additionally, I found that *rsa-1(or598)* embryos exhibited asynchronous nuclear envelope breakdown, posterior positioning of the spindle, and that the first cell division was more asymmetric than in wild-type embryos. The pronuclear migration and spindle positioning defects could be rescued by *klp-7(RNAi)* which increased the number of microtubules in the embryos. These result indicate that these phenotypes are secondary effects to the loss of microtubule number in *rsa-1(or598)* embryos.

Adult sterility was previously observed in both *rsa-1(RNAi)* (Sonnichsen et al., 2005) and *rsa-1(or598)* (O'Rourke et al., 2011), but the biological basis for this sterility was not investigated. I found that oocytes were never observed in the gonads of *rsa-1(or598)* hermaphrodites that were shifted to the restrictive temperature of 26 °C as L1 larvae. The most apparent cause for this sterility was gonad migration defects that were observed in most of the hermaphrodites. The molecular role of *rsa-1* in gonad migration is unclear; cell migration is known to require precise regulation of both the actin and microtubule cytoskeletons, therefore, *rsa-1* may modulate the microtubule cytoskeleton for post-embryonic non-mitotic functions during development. A potential regulatory role for RSA-1 in cell migration is explored in section 5.7 of this thesis.

## 5.2 **Suppressor screen of *rsa-1(or598)***

The genetic screen for suppressors of *rsa-1(or598)* identified 25 independent suppressor mutations. Six of the suppressors were second site mutations in the *rsa-1* gene, sixteen were in *paa-1*, and three suppressor alleles did not affect any proteins in the RSA-1/PP2A complex.

During the genetic screen the F2 generation was separated into pools so the progeny could be synchronized and shifted to the restrictive temperature as L4 larvae. A maximum of one suppressor was isolated from each of the pools. This step was necessary to synchronize the mutagenized worms and to allow a larger number of genomes to be screened. Since only one suppressor was isolated from a pool, this limited the maximum number of suppressors that could be isolated and biased the screen towards strong suppressors. If a weak and strong suppressor were both present in the same pool, the strong suppressor would be more likely to be selected based on representation in the population.

A general rule to determine if a genetic screen has been completed to saturation is that multiple alleles of all target genes are isolated. While many alleles of the interaction suppressors were isolated, preliminary mapping data suggests that only one allele of each of the unidentified suppressors was found in the screen. It is possible that some suppressor mutations generated in the screen were lost in the pooling and selection

process. Also any unrelated mutations that caused even a small amount to embryonic lethality could prevent a weak suppressor from being isolated in this screen.

### 5.2.1 *rsa-1(or598)* disrupts PAA-1 recruitment to the centrosome

I found that the RSA-1(or598) protein was able to localize to the centrosome, however the mutation causes a very similar phenotype to what has previously been observed in *rsa-1(RNAi)* embryos (Schlaitz et al., 2007; Srayko et al., 2005). This result suggested that even though the RSA-1(or598) protein is able to locate to the centrosomes, it is not functional.

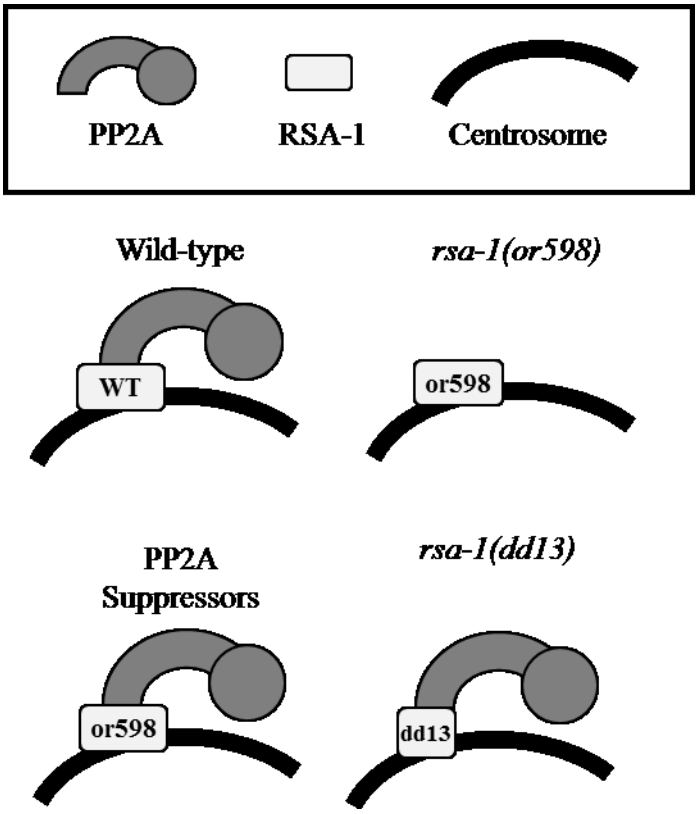


**Figure 5-1. PP2A centrosomal location in mutants**
Schematic of how *rsa-1* and suppressor mutations affect the centrosomal recruitment of PP2A.

I discovered that the *rsa-1(or598)* allele specifically disrupted recruitment of PAA-1 to the centrosome. This phenotype was able to be efficiently suppressed by interaction suppressors. A summary of the protein interactions of the RSA-1/PP2A holoenzyme are presented in Figure 5-1.

### 5.2.2 Interaction domains in PP2A structural and B'' regulatory subunit

The amino acids identified in the interaction suppressors likely highlight key residues involved in the protein-protein interaction between the B'' regulatory subunit and the PP2A structural subunit. These mutations were used to define a probable interaction domain in each of these proteins.

The intragenic mutations in RSA-1 result in amino acid substitutions in the protein that are clustered near the original *or598* lesion. Since these mutations are able to restore the protein interaction with PAA-1 they likely affect a region of the protein that contacts PAA-1. As was suggested in Lange et al. (2013), it is likely that these amino acids identify the region of RSA-1 that contacts PAA-1 (Figure 5-3). This hypothesis is consistent with previous observations that the human B'' regulatory subunit, PR72, is unable to interact with the PP2A structural subunit when there are mutations in the EF2 domain in this region (Janssens et al., 2003).

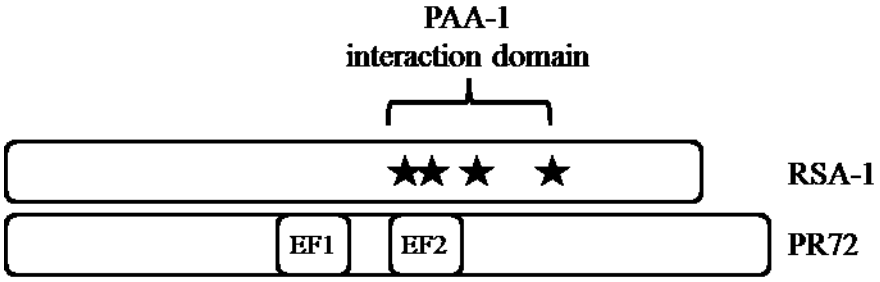


**Figure 5-2. Potential interaction domain in RSA-1**
Schematic of protein domains in RSA-1 and PR72, a human B'' regulatory subunit. Amino acids altered by the suppressor mutations are shown with black stars and the potential PAA-1 interaction domain is shown.

The PP2A structural subunit is highly conserved at the amino acid level. As such, it is likely that the structure of the protein is also conserved. The crystal structure of the human PP2A structural subunit has been solved several times both alone and in complex with other subunits of the PP2A complex (Cho and Xu, 2006; Groves et al., 1999; Strack et al., 2002; Xu et al., 2006; Xu et al., 2008). This protein is C-shaped and is composed of 15 tandem HEAT repeats, which are two anti-parallel α-helices separated by a short linker region joining them (Figure 5-3A). The PP2A structural subunit is a protein with an inner and outer layer of helices with a ridge on the top of the protein that forms an interface that interacts with the catalytic and regulatory subunits (Cho and Xu, 2006; Xu et al., 2006; Xu et al., 2008).

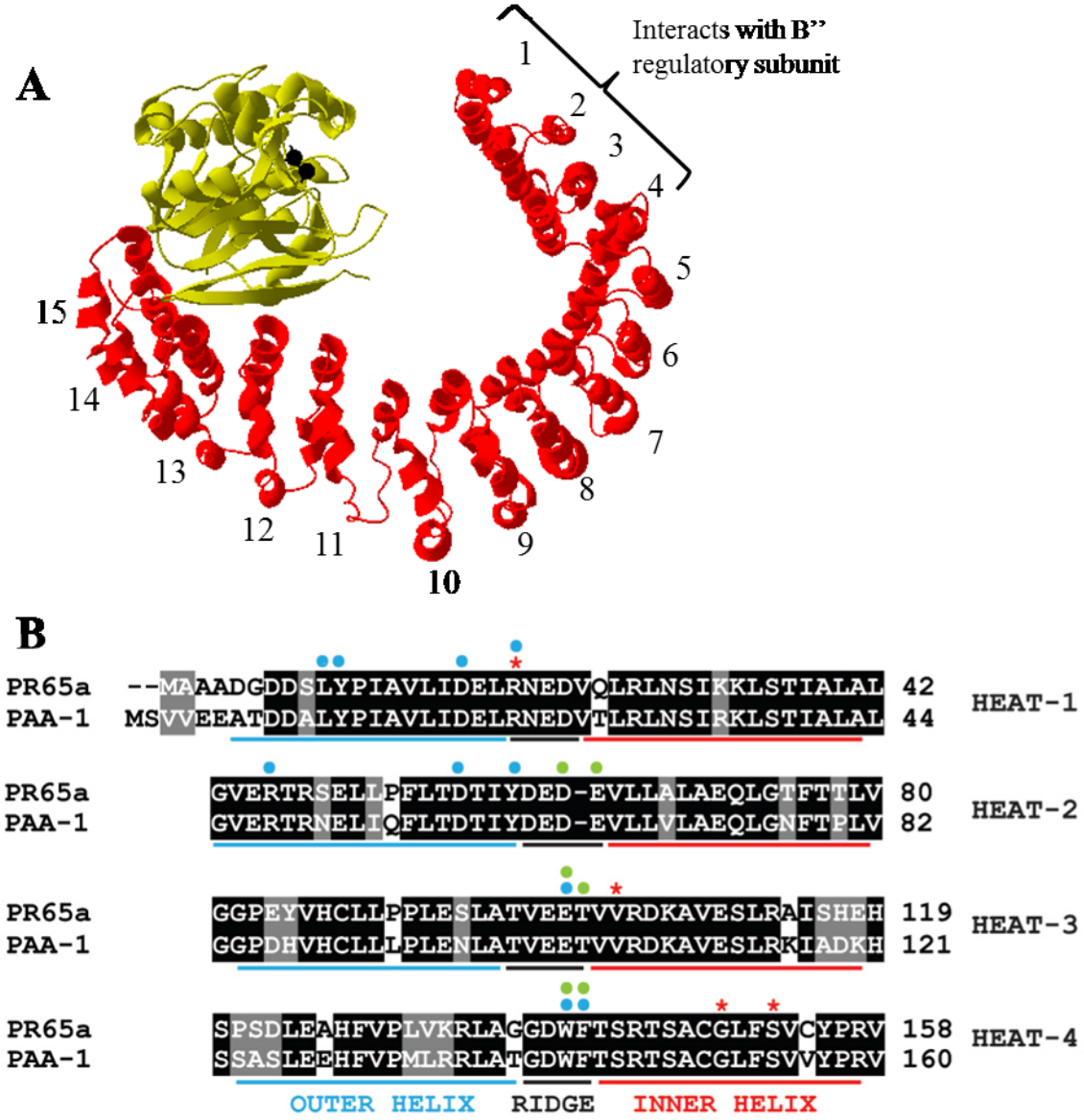


**Figure 5-3. Potential interaction domains in PAA-1**
A) Crystal structure of the PP2A holoenzyme MMDB ID: 84473 (Xu et al., 2008). Structural subunit is red and the catalytic subunit is yellow. The tandem HEAT repeats are labelled. The interaction domain with RSA-1 is indicated. B) Amino acid sequence of the first four HEAT repeats of PAA-1 and human PR65α. Amino acids altered in the suppressor strains are indicated with red asterisks. The circles indicate amino acids that physically interact with a B (blue) or B' (green) regulatory subunit. Black indicates identical residues and grey indicates similar residues.

The amino acids altered by the suppressors in PAA-1 are in the N-terminus of the protein. The suppressor mutations in PAA-1 affected the inner helix and ridge between the helices (Figure 5-3B). This is consistent with the previously published results that indicated that regulatory subunits interact with the N-terminus of the PP2A structural subunit (Cho and Xu, 2006; Xu et al., 2006; Xu et al., 2008). The B family of regulatory

subunits interacts with the N-terminal ridge and outer helices while the B' family only interacts with the ridge (Figure 5-3B). The interaction suppressors indicate that RSA-1 also interacts with the ridge of the HEAT repeats in the N-terminus. This provides an explanation for how the regulatory subunits bind the structural subunit in a mutually exclusive manner. Since each regulatory subunit family interacts with the N-terminal ridge, only one could be bound to the complex at a time. The mutations on the inner helix of HEAT-4 could mean that RSA-1 interacts with the inner helix or these mutations could alter the surface of the ridge that RSA-1 interacts with.

Since the PAA-1 suppressor mutations appeared wild-type on their own, it suggests that these amino acid substitutions do not affect the ability of PAA-1 to interact with other regulatory subunits in *C. elegans*.

### 5.2.3 PP2A B'' regulatory subunits and $Ca^{2+}$ binding

The EF-hand domain is a well characterized protein motif that binds calcium ions. A single EF-hand domain binds a calcium ion and a protein can contain any number of EF-hand domains. An EF-hand comprises two alpha helices joined by a loop. The loop motif is thirteen amino acids long and residues 1, 3, 5, 7, 9, and 12 make direct contact with the calcium ion (Persechini et al., 1989).

One of the best characterized human PP2A B'' regulatory subunits, PR72/PPP2R3A, is known to bind two calcium ions with two EF-hands termed EF1 and EF2 (Janssens et al., 2003). Furthermore, it has been argued that calcium binding by the EF2 motif is critical for the protein interaction with the structural subunit of the PP2A complex; mutations in EF2 that abolish calcium binding also eliminate the protein interaction between PR72 and the PP2A structural subunit (Janssens et al., 2003). The *rsa-1(or598)* mutation affects a key amino acid in the region that corresponds to EF2 in the human PR72 protein (Figure 5-2). Since the *rsa-1(or598)* allele disrupts the protein interaction with the PP2A structural subunit, I was interested if the reason for this disruption was due to a reduced affinity for calcium by RSA-1(or598).

Despite being a B'' regulatory subunit, the RSA-1 protein was not identified in a survey of the *C. elegans* genome for all EF-hand containing proteins (Kumar et al., 2012); RSA-1 does not contain a consensus EF-hand motif. To verify this, I compared the RSA-1 sequence with a consensus EF-hand sequence(http://prosite.expasy.org/PS00018).

The wild-type RSA-1 amino acid sequence varies from the consensus EF-hand motif at a single residue (Table 5-1). In wild-type RSA-1, the third amino acid in the potential EF-hand is a lysine while the consensus motif allows only an aspartic acid, asparagine, or serine at this position. The third amino acid in the motif is known to directly interact with the calcium ion (Persechini et al., 1989) and a positively charged lysine at this residue would not be expected to permit interaction with a positively charged calcium ion. Introduction of a lysine residue at position 1 or 12 of an EF hand can abolish calcium binding (Pottgiesser et al., 1994), but the third residue of the EF-hand has not been tested directly for amino acids that are compatible with $Ca^{2+}$ binding.

| | | | | Suppressors | |
|---|---|---|---|---|---|
| **Position** | **Consensus motif** | **RSA-1** | ***or598*** | ***abc6*** | ***abc24/27*** |
| 1 | D | D | **G** | **S** | **G** |
| 2 | ***Not*** W | L | L | L | L |
| 3 | D, N, or S | **K** | **K** | **K** | **K** |
| 4 | ***Not*** I, L, V, F, Y, or W | D | D | D | D |
| 5 | D, E, N, S, T, or G | D | D | D | **N** |
| 6 | D, N, Q, G, H, R , or K | G | G | G | G |
| 7 | ***Not*** G or P | L | L | L | L |
| 8 | L, I, V, M, or C | L | L | L | L |
| 9 | D, E, N, Q, S, T, A, G, or C | D | D | D | D |
| 10 | ***Any*** | E | E | E | E |
| 11 | ***Any*** | E | E | E | E |
| 12 | D or E | E | E | E | E |
| 13 | L, I, V, M, F, Y, or W | I | I | I | I |

**Table 5-1. RSA-1 deviates from consensus EF-hand motif**
Red amino acids indicate deviations from the consensus EF-hand motif.

I propose that the wild-type RSA-1 protein does not bind calcium and that calcium does not influence the propensity for protein-protein interactions between RSA-1 and the structural subunit of the PP2A complex. While a biochemical analysis is the only way to definitively determine that RSA-1 does not bind calcium ions, the interaction suppressors I identified provide support for this hypothesis. *abc6* affects the same residue as *or598* and changes this amino acid to a serine (Table 5-1). A serine at position 1 in an EF hand would also be inconsistent with the consensus calcium binding motif. Since this suppressor is able to restore PAA-1 recruitment to the centrosome and also restore the protein interaction in the yeast two hybrid assays it seems unlikely that this mutation affects calcium binding. Likewise, suppressor mutations that lie outside of the putative

EF-hand or are in PAA-1 can restore the PAA-1/RSA-1 interaction, suggesting that even if RSA-1 binds calcium, this is not necessary for the interaction since the *or598* lesion is still present.

The experiments that investigated the calcium binding by the human B'' regulatory subunit used site-directed mutagenesis to investigate the function of the EF-hands in PR72 (Janssens et al., 2003). In these experiments, the amino acids at position 1 and 12 of the EF-hands were both mutated to alanine residues. An alanine at position 1 (Jackson et al., 1996) or an alanine at position 12 (Dutt et al., 2000) abolishes calcium binding by EF-hand domains; it is unclear why the authors chose to mutate both residues in PR72. It is possible that in the PR72 protein the aspartic acid at position 1 of EF2 has two functions. Similar to RSA-1, it could be required for the protein interaction with the PP2A structural subunit. However, it could also contribute to calcium binding. It would be interesting to see if the single mutation at position 12 of EF2 is able to efficiently bind calcium. If calcium binding is abolished in that mutant, then it would be possible to investigate if calcium binding and the protein interaction with the PP2A structural subunit are always linked. Since the aspartic acid at position 1 would be intact, the protein may still efficiently interact with the PP2A holoenzyme without binding calcium, similar to the wild-type RSA-1 protein.

To determine if calcium binding is a conserved feature of other B'' regulatory subunits, I compared the amino acid sequences of various B'' proteins including three human proteins, one from *Arabidopsis*, and one from *C. elegans* (Figure 5-4). The human B'' subunits PR72 and PR70 have been experimentally shown to bind calcium and the amino acid sequence for EF2 agrees with the consensus EF motif, while EF1 has a single amino acid that deviates from the consensus. EF2 binds calcium with a higher affinity than EF1 (Janssens et al., 2003) and this deviation is likely the cause for the observed difference in affinities for calcium binding by these two domains. A different human B'' subunit, G5PR, as well as the *Arabidosis* regulatory subunit, TON2, have a consensus motif for EF1, but their EF2 sequences also have deviations in key residues (Figure 5-4). Since these EF2 motifs have variations in critical residues I do not expect them to bind calcium. Based on the sequence alone, it is likely that the first EF domain is functional in

G5PR and TON2, but there is no experimental data to support this claim. In comparison to these proteins, the RSA-1 EF-hand sequence deviates from the consensus in both the

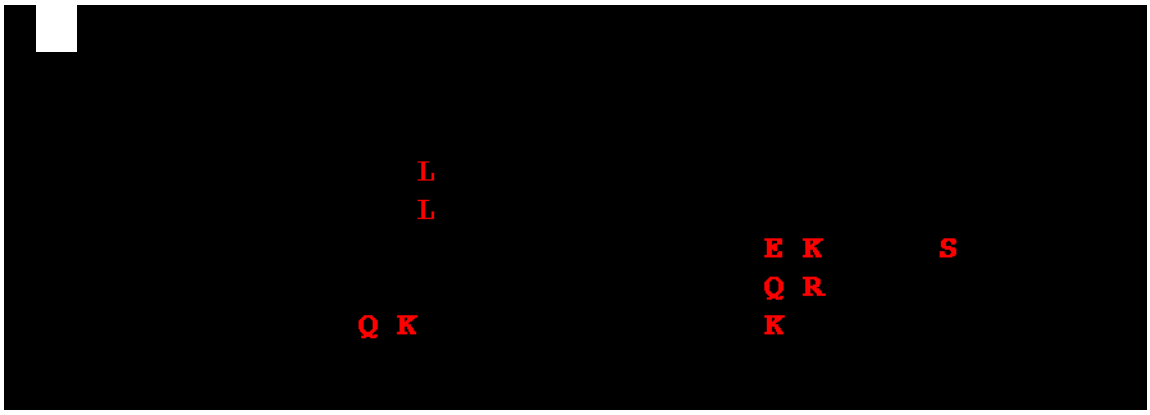


**Figure 5-4. EF hands in B'' subunits**
EF hands 1 and 2 in representative B'' regulatory subunits including *H. sapiens* PR72, PR70, and G5PR, *A. thaliania* TONNEAU2, and *C. elegans* RSA-1. Residues that interact with the $Ca^{2+}$ ion are bold. Amino acids that agree with the consensus EF hand sequence are black while amino acids that do not agree are red. Check marks indicate experimental evidence that the motif binds calcium. The underscore indicates the amino acid affected in the *rsa-1(or598)* mutant.

EF1 and EF2 regions. This suggests that RSA-1 does not bind any calcium ions with its EF-hand motifs. Therefore, it is likely that calcium binding by B'' regulatory subunits is not a conserved feature of this family of proteins and that calcium binding is not critical for protein-protein interactions between regulatory B'' subunits and PP2A structural subunits.

Although the relationship between calcium and B'' regulatory subunit behaviour is not clear, cellular fluctuations of calcium are well-known to regulate specific physiological processes. For example, muscle cells require appropriate calcium storage and release for proper development and function (Benavides and Egli, 2014). PR72 is expressed in skeletal and heart muscles (Hendrix et al., 1993), so it is possible that calcium links the activity of the PP2A phosphatase with physiological functions in the muscle. PR72 is targeted for degradation by a protease called calpain and mutations that disrupted calcium binding prevented calpain mediated degradation of PR72 (Janssens et al., 2009). It is possible that some B'' regulatory subunits bind calcium to regulate the activity or stability of the PP2A complex in response to specific physiological cues.

### 5.2.4 Crystal structures of PP2A holoenzymes

The crystal structure of the human PP2A holoenzyme bound to a B'' regulatory subunit has recently been solved by two independent research groups (Dovega et al., 2014; Wlodarchak et al., 2013). These new findings have facilitated the re-interpretation of the results from the *rsa-1(or598)* interaction suppressors. The published crystal structures for the human B'' regulatory subunits are consistent with the results I obtained from the interaction suppressors in the *rsa-1(or598)* genetic screen. This highlights the power of using traditional genetics techniques as a means to identify interaction domains in proteins that do not have any structural information available.

The three families of regulatory subunits (B, B', and B'') each interact with the ridge of the N-terminus of the PP2A structural subunit (Figure 5-5). The regions that interact with the regulatory subunits overlap, thus explaining how the regulatory subunits bind the holoenzyme in a mutually exclusive manner. The catalytic pocket of the catalytic subunit contains two manganese ions and faces the regulatory subunits. Since the catalytic pocket of the catalytic subunit faces the regulatory subunits it is likely that the regulatory subunits are responsible for positioning the substrates correctly for catalysis.

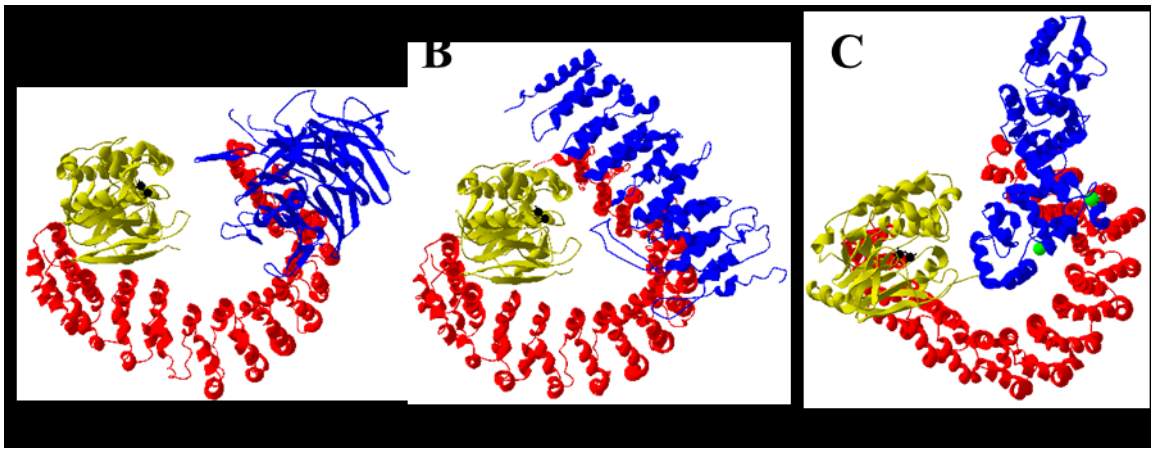


**Figure 5-5. Structure of three PP2A holoenzymes**
For each structure shown the structural subunit is red, the catalytic structure is yellow, and the regulatory subunits are blue. Manganese ions associated with the catalytic subunit are shown as black spheres. A) The PP2A holoenzyme with a B family regulatory subunit, PR55. MMDB ID: 84473 (Xu et al., 2008). B) The PP2A holoenzyme with a B' family regulatory subunit, PR61. MMDB ID: 84472 (Xu et al., 2006) C) The PP2A holoenzyme with a B'' family regulatory subunit, PR70. MMDB ID: 109894 (Wlodarchak et al., 2013). Calcium ions associated with the B'' regulatory subunit are shown as green spheres.

The suppressor mutations in the *C. elegans* structural subunit PAA-1 correspond to amino acids on the ridge of HEAT repeats 1 and 3 and on the inner helix of HEAT 4. Since these mutations restore the protein interaction with RSA-1(or598) I predicted that they may define the interface of the protein that interacts with RSA-1 (Lange et al., 2013). In the B'' crystal structure, the amino acids in HEAT repeats 1 and 3 interact with the regulatory subunit which is consistent with my predictions (Figure 5-6). However, the suppressors in HEAT repeat 4 are on the inner helix and do not directly contact the regulatory subunit. It is likely that these mutations change the conformation of the ridge to facilitate the protein interaction between PAA-1 and RSA-1(or598) (Figure 5-6). The ridge of HEAT repeat 4 is the portion of the protein of the structural subunit that directly contacts the EF2 calcium binding domain. The *rsa-1(or598)* mutation likely disrupts the interaction with this region.

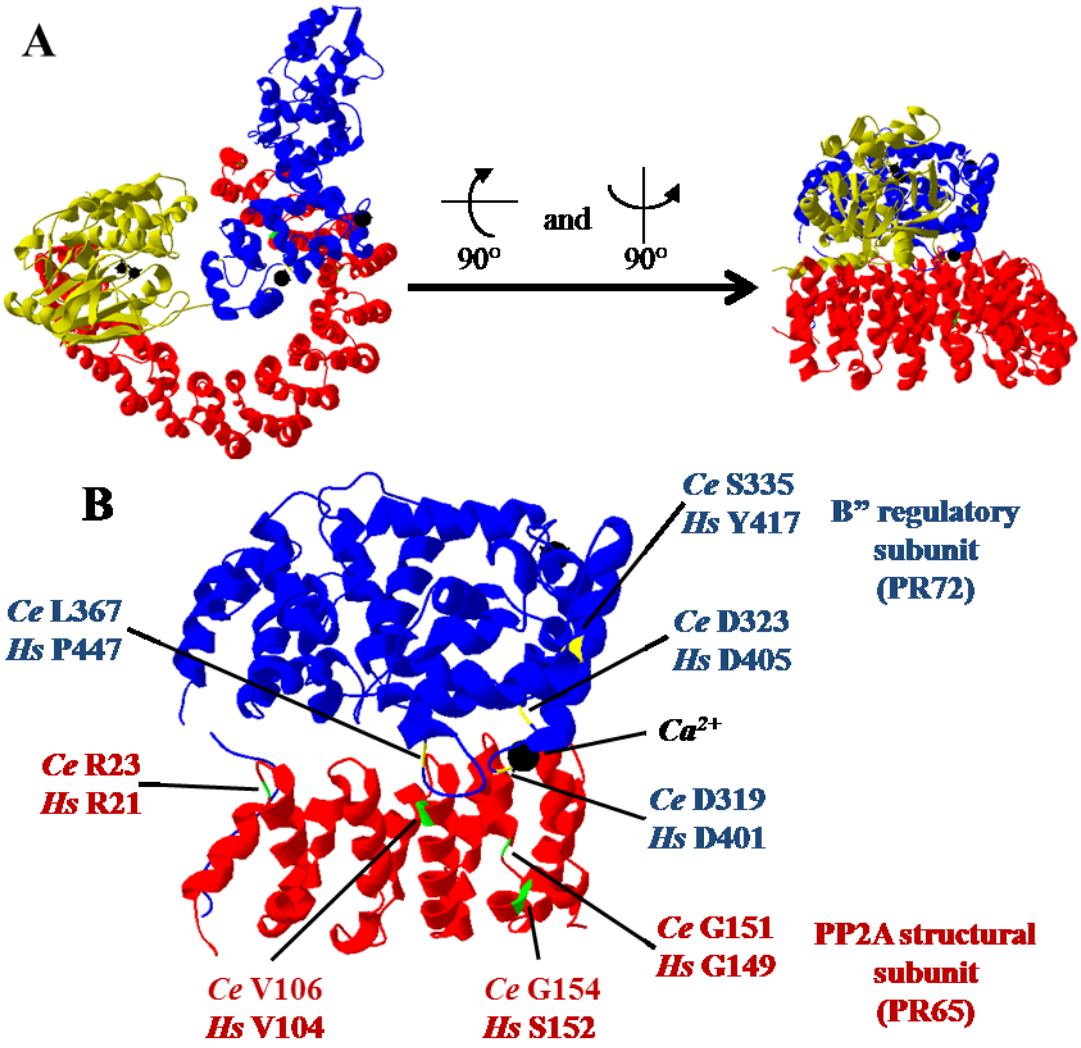


**Figure 5-6. Suppressor mutations in the PP2A/B'' crystal structure**
A) The PP2A holoenzyme with a B'' family regulatory subunit, PR70. MMDB ID: 109894 (Wlodarchak et al., 2013) shown from two angles. The manganese and calcium ions associated with the structure are shown as black spheres. B) A close up view of the rotated holoenzyme to show the interface between the structural and regulatory subunit. The catalytic subunit is not shown. Only the first five heat repeats in PR65 are visible (a.a. 8 - 196), but all amino acids in the regulatory subunit are shown. Amino acids altered in the *rsa-1(or598)* suppressors are shown in green and yellow on the structural and regulatory subunits respectively.

The intragenic suppressor mutations affected four amino acids that were located within a region of approximately 50 amino acids. In the three dimensional model, these amino acids are within close proximity to each other. Three of the four amino acids altered by the intragenic suppressors are on the interface of the B'' regulatory subunit and structural subunit interaction. The intragenic suppressor mutation that affects S335 (*H. sapiens* Y417) causes an amino acid substitution in the alpha helix that contains the EF2 hand calcium binding domain. Since the *C. elegans* RSA-1 protein likely does not bind

calcium ions, it could deviate from the three dimensional conformation of the human B'' regulatory subunits. I propose this is only a slight deviation because the suppressor mutations in both PAA-1 and RSA-1 correspond to the interface between the regulatory and structural subunits in the published crystal structures. While it is probable that the exact three dimensional structure of RSA-1 deviates from these published B'' regulatory subunit structures, the overall structure of the protein is likely conserved. It is possible that the EF-hand motif could impose the same structural restraints to the human and *C. elegans* B'' regulatory subunits, only that this region would no longer be modulated by calcium in *C. elegans.*

### 5.2.5 Instability of kinetochore-microtubule interaction as a mechanism to suppress of *rsa-1(or598)*

Preliminary results presented in Appendix B of this thesis have indicated that nonsense mutations in *ska-1* or depletion of *ska-1* with RNAi treatment are sufficient to restore embryonic viability to *rsa-1(or598)* embryos. The human Ska complex can interact with depolymerizing microtubules (Schmidt et la., 2012; Welburn et al., 2009) and is required to maintain stable kinetochore-microtubule interactions (Daum et al., 2009; Gaitos et al., 2009; Raaijmakers et al., 2009), likely by promoting the interaction of the kinetochore with dynamic depolymerizing microtubules. Depletion of *ska-1* does not result in embryonic lethality in *C. elegans* (Schmidt et la., 2012), however a systematic analysis of these embryos has not yet been published. While the function of *ska-1* in not known in *C. elegans*, the observation that loss of *ska-1* can suppress *rsa-1(or598)* strongly implicates it has a role in spindle assembly. Recently, overexpression of the human Ska1 protein has been shown to promote prostate tumourigenesis (Li et al., 2014) and cell growth of gastric cancer cells (Sun et al., 2014). Depletion of Ska1 in hepatocellular carcinoma cells is sufficient to inhibit proliferation (Qin et al., 2013). These results indicate that Ska1 may be a good target for novel anti-cancer treatments. Investigating the function of *ska-1* in *C. elegans* will generate a better understanding of the biology of the Ska complex and how it contributes to spindle assembly.

Preliminary results have also indicated that a missense mutation in a B' PP2A regulatory subunit, *pptr-1*, may be a suppressor of *rsa-1(or598)*. The human homolog of this regulatory subunit, PPP2R5A/B56α, is required for stable microtubule-kinetochore

attachments (Foley et al., 2011). Since *ska-1* also affects the stability of microtubule-kinetochore interactions, this may represent a general mechanism to suppress embryonic lethality caused by *rsa-1(or598)*. However, the *C. elegans* PPTR-1 protein does not currently have a characterized role in spindle assembly. In *C. elegans*, *pptr-1* has a role in regulating metabolism and stress response (Padmanabhan et al., 2009) and in the early embryo it is required for the asymmetric partitioning of P-granules (Gallo et al., 2010). It is possible that these known functions of *pptr-1* confer an ability to suppress *rsa-1(or598)* or that *pptr-1* has a currently uncharacterized role in *C. elegans* spindle assembly. Further work is required to distinguish between these possibilities.

### 5.3 Characterization of the *rsa-1(dd13)* allele

The *rsa-1(dd13)* allele disrupts a splice site and introduces a premature stop codon (Schlaitz et al., 2007). This mutation could either create a truncated protein that is missing the last 70 amino acids or the mRNA could be recognized by the non-sense mediated decay machinery and no protein would be translated from the transcript. The anti-RSA-1 antibodies were generated against a peptide, and only recognize the last eighteen amino acids of the protein (Schlaitz et al., 2007). If the *rsa-1(dd13)* allele creates a truncated protein, then this antibody would be unable to detect it, therefore immunostaining or a Western blot cannot be used to determine if this allele creates a truncated protein.

The complementation test between *rsa-1(dd13)* and *rsa-1(or598)* indicated that these mutations complement each other. It is likely *rsa-1(dd13)* and *rsa-1(or598)* each produce a mutant protein that is missing one key function and when both alleles are present the two mutations can functionally compensate for each other. This result indicated that the *rsa-1(dd13)* mutation does generate a protein that retains at least some function in the embryo.

The RSA-1 protein was not observed in immunostained early *rsa-1(dd13)* embryos. This is not surprising because the amino acids recognized by the RSA-1 antibody are not predicted to be present in the RSA-1(dd13) protein. However, in these embryos the PP2A structural subunit, PAA-1, was observed at the centrosomes. Since PAA-1 requires RSA-1 to localize to the centrosome (Schlaitz et al., 2007), the observation that PAA-1 is at the

centrosome strongly suggests that RSA-1(dd13) is also localizing correctly. These results are also consistent with the published crystal structure of the PP2A holoenzyme with B''/PR72 regulatory subunit (Wlodarchak et al., 2013). This structure indicated that the protein interaction between the B'' regulatory and PP2A structural subunit does not require the C-terminus of the protein. Therefore, the region of RSA-1 required to recruit PAA-1 to the centrosome would still be present in the RSA-1(dd13) truncated protein (Figure 5-7).

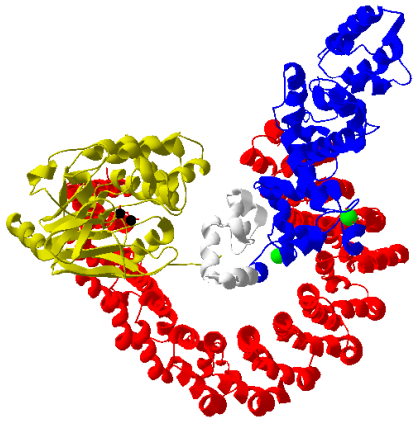

**Figure 5-7. Crystal structure of predicted truncation of B'' regulatory subunit**
The PP2A holoenzyme with a B'' family regulatory subunit, PR70. MMDB ID: 109894 (Wlodarchak et al., 2013). The amino acids corresponding to the truncation in *rsa-1(dd13)* are shown in white . Calcium ions, which are expected to be absent in the RSA-1 protein complex, are green and manganese ions are black.

Although not direct evidence, the PAA-1 staining suggests that the RSA-1 protein does not require the last 70 amino acids to localize to the centrosome. However, the last 70 amino acids do have an essential function since this allele is 100% embryonic lethal. Given the published crystal structures of human B'' regulatory subunits (Wlodarchak et al., 2013; Dovega et al., 2014) it is likely that the C-terminus of the protein is involved in interacting with substrates of the PP2A complex. The 70 amino acids that are missing in the *rsa-1(dd13)* allele (Figure 5-7) correspond to the portion of the human PR72 protein that interacts with a substrate, Cdc6, to mediate its dephosphorylation (Wlodarchak et al., 2013). The manganese ions in the active site of the catalytic subunit face the B'' regulatory subunit and amino acids in this region directly contact the catalytic subunit. In RSA-1 these amino acids likely also mediate the interaction with substrates of the RSA-1/PP2A complex.

Given these data, it is not surprising that the *paa-1(abc2)* suppressor was unable to suppress *rsa-1(dd13)*. The lethality observed in the *rsa-1(dd13)* strain is not the result of a decrease in PAA-1 levels at the centrosome. Since RSA-1(dd13) is already capable of recruiting PAA-1 to the centrosome, a suppressor mutation that restores recruitment of PAA-1 to the centrosome should not increase the embryonic viability. The unidentified suppressors *abc19* and *abc25* recruited PAA-1 to the centrosomes in a currently unknown mechanism and, by the same reasoning, it is unlikely that those mutations could suppress *rsa-1(dd13)*. However, the suppressor *abc17* was not observed to restore PAA-1 levels at the centrosome and appears to weakly suppress *rsa-1(or598)* through a mechanism that does not require centrosomal PAA-1. It is possible that *abc17* could suppress *rsa-1(dd13)* and it would be an interesting experiment to create the double mutant and determine if *abc17* can suppress *rsa-1(dd13)*. Both of these genes are linked to LG I but the map position of *abc17* was not refined, which impeded a direct test of this idea. Once the position of *abc17* is refined or the mutation is identified, then a genetic cross could be developed to generate the *rsa-1(dd13), abc17* strain.

### 5.4 **RSA-1 regulates spindle length**

The centrosomal recruitment of PP2A by RSA-1 is critical for spindle assembly and wild-type microtubule number in *C. elegans* embryos. A main focus of this thesis was to investigate why *rsa-1(or598)* embryos exhibit a spindle-collapse phenotype.

It has been proposed that TPXL-1 is the centrosomal component that regulates spindle length. Levels of TPXL-1 at centrosomes correlate directly with spindle size in many organisms including *C. elegans* (Greenan et al., 2010), human cells (Bird and Hyman, 2008), and in *Drosophila* (Goshima and Scholey, 2010).

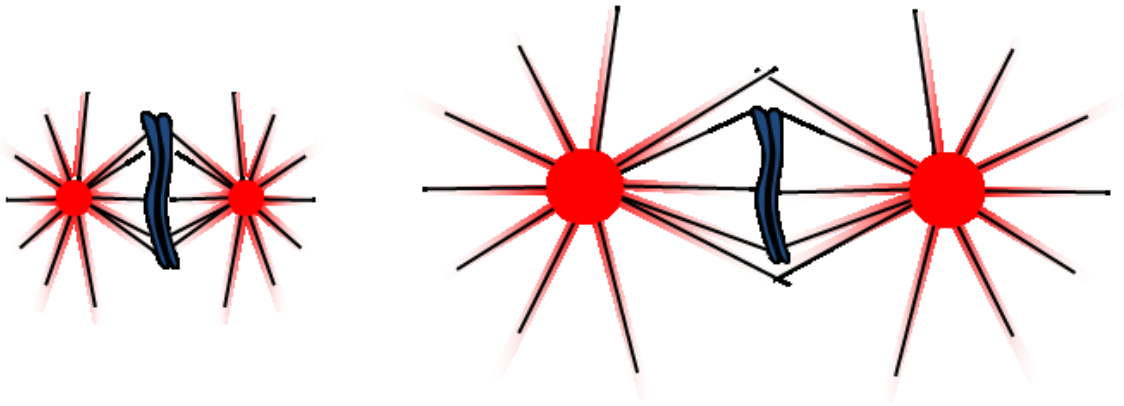

**Figure 5-8. Centrosomal TPXL-1 correlates with spindle length**
Centrosome size determines centrosomal levels of TPXL-1 (red). Centrosomal levels of TPXL-1 correlate directly with the gradient of TPXL-1 on the microtubules and spindle length.

In *C. elegans,* the gradient of TPXL-1 on the microtubules is dependent on centrosome size. It was observed that smaller centrosomes have less TPXL-1 and it was proposed that this is what leads to the limited TPXL-1 gradient on the spindle microtubules and smaller spindles (Greenan et al., 2010; Figure 5-8). Since TPXL-1 has several functions in cells, any or all of these functions could contribute to regulating spindle length. TPXL-1 is thought to bind microtubules so it could directly promote the stability or nucleation of microtubules. TPXL-1 could also function as an Aurora A activator on the spindle to indirectly promote spindle length through the phosphorylation of other spindle assembly factors. These are not mutually exclusive roles for TPXL-1 in spindle length regulation.

*rsa-1(RNAi)* embryos had significantly reduced levels of the TPXL-1 protein at the centrosomes and an extremely small spindle (Schlaitz et al., 2007) which supports the hypothesis that centrosomal levels of TPXL-1 ultimately determine spindle length. However, in *rsa-1(lf)* embryos, TPXL-1 is still observed on the astral microtubules and it is not possible to assess the gradient of TPXL-1 on the spindle microtubules of the collapsed spindles. To determine how RSA-1 regulates spindle length, I investigated Aurora A and several spindle assembly factors that contribute to spindle length regulation in other systems.

### 5.4.1 Spindle length is regulated by Aurora A on the microtubules

Locating to the spindle is critical for Aurora A function in spindle assembly. In vertebrate cells and *C. elegans* embryos, Aurora A requires TPXL-1 to locate to the spindle microtubules (Kufer et al., 2002; Ozlü et al., 2005). Mutations in TPXL-1 that prevent the protein interaction with Aurora A result in a change in Aurora A location, whereby Aurora A is observed at the centrosome but not on the microtubules (Ozlü et al., 2005). This suggests that the spindle collapse phenotype observed in *tpxl-1(RNAi)* (Bird and Hyman, 2008; Chen et al., 2014; Ozlü et al., 2005) embryos could be due to a change in Aurora A location or activity.

I discovered a new role for PP2A in modulating Aurora A localization in *C. elegans* embryos. From immunofluorescence and live imaging of *rsa-1(or598)* and *rsa-1(RNAi)*

embryos, Aurora A was observed at the centrosome but not on the microtubules during spindle assembly. This change in location was similar to that observed in *tpxl-1(RNAi)* embryos. These results indicated that RSA-1, like TPXL-1, is required for Aurora A to locate to the microtubules during spindle assembly.

A simple model where RSA-1 promotes the protein interaction between Aurora A and TPXL-1 can explain many of the phenotypes observed in *rsa-1(lf)* embryos (Figure 5-9). It was previously shown that the protein interaction between Aurora A and TPXL-1 is required for Aurora A to locate to microtubules (Ozlü et al., 2005), so loss of this protein interaction in *rsa-1(lf)* would prevent Aurora A from locating to the microtubules. The TPXL-1(F15D, F18D) mutant, which is unable to interact with Aurora A, was less abundant at the centrosome than wild-type TPXL-1. This suggests that the protein interaction between Aurora A and TPXL-1 is also required for the efficient recruitment of TPXL-1 to the centrosome. There is a significant decrease in the amount of TPXL-1 at the centrosome in *rsa-1(lf)* embryos, which I propose is a consequence of the decreased interaction between Aurora A and TPXL-1 proteins. RSA-1 could directly or indirectly promote this protein interaction. Since RSA-1 pulls down TPXL-1 in co-immunoprecipitation experiments (Schlaitz et al., 2007) it is likely that RSA-1 directly affects Aurora A and TPXL-1.

The microtubule localization of Aurora A may be of clinical significance. There is a colon cancer-associated missense mutation in Aurora A that disrupts the protein interaction between Aurora A and TPX2 (Bibby et al., 2009). This mutant Aurora A protein is located at the centrosome but not on the microtubules (Bibby et al., 2009). It is possible that a somatic mutation in Aurora A resulted in aneuploidy that drove tumorigenesis in these cells. Since mis-localization of Aurora A may contribute to aneuploidy, a better understanding of how the localization of Aurora A is regulated is required to better understand how this contributes to cancer formation.

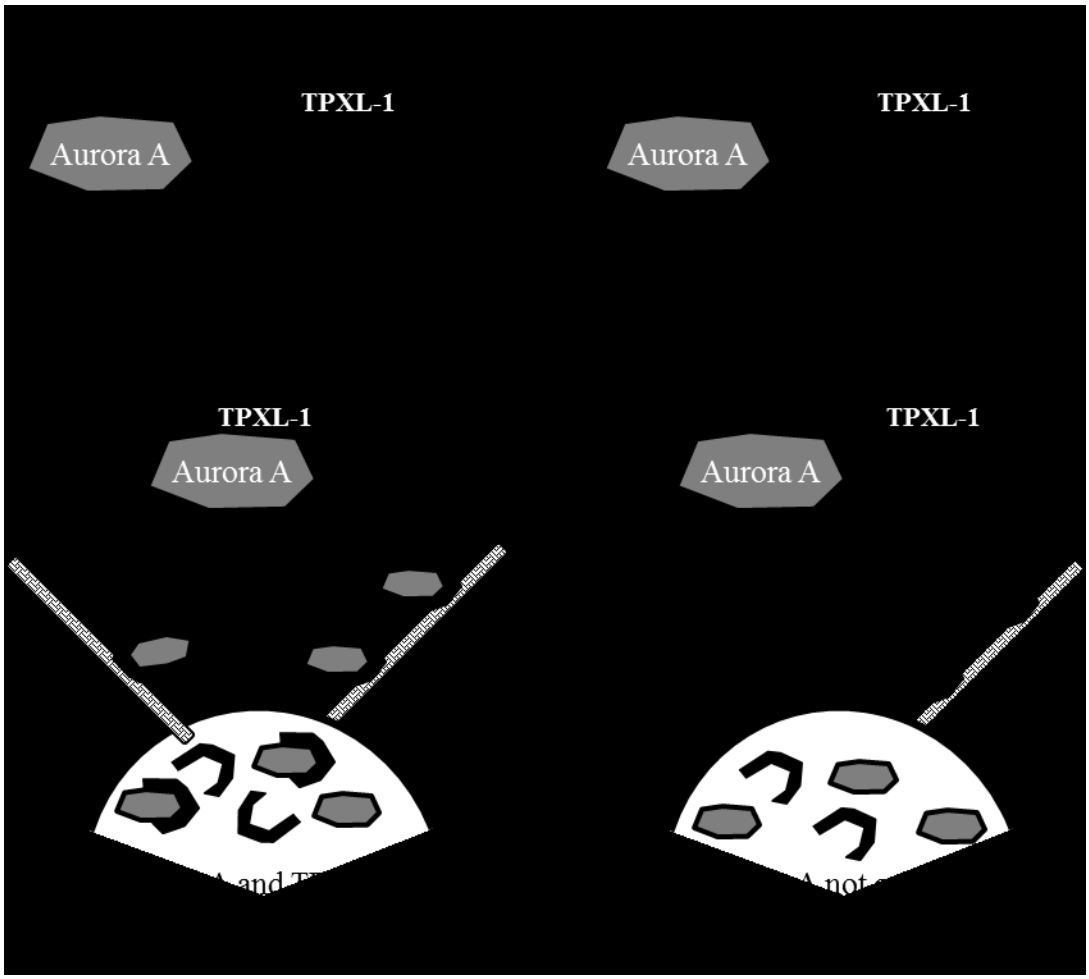


**Figure 5-9. RSA-1 mediated regulation of Aurora A localization**
Possible mechanisms for how RSA-1 could promote the centrosomal localization of TPXL-1 and the microtubule localization of Aurora A.

Unexpectedly, my analysis also revealed that the RSA-1-mediated regulation of Aurora A on the microtubules is dependent on the cell cycle. While RSA-1 was required for Aurora A localization to the microtubules during spindle assembly, this was not the case in anaphase; Aurora A was observed on the microtubules during anaphase in both *rsa-1(or598)* and *rsa-1(RNAi)* embryos. The microtubule localization of Aurora A has not previously been reported to change during the metaphase-to-anaphase transition. Recruitment of Aurora A to the centrosome during prophase is known to be negatively regulated by CDC-48 and an adaptor protein, UBXN-2 (Kress et al., 2014) but this is the first time that temporal regulation of Aurora A on the microtubules has been observed. These data indicate that the subcellular localization of Aurora A is highly regulated in the *C. elegans* embryo. Loss of Aurora A on the microtubules during spindle assembly

results in a severe spindle assembly defect even though Aurora A remains at the centrosome. This suggests that the targets that are regulated by Aurora A vary based on the location of the kinase in the spindle. The appropriate localization of Aurora A is critical for this major mitotic kinase to ensure spindle assembly proceeds correctly.

It remains unknown why RSA-1 is required for Aurora A to locate to the microtubules during spindle assembly but not after the onset of anaphase. Some spindle assembly factors, such as TPX2, avoid degradation by the anaphase promoting complex by associating with microtubules (Song et al., 2014). Since it has also been observed that Aurora A binding TPX2 prevents ubiquitin mediated degradation of Aurora A (Giubettini et al., 2010), it is possible that TPX2-mediated recruitment of Aurora A on the microtubules during anaphase prevents premature degradation of these proteins. This could help to maintain spindle integrity during anaphase by preserving a population of spindle assembly factors on the spindle to prevent premature spindle disassembly. This hypothesis implicates Aurora A in two similar, yet discrete, functions on the spindle microtubules. First, Aurora A is required to assemble the spindle and then it is required to maintain the spindle until the end of mitosis. RSA-1 would only regulate the spindle assembly functions of Aurora A while another, as of yet unidentified, cellular component would regulate Aurora A on the microtubules during anaphase.

### 5.4.2 Possible mechanisms for spindle length regulation

Since mutations in TPXL-1 that specifically disrupt Aurora A localization to the microtubules have a spindle collapse phenotype (Ozlü et al., 2005), it is likely that the loss of Aurora A on the microtubules is the primary cause of the spindle collapse phenotype in *rsa-1(or598)* embryos. Even though RSA-1 is required to locate Aurora A to microtubules during spindle assembly, the mechanism for the spindle assembly phenotype remains to be elucidated. Furthermore, it is possible that RSA-1 could regulate spindle assembly factors, in addition to Aurora A, that contribute to the spindle collapse phenotype.

The spindle collapse phenotype involves centrosomes moving towards the chromatin, implying that a pulling force drives this movement. There are several mechanisms in the cell that can generate this force. For example, depolymerization of microtubules that are anchored to the centrosome and kinetochore can provide the force for spindle shortening.

Microtubule motor proteins could also produce forces to move centrosomes and chromatin. In order to determine which factors contribute to the spindle collapse phenotype, I used RNAi treatment to disrupt various spindle components. If the spindle assembly factors generate the forces required for the spindle collapse in *rsa-1(or598)* embryos, then the spindle collapse would be suppressed by the RNAi treatment. I primarily focused on spindle components that have been reported to affect spindle length in other organisms.

#### *5.4.2.1 Microtubule-chromatin interaction*

Microtubules directly interact with the chromatin through a large protein-based complex called the kinetochore. In budding yeast, kinetochores are known to be critical to maintain proper spindle length because they provide an inward force that opposes spindle elongation (Nannas et al., 2014). I anticipated that kinetochores would be essential for the spindle collapse phenotype in *rsa-1(or598)* embryos because the *tpxl-1(RNAi)* spindle collapse required functional kinetochores (Ozlü et al., 2005). In support of this hypothesis, loss of kinetochores in *hcp-3(RNAi)* rescued the spindle collapse phenotype. Loss of HCP-3 prevents the entire kinetochore from forming on the centromere. It is likely that a subset of kinetochore proteins are involved in the spindle collapse phenotype and could suppress it while a functional kinetochore can still form. I predict that one or more of the kinetochore complexes that interact with microtubules are directly involved in the *rsa-1(lf)* spindle collapse. The kinetochore interacts with microtubules through various mechanisms. The KMN network comprises many proteins that provide a physical link to microtubules (Desai et al., 2003). The RZZ complex recruits dynein to the kinetochore and is important to establish lateral interactions with microtubules (Cheerambathur et al., 2013). The SKA complex is proposed to be required for the kinetochore to interact with depolymerizing microtubules (Schmidt et al., 2012). Since mutations in *ska-1* have been implicated in suppressing *rsa-1(or598)*, it will be interesting to see if the mechanism for the suppression is due to rescue of the spindle collapse.

#### *5.4.2.2 Microtubule motor proteins*

It is well established that microtubule motors can modulate spindle length in flies and vertebrates (reviewed in Gatlin and Bloom, 2010; Goshima and Scholey, 2010). In *C. elegans* the role of microtubule motor proteins in regulating spindle length is not well characterized. In this thesis I investigated if homologs of two well characterized vertebrate kinesins are involved in the *rsa-1(or598)* spindle collapse phenotype. Depletion of BMK-1 and KLP-18 did not affect the spindle collapse phenotype in *rsa-1(or598)* embryos.

There are many other microtubule motor proteins that have characterized roles in mitotic spindle assembly in eukaryotes. This includes minus-end directed motors such as dynein and kinesin-14 (Hepperla et al., 2014) or chromokinesins such as the kinesin-4 family (Kim and Stumpff, 2014). In this thesis I did not investigate the role of dynein in *C. elegans* spindle assembly because dynein is required for several aspects of mitosis prior to spindle assembly including pronuclear migration, centrosome separation, centrosome attachment to the pronuclei, and mitotic spindle orientation (Gönczy et al., 1999) so loss of dynein results in a pleiotropic phenotype. Even though *dhc-1(RNAi)* results in pleiotropic phenotypes, it may be possible to assess the spindle collapse in *rsa-1(or598), dhc-1(ts)* double mutant. *C. elegans* has four members of the kinesin-14 family of minus-end directed motors: KLP-3, KLP-15, KLP-16, and KLP-17. These motors have been shown to be important for chromosome movements in the *C. elegans* germ-line and during meiosis (Khan et al., 1997; Robin et al., 2005). These minus-end directed motors were not investigated in this thesis because they have no characterized roles in mitosis. *C. elegans* have one chromokinesin, KLP-19, that is related to the kinesin-4 family. KLP-19 has important roles during the germ-line mitotic divisions and meiosis (Powers et al., 2004). It has been shown that KLP-19 associates with the chromatin independently of kinetochores; in *hcp-3(RNAi)* embryos KLP-19 is observed on the chromatin during the first mitotic division (Powers et al., 2004). Since the spindle-collapse phenotype was suppressed in *rsa-1(or598)* embryos after *hcp-3(RNAi)* treatment, I did not investigate if KLP-19 has a role in the spindle collapse phenotype. Since KLP-19 is on the chromatin in *hcp-3(RNAi)* embryos and the spindle does not collapse when kinetochore formation is disrupted, this means that the spindle collapse can be prevented even when KLP-19 is

still on the chromatin. As such, it is not likely to be the driving in the spindle collapse in *rsa-1(lf)* embryos and was not investigated in this thesis.

#### *5.4.2.3 Microtubule dynamics and the spindle collapse*

Altering microtubule dynamics can affect spindle length. Conditions that depolymerize microtubules, such as cold or drug treatments, result in shorter spindles (Inoué & Salmon, 1995). Microtubule dynamics in the mitotic spindle are regulated through a variety of mechanisms however I only focused on microtubule depolymerization and polymerization in this thesis.

The microtubule depolymerizing protein MCAK tracks the growing plus end of microtubules and limits microtubule and spindle length during mitosis (Domnitz et al., 2012); over expression of MCAK resulted in shorter spindles (Domnitz et al., 2012). The role of the *C. elegans* MCAK protein, KLP-7, in the *rsa-1(or598)* spindle collapse was previously investigated by Schlaitz et al. They found that *rsa-1(RNAi)* embryos had increased levels of KLP-7 at the centrosomes but that *klp-7(RNAi)* was unable to rescue the *rsa-1(RNAi)* spindle collapse phenotype. These data suggested that the increased levels of KLP-7 at the centrosome are not responsible for the spindle collapse phenotype. Unexpectedly, when I performed live imaging of *rsa-1(or598); klp-7(RNAi)* embryos, 25% (n=2/8) did not assemble a bipolar spindle, but the mono-polar spindles that formed still collapsed. These data suggested that microtubule disassembly by KLP-7 is not the cause of the spindle collapse phenotype. Since mono-polar spindles are not observed in *rsa-1(or598)* or *klp-7(RNAi)* embryos alone these data suggest that RSA-1 and KLP-7 may be required in redundant pathways to promote bipolar spindle assembly in *C. elegans*. It is unclear why the phenotype is not observed in all embryos and further analysis is required to interpret this result.

In human cells, loss of the microtubule polymerase, ch-TOG/XMAP215, leads to shorter mitotic spindles (Barr and Gergely, 2008). A similar phenotype is observed when the *C. elegans* homolog, ZYG-9, is depleted in embryos (Bellanger and Gönczy, 2003; Le Bot, et al., 2003; Matthews et al., 1998; Srayko et al., 2003). *zyg-9(RNAi)* and mutant embryos exhibit a small spindle, though it is not as small as the collapsed spindles observed in *rsa-1(lf)* embryos. Centrosomal levels of ZYG-9 were not altered in *rsa-1(or598)* embryos (Lange et al., 2013) so this regulator of microtubule dynamics was not

investigated further for a role in the spindle collapse. It is possible that RSA-1 regulates the activity of ZYG-9 but does not affect its ability to locate to the centrosome. Another possibility is that RSA-1 is required for ZYG-9 to interact with the plus-end of microtubules. Since *zyg-9(RNAi)* results in small spindles it does not seem likely that a reduction of *zyg*-9 could rescue the spindle collapse in *rsa-1(or598)* embryos, but I did not perform this experiment.

## 5.5 **Potential substrates of the RSA-1/PP2A complex**

The regulatory subunits of PP2A complexes determine the subcellular location of the complex as well as the substrates of the complex. RSA-1 is a B'' regulatory subunit member for PP2A phosphatases and RSA-1 is required to recruit the PP2A holoenzyme to the centrosomes. However, it is unknown what the substrates of the PP2A complex are at the centrosome. The currently identified substrates of the human B'' regulatory subunits are not involved in spindle assembly (Davis et al., 2008). Previously two candidate substrates of the RSA-1/PP2A complex were proposed: KLP-7 and TPXL-1. *rsa-1(RNAi)* embryos exhibited an increase in the centrosomal levels of KLP-7 and a decrease in the levels of TPXL-1 at the centrosome (Schlaitz et al., 2007). This suggests that RSA-1 could be a negative regulator of KLP-7 and a positive regulator of TPXL-1 at the centrosome, but it does not necessarily mean that they are direct substrates of the RSA-1/PP2A complex.

### 5.5.1 KLP-7 as a substrate of RSA-1/PP2A

The vertebrate homolog of KLP-7, MCAK, is known to be regulated by phosphorylation. Many aspects of MCAK biology are affected by phosphorylation including affinity for binding microtubules (Ems-McClung et al., 2013), microtubule depolymerization activity (Tanenbaum et al., 2011), stability of the MCAK protein (Sanhaji et al., 2014), interaction with proteins (Xia et al., 2014), and localization of MCAK in the cell (Pakala et al., 2012). MCAK is known to be phosphorylated by many different kinases including Aurora A (Zhang et al., 2008), Aurora B (Zhang et al., 2007), Cdk1 (Sanhaji et al., 2010), PAK1 (Pakala et al., 2012), and Plk1 (Sanhaji et al., 2014). Significantly less is known about how phosphatases contribute to the regulation of

MCAK activity. MCAK has been proposed to be a substrate of PP2A at the centromere (Huang et al., 2007) but this hypothesis has not been thoroughly tested.

When MCAK is phosphorylated by Aurora B kinase, it undergoes a conformational change that decreases its affinity for microtubules (Ems-McClung at al., 2013). The catalytic activity of MCAK requires microtubule binding and this phosphorylation leads to an inability of MCAK to depolymerize microtubules (Ems-McClung at al., 2013). If a similar mechanism regulates the affinity of KLP-7 microtubule binding, then loss of an opposing phosphatase would result in hyper-phosphorylated, inactive KLP-7. It is unlikely that RSA-1/PP2A is the opposing phosphatase to this phosphorylation because loss of *rsa-1* likely leads to an increase of KLP-7-mediated microtubule disassembly.

Phosphorylation of MCAK by Plk1, at a different residue, facilitates recognition of MCAK by the proteasome (Sanhaji et al., 2014). Loss of phosphorylation on this residue stabilizes MCAK and causes an increase in the levels of MCAK (Sanhaji et al., 2014). If KLP-7 is regulated by a similar mechanism in *C. elegans* embryos, then loss of the opposing phosphatase would result lead to more proteasome mediated degradation of KLP-7 and therefore less KLP-7 in the embryos. It is not likely that RSA-1/PP2A is involved in this process because loss of *rsa-1* leads to more KLP-7 protein at the centrosome which is unlikely if there was a total decrease in the protein levels.

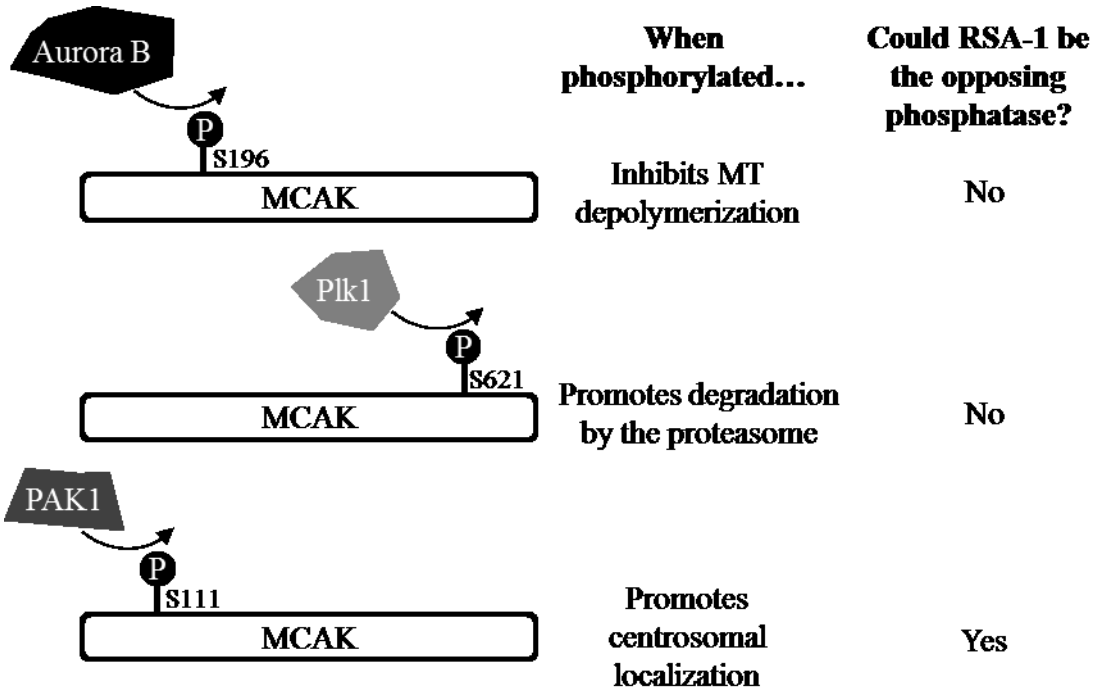


**Figure 5-10. Phosphorylation of MCAK**
The residues that are known to be phosphorylated on the human MCAK protein and how phosphorylation affects the protein. It is not known if the *C. elegans* KLP-7 protein is affected by phosphorylation in a similar manner to MCAK. If KLP-7 is phosphorylated in a similar manner to MCAK, then RSA-1/PP2A could be the opposing phosphatase.

Phosphorylation of MCAK at another amino acid by PAK1 is required for the centrosomal localization of MCAK (Pakala et al., 2012). When MCAK is not phosphorylated at this residue, the protein is not able to be recruited to the centrosome (Pakala et al., 2012). If a similar mechanism regulates the centrosomal localization of KLP-7 in *C. elegans* embryos, then loss of the opposing phosphatase would lead to an increase in the levels of KLP-7 at the centrosome. This is consistent with the observation that *rsa-1(RNAi)* embryos exhibit an increase in KLP-7 levels at the centrosome. This is the most likely mechanism for KLP-7 to be a direct substrate of the RSA-1/PP2A complex.

Analysis using Phos-tag reagent in poly-acrylamide gel electrophoresis has shown that decreased *rsa-1* function in embryos does not significantly affect the phosphorylation state of KLP-7 (Han, 2014). It is possible that Phos-tag containing gels are not sensitive enough to detect subtle changes to a protein with many phosphorylation sites. Indeed, Phos-tag gels were unable to detect changes in the phosphorylation of KLP-7 when Aurora A or Aurora B function was impaired by RNAi treatment, even though two-

dimensional gel electrophoresis could detect phosphorylation changes of KLP-7 under these conditions (Han, 2014). Two-dimensional gel electrophoresis and tandem mass spectrometry could be used to analyze protein phosphorylation with a higher resolution than Phos-tag PAGE.

Even though *rsa-1(RNAi)* embryos exhibited increased levels of KLP-7 at the centrosome, it does not mean that KLP-7 is a direct substrate of RSA-1/PP2A. It is possible that RSA-1 indirectly affects KLP-7 levels at the centrosome. For example, RSA-1 could promote the activity of an intermediate protein that negatively regulates the levels of KLP-7 at the centrosome.

### 5.5.2 TPXL-1 as a substrate of RSA-1/PP2A

It was shown that RSA-1 interacts with TPXL-1 in a co-immunoprecipitation assay so this supports the hypothesis that RSA-1 is a direct regulator of TPXL-1. Additionally, homologs of TPXL-1 are known to be regulated by phosphorylation in *Xenopus* extracts (Wittman et al., 2000) and human cells (Eckert et al., 2009).

It has previously been shown that an N-terminal fragment of TPXL-1 is phosphorylated by Aurora A *in vitro* on S30 (Ozlü et al., 2005; Han, 2014). I confirmed that TPXL-1 is phosphorylated *in vivo* in *C. elegans* embryos and TPXL-1 was more phosphorylated when PP2A activity was depleted in *paa-1(RNAi)* embryos. However, protein lysates from both *rsa-1(or598)* and *rsa-1(RNAi)* embryos did not show a change in mobility through the Phos-tag acrylamide matrix, suggesting no change in the phosphorylation state of TPXL-1. These data indicate that TPXL-1 may be a substrate of PP2A, but RSA-1 is not the primary regulatory subunit that mediates this dephosphorylation reaction.

Alternatively, it is possible that RSA-1 may dephosphorylate a small pool of TPXL-1 and that the Phos-tag PAGE was not sensitive enough to detect this change. It remains unknown what PP2A regulatory subunit is responsible for the observed change in TPXL-1 phosphorylation in the *paa-1(RNAi)* lysates.

### 5.5.3 Aurora A as a substrate of RSA-1/PP2A

Activation of Aurora A kinase activity occurs by phosphorylation of a threonine in the kinase domain or T-loop (Bayliss et al., 2003; Eyers et al., 2003). In human cells the

major phosphatase for this residue is protein phosphatase 6 (Zeng et al., 2010) but it has been proposed that at least two phosphatases are required to dephosphorylate this residue at the levels that are observed in human cells (Kang et al., 2014). The second phosphatase for this residue in human cells remains unknown. PP2A is found in a complex with Aurora A in human cells (Horn et al., 2007) and it has been shown to dephosphorylate a serine in an N-terminal "A-box" domain that promotes the proteasome dependent degradation of Aurora A (Horn et al., 2007; Littlepage and Ruderman, 2002). It is conceivable that PP2A could dephosphorylate multiple residues on Aurora A that could result in different biological consequences.

In *C. elegans*, the Aurora A T-loop phosphatase is unknown. Protein phosphatase 6 (PP6) is observed at the centrosomes and cell cortex in *C. elegans* embryos and has a role in spindle positioning (Afshar et al., 2010). *pph-6(RNAi)* embryos do exhibit a weakly penetrant chromosome segregation defect (Afshar et al., 2010) so this phosphatase may have a minor role in spindle assembly. In human cells, the loss of PP6 causes spindle assembly defects and severe chromosome segregation errors due to overactive Aurora A (Zeng et al., 2010). Given the discrepancy in phenotypes observed in *C.elegans* embryos and human cells, it seems improbable that PP6 is the major T-loop phosphatase in *C. elegans*.

Phosphorylation of the Aurora A T-loop affects the ability of Aurora A to associate with microtubules in *C. elegans* embryos; an Aurora A phospho-specific antibody has shown that the Aurora A T-loop is phosphorylated at the centrosomes but is not phosphorylated in the T-loop when on the microtubules (Toya et al., 2011). In human cells it has been shown that Aurora A kinase activity can be stimulated independently of T-loop phosphorylation by TPX2 binding (Dodson et al., 2012; Zorba et al., 2014), so it is possible that a population of Aurora A that is not phosphorylated on the T-loop could be active on the microtubules by its association with TPXL-1.

Given that T-loop phosphorylation of Aurora A is restricted spatially to the centrosome region in *C. elegans* embryos, it is plausible that dephosphorylation of the T-loop regulates Aurora A spatially. Since RSA-1 is required for Aurora A to associate with the microtubules during spindle assembly, I propose that RSA-1/PP2A dephosphorylates Aurora A on the T-loop during spindle assembly to facilitate localization onto the spindle

microtubules. This dephosphorylation could promote the protein interaction between Aurora A and TPXL-1. This hypothesis is inconsistent with observations in human cells and *Xenopus* cell extracts whereby TPX2 promotes T-loop phosphorylation of Aurora A (Bayliss et al., 2003; Brunet et al., 2004; Eckert et al., 2009). However, given that the *C. elegans* TPXL-1 primary amino acid sequence is very divergent from the vertebrate TPX2 protein, it is possible that TPXL-1 molecular behaviour has diverged as well.

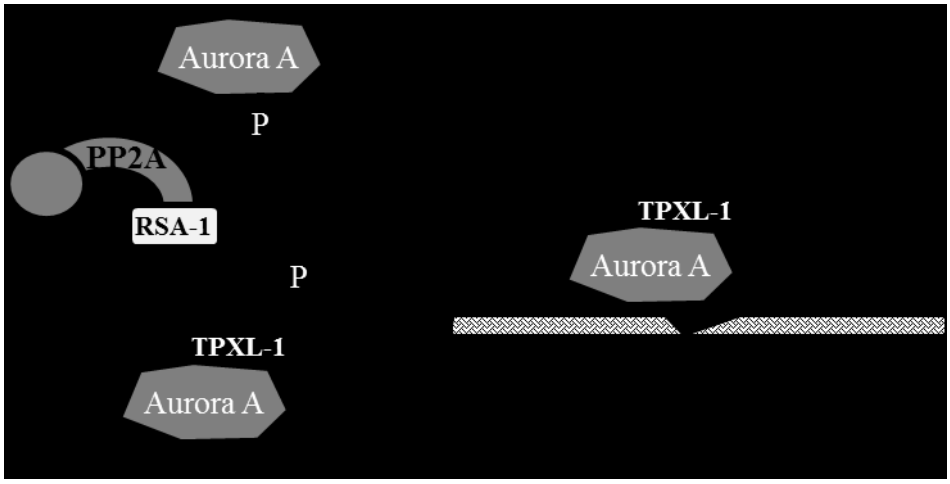


**Figure 5-11. Model for RSA-1/PP2A to dephosphorylate T-loop of Aurora A**
At the centrosome Aurora A is phosphorylated on the T-loop. RSA-1/PP2A could dephosphorylate the T-loop to promote the association of Aurora A with TPXL-1. The Aurora A/TPXL-1 complex can then translocate to the microtubules to phosphorylate spindle assembly factors and promote spindle integrity.

### 5.6 TPXL-1 on the chromatin

Vertebrate TPX2 has several well characterized roles in mitosis including Ran-mediated microtubule nucleation, localizing Aurora A to the mitotic spindle, and activating the kinase activity of Aurora A. In *C. elegans* embryos, TPXL-1 activates Aurora A and is required to locate Aurora A to spindle microtubules, but it was not known if it had a similar role in Ran-mediated microtubule nucleation. TPXL-1 lacks the C-terminal domain that interacts with Ran in the vertebrate TPX2 protein so it was proposed that TPXL-1 does not have a chromatin based microtubule nucleation function in spindle assembly in *C. elegans* (Karsenti, 2005).

I observed TPXL-1 on the chromatin in wild-type embryos using both immunofluorescence and live imaging of a transgenic TPXL-1::GFP protein. While the biological function of TPXL-1 on the chromatin has yet to be determined, I propose that it has a similar role at the chromatin as the vertebrate TPX2 protein. In response to high

levels of RanGTP around the chromatin, TPXL-1 could associate with the chromatin to promote microtubule nucleation/stabilization to stimulate robust spindle assembly. Consistent with this hypothesis, RanGTP was required for TPXL-1 to associate with the chromatin. Both Ran and RCC1 were required to establish high levels of RanGTP around the chromatin; in *ran-1(RNAi)* and *ran-3(RNAi)* embryos, TPXL-1 was not observed on the chromatin. TPXL-1 was not observed on the chromatin in conditions where RanGTP levels were depleted. On the other hand, RanGAP is important to limit the levels of RanGTP in the embryo and *ran-2(RNAi)* did not affect TPXL-1 at the chromatin.

Since TPXL-1 lacks any obvious homology to the TPX2 Ran binding domain, it is unclear how Ran regulates TPXL-1 localization to the chromatin. In canonical nuclear import, Ran interacts with proteins to promote their dissociation from importin α/β. Importin binds to substrates that have a nuclear localization sequence (NLS) to import them into the nucleus through the nuclear pore. Using NLS prediction software, NLStradamus (Ba et al., 2009), TPXL-1 has one predicted NLS (a.a. 151-RRRSEQRKK-159). This suggests that TPXL-1 could be imported into the nucleus; however, the predicted sequence may not be biologically relevant. Interestingly, two consensus Aurora A phosphorylation sites (R-X-S/T) are found in close proximity to the predicted NLS at amino acids 149 and 154. There are many examples where phosphorylation near or in an NLS can affect nuclear import of proteins (reviewed in Nardozzi et al., 2010). If the TPXL-1 NLS sequence is bona fide, then it is possible that nuclear localization of TPXL-1 is regulated by phosphorylation by Aurora A.

It remains to be elucidated how the TPXL-1 protein associates with the chromatin. Known chromatin-associated proteins such as components of the kinetochores or the chromosome passenger complex were not required for TPXL-1 to locate to the chromatin. It is possible that TPXL-1 interacts with DNA or histones directly, or via an interaction with a currently unidentified protein is required to stabilize TPXL-1 at the chromatin.

In *rsa-1(or598)* embryos the levels of TPXL-1 were significantly reduced at the chromatin. There are several possible explanations for this observation. Depletion of *rsa-1* is known to affect centrosomal levels of TPXL-1, so it is possible that centrosomal and chromatin levels of TPXL-1 correlate directly. One possible mechanism for this could be

that TPXL-1 is modified at the centrosome to allow it to be imported into the nucleus and/or associate with the chromatin. In *rsa-1(or598)* embryos there is a significant decrease in the number of microtubules in the embryo. To determine if the catalytic activity of the RSA-1/PP2A complex is required for the chromatin association of TPXL-1 I investigated *paa-1(RNAi)* embryos. However, the pleiotropic phenotypes in these embryos precluded simple interpretation. It would be better to use a small molecule inhibitor of PP2A, such as okadaic acid or calyculin A, to limit phosphatase activity at a specific point in time. Similar microscopy experiments have successfully been performed in *C. elegans* using permeabilized embryos to allow the drugs to enter the embryo (Bajaj and Srayko, 2013).

Aurora A was required for TPXL-1 to associate with the chromatin. Since centrosome maturation is impeded in *air-1(RNAi)*, there is a visible decrease in the centrosomal levels of TPXL-1 in these embryos. It is possible that robust TPXL-1 levels at the centrosome are required for TPXL-1 to be observed at the chromatin. However, Aurora A also co-localizes with TPXL-1 on the microtubules and perhaps even on the chromatin (Toya et al., 2011). Mutations that disrupted the Aurora A/TPXL-1 protein interaction affected the ability of TPXL-1 to locate to the chromatin. In the TPXL-1(F15D, F18D) mutant, TPXL-1 was not observed on the chromatin, however the expression was low and difficult to detect on the chromatin. It is possible that the chromatin levels of TPXL-1(F15D, F18D) mutant protein were below the limit of detection for this assay.

Unexpectedly, *zyg-9(RNAi)* embryos did not exhibit chromatin localization of TPXL-1 even though the centrosomal and microtubule localization of TPXL-1 appeared unaffected. ZYG-9 is a centrosomal protein that promotes the polymerization of long microtubules (Bellanger and Gönczy, 2003; Le Bot, et al., 2003; Matthews et al., 1998; Srayko et al., 2003). It is unclear why this microtubule polymerase affects TPXL-1 at the chromatin. The ZYG-9 homolog, XMAP215, associates with the chromatin in *Drosophila* and *Xenopus* (Bucciarelli et al., 2009; Groen et al, 2009) and in *Xenopus* extracts Ran-mediated microtubule nucleation depends on XMAP215 (Wilde and Zheng, 1999). It is possible that ZYG-9 could have a role at the chromatin in *C. elegans*.

In *Xenopus* extracts, Ran promotes the association of TPX2 and Aurora A (Tsai et al., 2003) and is thought to contribute to microtubule stabilization and spindle assembly

where RanGTP levels are high near the chromatin. In *C. elegans,* Aurora A has also been proposed to play a role in the stabilization of chromatin-nucleated microtubules (Toya et al., 2011). I propose that in *C. elegans* TPXL-1 is also involved in this process and that the chromatin localization of TPXL-1 is specifically required for this function. It is important to note that centrosomes are essential for spindle assembly in *C. elegans*. Unlike in *Xenopus* extracts, the microtubules that nucleate proximal to the chromosomes in *C. elegans* embryos are unable to be organized into a bipolar structure. As such, the microtubules that nucleate around the chromatin may play a role in promoting spindle integrity or structure rather than spindle assembly *per se*.

### 5.7 **A potential role for RSA-1 and Aurora A in cell migration**

Cell migration requires precise and coordinated changes to the cytoskeleton. While the role of the actin cytoskeleton in cell migration is well established (Reviewed by Carlier and Pantaloni, 2007), the microtubule cytoskeleton is also essential for cell migration (Reviewed by Etienne-Manneville, 2013). Treatment of migrating endothelial cells with drugs that inhibit microtubule dynamics impedes migration (Kamath et al., 2014) and the regulation of microtubule dynamics is required for the migration of *Drosophila* cells as well (Zhang et al., 2011). These observations highlight the importance of microtubules and microtubule dynamics in cell migration.

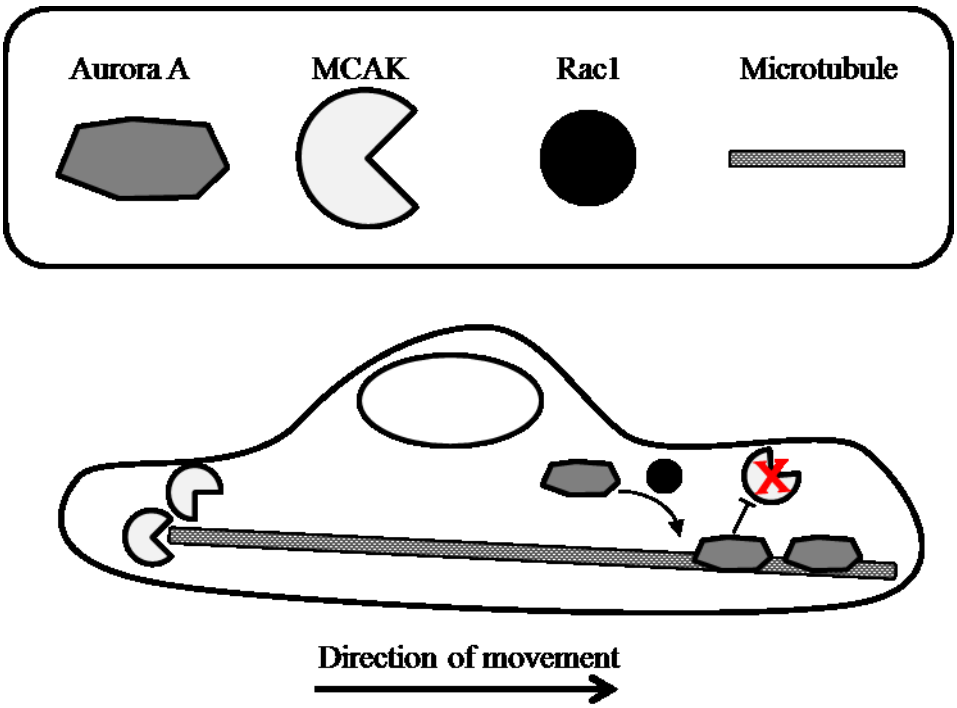


**Figure 5-12. Regulation of microtubule dynamics during cell migration**
Graphic summary of the results presented in Braun et al., 2014. Rac1 promotes the association of Aurora A with microtubules at the leading edge of endothelial cells. This promotes microtubule stability at the leading edge by inhibiting MCAK. MCAK is active at the trailing edge of the cell.

In migrating epithelial cells, microtubule ends at the leading edge of the cell are more stable than microtubule ends elsewhere in the cell which have a higher rate of catastrophe (Wadsworth, 1999). It has recently been shown that Aurora A localizes to microtubules in migrating human endothelial cells to regulate microtubule dynamics (Braun et al., 2014). Aurora A inhibits microtubule disassembly at the leading edge of migrating cells by limiting the activity of a protein that disassembles microtubules, MCAK (Figure 5-12; Braun et al., 2014). This Aurora A dependent regulation of MCAK activity is required for directional migration of the endothelial cells (Braun et al., 2014).

Rac1, a small GTPase, promotes Aurora A activation and the association of Aurora A with microtubules (Braun et al., 2014). The CED-10 protein, which is orthologous to human Rac1, is involved in cytoskeleton rearrangement and cell migration at various times in *C. elegans* development including phagocytosis of apoptotic cells (Wu and Horvitz, 1998), axon guidance (Wu et al., 2002), migration of vulva cells (Kishore and Sundaram, 2002), and migration of the distal tip cell during gonadogenesis (Wu and

Horvitz, 1998). In *ced-10* mutants the distal tip cell will often make additional turns or stop migrating prematurely (Wu and Horvitz, 1998).

The gonad migration phenotypes observed in *ced-10* mutants are similar to those observed in *rsa-1(or598)* larvae that were shifted to the restrictive temperature of 26 °C at L1. Migration of the distal tip cell in gonad development is known to require rearrangements of the actin cytoskeleton but less is known about the dynamics of the microtubules in these cells. It is possible that RSA-1 contributes to gonadogenesis by regulating microtubule dynamics in these cells. In early *rsa-1(or598)* embryos at 26 °C Aurora A was not observed on the microtubules during prophase and metaphase. This suggests that at some points during mitosis the microtubule localization of Aurora A depends on RSA-1 activity. It is possible that Aurora A may require RSA-1 to localize to microtubules at other times in development of the organism. Similar to the defects in the migration of human endothelial cells, loss of Aurora A on the microtubules could impede migration of the distal tip cell and cause the gonad migration defects observed in *rsa-1(or598)* worms. Consistent with this hypothesis, depletion *klp-7(RNAi)* and *tpxl-1(RNAi)* altered microtubule dynamics in the developing egg laying structure (Lacroix et al., 2014).

During embryogenesis many events require precise cell migration such as gastrulation and elongation of the body. It is possible that RSA-1 contributes to these cell migration events and the zygotic lethality and L1 arrest phenotypes are due to defects in these processes. Since the L1 arrested worms were not inspected for cell migration defects, it was not possible to determine the precise developmental defects involved in the arrest.

## 5.8 **Future directions**

### 5.8.1 Elucidate relationship between RSA-1, TPXL-1 and Aurora A

RSA-1 is required for Aurora A to associate with microtubules during spindle assembly. Since a protein interaction between Aurora A and TPXL-1 is required for Aurora A to locate to the microtubules, it is possible that RSA-1 regulates the Aurora A/TPXL-1 protein interaction. A phospho-specific Aurora A antibody has previously shown that Aurora A is phosphorylated on T201 when localized to the centrosome but not when on the microtubules (Toya et al., 2011). It is possible that RSA-1/PP2A

dephosphorylates this residue to promote the association of Aurora A with the microtubules via an interaction with TPXL-1. This phospho-specific antibody could be acquired and used in Western blots to determine if there is an increase in phosphorylation at this residue in *rsa-1(lf)* embryos. This reagent is only capable of detecting the phosphorylation state of a single residue and Aurora A in human cells is known to be phosphorylated on additional residues. Phos-tag PAGE can be done with an Aurora A antibody to detect changes in the phosphorylation state of the entire Aurora A protein.

To determine if the protein interaction between Aurora A and TPXL-1 is impeded in *rsa-1(lf)* embryos, co-immunoprecipitations could be performed. My hypothesis predicts that Aurora A and TPXL-1 would co-immunoprecipitate in wild-type protein lysates but that this interaction would be significantly diminished in *rsa-1(lf)* protein lysates. However, the interaction between Aurora A and TPXL-1 would only be impeded during spindle assembly and not during anaphase or telophase. If the protein lysate is from a mixed stage population of embryos the results may not be clear. Unfortunately, it is not possible to arrest *C. elegans* embryos in metaphase. It is possible to arrest embryos prior to mitosis by preventing CDK1 activation by either using RNAi treatment to deplete multiple cyclins (van der Voet et al., 2009) or by affecting a metabolic process that prevents mitotic entry (Rahman et al., 2014). In both of these situations the embryos arrest prior to NEBD and the centrosomes are able to nucleate microtubules. Since these embryos are not actually in mitosis, it is possible that RSA-1, TPXL-1, and Aurora A will not behave as observed during prophase and metaphase. Immunofluorescence and live imaging can be performed in these embryos to verify that TPXL-1 and Aurora A are localized as expected.

It is unknown what factor promotes Aurora A association with the microtubules during anaphase. This is likely a centrosomal protein and may be a phosphatase to fill the same role as RSA-1 during spindle assembly. One candidate is protein phosphatase 6/PPH-6 because this is a centrosomal phosphatase that is known to dephosphorylate Aurora A in other systems. The *pph-6(RNAi)* has weakly penetrant chromosome segregation defects and this could be the result of Aurora A not being properly maintained on the spindle during anaphase. Immunofluorescence and live imaging can be done to determine if *pph-6(RNAi)* affects the localization of Aurora A in the embryos. If PPH-6 does regulate the

localization of Aurora A during anaphase, then Aurora A would not be observed on the microtubules in *rsa-1(or598);pph-6(RNAi)* at any stage of mitosis.

### 5.8.2 Confirm *ska-1* and *pptr-1* are suppressors of *rsa-1(or598)*

Preliminary results from whole genome sequencing of the suppressor strains containing *abc17, abc19,* and *abc25* indicate that *ska-1* and *pptr-1* are excellent candidates to be suppressors of *rsa-1(or598)*. In human cells, both of these proteins are implicated in stabilizing or maintaining kinetochore-microtubule interactions, so they might have a common mechanism of suppression of *rsa-1(or598)*. Additional non-essential kinetochore proteins may also be able to suppress *rsa-1(or598)*. A targeted RNAi screen against kinetochore components can be done to determine if compromising any kinetochore components can suppress *rsa-1(or598)* or if this observation is specific to *ska-1*.

It is unknown if the non-sense mutations in *ska-1* result in a truncated protein or if non-sense mediated decay prevents translation of the protein. An anti-SKA-1 antibody or GFP tagged lines can be used to determine the location of SKA-1 protein under mutant conditions. Microscopy based experiments should be performed to determine if loss of *ska-1* rescues the spindle collapse phenotype in *rsa-1(or598)* embryos.

Since PPTR-1 is a PP2A regulatory subunit, it will be more difficult to determine if it directly or indirectly suppresses *rsa-1(or598)*. Firstly, *pptr-1* needs to be cloned into an RNAi feeding vector to determine if *pptr-1(RNAi)* is able to suppress *rsa-1(or598)*. To determine if PPTR-1 has a role in the stability of kinetochore-microtubules, cold depolymerization of microtubules can be performed. Kinetochore microtubules are more cold resistant than other populations of microtubules and are resistant to cold-induced depolymerization.

### 5.8.3 Determine cause for spindle collapse in *rsa-1(lf)* embryos

In this thesis many factors were investigated to determine if they play a role in the *rsa-1* spindle collapse phenotype. The only component identified that was required for the spindle collapse phenotype was the core kinetochore component, *hcp-3*. It remains unknown if microtubule dynamics or microtubule motor proteins generate the force for the spindle collapse.

To determine if microtubule depolymerization plays a role in the spindle collapse microtubule dynamics can be manipulated using microtubule binding drugs. Taxol is a microtubule stabilizing drug and can penetrate permeabilized *C. elegans* embryos (Bajaj and Srayko, 2013). If microtubule depolymerization is required for the spindle collapse, then the spindle should not collapse in Taxol treated *rsa-1(or598)* embryos. While this experiment could illuminate the role for microtubule dynamics in the spindle collapse, it would not reveal the entire molecular mechanism.

Additionally, I did not test if any minus-end directed motors have a role in the *rsa-1(or598)* spindle collapse phenotype. The kinesin-4 family members in *C. elegans* have no known roles during the mitotic divisions, however they could have redundant functions and more than one may need to be depleted to observe a phenotype. Since *dhc-1(RNAi)* embryos have pleiotropic phenotypes, a double mutant with the weak conditional allele, *dhc-1(or195)* (Hamill et al., 2002), can be generated to investigate dynein function during spindle assembly.

### 5.8.4 RSA-1 and KLP-7

It remains unknown why there is an increase in the level of the KLP-7 protein at the centrosome when RSA-1 function is compromised. Since it has been shown that a homolog of KLP-7 requires phosphorylation to locate to the centrosome (Pakala et al, 2012), it is possible that a phosphatase could be required to limit KLP-7 levels at the centrosome. If RSA-1 is required to dephosphorylate KLP-7 to limit the levels of the microtubule depolymerase at the centrosome, then in *rsa-1(or598)* embryos the KLP-7 protein should be more phosphorylated. A sensitive technique such as two dimensional gel electrophoresis or mass spectrometry can be used to detect changes in the phosphorylation of KLP-7 in *rsa-1(or598)* embryos.

Live imaging of *rsa-1(or598); klp-7(RNAi)* embryos revealed that one quarter of embryos did not form a bipolar spindle. Since this phenotype is not observed in *rsa-1(or598)* or *klp-7(RNAi)* embryos alone, it suggests that these proteins may be involved in a redundant spindle assembly pathway. This should be further investigated by repeating the live imaging experiment with an *rsa-1(or598); klp-7(tm2143)* double mutant. If the same results are observed with the double mutant embryos then it would be

worthwhile to investigate why these embryos are sometimes unable to make a bi-polar spindle.

#### 5.8.5 Additional genetic screens with *rsa-1*

A genetic screen for suppressors of *rsa-1(dd13)* would be an excellent way to identify mutations in substrates of the PP2A complex. A suppressor screen of this allele would likely only give rise to revertants and bypass suppressors. The bypass suppressors could be substrates of the complex that no longer require dephosphorylation by PP2A to function appropriately in the embryo. If RSA-1 is required to regulate several essential substrates, then a mutation in only one would not be expected to restore viability to the embryo.

Another way to identify genes that genetically interact with *rsa-1* is to do RNAi suppressor and enhancer screens. The suppressor screen would be done with L4 hermaphrodites at a restrictive temperature of 25 °C and the enhancer screen would be done at 20 °C. An enhancer would be any RNAi treatment that increases embryonic lethality in *rsa-1(or598)* at the permissive temperature but does not cause lethality in wild-type worms. A suppressor would be any RNAi treatment that increases embryonic viability at the restrictive temperature. Since RSA-1 has roles later in development, it may be possible to identify suppressors that can suppress the embryonic lethality but not rescue the developmental defects of *rsa-1(or598)*. For example, in the EMS screen, suppressors that did not restore gonadogenesis to the hermaphrodites would not be isolated. An RNAi-based screen would allow for the identification of suppressors that may not be able to suppress the post embryonic phenotypes of *rsa-1*.

### 5.9 **Concluding remarks**

Using a traditional EMS genetic screen, I was able to accurately identify the interaction domains between RSA-1 and PAA-1. My analysis highlights key amino acids that promote the association between the PP2A holoenzyme and a B'' regulatory subunit family member. PP2A phosphatase have been proposed as excellent targets for anti-cancer therapies (reviewed in Kalev and Sablina, 2011; Khanna et al., 2013; Perrotti and Neviani, 2013) as well as viable drug targets for other diseases such as Alzheimer's (Voronkov et al., 2011). However, small molecules that disrupt catalytic activity of the

phosphatase have many off target effects because the enzyme is involved in many cellular functions. Identification of key residues that mediate the interaction between the holoenzyme and regulatory subunits means that new small molecules can be designed that would disrupt the interaction of the holoenzyme with a specific regulatory subunit without affecting all PP2A functions in the cell.

I have established that the *C. elegans* TPXL-1 protein appears to contribute to Ran-mediated mitotic spindle assembly which is similar to the vertebrate TPX2 protein. I have also discovered that the RSA-1/PP2A complex regulates both TPXL-1 and Aurora A during spindle assembly. Since mis-regulation of Aurora A kinase and TPX2 is implicated in many types of cancers and hyperactive Aurora A confers resistance to Taxol treatment, understanding how phosphatases contribute to their regulation is critical to better our understanding of how they contribute to cancer.

My investigation has also implicated RSA-1/PP2A in cell migration, possibly through regulation of Aurora A kinase. Understanding this process is also important for cancer treatments because endothelial cell migration is required for angiogenesis in tumours. It has been shown that drug treatments that block Aurora A activity are able to limit mitosis and cell migration, which is more effective for cancer treatment than blocking either process alone (Do et al., 2014). A better understanding of how Aurora A is regulated in these processes could greatly improve the efficacy of existing anti-mitotic cancer therapies.

# Bibliography


Afshar, K., Werner, M. E., Tse, Y. C., Glotzer, M., & Gönczy, P. (2010). Regulation of cortical contractility and spindle positioning by the protein phosphatase 6 PPH-6 in one-cell stage *C. elegans* embryos. *Development, 137*(2), 237-247.

Aguirre-Portolés, C., Bird, A. W., Hyman, A., Cañamero, M., Pérez de Castro, I., & Malumbres, M. (2012). Tpx2 controls spindle integrity, genome stability, and tumor development. *Cancer Research, 72*(6), 1518-1528.

Albee, A. J., Tao, W., & Wiese, C. (2006). Phosphorylation of maskin by aurora-A is regulated by RanGTP and importin β. *Journal of Biological Chemistry, 281*(50), 38293-38301.

Alexander, J., Lim, D., Joughin, B. A., Hegemann, B., Hutchins, J. R. A., Ehrenberger, T., et al. (2011). Spatial exclusivity combined with positive and negative selection of phosphorylation motifs is the basis for context-dependent mitotic signaling. *Science Signalling, 4*(179), ra42.

Anand, S., Penrhyn-Lowe, S., & Venkitaraman, A. R. (2003). AURORA-A amplification overrides the mitotic spindle assembly checkpoint, inducing resistance to taxol. *Cancer Cell, 3*(1), 51-62.

Arquint, C., Gabryjonczyk, A. M., & Nigg, E. A. (2014). Centrosomes as signalling centres. *Philosophical Transactions of the Royal Society of London, Biological Sciences, 369*(1650), pii: 20130464.

Asencio, C., Davidson, I. F., Santarella-Mellwig, R., Ly-Hartig, T. B. N., Mall, M., Wallenfang, M. R., et al. (2012). Coordination of kinase and phosphatase activities by Lem4 enables nuclear envelope reassembly during mitosis. *Cell, 150*(1), 122-135.

Askjaer, P., Galy, V., Hannak, E., & Mattaj, I. W. (2002). Ran GTPase cycle and importins alpha and beta are essential for spindle formation and nuclear envelope assembly in living *Caenorhabditis elegans* embryos. *Molecular Biology of the Cell, 13*(12), 4355-4370.

Azimzadeh, J., Nacry, P., Christodoulidou, A., Drevensek, S., Camilleri, C., Amiour, N., et al. (2008). *Arabidopsis* TONNEAU1 proteins are essential for preprophase band formation and interact with centrin. *The Plant Cell Online, 20*(8), 2146-2159.

Ba, A. N. N., Pogoutse, A., Provart, N., & Moses, A. M. (2009). NLStradamus: A simple hidden markov model for nuclear localization signal prediction. *BMC Bioinformatics, 10*(1), 202-212.

Bai, M., Ni, J., Wu, J., Wang, B., Shen, S., & Yu, L. (2014). A novel mechanism for activation of aurora-A kinase by ajuba. *Gene, 543*(1), 133-139.

Bajaj, M., & Srayko, M. (2013). Laulimalide induces dose-dependent modulation of microtubule behaviour in the *C. elegans* embryo. *Plos One, 8*(8), e71889.

Baker, D. J., Jeganathan, K. B., Cameron, J. D., Thompson, M., Juneja, S., Kopecka, A., et al. (2004). BubR1 insufficiency causes early onset of aging-associated phenotypes and infertility in mice. *Nature Genetics, 36*(7), 744-749.

Baker, D. J., Jeganathan, K. B., Malureanu, L., Perez-Terzic, C., Terzic, A., & van Deursen, J. M. A. (2006). Early aging–associated phenotypes in Bub3/Rae1 haploinsufficient mice. *The Journal of Cell Biology, 172*(4), 529-540.

Bamba, C., Bobinnec, Y., Fukuda, M., & Nishida, E. (2002). The GTPase ran regulates chromosome positioning and nuclear envelope assembly *in vivo*. *Current Biology, 12*(6), 503-507.

Banerjee, B., Kestner, C. A., & Stukenberg, P. T. (2014). EB1 enables spindle microtubules to regulate centromeric recruitment of aurora B. *The Journal of Cell Biology, 204*(6), 947-963.

Barr, A. R., & Gergely, F. (2008). MCAK-independent functions of ch-Tog/XMAP215 in microtubule plus-end dynamics. *Molecular and Cellular Biology, 28*(23), 7199-7211.

Barr, F. A., Elliott, P. R., & Gruneberg, U. (2011). Protein phosphatases and the regulation of mitosis. *Journal of Cell Science, 124*(14), 2323-2334.

Basto, R., Lau, J., Vinogradova, T., Gardiol, A., Woods, C. G., Khodjakov, A., et al. (2006). Flies without centrioles. *Cell, 125*(7), 1375-1386.

Bayliss, R., Fry, A., Haq, T., & Yeoh, S. (2012). On the molecular mechanisms of mitotic kinase activation. *Open Biology*, 2(11).

Bayliss, R., Sardon, T., Vernos, I., & Conti, E. (2003). Structural basis of aurora-A activation by TPX2 at the mitotic spindle. *Molecular Cell, 12*(4), 851-862.

Bellanger, J., & Gönczy, P. (2003). TAC-1 and ZYG-9 form a complex that promotes microtubule assembly in *C. elegans* embryos. *Current Biology, 13*(17), 1488-1498.

Benavides, D. T., & Egli, M. (2014). Calcium's role in mechanotransduction during muscle development. *Cellular Physiology and Biochemistry, 33*, 249-272.

Bibby, R., Tang, C., Faisal, A., Drosopoulos, K., Lubbe, S., Houlston, R., et al. (2009). A cancer-associated aurora A mutant is mislocalized and misregulated due to loss of interaction with TPX2. *Journal of Biological Chemistry, 284*, 33177-33184.

Bird, A. W., & Hyman, A. A. (2008). Building a spindle of the correct length in human cells requires the interaction between TPX2 and aurora A. *The Journal of Cell Biology, 182*(2), 289-300.

Bishop, J. D., Han, Z., & Schumacher, J. M. (2005). The *Caenorhabditis elegans* aurora B kinase AIR-2 phosphorylates and is required for the localization of a BimC kinesin to meiotic and mitotic spindles. *Molecular Biology of the Cell, 16*(2), 742-756.

Blower, M. D., Nachury, M., Heald, R., & Weis, K. (2005). A Rae1-containing ribonucleoprotein complex is required for mitotic spindle assembly. *Cell, 121*(2), 223-234.

Bonner, M. K., Poole, D. S., Xu, T., Sarkeshik, A., Yates,John R., I.,II, & Skop, A. R. (2011). Mitotic spindle proteomics in chinese hamster ovary cells. *Plos One, 6*(5), e20489.

Booth, D., Hood, F. E., Prior, I. A., & Royle, S. J. (2011). A TACC3/ch-TOG/clathrin complex stabilises kinetochore fibres by inter-microtubule bridging. *EMBO Journal, 30*(5), 906-919.

Boxem, M., Maliga, Z., Klitgord, N., Li, N., Lemmens, I., Mana, M., et al. (2008). A protein domain-based interactome network for *C. elegans* early embryogenesis. *Cell, 134(3)*, 534-545.

Braun, A., Dang, K., Buslig, F., Baird, M. A., Davidson, M. W., Waterman, C. M., et al. (2014). Rac1 and aurora A regulate MCAK to polarize microtubule growth in migrating endothelial cells. *The Journal of Cell Biology, 206*(1), 97-112.

Brenner, S. (1974). The genetics of *Caenorhabditis elegans*. *Genetics, 77*(1), 71-94.

Brouhard, G. J., Stear, J. H., Noetzel, T. L., Al-Bassam, J., Kinoshita, K., Harrison, S. C., et al. (2008). XMAP215 is a processive microtubule polymerase. *Cell, 132*(1), 79-88.

Brown, K. S., Blower, M. D., Maresca, T. J., Grammer, T. C., Harland, R. M., & Heald, R. (2007). *Xenopus tropicalis* egg extracts provide insight into scaling of the mitotic spindle. *The Journal of Cell Biology, 176*(6), 765-770.

Brunet, S., Sardon, T., Zimmerman, T., Wittmann, T., Pepperkok, R., Karsenti, E., et al. (2004). Characterization of the TPX2 domains involved in microtubule nucleation and spindle assembly in *Xenopus* egg extracts. *Molecular Biology of the Cell, 15*(12), 5318-5328.

Bucciarelli, E., Pellacani, C., Naim, V., Palena, A., Gatti, M., & Somma, M. P. (2009). *Drosophila* Dgt6 interacts with Ndc80, Msps/XMAP215, and γ-tubulin to promote kinetochore-driven MT formation. *Current Biology, 19*(21), 1839-1845.

Burbank, K. S., Mitchison, T. J., & Fisher, D. S. (2007). Slide-and-cluster models for spindle assembly. *Current Biology, 17*(16), 1373-1383.

Burns, K. M., Wagenbach, M., Wordeman, L., & Schriemer, D. C. (2014). Nucleotide exchange in dimeric MCAK induces longitudinal and lateral stress at microtubule ends to support depolymerization. *Structure, 22*(8), 1173-1183.

Camilleri, C., Azimzadeh, J., Pastuglia, M., Bellini, C., Grandjean, O., & Bouchez, D. (2002). The *Arabidopsis* TONNEAU2 gene encodes a putative novel protein phosphatase 2A regulatory subunit essential for the control of the cortical cytoskeleton. *The Plant Cell Online, 14*(4), 833.

Carlier, M., & Pantaloni, D. (2007). Control of actin assembly dynamics in cell motility. *Journal of Biological Chemistry, 282*(32), 23005-23009.

Cheerambathur, D. K., Gassmann, R., Cook, B., Oegema, K., & Desai, A. (2013). Crosstalk between microtubule attachment complexes ensures accurate chromosome segregation. *Science*, 342(6163), 1239-1242.

Chang, P., Jacobson, M. K., & Mitchison, T. J. (2004). Poly(ADP-ribose) is required for spindle assembly and structure. *Nature, 432*(7017), 645-649.

Chavali, P. L., Peset, I., & Gergely, F. (2015). Centrosomes and mitotic spindle poles: A recent liaison? *Biochemical Society Transactions,* 43(1), 13-18.

Chen, G., Rubinstein, B., & Li, R. (2012). Whole chromosome aneuploidy: Big mutations drive adaptation by phenotypic leap. *Bioessays, 34*, 893-900.

Chen, H., Mohan, P., Jiang, J., Nemirovsky, O., He, D., Fleisch, M. C., et al. (2014). Spatial regulation of aurora A activity during mitotic spindle assembly requires RHAMM to correctly localize TPX2. *Cell Cycle, 13*(14), 2248-2261.

Chen, H., Mai, J., Wan, J., Gao, Y., Lin, L., Wang, S., et al. (2013). Role of a novel functional variant in the *PPP2R1A* promoter on the regulation of PP2A-aalpha and the risk of hepatocellular carcinoma. *Plos One, 8*(3), e59574.

Cheng, Y., Liu, W., Kim, S., Sun, J., Lu, L., Sun, J., et al. (2011). Evaluation of PPP2R2A as a prostate cancer susceptibility gene: A comprehensive germline and somatic study. *Cancer Genetics, 204*(7), 375-381.

Cho, U. S., & Xu, W. (2006). Crystal structure of a protein phosphatase 2A heterotrimeric holoenzyme. *Nature, 445*(7123), 53-57.

Clarke, P. R., & Zhang, C. (2008). Spatial and temporal coordination of mitosis by ran GTPase. *Nature Reviews Molecular Cell Biology, 9*(6), 464-477.

Cole, D. G., Saxton, W. M., Sheehan, K. B., & Scholey, J. M. (1994). A "slow" homotetrameric kinesin-related motor protein purified from drosophila embryos. *Journal of Biological Chemistry*, *269*(37), 22913-22916.

Connolly, A. A., Osterberg, V., Christensen, S., Price, M., Lu, C., Chicas-Cruz, K., et al. (2014). *Caenorhabditis elegans* oocyte meiotic spindle pole assembly requires microtubule severing and the calponin homology domain protein ASPM-1. *Molecular Biology of the Cell, 25*(8), 1298-1311.

Couwenbergs, C., Labbé, J.C., Goulding, M., Marty, T., Bowerman, B., & Gotta, M. (2007). Heterotrimeric G protein signaling functions with dynein to promote spindle positioning in *C. elegans. The Journal of Cell Biology,* 179(1), 15-22.

Curmi, P. A., Andersen, S. S. L., Lachkar, S., Gavet, O., Karsenti, E., Knossow, M., et al. (1997). The Stathmin/Tubulin interaction *in vitro*. *Journal of Biological Chemistry, 272*(40), 25029-25036.

Dammermann, A., Cipak, L., & Gregan, J. (2012). Microtubule organization: A pericentriolar material-like structure in yeast meiosis. *Current Biology, 22*(7), 229-231.

Daum, J. R., Wren, J. D., Daniel, J. J., Sivakumar, S., McAvoy, J. N., Potapova, T. A., et al. (2009). Ska3 is required for spindle checkpoint silencing and the maintenance of chromosome cohesion in mitosis. *Current Biology*, 19(17), 1467-1472.

Davis, A. J., Yan, Z., Martinez, B., & Mumby, M. C. (2008). Protein phosphatase 2A is targeted to cell division control protein 6 by a calcium-binding regulatory subunit. *Journal of Biological Chemistry, 283*(23), 16104-16114.

Decker, M., Jaensch, S., Pozniakovsky, A., Zinke, A., O'Connell, K., Zachariae, W., et al. (2011). Limiting amounts of centrosome material set centrosome size in *C. elegans* embryos. *Current Biology, 21*(15), 1259-1267.

Desai, A., Rybina, S., Muller-Reichert, T., Shevchenko, A., Shevchenko, A., Hyman, A., et al. (2003). KNL-1 directs assembly of the microtubule-binding interface of the kinetochore in *C. elegans. Genes & Development*, 17(19), 2421-2435.

Diaz-Rodríguez, E., Sotillo, R., Schvartzman, J., & Benezra, R. (2008). Hec1 overexpression hyperactivates the mitotic checkpoint and induces tumor formation *in vivo*. *Proceedings of the National Academy of Sciences, 105*(43), 16719-16724.

Do, T., Xiao, F., Bickel, L., Klein-Szanto, A., Pathak, H., Hua, X., et al. (2014). Aurora kinase A mediates epithelial ovarian cancer cell migration and adhesion. *Oncogene, 33*, 539-549.

Dodson, C. A., & Bayliss, R. (2012). Activation of aurora-A kinase by protein partner binding and phosphorylation are independent and synergistic. *The Journal of Biological Chemistry, 287*(2), 1150-1157.

Domnitz, S. B., Wagenbach, M., Decarreau, J., & Wordeman, L. (2012). MCAK activity at microtubule tips regulates spindle microtubule length to promote robust kinetochore attachment. *The Journal of Cell Biology, 197*(2), 231-237.

Dovega, R., Tsutakawa, S., Quistgaard, E. M., Anandapadamanaban, M., Löw, C., & Nordlund, P. (2014). Structural and biochemical characterization of human PR70 in isolation and in complex with the scaffolding subunit of protein phosphatase 2A. *PLoS One, 9*(7), e101846.

Dutt, P., Arthur, J. S. C., Grouchulski, P., Cygler, M., & Elce, J. (2000). Roles of individual EF-hands in the activation of m-calpain by calcium. *Biochemical Journal, 348*, 37-43.

Eckerdt, F., Eyers, P. A., Lewellyn, A. L., Prigent, C., & Maller, J. L. (2008). Spindle pole regulation by a discrete Eg5-interacting domain in TPX2. *Current Biology, 18*(7), 519-525.

Ems-McClung, S., Hainline, S., Devare, J., Zong, H., Cai, S., Carnes, S., et al. (2013). Aurora B inhibits MCAK activity through a phosphoconformational switch that reduces microtubule association. *Current Biology, 23*(24), 2491-2499.

Encalada, S., Willis, J. H., Lyczak, R., & Bowerman, B. (2004). A spindle checkpoint functions during mitosis in the early *Caenorhabditis elegans* embryo. *Molecular Biology of the Cell, 16*(3), 1056-1070.

Etienne-Manneville, S. (2013). Microtubules in cell migration. *Annual Review of Cell and Developmental Biology, 29*, 471-99.

Eyers, P. A., Erikson, E., Chen, L. G., & Maller, J. L. (2003). A novel mechanism for activation of the protein kinase aurora A. *Current Biology, 13*(8), 691-697.

Ferenz, N. P., Paul, R., Fagerstrom, C., Mogilner, A., & Wadsworth, P. (2009). Dynein antagonizes Eg5 by crosslinking and sliding antiparallel microtubules. *Current Biology, 19*(21), 1833-1838.

Fernandez, A. G., & Piano, F. (2006). MEL-28 is downstream of the ran cycle and is required for nuclear-envelope function and chromatin maintenance. *Current Biology, 16*(17), 1757-1763.

Floyd, S., Pines, J., & Lindon, C. (2008). APC/CCdh1 targets aurora kinase to control reorganization of the mitotic spindle at anaphase. *Current Biology, 18*(21), 1649-1658.

Foley, E. A., Maldonado, M., & Kapoor, T. M. (2011). Formation of stable attachments between kinetochores and microtubules depends on the B56-PP2A phosphatase. *Nature Cell Biology, 13*(10), 1265-1271.

Fumoto, K., Lee, P., Saya, H., & Kikuchi, A. (2008). AIP regulates stability of aurora-A at early mitotic phase coordinately with GSK-3beta. *Oncogene, 27*(32), 4478-4487.

Gable, A., Qiu, M., Titus, J., Balchand, S., Ferenz, N. P., Ma, N., et al. (2012). Dynamic reorganization of Eg5 in the mammalian spindle throughout mitosis requires dynein and TPX2. *Molecular Biology of the Cell, 23*(7), 1254-1266.

Gadea, B. B., & Ruderman, J. V. (2006). Aurora B is required for mitotic chromatin-induced phosphorylation of Op18/Stathmin. *Proceedings of the National Academy of Sciences of the United States of America, 103*(12), 4493-4498.

Gaitanos, T. N., Santamaria, A., Jeyaprakash, A. A., Wang, B., Conti, E., & Nigg, E. A. (2009). Stable kinetochore-microtubule interactions depend on the ska complex and its new component Ska3/C13Orf3. *The EMBO Journal*, 28(10), 1442-1452.

Gallo, C. M., Wang, J. T., Motegi, F., & Seydoux, G. (2010). Cytoplasmic partitioning of P granule components is not required to specify the germline in *C. elegans*. *Science, 330*(6011), 1685.

Galy, V., Askjaer, P., Franz, C., López-Iglesias, C., & Mattaj, I. W. (2006). MEL-28, a novel nuclear-envelope and kinetochore protein essential for zygotic nuclear-envelope assembly in *C. elegans*. *Current Biology, 16*(17), 1748-1756.

Gassmann, R., Carvalho, A., Henzing, A. J., Ruchaud, S., Hudson, D. F., Honda, R., et al. (2004). Borealin: A novel chromosomal passenger required for stability of the bipolar mitotic spindle. *The Journal of Cell Biology, 166*(2), 179-191.

Gatlin, J. C., & Bloom, K. (2010). Microtubule motors in eukaryotic spindle assembly and maintenance. *Seminars in Cell & Developmental Biology, 21*(3), 248-254.

Geles, K. G., Johnson, J. J., Jong, S., & Adam, S. A. (2002). A role for *Caenorhabditis elegans* importin IMA-2 in germ line and embryonic mitosis. *Molecular Biology of the Cell, 13*(9), 3138-3147.

Gillespie, P. J., Khoudoli, G. A., Stewart, G., Swedlow, J. R., & Blow, J. . (2007). ELYS/MEL-28 chromatin association coordinates nuclear pore complex assembly and replication licensing. *Current Biology, 17*(19), 1657-1662.

Giubettini, M., Asteriti, I., Scrofani, J., De Luca, M., Lindon, C., Lavia, P., et al. (2010). Control of aurora-A stability through interaction with TPX2. *Journal of Cell Science, 124*, 113-122.

Gönczy, P., Pichler, S., Kirkham, M., & Hyman, A. A. (1999). Cytoplasmic dynein is required for distinct aspects of mtoc positioning, including centrosome separation, in the one cell stage C*aenorhabditis elegans* embryo. *The Journal of Cell Biology, 147*(1), 135-150.

Good, M. C., Vahey, M. D., Skandarajah, A., Fletcher, D. A., & Heald, R. (2013). Cytoplasmic volume modulates spindle size during embryogenesis. *Science, 342*(6160), 856-860.

Goodwin, S. S., & Vale, R. D. (2010). Patronin regulates the microtubule network by protecting microtubule minus ends. *Cell, 143*(2), 263-274.

Gordon, D. J., Resio, B., & Pellman, D. (2012). Causes and consequences of aneuploidy in cancer. *Nature Reviews. Genetics, 13*(3), 189-203.

Goshima, G., & Scholey, J. M. (2010). Control of mitotic spindle length. *Annual Review of Cell and Developmental Biology, 26*, 21-57.

Goshima, G. (2011). Identification of a TPX2-like microtubule-associated protein in *Drosophila*. *Plos One, 6*(11), e28120.

Goshima, G., Mayer, M., Zhang, N., Stuurman, N., & Vale, R. D. (2008). Augmin: A protein complex required for centrosome-independent microtubule generation within the spindle. *The Journal of Cell Biology, 181*(3), 421-429.

Greenan, G., Brangwynne, C., Jaensch, S., Gharakhani, J., Julicher, F., & Hyman, A. (2010). Centrosome size sets mitotic spindle length in *Caenorhabditis elegans* Embryos. *Current Biology, 20*, 353-358.

Griffin, E. E., Odde, D. J., & Seydoux, G. (2011). Regulation of the MEX-5 gradient by a spatially segregated kinase/phosphatase cycle. *Cell, 146*(6), 955-968.

Grill, S. W., Gonczy, P., Stelzer, E. H. K., & Hyman, A. A. (2001). Polarity controls forces governing asymmetric spindle positioning in the *Caenorhabditis elegans* embryo. *Nature, 409*(6820), 630-633.

Grill, S. W., Howard, J., Schäffer, E., Stelzer, E. H. K., & Hyman, A. A. (2003). The distribution of active force generators controls mitotic spindle position. *Science, 301*(5632), 518-521.

Groen, A. C., Coughlin, M., & Mitchison, T. J. (2011). Microtubule assembly in meiotic extract requires glycogen. *Molecular Biology of the Cell, 22*(17), 3139-3159.

Groen, A. C., Maresca, T. J., Gatlin, J. C., Salmon, E. D., & Mitchison, T. J. (2009). Functional overlap of microtubule assembly factors in chromatin-promoted spindle assembly. *Molecular Biology of the Cell, 20*(11), 2766-2773.

Groves, M. R., Hanlon, N., Turowski, P., Hemmings, B. A., & Barford, D. (1999). The structure of the protein phosphatase 2A PR65/A subunit reveals the conformation of its 15 tandemly repeated HEAT motifs. *Cell*, 96(1), 99-110.

Gruss, O. J., Carazo-Salas, R. E., Schatz, C. A., Guarguaglini, G., Kast, J., Wilm, M., et al. (2001). Ran induces spindle assembly by reversing the inhibitory effect of importin α on TPX2 activity. *Cell, 104*(1), 83-93.

Guillet, V., Knibiehler, M., Gregory-Pauron, L., Remy, M., Chemin, C., Raynaud-Messina, B., et al. (2011). Crystal structure of gamma-tubulin complex protein GCP4 provides insight into microtubule nucleation. *Nature Structural Molecular Biology, 18*(8), 915-919.

Guo, Y., Kim, C., & Mao, Y. (2013). New insights into the mechanism for chromosome alignment in metaphase. *International Review of Cell and Molecular Biology, 303*(0), 237-262.

Guven-Ozkan, T., Nishi, Y., Robertson, S. M., & Lin, R. (2008). Global transcriptional repression in *C. elegans* germline precursors by regulated sequestration of TAF-4. *Cell, 135*(1), 149-160.

Hachet, V., Canard, C., & Gönczy, P. Centrosomes promote timely mitotic entry in *C. elegans* embryos. *Developmental Cell, 12*(4), 531-541.

Halpin, D., Kalab, P., Wang, J., Weis, K., & Heald, R. (2011). Mitotic spindle assembly around RCC1-coated beads in *Xenopus* egg extracts. *PLoS Biology, 9*(12), e1001225.

Hamill, D. R., Severson, A. F., Carter, J. C., & Bowerman, B. (2002). Centrosome maturation and mitotic spindle assembly in *C. elegans* require SPD-5, a protein with multiple coiled-coil domains. *Developmental Cell, 3*(5), 673-684.

Han, X. (2014). *Regulation of* Caenorhabditis elegans *MCAK by aurora kinase phosphorylation.* Unpublished PhD, University of Alberta, Edmonton, Alberta.

Hannak, E., Oegema, K., Kirkham, M., Gönczy, P., Habermann, B., & Hyman, A. A. (2002). The kinetically dominant assembly pathway for centrosomal asters in *Caenorhabditis elegans* is γ-tubulin dependent. *The Journal of Cell Biology, 157*(4), 591-602.

Hara, Y., & Kimura, A. (2009). Cell-size-dependent spindle elongation in the *Caenorhabditis elegans* early embryo. *Current Biology, 19*(18), 1549-1554.

Hayashi, H., Kimura, K., & Kimura, A. (2012). Localized accumulation of tubulin during semi-open mitosis in the *Caenorhabditis elegans* embryo. *Molecular Biology of the Cell, 23*(9), 1688-1699.

Heald, R., Tournebize, R., Blank, T., Sandaltzopoulos, R., Becker, P., Hyman, A., et al. (1996). Self-organization of microtubules into bipolar spindles around artificial chromosomes in *Xenopus* egg extracts. *Nature, 382*(6590), 420-425.

Hendrix, P., Mayer-Jackel, R. E., Cron, P., Goris, J., Hofsteenge, J., Merlevede, W., et al. (1993). Structure and expression of a 72-kDa regulatory subunit of protein phosphatase 2A. evidence for different size forms produced by alternative splicing. *Journal of Biological Chemistry, 268*(20), 15267-15276.

Hepperla, A., Willey, P., Coombes, C., Schuster, B., Gerami-Nejad, M., McClellan, M., et al. (2014). Minus-end-directed kinesin-14 motors align antiparallel microtubules to control metaphase spindle length. *Developmental Cell, 31*(1), 61-72.

Hoang, L. N., McConechy, M. K., Meng, B., McIntyre, J. B., Ewanowich, C., Blake Gilks, C., et al. (2014). Targeted mutation analysis of endometrial clear cell carcinoma. *Histopathology,* Accepted Article, doi: 10.1111/his.12581.

Holy, T. E., & Leibler, S. (1994). Dynamic instability of microtubules as an efficient way to search in space. *Proceedings of the National Academy of Sciences, 91*(12), 5682-5685.

Horn, V., Thélu, J., Garcia, A., Albigès-Rizo, C., Block, M., & Viallet, J. (2007). Functional interaction of aurora-A and PP2A during mitosis. *Molecular Biology of the Cell, 18*(4), 1233-1241.

Huang, H., Feng, J., Famulski, J., Rattner, J. B., Liu, S. T., Kao, G. D., et al. (2007). Tripin/hSgo2 recruits MCAK to the inner centromere to correct defective kinetochore attachments. *The Journal of Cell Biology, 177*(3), 413-424.

Inoué, S., & Salmon, E. D. (1995). Force generation by microtubule Assembly/Disassembly in mitosis and related movements. *Molecular Biology of the Cell, 6*(12), 1619-1640.

Iyer, J., & Tsai, M. (2012). A novel role for TPX2 as a scaffold and co-activator protein of the chromosomal passenger complex. *Cellular Signalling, 24*(8), 1677-1689.

Jackson, D. E., Poncz, M., Holyst, M. T., & Newman, P. J. (1996). Inherited mutations within the calcium-binding sites of the integrin αIIb subunit (platelet glycoprotein IIb). *European Journal of Biochemistry, 240*(1), 280-287.

Jakobsen, L., Vanselow, K., Skogs, M., Toyoda, Y., Lundberg, E., Poser, I., et al. (2011). Novel asymmetrically localizing components of human centrosomes identified by complementary proteomics methods. *The EMBO Journal, 30*(8), 1520-1535.

Janssens, V., Derua, R., Zwaenepoel, K., Waelkens, E., & Goris, J. (2009). Specific regulation of protein phosphatase 2A PR72/B″ subunits by calpain. *Biochemical and Biophysical Research Communications, 386*(4), 676-681.

Janssens, V., Jordens, J., Stevens, I., Van Hoof, C., Martens, E., De Smedt, H., et al. (2003). Identification and functional analysis of two $Ca^{2+}$ binding EF-hand motifs in the B"/PR72 subunit of protein phosphatase 2A. *Journal of Biological Chemistry, 278*(12), 10697-10706.

Joglekar, A. P., Bouck, D. C., Molk, J. N., Bloom, K. S., & Salmon, E. D. (2006). Molecular architecture of a kinetochore-microtubule attachment site. *Nature Cell Biology, 8*(6), 581-585.

Joglekar, A. P., Bouck, D., Finley, K., Liu, X., Wan, Y., Berman, J., et al. (2008). Molecular architecture of the kinetochore-microtubule attachment site is conserved between point and regional centromeres. *The Journal of Cell Biology, 181*(4), 587-594.

Kalab, P., Weis, K., & Heald, R. (2002). Visualization of a ran-GTP gradient in interphase and mitotic *Xenopus* egg extracts. *Science (New York, N.Y.), 295*(5564), 2452-2456.

Kalev, P., & A Sablina, A. (2011). Protein phosphatase 2A as a potential target for anticancer therapy. *Anti-Cancer Agents in Medicinal Chemistry, 11*(1), 38-46.

Kamath, R. S., Fraser, A. G., Dong, Y., Poulin, G., Durbin, R., Gotta, M., et al. (2003). Systematic functional analysis of the *Caenorhabditis elegans* genome using RNAi. *Nature, 421*(6920), 231-237.

Kamath, K., Smiyun, G., Wilson, L., & Jordan, M. A. (2014). Mechanisms of inhibition of endothelial cell migration by taxanes. *Cytoskeleton, 71*(1), 46-60.

Kang, Q., Srividhya, J., Ipe, J., & Pomerening, J. R. (2014). Evidence towards a dual phosphatase mechanism that restricts aurora A (T295) phosphorylation during the early embryonic cell cycle. *Journal of Biological Chemistry,* 289(25), 17480-17496.

Kapitein, L. C., Peterman, E. J., Kwok, B. H., Kim, J. H., Kapoor, T. M., & Schmidt, C. F. (2005). The bipolar mitotic kinesin Eg5 moves on both microtubules that it crosslinks. *Nature, 435*(7038), 114-118.

Kapoor, T. M., Mayer, T. U., Coughlin, M. L., & Mitchison, T. J. (2000). Probing spindle assembly mechanisms with monastrol, a small molecule inhibitor of the mitotic kinesin, Eg5. *The Journal of Cell Biology, 150*(5), 975-988.

Karsenti, E. (2005). TPX or not TPX? *Molecular Cell, 19*(4), 431-432.

Katayama, H., Sasai, K., Kloc, M., Brinkley, B. R., & Sen, S. (2008). Aurora kinase-A regulates kinetochore/chromatin associated microtubule assembly in human cells. *Cell Cycle, 7*(17), 2691-2704.

Keck, J. M., Jones, M. H., Wong, C. C. L., Binkley, J., Chen, D., Jaspersen, S. L., et al. (2011). A cell cycle phosphoproteome of the yeast centrosome. *Science*, *332*(6037), 1557-1561.

Kerssemakers, J. W. J., Laura Munteanu, E., Laan, L., Noetzel, T. L., Janson, M. E., & Dogterom, M. (2006). Assembly dynamics of microtubules at molecular resolution. *Nature, 442*(7103), 709-712.

Khan, M. L. A., Gogonea, C. B., Siddiqui, Z. K., Ali, M. Y., Kikuno, R., Nishikawa, K., et al. (1997). Molecular cloning and expression of the *Caenorhabditis elegans klp-3*, an ortholog of C terminus motor kinesins kar3 and ncd. *Journal of Molecular Biology, 270*(5), 627-639.

Khanna, A., Pimanda, J. E., & Westermarck, J. (2013). Cancerous inhibitor of protein phosphatase 2A, an emerging human oncoprotein and a potential cancer therapy target. *Cancer Research, 73*(22), 6548-6553.

Khodjakov, A., Cole, R. W., Oakley, B. R., & Rieder, C. L. (2000). Centrosome-independent mitotic spindle formation in vertebrates. *Current Biology, 10*(2), 59-67.

Kim, H., Fonseca, C., & Stumpff, J. (2014). A unique kinesin-8 surface loop provides specificity for chromosome alignment. *Molecular Biology of the Cell, 25*(21), 3319-3329.

Kinoshita, E., Kinoshita-Kikuta, E., Takiyama, K., & Koike, T. (2006). Phosphate-binding tag, a new tool to visualize phosphorylated proteins. *Molecular & Cellular Proteomics*, 5(4), 749-757.

Kirik, A., Ehrhardt, D. W., & Kirik, V. (2012). TONNEAU2/FASS regulates the geometry of microtubule nucleation and cortical array organization in interphase arabidopsis cells. *The Plant Cell Online, 24*(3), 1158-1170.

Kishore, R. S., & Sundaram, M. V. (2002). *ced-10,* rac, and *mig-2* function redundantly and act with *unc-73* trio to control the orientation of vulval cell divisions and migrations in *Caenorhabditis elegans*. *Developmental Biology, 241*(2), 339-348.

Kitagawa, R. (2009). Key players in chromosome segregation in *Caenorhabditis elegans*. *Frontiers in Bioscience, 14*, 1529-1557.

Kitagawa, D., Flückiger, I., Polanowska, J., Keller, D., Reboul, J., & Gönczy, P. (2011). PP2A phosphatase acts upon SAS-5 to ensure centriole formation in *C. elegans* embryos. *Developmental Cell*, 20(4), 550-562.

Kollman, J. M., Polka, J. K., Zelter, A., Davis, T. N., & Agard, D. A. (2010). Microtubule nucleating gamma-TuSC assembles structures with 13-fold microtubule-like symmetry. *Nature, 466*(7308), 879-882.

Kollu, S., Bakhoum, S. F., & Compton, D. A. (2009). Interplay of microtubule dynamics and sliding during bipolar spindle formation in mammalian cells. *Current Biology, 19*(24), 2108-2113.

Kono, Y., Maeda, K., Kuwahara, K., Yamamoto, H., Miyamoto, E., Yonezawa, K., et al. (2002). MCM3-binding GANP DNA-primase is associated with a novel phosphatase component G5PR.*Genes to Cells, 7*(8), 821-834.

Kress, E., Schwager, F., Holtackers, R., Seiler, J., Prodon, F., Zanin, E., et al. (2013). The UBXN-2/p37/p47 adaptors of CDC-48/p97 regulate mitosis by limiting the centrosomal recruitment of aurora A. *The Journal of Cell Biology, 201*(4), 559-575.

Kruse, T., Zhang, G., Larsen, M. S. Y., Lischetti, T., Streicher, W., Kragh Nielsen, T., et al. (2013). Direct binding between BubR1 and B56–PP2A phosphatase complexes regulate mitotic progression. *Journal of Cell Science, 126*(5), 1086-1092.

Kufer, T. A., Silljé, H. H. W., Körner, R., Gruss, O. J., Meraldi, P., & Nigg, E. A. (2002). Human TPX2 is required for targeting aurora-A kinase to the spindle. *The Journal of Cell Biology, 158*(4), 617-623.

Kuhn, M., Hyman, A. A., & Beyer, A. (2014). Coiled-coil proteins facilitated the functional expansion of the centrosome. *PLOS Computational Biology, 10*(6), e1003657.

Kumar, M., Ahmad, S., Ahmad, E., Saifi, M. A., & Khan, R. H. (2012). *In silico* prediction and analysis of *Caenorhabditis* EF-hand containing proteins. *Plos One, 7*(5), e36770.

Labbé, J.C., McCarthy, E. K., & Goldstein, B. (2004). The forces that position a mitotic spindle asymmetrically are tethered until after the time of spindle assembly. *The Journal of Cell Biology*, 167(2), 245-256.

Labbé, J. C., & Roy, R. (2006). New developmental insights from high-throughput biological analysis in *Caenorhabditis elegans. Clinical Genetics*, 69(4), 306-314.

Lacroix, B., Bourdages, K. G., Dorn, J. F., Ihara, S., Sherwood, D. R., Maddox, P. S., et al. (2014). *In situ* imaging in *C. elegans* reveals developmental regulation of microtubule dynamics. *Developmental Cell, 29*(2), 203-216.

Lambrecht, C., Haesen, D., Sents, W., Ivanova, E., & Janssens, V. (2013). Structure, regulation, and pharmacological modulation of PP2A phosphatases. In J. L. Millán (Ed.), (pp. 283-305) Humana Press.

Lange, K. I., Heinrichs, J., Cheung, K., & Srayko, M. (2013). Suppressor mutations identify amino acids in PAA-1/PR65 that facilitate regulatory RSA-1/B″ subunit targeting of PP2A to centrosomes in *C. elegans*. *Biology Open, 2*(1), 88-94.

Le Bot, N., Tsai, M., Andrews, R. K., & Ahringer, J. (2003). TAC-1, a regulator of microtubule length in the *C. elegans* embryo. *Current Biology, 13*(17), 1499-1505.

Leontovich, A., Salisbury, J., Veroux, M., Tallarita, T., Billadeau, D., McCubrey, J., et al. (2013). Inhibition of Cdk2 activity decreases aurora-A kinase centrosomal localization and prevents centrosome amplification in breast cancer cells. *Oncology Reports, 29*(5), 1785-1788.

Li, J., Xuan, J. W., Khatamianfar, V., Valiyeva, F., Moussa, M., Sadek, A., et al. (2014). SKA1 over-expression promotes centriole over-duplication, centrosome amplification and prostate tumourigenesis. *The Journal of Pathology*, 234(2), 178-189.

Li, Y., Tang, K., Zhang, H., Zhang, Y., Zhou, W., & Chen, X. (2011). Function of aurora kinase A in taxol-resistant breast cancer and its correlation with P-gp. *Molecular Medicine Reports, 4*(4), 739-746.

Littlepage, L., & Ruderman, J. (2002). Identification of a new APC/C recognition domain, the A box, which is required for the Cdh1-dependent destruction of the kinase aurora-A during mitotic exit. *Genes & Development, 16*, 2274-2285.

Littlepage, L. E., Wu, H., Andresson, T., Deanehan, J. K., Amundadottir, L. T., & Ruderman, J. V. (2002). Identification of phosphorylated residues that affect the activity of the mitotic kinase aurora-A. *Proceedings of the National Academy of Sciences, 99*(24), 15440-15445.

Loughlin, R., Heald, R., & Nédélec, F. (2010). A computational model predicts *Xenopus* meiotic spindle organization. *The Journal of Cell Biology, 191*(7), 1239-1249.

Ma, H. T., & Poon, R. Y. C. (2011). How protein kinases co-ordinate mitosis in animal cells. *Biochemical Journal, 435*(1), 17-31.

Maddox, P. S., Oegema, K., Desai, A., & Cheeseman, I. M. (2004). "Holo"er than thou: Chromosome segregation and kinetochore function in *C. elegans*. *Chromosome Research, 12*(6), 641-653.

Malone, C. J., Misner, L., Le Bot, N., Tsai, M., Campbell, J. M., Ahringer, J., et al. (2003). The *C. elegans* hook protein, ZYG-12, mediates the essential attachment between the centrosome and nucleus. *Cell, 115*(7), 825-836.

Malumbres, M., & Pérez de Castro, I. (2014). Aurora kinase A inhibitors: Promising agents in antitumoral therapy. *Expert Opinion on Therapeutic Targets,18*(12), 1377-1393.

Maresca, T. J., Groen, A. C., Gatlin, J. C., Ohi, R., Mitchison, T. J., & Salmon, E. D. (2009). Spindle assembly in the absence of a RanGTP gradient requires localized CPC activity. *Current Biology, 19*(14), 1210-1215.

Matthews, L. R., Carter, P., Thierry-Mieg, D., & Kemphues, K. (1998). ZYG-9, A *Caenorhabditis elegans* protein required for microtubule organization and function, is a component of meiotic and mitotic spindle poles. *The Journal of Cell Biology, 141*(5), 1159-1168.

Maurer, S., Cade, N., Bohner, G., Gustafsson, N., Boutant, E., & Surrey, T. (2014). EB1 accelerates two conformational transitions important for microtubule maturation and dynamics. *Current Biology, 24*(4), 372-384.

McCright, B., Rivers, A. M., Audlin, S., & Virshup, D. M. (1996). The B56 family of protein phosphatase 2A (PP2A) regulatory subunits encodes differentiation-induced phosphoproteins that target PP2A to both nucleus and cytoplasm. *Journal of Biological Chemistry, 271*(36), 22081-22089.

McEwen, B. F., Heagle, A. B., Cassels, G. O., Buttle, K. F., & Rieder, C. L. (1997). Kinetochore fiber maturation in PtK1 cells and its implications for the mechanisms of chromosome congression and anaphase onset. *The Journal of Cell Biology, 137*(7), 1567-1580.

Meunier, S., & Vernos, I. (2011). K-fibre minus ends are stabilized by a RanGTP-dependent mechanism essential for functional spindle assembly. *Nature Cell Biology, 13*(12), 1406-1414.

Mitchison, T. (1993). Localization of an exchangeable GTP binding site at the plus end of microtubules. *Science, 261*(5124), 1044-1047.

Mitchison, T., & Kirschner, M. (1984). Dynamic instability of microtubule growth. *Nature, 312*, 237-42.

Mitchison, T. J., & Kirschner, M. W. (1985). Properties of the kinetochore *in vitro*. I. microtubule nucleation and tubulin binding. *The Journal of Cell Biology, 101*(3), 755-765.

Mitchison, T. J., Maddox, P., Gaetz, J., Groen, A., Shirasu, M., Desai, A., et al. (2005). Roles of polymerization dynamics, opposed motors, and a tensile element in governing the length of *Xenopus* extract meiotic spindles. *Molecular Biology of the Cell, 16*(6), 3064-3076.

Mori, D., Yano, Y., Toyo-oka, K., Yoshida, N., Yamada, M., Muramatsu, M., et al. (2007). NDEL1 phosphorylation by aurora-A kinase is essential for centrosomal maturation, separation, and TACC3 recruitment. *Molecular and Cellular Biology, 27*(1), 352-367.

Morris, E. J., Nader, G. P. F., Ramalingam, N., Bartolini, F., & Gundersen, G. G. (2014). Kif4 interacts with EB1 and stabilizes microtubules downstream of rho-mDia in migrating fibroblasts. *Plos One, 9*(3), e91568.

Mukherjee, S., Valencia, J. D., Stewman, S., Metz, J., Monnier, S., Rath, U., et al. (2012). Human fidgetin is a microtubule severing the enzyme and minus-end depolymerase that regulates mitosis. *Cell Cycle, 11*(12), 2359-2366.

Müller, H., Schmidt, D., Steinbrink, S., Mirgorodskaya, E., Lehmann, V., Habermann, K., et al. (2010). Proteomic and functional analysis of the mitotic *Drosophila* centrosome. *The EMBO Journal, 29*(19), 3344-3357.

Müller-Reichert, T., Greenan, G., O'Toole, E., & Srayko, M. (2010). The *elegans* of spindle assembly. *Cellular and Molecular Life Sciences, 67*(13), 2195-2213.

Nannas, N., O'Toole, E. T., Winey, M., & Murray, A. (2014). Chromosomal attachments set length and microtubule number in the *S. cerevisiae* mitotic spindle. *Molecular Biology of the Cell, 25*(25), 4034-4048.

Nardozzi, J. D., Lott, K., & Cingolani, G. (2010). Phosphorylation meets nuclear import: A review. *Cell Communication and Signaling, 8*(32).

Nazarova, E., O'Toole, E., Kaitna, S., Francois, P., Winey, M., & Vogel, J. (2013). Distinct roles for antiparallel microtubule pairing and overlap during early spindle assembly. *Molecular Biology of the Cell*, 24(20), 3238-3250.

Nguyen-Ngoc, T., Afshar, K., & Gonczy, P. (2007). Coupling of cortical dynein and galpha] proteins mediates spindle positioning in *Caenorhabditis elegans. Nature Cell Biology, 9*(11), 1294-1302.

Nikonova, A., Astsaturov, I., Serebriiskii, I., Dunbrack, R., Jr., & Golemis, E. (2013). Aurora A kinase (AURKA) in normal and pathological cell division. *Cellular and Molecular Life Sciences, 70*(4), 661-687.

Noatynska, A., Gotta, M., & Meraldi, P. (2012). Mitotic spindle (DIS)orientation and DISease: Cause or consequence? *The Journal of Cell Biology, 199*(7), 1025-1035.

Oegema, K., Desai, A., Rybina, S., Kirkham, M., & Hyman, A. A. (2001). Functional analysis of kinetochore assembly in *Caenorhabditis elegans*. *The Journal of Cell Biology, 153*(6), 1209-1226.

Ohi, R., Sapra, T., Howard, J., & Mitchison, T. J. (2004). Differentiation of cytoplasmic and meiotic spindle assembly MCAK functions by aurora B-dependent phosphorylation. *Molecular Biology of the Cell, 15*(6), 2895-2906.

Olsen, J. V., Vermeulen, M., Santamaria, A., Kumar, C., Miller, M. L., Jensen, L. J., et al. (2010). Quantitative phosphoproteomics reveals widespread full phosphorylation site occupancy during mitosis. *Science Signalling, 3*(104), ra3.

O'Rourke, S. M., Carter, C., Carter, L., Christensen, S. N., Jones, M. P., Nash, B., et al. (2011). A survey of new temperature-sensitive, embryonic-lethal mutations in *C. elegans*: 24 alleles of thirteen genes. *PLoS One, 6*(3), e16644.

O'Toole, E., Greenan, G., Lange, K. I., Srayko, M., & Müller-Reichert, T. (2012). The role of γ-tubulin in centrosomal microtubule organization. *PLoS One, 7*(1), e29795.

Ozlü, N., Srayko, M., Kinoshita, K., Habermann, B., O'Toole, E. T., M ller-Reichert, T., et al. (2005). An essential function of the *C. elegans* ortholog of TPX2 is to localize activated aurora A kinase to mitotic spindles. *Developmental Cell, 9*(2), 237-248.

Padmanabhan, S., Mukhopadhyay, A., Narasimhan, S. D., Tesz, G., Czech, M. P., & Tissenbaum, H. A. (2009). A PP2A regulatory subunit Regulates *C. elegans* Insulin/IGF-1 signaling by modulating AKT-1 phosphorylation. *Cell,* 136(5), 939-951.

Pakala, S. B., Nair, V. S., Reddy, S. D., & Kumar, R. (2012). Signaling-dependent phosphorylation of mitotic centromere-associated kinesin regulates microtubule depolymerization and its centrosomal localization. *Journal of Biological Chemistry, 287*(48), 40560-40569.

Perrotti, D., & Neviani, P. (2013). Protein phosphatase 2A: A target for anticancer therapy. *The Lancet Oncology, 14*(6), e229-e238.

Persechini, A., Moncrief, N. D., & Kretsinger, R. H. (1989). The EF-hand family of calcium-modulated proteins. *Trends in Neurosciences, 12*(11), 462-467.

Petry, S., Groen, A., Ishihara, K., Mitchison, T., & Vale, R. (2013). Branching microtubule nucleation in *Xenopus* egg extracts mediated by augmin and TPX2. *Cell, 152*(4), 768-777.

Pinson, L., Mannini, L., Willems, M., Cucco, F., Sirvent, N., Frebourg, T., et al. (2014). CEP57 mutation in a girl with mosaic variegated aneuploidy syndrome. *American Journal of Medical Genetics, 164*(1), 177-181.

Pinyol, R., Scrofani, J., & Vernos, I. (2013). The role of NEDD1 phosphorylation by aurora A in chromosomal microtubule nucleation and spindle function. *Current Biology, 23*(2), 143-149.

Portier, N., Audhya, A., Maddox, P. S., Green, R. A., Dammermann, A., Desai, A., et al. (2007). A microtubule-independent role for centrosomes and aurora a in nuclear envelope breakdown. *Developmental Cell, 12*(4), 515-529.

Pottgiesser, J., Maurer, P., Mayer, U., Nischt, R., Mann, K., Timpl, R., et al. (1994). Changes in calcium and collagen IV binding caused by mutations in the EF hand and other domains of extracellular matrix protein BM-40 (SPARC, osteonectin). *Journal of Molecular Biology, 238*(4), 563-574.

Powers, J., Rose, D. J., Saunders, A., Dunkelbarger, S., Strome, S., & Saxton, W. M. (2004). Loss of KLP-19 polar ejection force causes misorientation and missegregation of holocentric chromosomes. *The Journal of Cell Biology, 166*(7), 991-1001.

Qin, X., Yuan, B., Xu, X., Huang, H., & Liu, Y. (2013). Effects of short interfering RNA-mediated gene silencing of SKA1 on proliferation of hepatocellular carcinoma cells. *Scandinavian Journal of Gastroenterology,* 48(11), 1324-1332.

Raaijmakers, J. A., Tanenbaum, M. E., Maia, A. F., & Medema, R. H. (2009). RAMA1 is a novel kinetochore protein involved in kinetochore-microtubule attachment. *Journal of Cell Science*, 122(14), 2436-2445.

Rabilotta, A., Amini, R., & Labbé, J. C. (2012). Live imaging for studying asymmetric cell division in the *C. elegans* embryo. In K. A. Mace, & K. M. Braun (Eds.), Progenitor Cells (pp. 111-125) Humana Press.

Rahman, M. M., Rosu, S., Joseph-Strauss, D., & Cohen-Fix, O. (2014). Down-regulation of tricarboxylic acid (TCA) cycle genes blocks progression through the first mitotic division in *Caenorhabditis elegans* embryos. *Proceedings of the National Academy of Sciences, 111*(7), 2602-2607.

Rahman, M., Nakayama, K., Rahman, M. T., Nakayama, N., Katagiri, H., Katagiri, A., et al. (2013). PPP2R1A mutation is a rare event in ovarian carcinoma across histological subtypes. *Anticancer Research, 33*(1), 113-118.

Ricke, R. M., Jeganathan, K. B., & van Deursen, J. M. (2011). Bub1 overexpression induces aneuploidy and tumor formation through aurora B kinase hyperactivation. *The Journal of Cell Biology, 193*(6), 1049-1064.

Ricke, R. M., & van Deursen, J. M. (2013). Aneuploidy in health, disease, and aging. *The Journal of Cell Biology, 201*(1), 11-21.

Robin, G., DeBonis, S., Dornier, A., Cappello, G., Ebel, C., Wade, R. H., et al. (2005). Essential kinesins: Characterization of *Caenorhabditis elegans* KLP-15. *Biochemistry, 44*, 6526-6536.

Romano, A., Guse, A., Krascenicova, I., Schnabel, H., Schnabel, R., & Glotzer, M. (2003). CSC-1: A subunit of the aurora B kinase complex that binds to the survivin-like protein BIR-1 and the incenp-like protein ICP-1. *The Journal of Cell Biology, 161*(2), 229-236.

Ruediger, R., Ruiz, J., & Walter, G. (2011). Human cancer-associated mutations in the Aα subunit of protein phosphatase 2A increase lung cancer incidence in Aα knock-in and knockout mice. *Molecular and Cellular Biology, 31*(18), 3832-3844.

Sacristan, C., & Kops, G. J. P. L. (2014). Joined at the hip: Kinetochores, microtubules, and spindle assembly checkpoint signaling. *Trends in Cell Biology,* (0)

Sampath, S. C., Ohi, R., Leismann, O., Salic, A., Pozniakovski, A., & Funabiki, H. (2004). The chromosomal passenger complex is required for chromatin-induced microtubule stabilization and spindle assembly. *Cell, 118*(2), 187-202.

Sanhaji, M., Ritter, A., Belsham, H. R., Friel, C. T., Roth, S., Louwen, F., et al. (2014). Polo-like kinase 1 regulates the stability of the mitotic centromere-associated kinesin in mitosis. *Oncotarget, 5*(10), 3130-3144.

Sanhaji, M., Friel, C. T., Kreis, N., Krämer, A., Martin, C., Howard, J., et al. (2010). Functional and spatial regulation of mitotic centromere-associated kinesin by cyclin-dependent kinase 1. *Molecular and Cellular Biology, 30*(11), 2594-2607.

Santamaria, A., Wang, B., Elowe, S., Malik, R., Zhang, F., Bauer, M., et al. (2011). The Plk1-dependent phosphoproteome of the early mitotic spindle. *Molecular & Cellular Proteomics, 10*(1).

Sarangapani, K. K., Akiyoshi, B., Duggan, N. M., Biggins, S., & Asbury, C. L. (2013). Phosphoregulation promotes release of kinetochores from dynamic microtubules via multiple mechanisms. *Proceedings of the National Academy of Sciences, 110*(18), 7282-7287.

Sardon, T., Peset, I., Petrova, B., & Vernos, I. (2008). Dissecting the role of aurora A during spindle assembly. *The EMBO Journal, 27*(19), 2567-2579.

Sauer, G., Körner, R., Hanisch, A., Ries, A., Nigg, E. A., & Silljé, H. H. W. (2005). Proteome analysis of the human mitotic spindle. *Molecular & Cellular Proteomics, 4*(1), 35-43.

Saunders, A. M., Powers, J., Strome, S., & Saxton, W. M. (2007). Kinesin-5 acts as a brake in anaphase spindle elongation. *Current Biology, 17*(12), 453-454.

Scharer, C. D., Laycock, N., Osunkoya, A. O., Logani, S., McDonald, J. F., Benigno, B. B., et al. (2008). Aurora kinase inhibitors synergize with paclitaxel to induce apoptosis in ovarian cancer cells. *Journal of Translational Medicine, 6*(79).

Schatz, C. A., Santarella, R., Hoenger, A., Karsenti, E., Mattaj, I. W., Gruss, O. J., et al. (2003). Importin alpha-regulated nucleation of microtubules by TPX2. *The EMBO Journal, 22*(9), 2060-2070.

Schlaitz, A., Srayko, M., Dammermann, A., Quintin, S., Wielsch, N., MacLeod, I., et al. (2007). The *C. elegans* RSA complex localizes protein phosphatase 2A to centrosomes and regulates mitotic spindle assembly. *Cell, 128*(1), 115-127.

Schliekelman, M., Cowley, D. O., O'Quinn, R., Oliver, T. G., Lu, L., Salmon, E. D., et al. (2009). Impaired Bub1 function in vivo compromises tension-dependent checkpoint function leading to aneuploidy and tumorigenesis. *Cancer Research, 69*(1), 45-54.

Schmid, M., Steinlein, C., Tian, Q., Hanlon Newell, A., Gessler, M., Olson, S., et al. (2014). Mosaic variegated aneuploidy in mouse BubR1 deficient embryos and pregnancy loss in human. *Chromosome Research, 22*(3), 375-392.

Schmidt, J., Arthanari, H., Boeszoermenyi, A., Dashkevich, N., Wilson-Kubalek, E., Monnier, N., et al. (2012). The kinetochore-bound Ska1 complex tracks depolymerizing microtubules and binds to curved protofilaments. *Developmental Cell, 23*(5), 968-980.

Schmitz, M. H. A., Held, M., Janssens, V., Hutchins, J. R. A., Hudecz, O., Ivanova, E., et al. (2010). Live-cell imaging RNAi screen identifies PP2A-B55alpha and importin-beta1 as key mitotic exit regulators in human cells. *Nature Cell Biology, 12*(9), 886-893.

Scrofani, J., Sardon, T., Meunier, S., & Vernos, I. (2015). Microtubule nucleation in mitosis by a RanGTP-dependent protein complex. *Current Biology, 25*(2), 131-140.

Schumacher, J. M., Ashcroft, N., Donovan, P. J., & Golden, A. (1998). A highly conserved centrosomal kinase, AIR-1, is required for accurate cell cycle progression and segregation of developmental factors in *Caenorhabditis elegans* embryos. *Development, 125*(22), 4391-4402.

Segbert, C., Barkus, R., Powers, J., Strome, S., Saxton, W. M., & Bossinger, O. (2003). KLP-18, a Klp2 kinesin, is required for assembly of acentrosomal meiotic spindles in *caenorhabditis elegans*. *Molecular Biology of the Cell, 14*(11), 4458-4469.

Seki, A., Coppinger, J. A., Jang, C., Yates, J. R., & Fang, G. (2008). Bora and the kinase aurora A cooperatively activate the kinase Plk1 and control mitotic entry. *Science, 320*(5883), 1655-1658.

Sents, W., Ivanova, E., Lambrecht, C., Haesen, D., & Janssens, V. (2013). The biogenesis of active protein phosphatase 2A holoenzymes: A tightly regulated process creating phosphatase specificity. *FEBS Journal, 280*(2), 644-661.

Shagisultanova, E., Dunbrack, R., & Golemis, E. (2015). Issues in interpreting the in vivo activity of aurora-A. *Expert Opinion on Therapeutic Targets, 19*(2), 187-200.

Shaye, D. D., & Greenwald, I. (2011). OrthoList: A compendium of *C. elegans* genes with human orthologs. *Plos One, 6*(5), e20085.

Song, L., Craney, A., & Rape, M. (2014). Microtubule-dependent regulation of mitotic protein degradation. *Molecular Cell, 53*(2), 179-192.

Song, M., Liu, Y., Anderson, D., Jahng, W., & O'Connell, K. (2011). Protein phosphatase 2A-SUR-6/B55 regulates centriole duplication in *C. elegans* by controlling the levels of centriole assembly factors. *Developmental Cell, 20*(4), 563-571.

Sonnichsen, B., Koski, L. B., Walsh, A., Marschall, P., Neumann, B., Brehm, M., et al. (2005). Full-genome RNAi profiling of early embryogenesis in *Caenorhabditis elegans*. *Nature, 434*(7032), 462-469.

Sontag, E., Nunbhakdi-Craig, V., Bloom, G. S., & Mumby, M. C. (1995). A novel pool of protein phosphatase 2A is associated with microtubules and is regulated during the cell cycle. *The Journal of Cell Biology, 128*(6), 1131-1144.

Speliotes, E. K., Uren, A., Vaux, D., & Horvitz, H. R. (2000). The survivin-like *C. elegans* BIR-1 protein acts with the aurora-like kinase AIR-2 to affect chromosomes and the spindle midzone. *Molecular Cell, 6*(2), 211-223.

Srayko, M., Kaya, A., Stamford, J., & Hyman, A. A. (2005). Identification and characterization of factors required for microtubule growth and nucleation in the early *C. elegans* embryo. *Developmental Cell, 9*(2), 223-236.

Srayko, M., O'Toole, E. T., Hyman, A. A., & Müller-Reichert, T. (2006). Katanin disrupts the microtubule lattice and increases polymer number in *C. elegans* meiosis. *Current Biology*, 16(19), 1944-1949.

Srayko, M., Quintin, S., Schwager, A., & Hyman, A. A. (2003). *Caenorhabditis elegans* TAC-1 and ZYG-9 form a complex that is essential for long astral and spindle microtubules. *Current Biology, 13*(17), 1506-1511.

Strack, S., Zaucha, J. A., Ebner, F. F., Colbran, R. J., & Wadzinski, B. E. (1998). Brain protein phosphatase 2A: Developmental regulation and distinct cellular and subcellular localization by B subunits. *The Journal of Comparative Neurology, 392*(4), 515-527.

Strack, S., Ruediger, R., Walter, G., Dagda, R. K., Barwacz, C. A., & Cribbs, J. T. (2002). Protein phosphatase 2A holoenzyme assembly: Identification of contacts between B-family regulatory subunits and scaffolding A subunits.*Journal of Biological Chemistry*, 277(23), 20750-20755.

Sturgill, E. G., Das, D. K., Takizawa, Y., Shin, Y., Collier, S. E., Ohi, M. D., et al. (2014). Kinesin-12 Kif15 targets kinetochore fibers through an intrinsic two-step mechanism. *Current Biology, 24*(19), 2307-2313.

Sturgill, E. G., & Ohi, R. (2013). Kinesin-12 differentially affects spindle assembly depending on its microtubule substrate. *Current Biology, 23*(14), 1280-1290.

Suganuma, M., Fujiki, H., Suguri, H., Yoshizawa, S., Hirota, M., Nakayasu, M., et al. (1988). Okadaic acid: An additional non-phorbol-12-tetradecanoate-13-acetate-type tumor promoter. *Proceedings of the National Academy of Sciences, 85*(6), 1768.

Sun, W., Yao, L., Jiang, B., Guo, L., & Wang, Q. (2014). Spindle and kinetochore-associated protein 1 is overexpressed in gastric cancer and modulates cell growth. *Molecular and Cellular Biochemistry*, 391(1-2), 167-174.

Syrovatkina, V., Fu, C., & Tran, P. (2013). Antagonistic spindle motors and MAPs regulate metaphase spindle length and chromosome segregation. *Current Biology, 23*(23), 2423-2429.

Tanenbaum, M. E., Macurek, L., van der Vaart, B., Galli, M., Akhmanova, A., & Medema, R. H. (2011). A complex of Kif18b and MCAK promotes microtubule depolymerization and is negatively regulated by aurora kinases. *Current Biology, 21*(16), 1356-1365.

Tanenbaum, M. E., Macůrek, L., Janssen, A., Geers, E. F., Alvarez-Fernández, M., & Medema, R. H. (2009). Kif15 cooperates with eg5 to promote bipolar spindle assembly. *Current Biology, 19*(20), 1703-1711.

Tegha-Dunghu, J., Gusnowski, E., & Srayko, M. (2014). Measuring microtubule growth and gliding in *Caenorhabditis elegans* embryos. In D. J. Sharp (Ed.), (pp. 103-116) Springer New York.

The *C. elegans* Sequencing Consortium. (1998). Genome sequence of the nematode *C. elegans*: A platform for investigating biology. *Science, 282*(5396), 2012-2018.

Tipton, A., Wang, K., Oladimeji, P., Sufi, S., Gu, Z., & Liu, S. (2012). Identification of novel mitosis regulators through data mining with human centromere/kinetochore proteins as group queries. *BMC Cell Biology, 13*(1), 15.

Toya, M., Terasawa, M., Nagata, K., Iida, Y., & Sugimoto, A. (2011). A kinase-independent role for aurora A in the assembly of mitotic spindle microtubules in *Caenorhabditis elegans* embryos. *Nature Cell Biology, 13*(6), 708-714.

Tsai, M., Wiese, C., Cao, K., Martin, O., Donovan, P., Ruderman, J., et al. (2003). A ran signalling pathway mediated by the mitotic kinase aurora A in spindle assembly. *Nature Cell Biology, 5*(3), 242-248.

Uteng, M., Hentrich, C., Miura, K., Bieling, P., & Surrey, T. (2008). Poleward transport of Eg5 by dynein–dynactin in *Xenopus laevis* egg extract spindles. *The Journal of Cell Biology, 182*(4), 715-726.

van der Horst, A., & Lens, S. M. (2014). Cell division: Control of the chromosomal passenger complex in time and space. *Chromosoma, 123*(1-2), 25-42.

van der Voet, M., Lorson, M., Srinivasan, D. G., Bennett, K. L., & van den Heuvel, s. (2009). *C. elegans* mitotic cyclins have distinct as well as overlapping functions in chromosome segregation. *Cell Cycle*, 8(24), 4091-4102.

van Heesbeen, R. H. P., Tanenbaum, M., & Medema, R. (2014). Balanced activity of three mitotic motors is required for bipolar spindle assembly and chromosome segregation. *Cell Reports, 8*(4), 948-956.

Varma, D., & Salmon, E. D. (2012). The KMN protein network – chief conductors of the kinetochore orchestra. *Journal of Cell Science, 125(*24), 5927-5936.

Voronkov, M., Braithwaite, S. P., & Stock, J. B. (2011). Phosphoprotein phosphatase 2A: A novel druggable target for Alzheimer's disease. *Future Medicinal Chemistry, 3*(7), 821-833.

Vos, J. W., Pieuchot, L., Evrard, J., Janski, N., Bergdoll, M., de Ronde, D., et al. (2008). The plant TPX2 protein regulates prospindle assembly before nuclear envelope breakdown. *The Plant Cell Online, 20*(10), 2783-2797.

Wadsworth, P. (1999). Regional regulation of microtubule dynamics in polarized, motile cells. *Cell Motility and the Cytoskeleton, 42*(1), 48-59.

Wadsworth, P., & Salmon, E. D. (1986). Analysis of the treadmilling model during metaphase of mitosis using fluorescence redistribution after photobleaching. *The Journal of Cell Biology, 102*(3), 1032-1038.

Weaver, L. N., & Walczak, C. E. (2015). Spatial gradients controlling spindle assembly. *Biochemical Society Transactions*, 43(1), 7-12.

Welburn, J. P. I., Grishchuk, E. L., Backer, C. B., Wilson-Kubalek, E. M., Yates III, J. R., & Cheeseman, I. M. (2009). The human kinetochore Ska1 complex facilitates microtubule depolymerization-coupled motility. *Developmental Cell*, 16(3), 374-385.

Wicks, S. R., Yeh, R. T., Gish, W. R., Waterston, R. H., & Plasterk, R. H. A. (2001). Rapid gene mapping in *Caenorhabditis elegans* using a high density polymorphism map. *Nature Genetics, 28*(2), 160-164.

Wijshake, T., Malureanu, L. A., Baker, D. J., Jeganathan, K. B., van, d. S., & van Deursen, J. M. (2012). Reduced life- and healthspan in mice carrying a mono-allelic *BubR1* MVA mutation. *PLoS Genet, 8*(12), e1003138.

Wilde, A., Lizarraga, S. B., Zhang, L., Wiese, C., Gliksman, N. R., Walczak, C. E., et al. (2001). Ran stimulates spindle assembly by altering microtubule dynamics and the balance of motor activities. *Nature Cell Biology, 3*(3), 221-227.

Wilde, A., & Zheng, Y. (1999). Stimulation of microtubule aster formation and spindle assembly by the small GTPase ran. *Science, 284*(5418), 1359-1362.

Wittmann, T., Wilm, M., Karsenti, E., & Vernos, I. (2000). Tpx2, a novel *Xenopus* map involved in spindle pole organization. *Journal of Cell Biology, 149*, 1405-1418.

Wlodarchak, N. J., Guo, F., Satyshur, K. A., Jiang, L., Jeffrey, P. D., Sun, T., et al. (2013). Structural mechanism of trimeric PR70 PP2A holoenzyme: Insights into Cdc6 dephosphorylation. *The FASEB Journal, 27*, 1043.2.

Wollman, R., Cytrynbaum, E. N., Jones, J. T., Meyer, T., Scholey, J. M., & Mogilner, A. (2005). Efficient chromosome capture requires a bias in the 'search-and-capture' process during mitotic-spindle assembly. *Current Biology, 15*(9), 828-832.

Wong, J., Lerrigo, R., Jang, C., & Fang, G. (2008). Aurora A regulates the activity of HURP by controlling the accessibility of its microtubule-binding domain. *Molecular Biology of the Cell, 19*(5), 2083-2091.

Wu, Y., Cheng, T., Lee, M., & Weng, N. (2002). Distinct rac activation pathways Control *Caenorhabditis elegans* cell migration and axon outgrowth. *Developmental Biology, 250*(1), 145-155.

Wu, Y., & Horvitz, H. R. (1998). *C. elegans* phagocytosis and cell-migration protein CED-5 is similar to human DOCK180. *Nature, 392*(6675), 501-504.

Wühr, M., Tan, E. S., Parker, S. K., Detrich, H. W., & Mitchison, T. J. (2010). A model for cleavage plane determination in early amphibian and fish embryos. *Current Biology, 20*(22), 2040-2045.

Wühr, M., Chen, Y., Dumont, S., Groen, A. C., Needleman, D. J., Salic, A., et al. (2008). Evidence for an upper limit to mitotic spindle length. *Current Biology, 18*(16), 1256-1261.

Xia, P., Zhou, J., Song, X., Wu, B., Liu, X., Li, D., et al. (2014). Aurora A orchestrates entosis by regulating a dynamic MCAK–TIP150 interaction. *Journal of Molecular Cell Biology, 6*(3), 240-254.

Xu, Y., Chen, Y., Zhang, P., Jeffrey, P. D., & Shi, Y. (2008). Structure of a protein phosphatase 2A holoenzyme: Insights into B55-mediated tau dephosphorylation. *Molecular Cell, 31*(6), 873-885.

Xu, Y., Xing, Y., Chen, Y., Chao, Y., Lin, Z., Fan, E., et al. (2006). Structure of the protein phosphatase 2A holoenzyme. *Cell, 127*(6), 1239-1251.

Yang, C., & Fan, S. (2008). *Drosophila* mars is required for organizing kinetochore microtubules during mitosis. *Experimental Cell Research, 314*(17), 3209-3220.

Yokoyama, H., & Gruss, O. J. (2013). New mitotic regulators released from chromatin. *Frontiers in Oncology, 3*(308).

Yokoyama, H., Koch, B., Walczak, R., Ciray-Duygu, F., González-Sánchez, J. C., Devos, D. P., et al. (2014). The nucleoporin MEL-28 promotes RanGTP-dependent γ-tubulin recruitment and microtubule nucleation in mitotic spindle formation. *Nature Communications, 5*, 3270.

Yokoyama, H., Nakos, K., Santarella-Mellwig, R., Rybina, S., Krijgsveld, J., Koffa, M., et al. (2013). CHD4 is a RanGTP-dependent MAP that stabilizes microtubules and regulates bipolar spindle formation. *Current Biology, 23*(24), 2443-2451.

Zeng, K., Bastos, R. N., Barr, F. A., & Gruneberg, U. (2010). Protein phosphatase 6 regulates mitotic spindle formation by controlling the T-loop phosphorylation state of aurora A bound to its activator TPX2. *The Journal of Cell Biology, 191*(7), 1315.

Zhang, D., Grode, K. D., Stewman, S. F., Diaz-Valencia, J., Liebling, E., Rath, U., et al. (2011). *Drosophila* katanin is a microtubule depolymerase that regulates cortical-microtubule plus-end interactions and cell migration. *Nature Cell Biology, 13*(4), 361-369.

Zhang, X., Ems-McClung, S. C., & Walczak, C. E. (2008). Aurora A phosphorylates MCAK to control ran-dependent spindle bipolarity. *Molecular Biology of the Cell, 19*(7), 2752-2765.

Zhang, X., Lan, W., Ems-McClung, S. C., Stukenberg, P. T., & Walczak, C. E. (2007). Aurora B phosphorylates multiple sites on mitotic centromere-associated kinesin to spatially and temporally regulate its function. *Molecular Biology of the Cell, 18*(9), 3264-3276.

Zhao, Z., Lim, J. P., Ng, Y., Lim, L., & Manser, E. (2005). The GIT-associated kinase PAK targets to the centrosome and regulates aurora-A. *Molecular Cell, 20*(2), 237-249.

Zolnierowicz, S., Csortos, C., Bondor, J., Verin, A., Mumby, M. C., & DePaoli-Roach, A. (1994). Diversity in the regulatory B-subunits of protein phosphatase 2A: Identification of a novel isoform highly expressed in brain. *Biochemistry, 33*(39), 11858-11867.

Zorba, A., Buosi, V., Kutter, S., Kern, N., Pontiggia, F., Cho, Y., et al. (2014). Molecular mechanism of aurora A kinase autophosphorylation and its allosteric activation by TPX2. *Elife, 3*, e02667.

Zwaenepoel, K., Louis, J., Goris, J., & Janssens, V. (2008). Diversity in genomic organisation, developmental regulation and distribution of the murine PR72/B. *BMC Genomics, 9*(1), 393.

# Appendix A – Primers and optimized PCR conditions

## 1 Amplifying and sequencing the coding region of candidate suppressors

50 µl PCR reactions were performed with 5 µl gDNA as the template. Annealing temperatures were optimized using gradient PCR and extension times were estimated based on predicted product size. PCR products were isolated with Qiagen Gel Extraction or PCR Clean-Up kits and sequenced with Big Dye 2.0.

- ***air-1*, K07C11.2**

2028 bp PCR product includes all introns and exons, the 5'UTR, and some of the 3'UTR.

| | | |
|---|---|---|
| 94°C | x 2 minutes | |
| 94°C | x 15 seconds | 30 cycles |
| 55°C | x 30 seconds | |
| 72°C | x 2 minutes | |
| 4°C | x ∞ | |

*air-1* PCR primer pair 1:
5′CGTGTTGTTTAGCAATGCCGCTCAAC
5′GAAGTTAGTAGCCGTATGATATACGGTTC

*air-1* sequencing primers:
5′AGCTGTCGCACAAATCTGAG
5′CAGTCATCAGTTGAAGAGAGAGATCG
5′ATCTGGTTCCTTTTCTCCTCGGGAC
5′AGCCGAAAGAAGTCACTAGCTG
5′AGCCGAAAGAAGTCACTAGCTG

---

- ***air-2*, B0207.4**

1849 bp PCR product includes all introns and exons, the 5'UTR, and the 3'UTR.

| | | |
|---|---|---|
| 94°C | x 2 minutes | |
| 94°C | x 15 seconds | 30 cycles |
| 62°C | x 30 seconds | |
| 72°C | x 1.5 minutes | |
| 4°C | x ∞ | |

*air-2* PCR primer pair 1:
5′GACGACATATTGCGGACCATTG
5′CGAGTCTACGCGACATCTGAAA

*air-2* sequencing primers:
5′AATCGCAACTCATCTCAGGAGG
5′CGCAGTTGACTTATGGGCAATC
5′GCTGTTGGCTCTGAGAATCTCT

---

- ***cdc-25.1*, K06A5.7**

2251 bp PCR product includes all introns and exons, the 5'UTR, and the 3'UTR.

| | | |
|---|---|---|
| 94°C | x 2 minutes | |
| 94°C | x 15 seconds | 30 cycles |
| 63°C | x 30 seconds | |
| 72°C | x 2.5 minutes | |
| 4°C | x ∞ | |

*cdc-25.1* PCR primer pair 1:
5′TAGTTGAGGGCTGTGCATC
5′GAAACGGAGACCTGCAAAG

*cdc-25.1* sequencing primers:
5′GAGAGTTTCTGACGTTGCTC
5′TCGGTGATGAAGACGATGAG
5′GCTGAATGTCGTCAGATATGTG

- **paa-1, F48E8.5**

1933 bp PCR product includes all introns and exons, and the 5'UTR.

| | | |
|---|---|---|
| 94°C | x 2 minutes | |
| 94°C | x 15 seconds | 30 cycles |
| 62°C | x 30 seconds | |
| 72°C | x 2 minutes | |
| 4°C | x ∞ | |

*paa-1* PCR primer pair:
5′CTCCTTTGAATAGCCGCGAG
5′TTATTCGCGTGCTCGGGAAC

*paa-1* sequencing primers:
5′GCAACGAAGATGTCACGTTG
5′GGATGGAAAATGGAGAGTTCG
5′GCTCATCAACATGAAGATCAGTG
5′CGTTATATGGTTGCCGAGAAGC

---

- ***rsa-1*, C25A1.9b**

The *rsa-1* introns and exons are amplified with two overlapping PCR products. The PCR1 product is 1133 bp and the PCR2 product is 1087 bp.

| | | |
|---|---|---|
| 94°C | x 2 minutes | |
| 94°C | x 15 seconds | 30 cycles |
| 61°C | x 30 seconds | |
| 72°C | x 2 minutes | |
| 4°C | x ∞ | |

*rsa-1* PCR primer pair 1:
5′ACTATGCCAACCGACGAACCTT
5′TGAAATTTCGAAGATTCGCTTGGTG

*rsa-1* PCR primer pair 2:
5′CAGAGGAGCTTGTACGAACAGTCA
5′AATTAGCGGGACTGCTATTGCTCG

Sequencing primers for *rsa-1* PCR1:
5′ GGGAGAAAGTAGATATGTGACG
5′ CTTTGATTGATTGTGGTGAAG

Sequencing primers for *rsa-1* PCR2:
5′ TACAGCTTACGCAGTTGG
5′ AATTTCCAGACCACTGCC
5′ TTGAAGCTGAAATGATGACT

---

- **tpxl-1, Y39G10AR.12**

The *tpxl-1* exons and introns 1-3* are all amplified with two non-overlapping PCR products. The PCR1 product is 1806 bp and the PCR2 product is 1586 bp.

| | | |
|---|---|---|
| 94°C | x 2 minutes | |
| 94°C | x 15 seconds | 30 cycles |
| 59°C | x 30 seconds | |
| 72°C | x 2 minutes | |
| 4°C | x ∞ | |

*tpxl-1* PCR primer pair 1:
5′CAAGGATGAGCAAAAGTCAAACC
5′TCGGAAGAGAAGGCTGAATGGG

*tpxl-1* PCR primer pair 2:
5′AGCTGCTGCGACATTGATAAG
5′GCTCAGAAGAAACCTTTCGCA

*tpxl-1* sequencing primers PCR1:
5′GACGCTGCGAAAGACGTTCCTCTG
5′CAGAGGAACGTCTTTCGCAGCGTC
5′CAACAGCCAATCGCTCATCG

*tpxl-1* sequencing primers PCR2:
5′ATTTCCGGTTCGCCGATTTC
5′GGTGGAGGAGACACAACAATA

* Intron 4 is 4906 bp long and is not sequenced in these reactions.

## 2 Genotyping *klp-7(tm2143)* by PCR

The *tm2143* null allele in *klp-7* is an 877 bp deletion spanning from intron 2 to exon 4 of K11D9.1a. To detect the deletion by PCR, a reaction was performed with primers that flank the deletion. This PCR product was then run on an agarose gel to determine the size of the PCR product. Wild-type genomic DNA as a template this reaction generates a 1978 bp band and with *tm2143* mutant genomic DNA as the template the reaction generates a 1101 bp band.

| | | | |
|---|---|---|---|
| Forward Primer: | 95°C | x 2 minutes | |
| 5′ - CTTGTCGTCGGGATGCATGT | 95°C | x 30 seconds | 26 cycles |
| Reverse Primer: | 56°C | x 30 seconds | |
| 5′ - TCACTGTCCTGGACTTCTCA | 72°C | x 2 minutes | |
| | 4°C | x ∞ | |

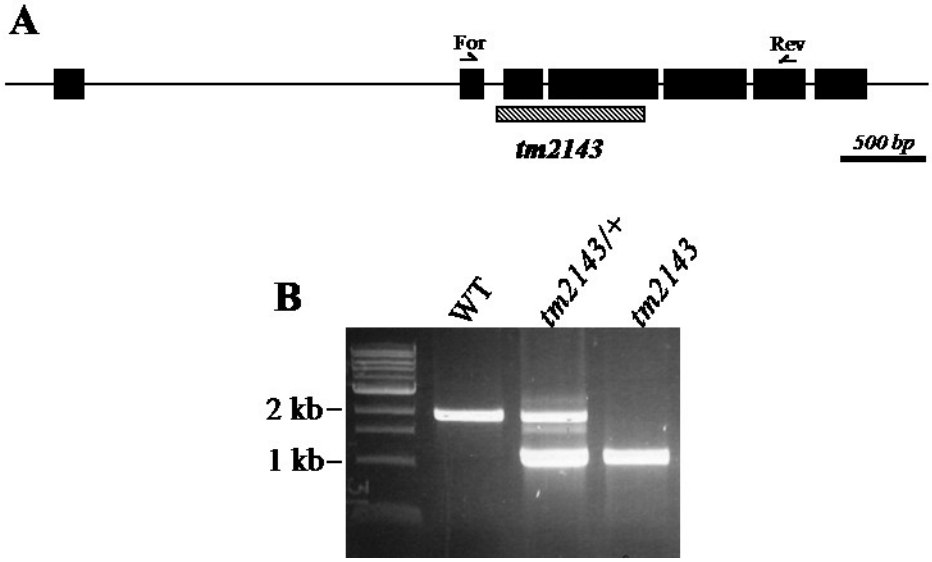


***klp-7(tm2143)* genotyping PCR.** (A) Gene structure for *klp-7*, K11D9.1a. Black boxes represent exons, lined box shows the region of the gene missing in the klp-7(*tm2143)* mutant, and arrows show approximate binding of the PCR primers. (B) Representative genotyping gel showing wild-type, heterozygous, and homozygous mutant PCR products.

## 3 Genotyping *rsa-1(or598)* by PCR and restriction digest

The *or598* allele in *rsa-1* is a base pair substitution that abolishes a restriction enzyme cut site. To detect the base pair substitution a PCR is done which results in a 627 bp PCR product with the substitution near the center of the product. The PCR product is then digested with BspPI in Tango buffer with BSA added and incubated for 16 hours at 55°C. The PCR product and digested product are then run on an agarose gel. The wild-type has a 321 bp and 306 bp band which are usually not distinct on the gel while the *or598* allele is not cut.

| | | | |
|---|---|---|---|
| Forward Primer: | 95°C | x 2 minutes | |
| 5′ - TTCCTTGACTCCCAACGAAAGGGA | 95°C | x 30 seconds | 25 cycles |
| Reverse Primer: | 57°C | x 30 seconds | |
| 5′ - AATTAGCGGGACTGCTATTGCTCG | 72°C | x 1 minutes | |
| | 4°C | x ∞ | |

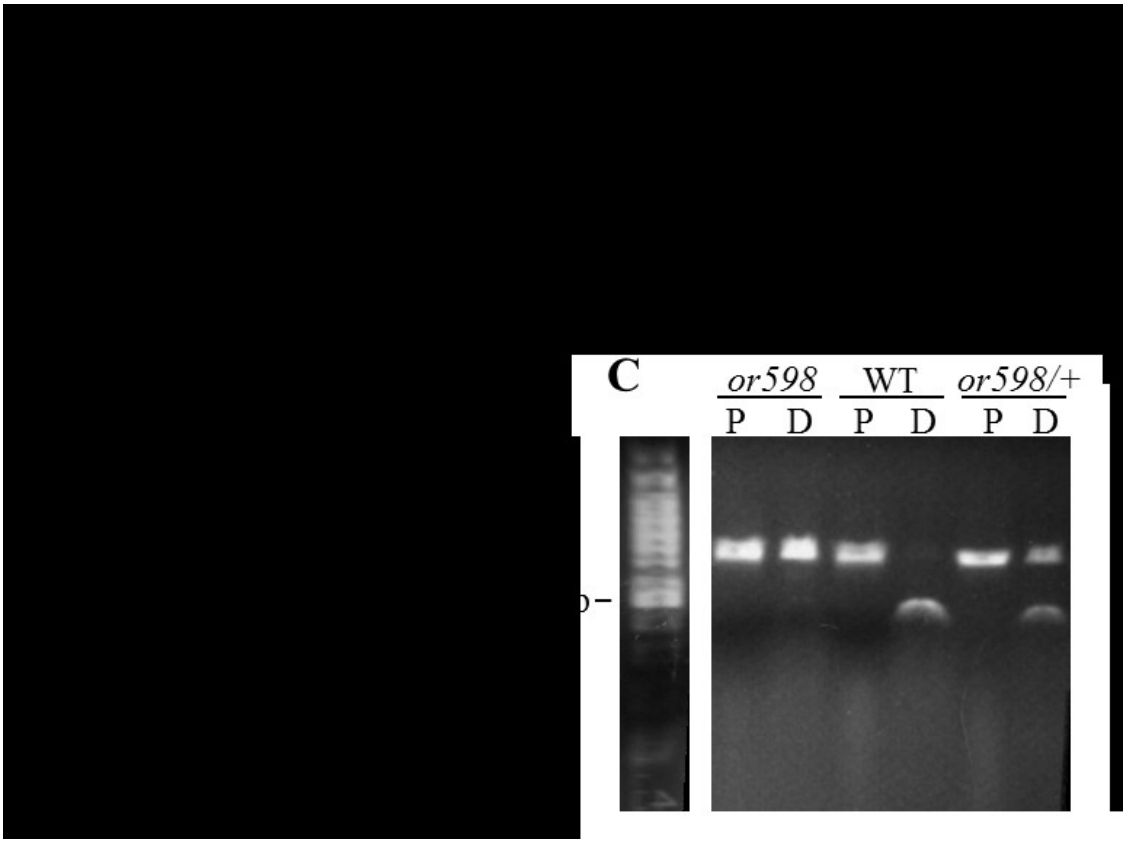


***or598* genotyping PCR and restriction digest.** (A) Gene structure for *rsa-1*, C25A1.9b. Black boxes represent exons, asterisk marks the approximate location of the *or598* base pair substitution, and arrows show approximate binding of the PCR primers. (B) The wild-type *rsa-1* sequence contains DNA seuqnece recognized by the restriction enzyme BspPI while the *or598* sequence does not. (C) P is the PCR product and D is the PCR product after digestion with BspPI.

## 4 Cloning gDNA into L4440 RNAi vector

Wild-type gDNA was cloned into L4440 using traditional cloning techniques and the following primers:

| |
|---|
| ***tpxl-1:*** 414 bp at the 5' end of the gene |
| 5′TTT**GCGGCCGC**CAAACCATTCAGGAATTCGAT |
| 5′TTT**AAGCTT**TTCTCCACCGCTTCCTG |
| ***ebp-1/2/3****: ebp-2* was cloned and then *ebp-1* (which is an identical sequence to *ebp-3*) |
| Step 1: *ebp-2* exon 4 |
| 5′TTT**GCGGCCGC**AAACACAAGGCCGCCAG |
| 5′TTT**AAGCTT**GAAAGTCTCCGTATCGTCCA |
| Step 2: *ebp-1/3* exon 4, |
| 5′TTT**AAGCTT**ACCAGTGACCACAATGAGAAC |
| 5′TTT**CTCGAGTG**ACGTGTAACTTCTTCCAG |
| ***ran-2*:** |
| 5′TTT**GTCGAC**CGTGAAACCGTGATAGATCG |
| 5′TTT**GTCGAC**TCCAAACGATTTCTTCCAGC |
| ***klp-18*:** |
| 5′TTT**GTCGAC**ATCAAGTGCTACGGCAG |
| 5′TTT**GTCGAC**GCAAGAAGACGGATGCAAC |
| Restriction enzyme cut sites are bold and underlined. |

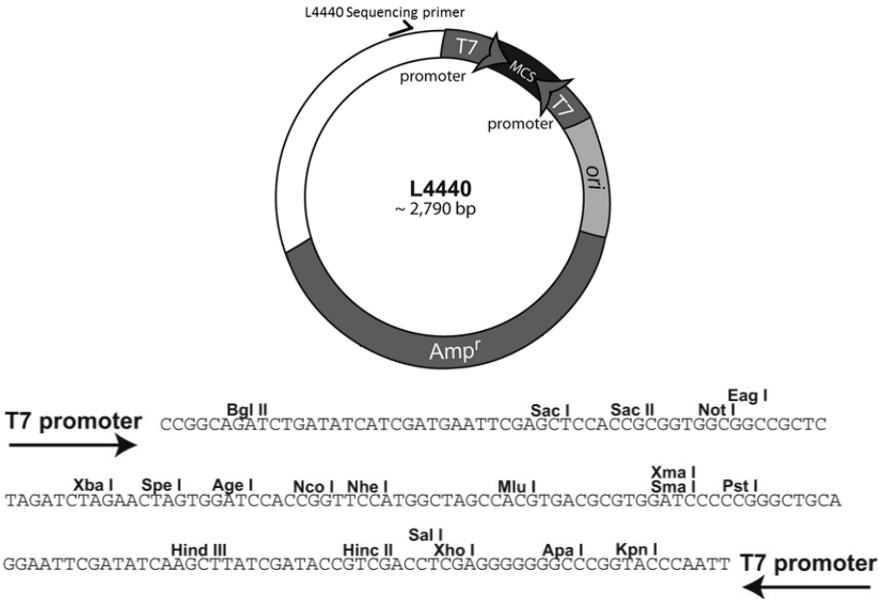


**L4440 RNAi plasmid.** Plasmid map of L4440 and sequence of the multiple cloning site. Image adapted from www.addgene.org/1654/.

## 5 Cloning cDNA into yeast two hybrid vectors

Primers for yeast two hybrid cloning:

| | |
|---|---|
| *paa-1* into pAct2.2 | 5′TTT**CCCGGG**CTTGTCGGTTGTCGAAGAAGCC<br>5′TTT**CCCGGG**AGGTACAAGCCGAGTGAGTTCTTGG |
| *let-92* into pLexA | 5′TTT**CCCGGG**CGCAGGCTTGGCTGCTGCC<br>5′TTT**CTGCAG**GGTACAGGAAGTAGTCAGGC |
| *rsa-1* into pLexA and pACT2.2 | 5′TTT**GGATCC**GCTTGCCAACCGACGAACCTTC<br>5′TTT**CTGCAG**GGTATTGCTCGCGTCGTTCG |

Restriction enzyme cut sites are bold and underlined.

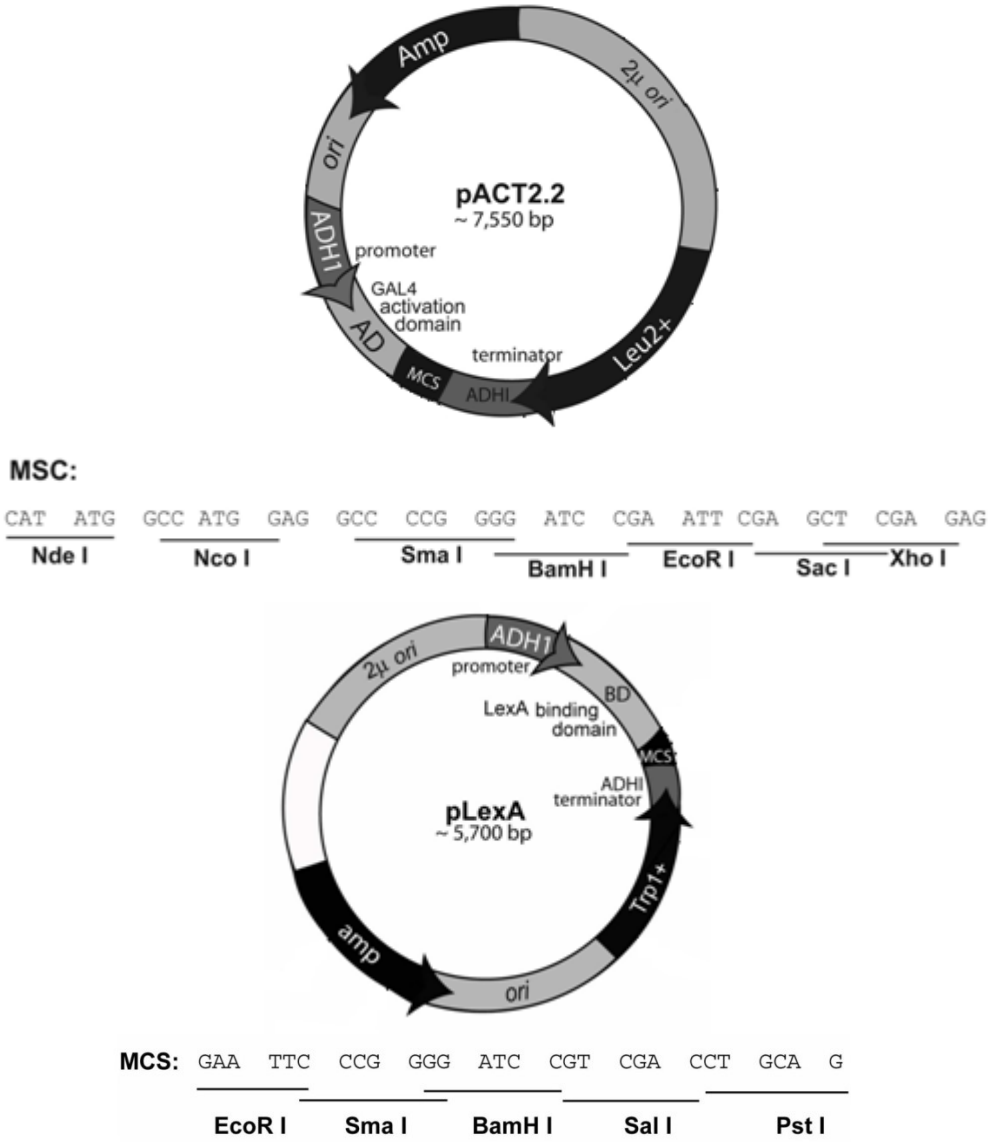


**pLexA and pAct2.2.** Plasmid maps and sequence of the multiple cloning site of yeast two hybrid vectors. Images adapted from www.addgene.org/11342/ and www.addgene.org/11343/.

## 6 PCR mutagenesis primers

The mutations introduced in the PCR are bold and underlined.

*rsa-1(or598)*

5′/Phos/TACCATTTCGAAATTCTGG**G**TCTAAAGGATGATGGACTGTTG

5′/Phos/CAACAGTCCATCATCCTTTAGA**C**CCAGAATTTCGAAATGGTA

*rsa-1(abc6)*

5′/Phos/CAAATACCATTTCGAAATTCTG**A**GTCTAAAGGATGATGGACTG

5′/Phos/CAGTCCATCATCCTTTAGAC**T**CAGAATTTCGAAATGGTATTTG

*paa-1(abc8)*

5′/Phos/GCCACAGTCGAGGAGACCGTG**A**TCCGTGACAAAGCCGTTGAG

5′/Phos/CTCAACGGCTTTGTCACGGA**T**CACGGTCTCCTCGACTGTGGC

PCR mutagenesis reactions were hot-started with 17 µl PT1.1x Master Mix (500 mM KCl, 15 mM MgCl2, 100 mM Tris-HCl pH8, 0.1% BSA), 1 µl 10mM NAD, 0.5 µl each phosphorylated primer, 0.5 µl DMSO, 0.3 µl Taq ligase, 10 ng of template. Then 1 µl of Pfu was added and the PCR conditions were as follows: 95°C x 2 min, (95°C x 1 min, 55°C x 1 min, 65°C x 10 min) x30 cycles, and 65°C x 7 min.

## 7 Snip-SNP mapping primers, PCRs, and digests

SNP PCR reactions were 15 µl $ddH_20$, 2.5 µl 10x Taq buffer, 1.25 µl of each 10 mM primer, 1 µl of 10mM dNTPs, 1µl Taq, and 3 µl of gDNA as template. All snip-SNPs used the same PCR program as follows: 95 °C for 2 minutes and 30 cycles of 95 °C for 30 seconds, 57 °C for 30 seconds, and 72 °C for 1 minute. All restriction enzymes were used according to manufacturer's instructions. Agarose gel electrophoresis with ethidium bromide was used to visualize the RFLPs. Primers and restriction enzymes are listed below.

**Snip-SNP primers and restriction enzymes.**

| SNP Name | Location | Sequence (5' → 3') | Enzyme |
|---|---|---|---|
| **pkP3055** | III: -14.86 | ATGTGGTATGGATCAGTGGTGG<br>GTTGAGCTCGTGTAGACCTTTC | Bsh1236I |
| **pkP3094** | III: -8.89 | TGGGCTTAACAATGATGGG<br>CGCTGAAATTGAGGAGCAG | AvaII |
| **dbP8** | III: -7.39 | TAGTCGAAAAGCTGTAAAAC<br>GTTCTGTAGGAGGGTCTCAATG | SspI |
| **pkP3046** | III: -5.39 | TACGCACATGCCTACAAAGG<br>CTTCATTGCGCTCACTTCTG | MboI |
| **pkP3096** | III: -4.12 | AATTCCGTGTAGCGAATCG<br>CCAACTGTCGACGATAGAGATG | EcoRI |
| **snp_B02841** | III: -3.18 | CAAAGATCTTAGTTAGGTGCG<br>ACCTGGTGTGCCATTGAG | RsaI |
| **pkP3047** | III: -1.71 | GAGTACGCGGGTCATTTTTG<br>CAGACATTTAGGAGTAGGCAGG | MseI |
| **pkP3099** | III: -1.47 | AAACAAGGATCAGTGGAATGTG<br>GACCGAATCGAATCGGAAG | HpyCH4V |
| **snp_C05D111** | III: -1.29 | ACACCTTCTATCTCGGCAGTC<br>TAGTTATGTCGGACGGACGTC | BslI |
| **pkP3101** | III: -0.91 | ATAAACAATTTCAGTGCCGC<br>CCAAGTGCAAACTATGGTGC | HinfI |
| **pkP3102** | III: -0.85 | TGGATTTGAGAGGTGTCCATAG<br>CATTAGGAAGTGATGCAAGTGG | AvaII |
| **pkP3071** | III: 4.81 | GGGGGATTCTGGATTTATGG<br>CCTTGATATCCTTCTGGTGG | Bsp119I |
| **pkP3074** | III: 11.76 | AAGAGAGGAAAAAGGCGC<br>CAGACACTTCTCCCAAATCC | BfaI |
| **pkP3075** | III: 16.34 | AGCCTAAGCCCAAGCTTTAG<br>AAACAGCATTGTCGACGAGC | HindIII |

# Appendix B – Whole genome sequencing of *abc17*, *abc19*, and *abc25*

## 8 Whole genome sequencing of *rsa-1(or598)* suppressors

The genetic screen for *rsa-1(or598)* suppressors isolated twenty-five independent suppressor alleles. Twenty-two of these mutations were identified in the *rsa-1* and *paa-1* genes but three of these suppressors, *abc17, abc19,* and *abc25,* were not. Whole genome sequencing of the outcrossed suppressors was performed and the results are presented here. Preliminary results to confirm the identity of the suppressors mutations are also presented, however more experiments are required to establish which lesions are responsible for the suppression.

## 9 Summary of WGS data

In the three strains that were sequenced, there were between 800 and 900 unique variations in the genome. Of these, approximately 90% were single nucleotide polymorphisms (SNPs) and 10% were insertions/deletions (InDels). This was consistent with previous reports of EMS mutation profiles in *C. elegans* (Flibotte et al., 2010).

| Allele | Total | SNPs | InDels |
|---|---|---|---|
| *abc17* | 896 | 815 | 81 |
| *abc19* | 873 | 780 | 93 |
| *abc25* | 796 | 712 | 84 |

**Total number of variations in the genomes of the suppressors that were sequenced.**

Most of these mutations were found outside of genes in non-coding, intergenic regions. For each genome sequenced, less than 100 of the variations in the genome were predicted to affect a protein. For subsequent analysis, only mutations that were predicted to affect a protein sequence were considered.

| Allele | Nonsense | Missense | Splice variant | In frame InDel | Silent | 5' or 3' UTR | Intronic | Non-coding region |
|---|---|---|---|---|---|---|---|---|
| *abc17* | 4 | 84 | 9 | 1 | 40 | 17 | 298 | 443 |
| *abc19* | 1 | 80 | 6 | 2 | 27 | 10 | 285 | 462 |
| *abc25* | 6 | 66 | 9 | 0 | 28 | 15 | 250 | 422 |

**Breakdown of the mutations in the suppressor strains that were sequenced.**
Nonsense, missense, splice variant, and in frame InDels are predicted to affect protein amino acid sequences.

### 9.1 *abc17*

In mapping experiments, the *abc17* allele appeared to be linked to all chromosomes except LG II. This suggests either that the mapping data is unreliable or that the suppressor phenotype is the result of variations on multiple chromosomes. Preliminary inspection of the list of variations in this strain revealed a nonsense mutation in *ska-1*.

| LG I | LG II | LG V | LG X |
|---|---|---|---|
| C01H6.9 | C16C4.5/*math-1* | C03A7.8/*abu-7* | C02C6.1/*dyn-1* |
| C34G6.6/*noah-1* | C23H3.3 | C05C8.4/*gei-6* | C18B12.4 |
| C35E7.5 | C32B5.5/*fbxc-14* | C14C6.6 | C30G4.2 |
| E02D9.1 | F10E7.2 | C17E7.2/*srh-190* | C46E1.3 |
| E03H4.5 | F56D12.5/*vig-1* | C18B10.5/*srbc-8* | F01G12.5/*let-2* |
| F11C3.3/*unc-54* | R07C3.12/*clec-44* | C27H6.4/*rmd-2* | F11C1.2/*mff-1* |
| F22G12.5 | W01G7.1/*daf-5* | F16H6.9 | F22E10.3/*pgp-14* |
| F25H2.2/*snx-27* | W07E6.2 | F17C11.10 | F31F6.6/*nac-1* |
| F33D11.2 | Y39F10C.3 | F31D4.7/*twk-35* | F54E4.3 |
| F46A9.6/*mec-8* | Y53F4B.31/*gst-28* | F31F4.7/*ugt-42* | K08H2.10 |
| F56H1.4/*rpt-5* | | F36D3.9/*cpr-2* | R03G8.3 |
| K04G2.10 | **LG III** | F40F9.5 | T07H6.4 |
| T04D3.4/*gcy-35* | C05D10.3/*wht-1* | F44C4.3/*cpr-4* | T27A8.1/*cpd-2* |
| T08B2.7 | F11F1.8 | F44C8.6/*nhr-56* | VF11C1L.1/*ppk-3* |
| T23D8.1/*mom-5* | F43C1.1 | F57F4.1 | ZK662.4/*lin-15B* |
| W09C5.8 | Y49E10.23/*cccp-1* | H24K24.2 | |
| Y105E8A.2 | Y66D12A.30 | K04F1.15/*alh-2* | |
| **Y106G6H.15/*ska-1*** | Y75B8A.26/*mrp-8* | M02H5.6/*nhr-98* | |
| Y106G6H.7/*sec-8* | ZK112.7/*cdh-3* | T15B7.8 | |
| Y6B3B.4 | ZK1128.1 | T16G1.4 | |
| Y87G2A.17 | | T18H9.1 | |
| Y87G2A.7 | **LG IV** | W06H8.8/*ttn-1* | |
| ZC247.1 | C18H7.6 | Y38H6C.10/*fbxa-149* | |
| ZK337.1/*tep-1* | Y116A8C.26 | Y59A8B.21 | |
| | Y37E11AM.1/*smgl-2* | ZC178.1 | |
| | Y41D4A.8/*frpr-19* | ZK384.1/*scl-19* | |
| | Y69E1A.6/*sri-19* | ZK863.2/*col-37* | |

**Mutations that affect protein coding genes in an *abc17* carrying strain**
The whole genome sequencing of a strain carrying *abc17* revealed 98 mutations that would result in amino acid changes in proteins encoded by 89 genes.

*ska-1* (*spindle and kinetochore associated protein-1)* is the *C. elegans* homolog of human Ska1. Human Ska1 is a kinetochore protein that is also observed on spindle microtubules (Hanisch et al., 2006). Loss of Ska1 results in activation of the spindle assembly checkpoint even though the spindle appears to be assembled and chromosomes correctly bi-oriented (Hanisch et al., 2006). In *C. elegans*, depletion of *ska-1* does not result in embryonic lethality (Schmidt et al., 2012), although a thorough characterization of the *ska*-1 loss-of-function phenotype has not yet been published.

Human Ska1 forms a complex with Ska2 and Ska3 (Daum et al., 2009; Gaitanos et al., 2009; Raaijmakers et al., 2009; Theis et al., 2009; Welburn et al., 2009). *C. elegans* lacks a Ska2 protein but a Ska3 ortholog is present (Schmidt et al., 2012). The Ska complex can interact with depolymerizing microtubules (Schmidt et la., 2012; Welburn et al., 2009) and is proposed to have a function that is similar to the Dam1 complex in budding yeast. The Ska complex is required to maintain kinetochore-microtubule interactions (Daum et al., 2009; Gaitos et al., 2009; Raaijmakers et al., 2009), likely by promoting the interaction of the kinetochore with dynamic depolymerizing microtubules.

The C-terminus of human Ska1 has a microtubule binding domain (Jeyaprakesh et al., 2012; Schmidt et al., 2012). The microtubule binding domain in the *C. elegans* SKA-1 protein is also at the C-terminus, from amino acids 118 to 243 (Schmidt et al., 2012). The nonsense mutation present in the *abc17* strain introduces a stop codon at amino acid 89 of the SKA-1 protein. This mutation is expected to result in either a truncated SKA-1 protein or nonsense-mediated decay of the transcript.

### 9.2 ***abc25***

In mapping experiments, the *abc25* allele appeared to be linked to LG II and LG X. This could suggest that the mapping data is unreliable or that the suppressor phenotype is the result of variations on multiple chromosomes. There were no obvious candidate suppressors on either of these chromosomes. Like *abc17,* this strain also contained a non-sense mutation in *ska-1*. This mutation introduces a stop codon amino acid 125 of the SKA-1 protein. Since the *abc17* strain also contained a non-sense mutation in *ska-1*, this result further supports the possibility that *ska-1* is a bona fide suppressor of *rsa-1(or598).*

| LG I | LG V | LG X |
|---|---|---|
| F13G3.8/*eat-5* | C06B3.13/*srxa-12* | CE7X_3.2 |
| T03F1.6 | C03G6.14/*cyp-35A1* | C30E1.5/*fbxb-114* |
| T09E11.8 | C36C5.7/srab-10 | F35A5.1 |
| VH15N14R.1 | C10F3.7 | F02D10.7/*set-8* |
| VH15N14R.1 | C14C6.8 | F52H2.15 |
| Y105E8A.26/*zoo-1* | F13H6.5 | H42K12.3 |
| Y105E8A.9/*apg-1* | C38C3.1/*sru-28* | F56B6.4/*gyg-1* |
| **Y106G6H.15/*ska-1*** | B0348.4/*egl-8* | C27C12.5/*acd-3* |
| Y47H9C.14 | C50H11.3/*srt-71* | H02F09.3 |
| Y53C10A.10 | C24B9.4/*srt-28* | F54B11.7 |
| | F14F8.10/*srw-41* | R04D3.9/*srd-43* |
| **LG II** | F31F4.7/*ugt-42* | R12H7.4 |
| T05A6.5 | F35E8.1 | T18D3.3/*cdf-2* |
| T06D8.1 | F36D4.3/*hum-2* | VF11C1L.1/*ppk-3* |
| | K09C6.8 | |
| **LG III** | K11C4.5/*unc-68* | **LG IV** |
| C38H2.1/*tbc-8* | M04C3.2 | C09G12.10/*srz-83* |
| F11F1.1 | R08F11.7 | F42A6.8/*fbxa-130* |
| K08E3.1/*tyr-2* | T08G5.2 | F45E4.6 |
| M04D8.6/*xbx-3* | T09D3.2/*srg-28* | F53H1.1 |
| Y66D12A.7 | T27B7.6/*nhr-228* | Y37E11B.10 |
| | VC5.2 | Y45F10B.14/*srd-10* |
| | W02H5.16 | Y54G2A.38 |
| | W06H8.8/*ttn-1* | Y55F3BR.1 |
| | Y37H2A.7 | Y69A2AR.14 |
| | Y45G5AM.2 | Y69A2AR.19 |
| | Y58A7A.3 | Y69A2AR.24 |
| | ZC142.1/*srt-13* | |
| | ZK1055.6 | |

**Mutations that affect protein coding genes in an *abc25* carrying strain**
The whole genome sequencing of a strain carrying *abc25* revealed 81 mutations that would result in amino acid changes in proteins encoded by 76 genes.

### 9.3 *abc19*

In mapping experiments, the *abc19* allele appeared to be linked to both LG IV and LG V. This could suggest that the mapping data is unreliable or that the suppressor phenotype is the result of variations on both of these chromosomes. Preliminary analysis of the sequencing data revealed a missense mutation in *pptr-1*.

*pptr-1* is member of the B56/B' PP2A regulatory subunit family. In adult worms, *pptr-1* has a role in regulating metabolism and stress response (Padmanabhan et al., 2009). In the early embryo, *pptr-1* is required for the posterior partitioning of P-granules (Gallo et al., 2010). Loss of *pptr-1* resulted in loss of asymmetric partitioning of the P-granules, although this did not affect the fate of germ-line development (Gallo et al., 2010). *pptr-1(RNAi)* embryos do not exhibit embryonic lethality.

| LGI | LG III | LG V |
|---|---|---|
| F33E2.8 | C04D8.1/*pac-1* | B0024.14/*crm-1* |
| K08C9.2 | C30A5.10 | B0331.2 |
| T12F5.4/*lin-59* | F48E8.3 | C03E10.5/*clec-223* |
| W04G5.9 | F54E7.8 | C05C8.5 |
| Y48G1BM.7 | H04J21.3/*gip-1* | C06C6.7 |
| Y54E10BR.4 | K03H1.1/*gln-2* | C10G8.5/*ncx-2* |
| Y65B4A.8 | M01A8.2 | C50B6.3 |
| | R107.9 | F07B10.7 |
| **LGII** | T23G5.2 | F10D2.5/*ugt-40* |
| C08F1.8 | Y39A1B.3/*dpy-28* | F13H6.1 |
| C09E8.1 | ZK328.5/*npp-10* | F15E11.2 |
| C34C6.2 | | F20E11.5 |
| C54A12.1/*ptr-6* | **LG IV** | F32D1.3 |
| C56C10.7 | W01B6.6 | F36D3.5 |
| F19B10.4 | Y42H9B.1 | F36F12.3 |
| F23F1.6 | Y9C9A.7/*str-153* | F37B4.4/*srh-272* |
| F28C6.7/*rpl-26* | | F58G11.5/*tag-65* |
| F58F12.1 | **LG X** | K09H11.2 |
| K01C8.6/*mrpl-10* | B0272.1/*tbb-4* | K10C8.1 |
| M151.8/*fbxb-33* | C18A11.3 | K12F2.1/*myo-3* |
| R10H1.5/*nas-23* | C35C5.1/*sdc-2* | R31.1/*sma-1* |
| T12C9.3/*twk-2* | F08F1.7/*tag-123* | T21C9.5/*lpd-9* |
| T19D12.1 | F15A2.6/*sad-1* | T27B7.6/*nhr-228* |
| T27D12.1 | F32A6.5/*sto-2* | W06H8.8/*ttn-1* |
| W06A11.1 | H28G03.3 | **W08G11.4/*pptr-1*** |
| W10G11.19 | R09A8.1 | Y39B6A.29 |
| W10G11.5/*clec-127* | W03G11.2 | Y45G5AM.1/*nhr-114* |
| Y38E10A.7/*lips-15* | | ZC455.3/*ugt-3* |
| Y53C12B.3/*nos-3* | | |

**Mutations that affect protein coding genes in an *abc19* carrying strain**
The whole genome sequencing of a strain carrying *abc19* revealed 89 mutations that would result in amino acid changes in proteins encoded by 78 genes.

During characterization of the *rsa-1(or598)* suppressors, I noted that in *abc19* embryos the P-granules were either not visible or weakly fluorescent upon immunostaining with anti-PAA-1 antibodies. Since the P-granule localization of PAA-1 was disrupted in this suppressor strain and *pptr-1* is implicated in P-granule related functions, this was chosen for further testing as an *rsa-1(or598)* suppressor.

### *10* Investigating *ska-1* as a suppressor of *rsa-1(or598)*

Since two non-sense mutations in *ska-1* were identified in the whole genome sequencing data, I investigated if *ska-1(RNAi)* was able to restore embryonic viability to *rsa-1(or598)* embryos. *ska-1(RNAi)* embryos are viable, so it was difficult to determine if the RNAi treatment was successful. Western blotting with an anti-SKA-1 antibody or

loss of SKA-1::GFP signal could be used to verify that the RNAi is successful, however these reagents are not currently available in the Srayko laboratory.

Despite being unable to confirm the efficacy of *ska-1(RNAi)*, I proceeded with the experiment, looking for any evidence of suppression of *rsa-1(or598)* by *ska-1(RNAi)*. As expected, *ska-1(RNAi)* did not affect the embryonic viability of embryos produced by wild-type hermaphrodites. At 26 °C *rsa-1(or598)* homozygotes exhibit 0% embryonic viability, however *rsa-1(or598) ska-1(RNAi)* resulted in a significant increase in viability (2.2 %, s.d. 1.9%, n=226). This indicated that depletion of *ska-1* in *C. elegans* was able to restore embryonic viability to *rsa-1(or598)* embryos. Since I am unable to assess the efficiency of the *ska-1* RNAi treatment, it is unclear if this is due to a partial or complete depletion of SKA-1. While this is a modest level of suppression, it is comparable to the embryonic viability of the *abc17* and *abc25* strains which were 8.3% and 6.6% respectively. These data strongly suggest that the non-sense mutations in *ska-1* are the variations in the *abc17* and *abc25* strains that confer suppression.

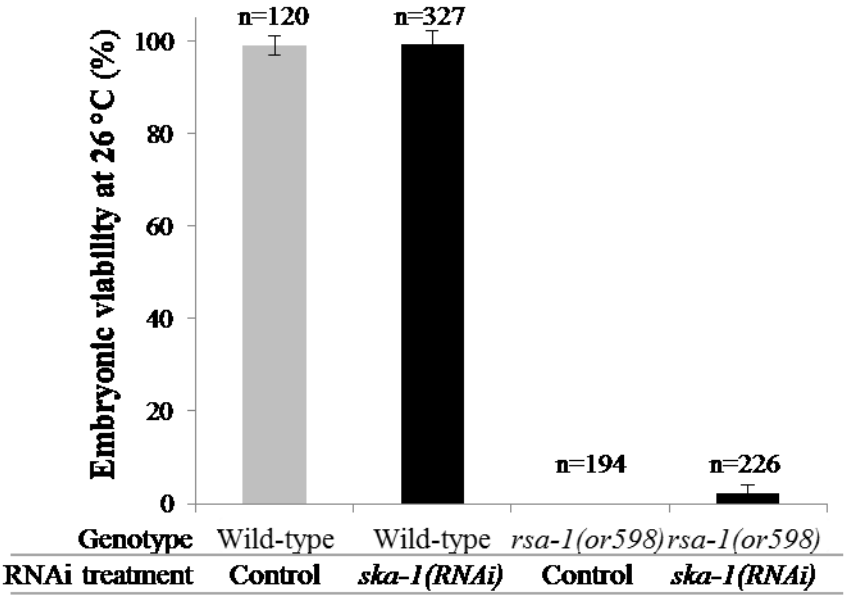


**Embryonic viability at 26 °C after *ska-1(RNAi)***

It remains unknown if the *ska-1(abc17)* and *ska-1(abc25)* mutations generate a truncated protein or not. Since *ska-1(RNAi)* phenocopies these mutations, it suggests that even if a truncated protein is generated it is not functional. Both of these mutations are

predicted to generate a truncated protein that lacks an intact microtubule binding domain. In human cells, loss of the microtubule binding domain confines the localization of Ska1 to the kinetochore (Schmidt et al., 2012). An anti-SKA-1 antibody could be generated to determine the localization of SKA-1 in these suppressor strains.

There are several possible mechanisms for how mutations in *ska-1* could suppress *rsa-1(or598)*. Since the Ska1 complex is implicated in maintaining kinetochore-microtubule interactions in human cells (Daum et al., 2009; Gaitos et al., 2009; Raaijmakers et al., 2009), it is possible that this function is conserved in *C. elegans*. If the kinetochore-microtubule interactions are weakened in *rsa-1(or598)* embryos, this could limit the spindle collapse and allow proper spindle assembly to occur. The primary phenotype in Ska1-depleted human cells is a delay of anaphase onset (Hanisch et al., 2006). If this phenotype is also observed in *C. elegans* embryos, then it could be possible that a prolonged mitosis in these embryos could allow for more time for spindle assembly and this could allow the *rsa-1(or598)* embryos enough time to assemble a spindle. Ska1 has been shown to be phosphorylated in human cells (Chan et al., 2012). It is possible that RSA-1 contributes to the regulation of SKA-1 in *C. elegans* and that loss of *rsa-1* results in a hyper-active SKA-1 protein. Further experiments are required to elucidate the mechanism of how *ska-1* mutations and RNAi suppress *rsa-1(or598).*

In humans, the Ska complex is composed of three proteins termed Ska1, Ska2, and Ska3. *C. elegans* SKA-1 and SKA-3 also form a complex (Schmidt et al., 2012). A *ska-3* RNAi clone was not available in the RNAi library so it remains unknown if depletion of *ska-3* can also suppress *rsa-1(or598)* or if this phenotype is specific to *ska-1*. Future experiments will include cloning *ska-3* to determine if it genetically interacts with *rsa-1*.

The human Ska complex is regulated by phosphorylation. Both Ska1 and Ska3 are phosphorylated by Aurora B in human cells (Chan et al., 2012) and Ska3 is dephosphorylated at the end of mitosis by PP2A with a B regulatory subunit, PPP2R2B/B55β (Theis et al., 2009). It is currently unknown if the *C. elegans* Ska proteins are phosphorylated, but this is a possible mechanism to explain the observed genetic interactions between *ska-1* and *rsa-1*.

In PAA-1 immunostaining experiments, PAA-1 was observed at the centrosome in the suppressor strain containing *abc25* but not in the strain containing *abc17*. Since both of

these strains have mutations in *ska-1*, it is unknown why they would not have the same PAA-1 localization in the early embryo. Although the different results could be due to variability in the immunostaining procedure, it is possible that one of the mutations generates a truncated protein while the other results in non-sense mediated decay of the transcript, which could result in different effects in the embryo.

## 11 Investigating *pptr-1* as a suppressor of *rsa-1(or598)*

The *pptr-1* mutation found in *abc19* is a missense mutation that causes an amino acid substitution, C95Y. Therefore, RNAi may not be able to phenocopy the suppression phenotype. Unfortunately, a *pptr-1* clone was not available in the bacterial RNAi feeding library. *pptr-1* needs to be cloned into the RNAi vector in order to perform this experiment.

The PPTR-1 protein is very well conserved with the human PPP2R5A/B56α protein with 66.8% identity and 80.5% similarity. The residue affected by the mutation is highly conserved among the proteins in this family. In the crystal structure for the PP2A holoenzyme bound of a B' regulatory subunit, this amino acid is found on the outer face of the enzyme. From this location is seems unlikely that this amino acid is critical for protein interactions within the PP2A complex. Since PAA-1 was not recruited to the P-granules in this strain, it is possible that this region of the protein is important for subcellular localization of the complex.

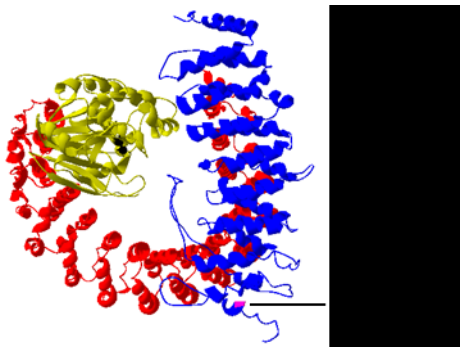

**PP2A holoenzyme with a B' regulatory subunit**
The PP2A holoenzyme with a B' family regulatory subunit, PR61. MMDB ID: 84472 (Xu et al., 2006). The cysteine that is mutated in the *abc19* containing strain is shown in pink.

The most obvious mechanism for how this mutation in *pptr-1* could act as a suppressor of *rsa-1(or598)* is if PAA-1 that is displaced from the P-granules is able to locate to the centrosome. Even though the protein interaction between RSA-1(or598) and PAA-1 would still be inefficient, and increased level of available PAA-1 for centrosome functions might allow proper mitosis in the *ras-1(or598)* background.

It is possible that PPTR-1 plays a more direct role in spindle assembly and that this function contributes to its ability to act as a suppressor of *rsa-1(or598).* The human B' subunit that is most similar to PPTR-1, PPP2R5A, has a role in generating stable microtubule-kinetochore attachments (Foley et al., 2011). While the only characterized functions of PPTR-1 in the early *C. elegans* embryo involved partitioning of the P-granules, it is possible that it also has a role in the regulation of kinetochore-microtubule interactions. This mechanism of suppression would be similar to the current hypothesis for how *ska-1* is able to suppress *rsa-1(or598)*.

## 12 Materials and methods for WGS

Hermaphrodites were cultured on four or five 10 cm NGM agarose plates (2% agarose, 0.5% tryptone, 0.2% yeast extract, 0.5% NaCl, 5 µg/mL cholesterol, 2 mM $CaCl_2$, 2 mM $MgSO_4$, 25 mM $KPO_4$ pH 6.0). Gravid hermaphrodites were washed off the plates in M9. The worms were washed three times with M9 to remove as much *E.coli* as possible. The 100 µL pellet of gravid hermaphrodites was frozen at -80 °C overnight. 600 µL of worm lysis buffer (50 mM KCl, 10 mM Tris-HCl pH8.3, 2.5 mM $MgCl_2$, 0.45% NP-40/Igepal-CA-630, 0.45% Tween-20, 0.01% gelatin) with approximately 500 µg/ml of Proteinase K was added to the worm pellet and incubated overnight at 60 °C in a rotating hybridization oven. RNAse A was added to a final concentration of 37.5 µg/mL. Fresh PCI (50% phenol, 50% chloroform:isoamyl alcohol (24:1)) was added to the sampled and mixed for 5 minutes and centrifuged for 5 minutes at 15000g. The aqueous layer was added to chloroform:isoamyl alcohol (24:1) and mixed for 5 minutes and centrifuged for 5 minutes at 15000g. The aqueous layer was added to 0.1 volumes of 3 M sodium acetate pH 5.2, and 2 volumes of cold 95% ethanol was added. The tube was mixed and incubated at -20 °C for one hour. The sampled was centrifuged for 15 minutes at 15000g and the supernatant carefully removed. The pellet was washed twice with 1 mL

of 70% ethanol and spun for 5 minutes at 15000g. The ethanol was removed carefully and the pellet dried at room temperature for no more than 10 minutes. The pellet was then suspended in 100 µL of TE pH 8.0. Quality of the gDNA was determined on a NanoDrop ND-1000 spectrophotometer and the A260/A280 values ranged from 2.02 to 2.07 which indicated that the samples were composed of nucleic acids with minimal protein contamination. The A260/230 ranged from 2.57 to 2.97 which indicated that phenol/chloroform did not contaminate the samples. High quality gDNA samples should exhibit a range of molecular weights up to at least 10 Kbp on an agarose gel. Approximately 1 µg of each gDNA sample was digested with HinfI and run on an agarose gel. This confirmed that the genomic DNA was of sufficiently high quality to be submitted for whole genome sequencing.

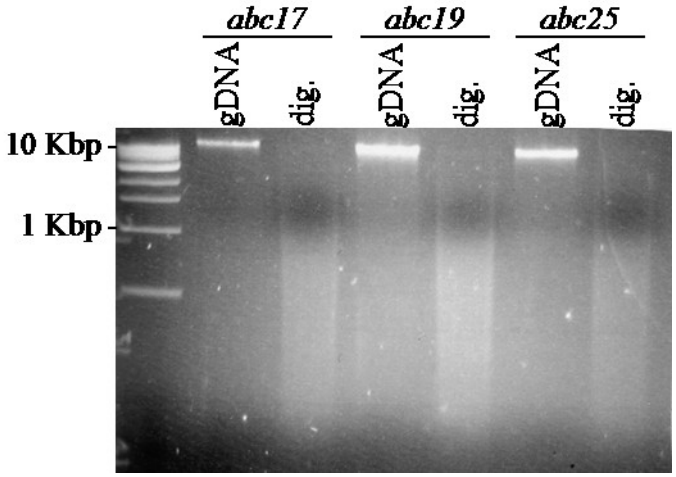


**gDNA preparation for whole genome sequencing**
Approximately 1 µg of gDNA from each of the homozygous suppressor strains and digested with HinfI.

The DNA sample was delivered to Delta Genomics (Edmonton, Alberta) for sequencing. Analysis of the sequencing results was performed by Paul Stothard (Department of Agricultural Food and Nutritional Science, University of Alberta).

## 13 Bibliography


Chan, Y. W., Jeyaprakash, A. A., Nigg, E. A., & Santamaria, A. (2012). Aurora B controls kinetochore–microtubule attachments by inhibiting ska complex–KMN network interaction. *The Journal of Cell Biology*, 196(5), 563-571.

Daum, J. R., Wren, J. D., Daniel, J. J., Sivakumar, S., McAvoy, J. N., Potapova, T. A., et al. (2009). Ska3 is required for spindle checkpoint silencing and the maintenance of chromosome cohesion in mitosis. *Current Biology*, 19(17), 1467-1472.

Flibotte, S., Edgley, M. L., Chaudhry, I., Taylor, J., Neil, S. E., Rogula, A., et al. (2010). Whole-genome profiling of mutagenesis in caenorhabditis elegans. *Genetics,* 185(2), 431-441.

Foley, E. A., Maldonado, M., & Kapoor, T. M. (2011). Formation of stable attachments between kinetochores and microtubules depends on the B56-PP2A phosphatase. *Nature Cell Biology*, 13(10), 1265-1271.

Gaitanos, T. N., Santamaria, A., Jeyaprakash, A. A., Wang, B., Conti, E., & Nigg, E. A. (2009). Stable kinetochore-microtubule interactions depend on the ska complex and its new component Ska3/C13Orf3. *The EMBO Journal*, 28(10), 1442-1452.

Gallo, C. M., Wang, J. T., Motegi, F., & Seydoux, G. (2010). Cytoplasmic partitioning of P granule components is not required to specify the germline in *C. elegans. Science,* 330(6011), 1685.

Hanisch, A., Silljé, H. H., & Nigg, E. A. (2006). Timely anaphase onset requires a novel spindle and kinetochore complex comprising Ska1 and Ska2. *The EMBO Journal,* 25(23), 5504-5515.

Jeyaprakash, A., Santamaria, A., Jayachandran, U., Chan, Y., Benda, C., Nigg, E., et al. (2012). Structural and functional organization of the ska complex, a key component of the kinetochore-microtubule interface. *Molecular Cell*, 46(3), 274-286.

Padmanabhan, S., Mukhopadhyay, A., Narasimhan, S. D., Tesz, G., Czech, M. P., & Tissenbaum, H. A. (2009). A PP2A regulatory subunit Regulates *C. elegans* Insulin/IGF-1 signaling by modulating AKT-1 phosphorylation. *Cell,* 136(5), 939-951.

Raaijmakers, J. A., Tanenbaum, M. E., Maia, A. F., & Medema, R. H. (2009). RAMA1 is a novel kinetochore protein involved in kinetochore-microtubule attachment. *Journal of Cell Science*, 122(14), 2436-2445.

Schmidt, J., Arthanari, H., Boeszoermenyi, A., Dashkevich, N., Wilson-Kubalek, E., Monnier, N., et al. (2012). The kinetochore-bound Ska1 complex tracks depolymerizing microtubules and binds to curved protofilaments. *Developmental Cell,* 23(5), 968-980.

Theis, M., Slabicki, M., Junqueira, M., Paszkowski-Rogacz, M., Sontheimer, J., Kittler, R., et al. (2009). Comparative profiling identifies C13orf3 as a component of the ska complex required for mammalian cell division. *The EMBO Journal*, 28(10), 1453-1465.

Welburn, J. P. I., Grishchuk, E. L., Backer, C. B., Wilson-Kubalek, E. M., Yates III, J. R., & Cheeseman, I. M. (2009). The human kinetochore Ska1 complex facilitates microtubule depolymerization-coupled motility. *Developmental Cell*, 16(3), 374-385.

Xu, Y., Xing, Y., Chen, Y., Chao, Y., Lin, Z., Fan, E., et al. (2006). Structure of the protein phosphatase 2A holoenzyme. *Cell*, 127(6), 1239-1251.